

Palladium-Catalyzed Oxidative Functionalization of C–H Bonds

by

Kami Lee Hull

A dissertation submitted in partial fulfillment
of the requirements for the degree of
Doctor of Philosophy
(Chemistry)
in The University of Michigan
2009

Doctoral Committee:

Associate Professor Melanie S. Sanford, Chair
Professor Johannes Schwank
Professor Adam J. Matzger
Associate Professor John P. Wolfe

© Kami Lee Hull

2009

To Dr. Melanie S. Sanford
and
My Family

Acknowledgements

It is impossible for me to accurately represent how truly grateful I am to all of my family, friends, lab mates, professors, and, especially, my advisor, Melanie. Nothing in this thesis would have been possible without each and every one of you. Thank you.

Melanie, thank you for giving me the opportunity to work in your lab. As one of your first graduate students, I had a unique opportunity to be there as your lab grew from a few graduate students to the hustle and bustle it is today. You were a great advisor to me, you always had enthusiasm for the chemistry, even when it didn't want to cooperate. Thank you for having my back, teaching me and guiding me with in the chemistry community, and encouraging me in my ambitions. Your believing in me as a chemist gives the confidence to go forward and peruse my highest ambitions.

Drs. Wolfe, Matzger, and Schwank thank you for being on my committee: I look forward to your questions at my defense and your input on my thesis. Additionally, Dr. Wolfe, thank you for all the helpful comments and questions at my group meetings over the years. I really enjoyed having you there to ask probing questions to make me think that much harder, help us to learn to disconnect complex molecules, tell stories about other chemists, and crack jokes. I am thrilled that we had joint group meetings for so long, because it allowed me to learn how you approach chemistry. Dr. Matzger, thank you for all of your help over the years with suggestions NMR experiments, suggestions for lab, and your humor in the hallway – I always enjoy your dry humor.

To everyone in the Sanford Lab, past and present- Thank you! I consider my self very lucky to have a lab that became a family for me. Our lab is so much fun to work in, and be a part of... from the outside we probably look crazy, but they have no idea what they are missing!

Allison, thank you for being my deskmate – putting up with both my mess, npr, and my “angry girl” music. You and Ben really made me feel welcome when I first joined the lab and I really appreciate that.

I was very lucky to have amazing classmates, Dipa, Lopa, and Salena. I really feel that together we set the tone of the lab. Dipa, thank you for all the late nights working together, the moral support, and the sounding board for ideas, even when you are stressed you always find time to help with chemistry. Your work effort was inspirational; watching you made me work harder, longer, and smarter. I don't think I would be the chemist I am today if you were not in lab with me. Furthermore, thank you for all of the fun times - I loved our trip to Spain together, you with your ridiculously heavy suitcase and me with all of my plans! Lastly, thank you for being a wonderful friend – I don't think you realize how much we all love you.

Lopa thank you for being Lopa! You are amazing! You are so smart, crazy, loving, fun, and hard working all at the same time. Thank you for all the help on chemistry. You are always so generous and helpful; for just one example, when I was trying to finish a paper before I left for Spain you made my poster for me, not only that, you made all the figures perfect because you knew that's how I would like it. Just thinking of it makes me smile. Also, thank you for all the delicious Indian food and lessons in how to make it. Finally, thank you for having a fantastic husband – Smitesh you are amazing and I am really happy that I got to know you throughout grad school.

Salena thank you for always being so much fun in lab and being such an amazing baker... if it wasn't for your amazing homemade cakes inspiring me I would probably still be baking cakes from boxes today! But also, thank you for always being such a strong ground in the lab, not putting up with nonsense, and always speaking your mind.

Deprez! Nick are like my little brother, the one I never had (and never wanted.... Just kidding!) . Thank you for joining our lab, dominated by women, and putting up with all of our craziness. Also, thank you for never putting Dipa into the trashcan, which is a

further piece of evidence that in a fight, I would win! But seriously, thanks for all of our conversations, proofing my figures, and joking around, you are fantastic!

Leilani, I miss you! You are still my peeps, Dr. Weebles! Having you in lab was always so much fun, you were such a good chemist and good friend. I have learned that in grad school people come in and out of your life all the time, I am just happy that you were one my my best friends for that year, well really forever, because friendship is always there. Thanks also to Eric Kalberer and Paul Zinn, who where very helpful and informative postdocs.

To my first “husband”, Waseem: thank you for being the first student that I taught how to do organic research. Thank you for pioneering the fluorination project, you took on a lot and flourished. I know that you are going to be a fantastic doctor, even if you will just be an MD. Even when we were bickering like an old married couple, we were having fun doing it!

To the four guys who tried to change the gender balance of the lab: Tom, you are hilarious (you know it)! Thanks for all the sarcasm, fun stories, and tricking Lopa. Also, thank you for taking over the oxidative cross-coupling project from me – its my baby and I know its in good hands with you! Matt, thank you for all of your help and braving our lonely year in the Satellite lab together. Nick thank you for being such a fun bench mate, honest lab mate, and most importantly, thank you for being messier than me (or at least almost as messy). Andrew, thank you for always being there for me, to talk about chemistry and life. This last year as your bench mate has been so much fun, even if at times a little too distracting... You are so easy to talk to, and even if you are no ones moral compass, you are always willing to listen and give sound advise and I truly appreciate that.

Kara and Joy, you both joined the lab at a transition period, when our first people were graduating, Melanie was getting tenure, and the lab was settling down from the hard pre-tenure push. Thank you for continuing the tradition of working hard while having fun, I feel like you two are helping to keep the Sanford lab that I knew and loved.

Brannon, thank you for all of your help over the last year with chemistry and running computations; and I think that you are a great addition to our lab and I hope that you enjoy your time in it as much as I did. Janette, thank you for all the fun we had when we were in the Satellite lab together; I loved debating politics, hearing about Spanky and Stella, and just having you around. Sharon, Asako, and Amanda thanks for all of the fun over the past year! I think that you are all fantastic, and hope that your five years in the Sanford Lab are as good as mine were.

My family- Mom, Dad, Rena and Megan- have all been so supportive throughout graduate school – from the time I was a little kid to now they have always said that I could do anything that I set my mind to. Their believing in me made all of this possible. My family has grown over the past few years, so welcome to John and Ruth thank you as well. I love you all.

Finally, I would like to thank all of my friends, whom I love like family. The girls from college, kathRyn, Emily, Barb, Sarah, Rachel, and Lucy I love you all, and we should defiantly celebrate by trekking to London! I have missed seeing you all over the last few years, but I know that we all love each other all the same! To the wonderful friends I have made at Michigan – Katie and Jeremy, Pascale, Stacy, Erica, Susan, Eric, Donna, and everyone else, I love you, grad school would have been miserable without you, and I don't think I would have made it if I didn't have each and every one of you. Finally, I want to thank Bear for all of his support and kindness over the last few months, soon (I hope) I will no longer be Zombie-Kami.

Table of Contents

Dedication	ii
Acknowledgements	iii
List of Tables	ix
List of Schemes	xi
Chapter 1	
Introduction	1
1.1 References	12
Chapter 2	
Palladium-Catalyzed Regio and Chemoselective Oxidation of sp^3 C–H Bonds	14
2.1 Background and Significance	14
2.2 Methodology Development and Synthetic Scope	19
2.3 Developing Reaction Conditions for Asymmetric Catalysis	27
2.4 Subsequent Examples	31
2.5 Conclusions.....	34
2.6 Experimental Procedure.....	35
2.7 References.....	42
Chapter 3	
Palladium-Catalyzed Oxidative Fluorination of C–H Bonds	45
3.1 Background and Significance	45

3.2 Methodology Development and Synthetic Scope	49
3.3 Subsequent Examples	58
3.4 Conclusions.....	60
3.5 Experimental Procedure.....	61
3.6 References.....	80

Chapter 4

Palladium-Catalyzed Oxidative Homocoupling of 2-Phenylpyridine Derivatives	83
--	----

4.1 Background and Significance	83
4.2 Methodology Development and Synthetic Scope.....	90
4.3 Mechanistic Investigations	100
4.4 Subsequent Examples	108
4.5 Conclusions.....	109
4.6 Experimental Procedure.....	109
4.7 References	122

Chapter 5

Palladium-Catalyzed Oxidative Cross-Coupling of C–H Bonds	125
---	-----

5.1 Background and Significance	125
5.2 Methodology Development and Synthetic Scope.....	132
5.3 Mechanistic Investigations of Pd-Mediated Oxidative Cross-Coupling Reactions	143
5.4 Regioselectivity Studies	161
5.5 Subsequent Examples	173
5.6 Conclusions.....	175
5.7 Experimental Procedure.....	176
5.7 References	198

List of Tables

Chapter 2

Palladium-Catalyzed Regio and Chemoselective Oxidation of sp^3 C–H Bonds

Table 2.1: Developing Conditions which Minimize Racemization31

Table 2.2: Acetoxylation of 8-Methylquinoline with Recyclable Oxidant PS–I(OAc)₂
.....32

Chapter 3

Palladium-Catalyzed Oxidative Fluorination of C–H Bonds

Table 3.1: Oxidant Screening for the Fluorination of Benzylic C–H Bonds50

Table 3.2: Oxidant Screening for the Fluorination of Aryl C–H Bonds55

Table 3.3: Substrate Scope for the Pd-Catalyzed Oxidative Fluorination Reaction57

Chapter 4

Palladium-Catalyzed Oxidative Homocoupling of 2-Phenylpyridine Derivatives

Table 4.1: Solvent Screen for the Pd-Catalyzed Oxidative Coupling of 2-(*o*-Tolyl)
pyridine93

Table 4.2: Oxidant Screening for the Oxidative Homocoupling of 2-(*o*-Tolyl)pyridine
.....94

Table 4.3: Catalyst Screen for the Pd-Catalyzed Oxidative Coupling of 2-(*o*-
Tolyl)pyridine95

Table 4.4: Substrate Scope of the Oxidative Coupling Reactions97

Table 4.5: Oxidative Coupling of *meta*-Substituted 2-Arylpyridines98

Chapter 5

Palladium-Catalyzed Oxidative Cross-Coupling of C–H Bonds

Table 5.1: Oxidant Screening for the Pd-Catalyzed Oxidative Cross-Coupling of Benzo[<i>h</i>]quinoline (33) and Benzene	136
Table 5.2: Screening of Sulfoxide Additives for the Pd-Catalyzed Oxidative Coupling of Benzo[<i>h</i>]quinoline (33) and Benzene	136
Table 5.3: Screening of Ligands and their Ability to Promote the Oxidative Coupling Reaction	137
Table 5.4: Substrate Scope for the Oxidative Cross-Coupling of Benzoquinone and a Variety of 1,2- and 1,3-Disubstituted Arenes	141
Table 5.5: H/D Exchange Studies	160
Table 5.6: Effects of Changing the Sterics of the Carboxylate	165
Table 5.7: Effects of Changing the Sterics of the Carboxylate	166
Table 5.8: Changing the Electronics of the Carboxylate	129

List of Schemes

Chapter 1

Introduction

Scheme 1.1: C–H Bond Functionalization (a) and Traditional Functional Group Transformations (b)	1
Scheme 1.2: Transition Metal Mediated C–H Bond Functionalization	2
Scheme 1.3: Hydroboration vs. C–H Bond Oxidation	2
Scheme 1.4: IC ₅₀ of Four Derivatives of Indeno-Quinoline-6-Carboxamide	3
Scheme 1.5: Synthesis of Indeno-Quinoline-6-Carboxamides (1-4)	3
Scheme 1.6: Alternative Approach for Synthesis of 2-4 from 1	4
Scheme 1.7: Mechanisms of C–H Activation to Form of a C–[M] Bonds	4
Scheme 1.8: Possible Mechanisms of Electrophilic C–H Activation	5
Scheme 1.9: Indirect Activation of a C–H Bond.....	5
Scheme 1.10: Ligand Directed C–H Activation.....	6
Scheme 1.11: Intramolecular Indirect C–H Activation.....	6
Scheme 1.12: Cyclopalladation of Azobenzene.....	7
Scheme 1.13: Examples of Functionalization Reactions	7
Scheme 1.14: Pd-Catalyzed Acetoxylation of Toluene.....	8
Scheme 1.15: Proposed Mechanism for Pd-Catalyzed Acetoxylation of Benzene.....	8
Scheme 1.16: Pd-Catalyzed Acetoxylation of sp ³ C–H bonds.....	9
Scheme 1.17: Pd-Catalyzed Fluorination of C–H Bonds.....	9
Scheme 1.18: Pd-Catalyzed Direct Arylation of C–H Bonds	10
Scheme 1.19: Pd-Catalyzed Oxidative Coupling of Toluene.....	10
Scheme 1.20: Pd-Catalyzed Oxidative Homocoupling of 2-Arylpyridines	10
Scheme 1.21: Pd-Catalyzed Oxidative Cross-Coupling.....	11

Chapter 2

Palladium-Catalyzed Regio and Chemoselective Oxidation of sp^3 C–H Bonds

Scheme 2.1: Transition Metal-Catalyzed Approach for sp^3 C–H Bond Oxygenation	14
Scheme 2.2: Oxidation of Methane to Methanol with a Pt-Catalyst	15
Scheme 2.3: Examples of Palladacycles Formed through sp^3 C–H Bond Activation	15
Scheme 2.4: Pd-Mediated Oxygenation of an sp^3 C–H Bond	16
Scheme 2.5: Pt-Catalyzed Oxidative-Cyclization of Amino Acids	16
Scheme 2.6: Pd-Catalyzed Acetoxylation of Benzene	17
Scheme 2.7: Pd-Catalyzed Acetoxylation of Toluene	17
Scheme 2.8: Proposed Pd-Catalyzed Acetoxylation of 8-Methylquinoline	18
Scheme 2.9: Palladium-Catalyzed Acetoxylation of Benzo[<i>h</i>]quinoline	18
Scheme 2.10: Proposed Mechanism for the Pd-Catalyzed Regioselective Acetoxylation Reaction of Benzo[<i>h</i>]quinoline	19
Scheme 2.11: Cyclopalladation of 8-Methylquinoline with Palladium Acetate	19
Scheme 2.12: Palladium-Catalyzed Acetoxylation of 8-Methylquinoline	20
Scheme 2.13: Pd-Catalyzed Acetoxylation of 5,8-Dimethylquinoline	20
Scheme 2.14: Pd-Catalyzed Acetoxylation of 1-Methylnaphthalene	21
Scheme 2.15: Substrate Scope for Pd-Catalyzed Acetoxylation of Benzylic C–H Bonds	21
Scheme 2.16: Pd-Catalyzed Acetoxylation of 2-Methoxypyridine	22
Scheme 2.17: Heteroatom Activated Substrates for the Pd-Catalyzed Acetoxylation Reaction	22
Scheme 2.18: Pd-Catalyzed Acetoxylation of 2- <i>tert</i> -Butylpyridine	23
Scheme 2.19: Rationale for Formation of the Triacetylated Product	23
Scheme 2.20: Substrate Scope for the Pd-Catalyzed Acetoxylation Reaction of Unactivated C–H Bonds	24
Scheme 2.21: Pd-Catalyzed Acetoxylation of Oxime Ethers	25
Scheme 2.22: Proposed Mechanism for the Pd-Catalyzed Acetoxylation Reaction	25
Scheme 2.23: Palladium-Catalyzed Oxidative Functionalization: Acetoxylation vs. Etherification	26

Scheme 2.24: Pd-Catalyzed Oxidative Etherification of C–H Bonds	26
Scheme 2.25: Oxidation of Pt ^{II} to Pt ^{IV} in Alcohol Solvents	27
Scheme 2.26: Possible Pd ^{IV} Intermediates in the Pd-Catalyzed Etherification Reaction	27
Scheme 2.27: Initial Attempt Towards the Pd-Catalyzed Asymmetric Acetoxylation Reaction	28
Scheme 2.28: Three Possible Mechanisms for the Reductive Elimination from 54	29
Scheme 2.29: Resolution of the Two Diastereomeric 8-Ethylquinoline Palladacycles	30
Scheme 2.30: Oxidation of the Resolved Palladacycle Under the Catalytic Conditions	30
Scheme 2.31: Acetoxylation of an sp ³ C–H Bond with K ₂ S ₂ O ₈	32
Scheme 2.32: Acetoxylation of an sp ³ Bond with MeCOOO <i>t</i> -Bu as the Oxidant	33
Scheme 2.33: Pd-Catalyzed Acetoxylation of Boc Protected <i>N</i> -Methyl Amines	33
Scheme 2.34: Pd-Catalyzed Acetoxylation of Secondary C–H Bonds	34

Chapter 3

Palladium-Catalyzed Oxidative Fluorination of C–H Bonds

Scheme 3.1: Examples of pharmaceuticals containing C–F bonds	45
Scheme 3.2: Examples of (a) the Balz-Schiemann Reaction and (b) the Halex Process	46
Scheme 3.3: Proposed Pd ^{II} /Pd ⁰ Catalytic Cycle for C–F Bond Formation	46
Scheme 3.4: Synthesis of Pd ^{II} Fluoride Complexes	47
Scheme 3.5: Attempts to Reductively Eliminate Ar–F from Pd ^{II}	47
Scheme 3.6: Pd-Catalyzed Acyl Fluoride Formation	48
Scheme 3.7: Mechanism for the Pd-Mediated Acid Fluoride Formation	48
Scheme 3.8: Pd-Catalyzed Halogenation of C–H Bonds	49
Scheme 3.9: Proposed Pd-Catalyzed Oxidative Fluorination of C–H Bonds	49
Scheme 3.10: Optimized Conditions for Benzylic C–H Bond Fluorination	51

Scheme 3.11: Pd-Mediated Oxidative Coupling between 8-Methylquinone and Benzene	51
Scheme 3.12: Determining the Origin of 18b	52
Scheme 3.13: Reaction Between 18a and Anisole	52
Scheme 3.14: Competition Between Benzene and 1,4-Dimethoxybenzene	53
Scheme 3.15: Competing C–F and C–OAc Bond Forming Reductive Eliminations...53	
Scheme 3.16: Reaction of 18a and AcOH in the Presence of <i>N</i> -Fluoro-2,4,6-Trimethylpyridinium Tetrafluoroborate.....	54
Scheme 3.17: Optimized Conditions for the Fluorination of 23	55
Scheme 3.18: Proposed Mechanism for the Oxidative Fluorination Reaction	57
Scheme 3.19: Direct Oxidative Cleavage Mechanism for the Pd-Catalyzed Fluorination Reactions.....	58
Scheme 3.20: Oxidative of a Ar–Pd ^{II} –I with an <i>N</i> -fluoro-pyridinium salt.....	58
Scheme 3.21: Oxidation to an Isolable Pd ^{IV} Aryl Fluoride and Reductive Elimination to Afford the new C–F Bond.....	59
Scheme 3.22: Ritter's Example of C–F Bond Forming Reductive Elimination from Pd ^{IV}	59
Scheme 3.23: Stoichiometric Oxidative Fluorination of Aryl Boronic Acids	59
Scheme 3.24: Proposed Reductive Elimination of an Ar–F Bond From Pd ^{II}	60
Scheme 3.25: Grushin's Proposed Mechanism for the Formation of the Ar–F	60

Chapter 4

Palladium-Catalyzed Oxidative Homocoupling of 2-Phenylpyridine Derivatives

Scheme 4.1: Ar–Ar Bond Formation via Metal-Catalyzed Cross-Coupling.....	84
Scheme 4.2: General Mechanism for Pd-Catalyzed Cross-Coupling Reactions.....	84
Scheme 4.3: Direct Arylation of a C–H Bond.....	85
Scheme 4.4: Transition-Metal Catalyzed C–H Oxidative Coupling	85
Scheme 4.5: The First Example of Pd-Mediated Oxidative Coupling.....	86
Scheme 4.6: Two Likely Mechanisms for the Pd-Mediated Oxidative Coupling of Benzene.....	86

Scheme 4.7: Palladium-Catalyzed Oxidative Homocoupling of Toluene.....	87
Scheme 4.8: Oxidative Dimerization of Thiophenes and Furans.....	87
Scheme 4.9: Selective Reoxidation of Pd ⁰ with AgF.....	87
Scheme 4.10: Ligand Effects on the Regioselectivity of the Oxidative Coupling of Dimethyl Phthalate (3).....	88
Scheme 4.11: C–H Activation of Dimethyl Phthalate with (phen)Pd(OAc) ₂	88
Scheme 4.12: C–H Activation of Dimethyl Phthalate with Pd(acac) ₂	89
Scheme 4.13: The Regioselective Oxidative Coupling of Methylbenzoate.....	89
Scheme 4.14: Pyridine-Directed <i>ortho</i> -Selective Oxidative C–H Functionalization...90	90
Scheme 4.15: Proposed Oxidative Homocoupling of 2-Phenylpyridine.....	90
Scheme 4.16: Oxidative Homocoupling via Two C–H Activations.....	91
Scheme 4.17: Oxidative Homocoupling via a C–H activation Followed by a Transmetallation.....	91
Scheme 4.18: Palladium-Catalyzed Acetoxylation Utilizing Oxone [®] as the Oxidant.....	92
Scheme 4.19: Possible Oxidative Homocoupling of 2-Phenylpyridine.....	92
Scheme 4.20: Initial Result on the Oxidative Homocoupling of 2-(<i>o</i> -Tolyl)pyridine.....	92
Scheme 4.21: Optimized Conditions for the Oxidative Coupling of 2-(<i>o</i> -Tolyl)pyridine.....	96
Scheme 4.22: The Oxidative Coupling of <i>meta</i> -Substituted 2-Arylpyridine Derivatives.....	98
Scheme 4.23: High Regioselectivity in the Palladium-Catalyzed Acetoxylation of 2-(<i>m</i> -MeO-Phenyl)pyridine.....	98
Scheme 4.24: Substrates that were not Oxidatively Coupled Under Our Reaction Conditions.....	99
Scheme 4.25: Possible Transmetallation Mechanisms for Pd-Mediated Oxidative Homocoupling.....	100
Scheme 4.26: Possible Sequential C–H Activation Mechanisms for Pd-Mediated Oxidative Homocoupling.....	101
Scheme 4.27: Stoichiometric Oxidation of Cyclopalladated Complex 29	102
Scheme 4.28: Crossover Experiments Between 29 and 33	102
Scheme 4.29: Crossover Experiments Between 29 and Free 2- <i>o</i> -tolylpyridine 23	103

Scheme 4.30: Regioselectivity of the C–H Activation.....	104
Scheme 4.31: Oxidation of Intermediate 30	104
Scheme 4.32: Reaction of 30 with Oxone [®] in the Presence of Free Substrate 23	105
Scheme 4.33: Explanation for the Formation of the Crossover Product 34 in Scheme 4.32	105
Scheme 4.34: Reaction of 30 with AcOH	106
Scheme 4.35: Facile Protonation of Complex 38	106
Scheme 4.36: Probing Equilibration between 41 and 43 via the Transient Intermediate 42	107
Scheme 4.37: C–H Activation at Pt ^{IV}	108
Scheme 4.38: C–H Activation at a Cationic Pt ^{IV} is Faster than Ligand Association of Cl	108
Scheme 4.39: Possible Mechanism for the Second C–H Activation at Pd ^{IV}	108

Chapter 5

Palladium-Catalyzed Oxidative Cross-Coupling of C–H Bonds

Scheme 5.1: Oxidative Homocoupling of C–H Bonds	125
Scheme 5.2: Oxidative Cross-coupling of C–H Bonds	125
Scheme 5.3: Traditional Cross-Coupling	126
Scheme 5.4: Direct-Arylation of a C–H Bond	126
Scheme 5.5: Two Chemoselective, Sequential C–H Activations are Required for Selective Oxidative Cross-Coupling.....	127
Scheme 5.6: Oxygen as Oxidant for the Formation of Biaryls	128
Scheme 5.7: The First Example of Pd-Mediated Oxidative Cross-Coupling	128
Scheme 5.8: Oxidative Cross-Coupling of Activated Heterocycle 6 with Benzene	129
Scheme 5.9: Oxidative Coupling of <i>N</i> -Benzylpyrrole (8) with Benzene	129
Scheme 5.10: Proposed Mechanism for the Oxidative Cross Coupling of 6 and Benzene	130

Scheme 5.11: Fagnou's Oxidative Coupling of <i>N</i> -Acetylindole with Benzene	130
Scheme 5.12: DeBoef's Oxidative Coupling of Benzofuran with O ₂ as the Terminal Oxidant.....	131
Scheme 5.13: Proposed Mechanism for the Pd-Catalyzed Cross-Coupling of Indole and Benzene.....	131
Scheme 5.14: Pd-Catalyzed Oxidative Cross-Coupling of Naphthalene and Benzene	132
Scheme 5.15: Proposed Pd-Mediated Oxidative Cross-Coupling.....	132
Scheme 5.16: Proposed Oxidative Cross-Coupling Reaction	133
Scheme 5.17: Stoichiometric Reaction Between [BzqPdOAc] ₂ (28) and Benzene	133
Scheme 5.18: Addition of π -Acidic Ligands to Promote the Second C–H Activation	134
Scheme 5.19: Benzoquinone-Promoted Stoichiometric Oxidative Coupling	134
Scheme 5.20: BQ-Promoted Direct Coupling of Ar–H with Me ₄ Sn.....	134
Scheme 5.21: The Optimized Conditions for the Oxidative Cross-Coupling of Benzo[<i>h</i>]quinoline (33) and Benzene	138
Scheme 5.22: Cross-Coupling Products with Other Directing Groups.....	138
Scheme 5.23: Oxidative Coupling of Benzo[<i>h</i>]quinoline (33) with <i>p</i> -Xylene.....	139
Scheme 5.24: Fagnou's Oxidative Coupling of <i>N</i> -Acetylindole (16) and <i>p</i> -Xylene ...	139
Scheme 5.25: Sterically Controlled Selectivity in the Pd-Catalyzed Oxidative Homocoupling of Dimethyl Phthalate	140
Scheme 5.26: Sterically Controlled Selectivity in Ir-Catalyzed C–H Borylation	142
Scheme 5.27: Competition Studies Between Electronically Different Arene Substrates	143
Scheme 5.28: Effect of Benzoquinone Structure on Selectivity	144
Scheme 5.29: Scenario A, Involving a BQ Promoted C–H Activation.....	145
Scheme 5.30: Scenario B, Where the BQ Induces Reductive Elimination	145
Scheme 5.31: Stoichiometric Oxidative Coupling Between 28 and 1,2-Dimethoxybenzene	146
Scheme 5.32: Three Possible Mechanisms for Pd-Mediated Oxidative Cross-Coupling	147
Scheme 5.33: Standard Reaction Conditions for the Initial Rate Kinetic Experiment	148

Scheme 5.34: Derived Rate Equations for the Three Mechanisms Shown in Scheme 5.32	148
Scheme 5.35: Reaction Conditions for Determining the Order in BQ.....	149
Scheme 5.36: Order Studies in BQ.....	149
Scheme 5.37: A Linear Double Reciprocal Plot is Consistent with Saturation Kinetics	150
Scheme 5.38: Experiments Determining the Order in [BzqPdOAc] ₂ (28).....	150
Scheme 5.39: Determining the Order in 1,2-Dimethoxybenzene	151
Scheme 5.40: Determining the Order in DMSO	152
Scheme 5.41: Determining the Order in AcOH	153
Scheme 5.42: Synthesis of [BzqPdO ₂ C(<i>Ar</i>)] ₂ (62-68) Complexes	154
Scheme 5.43: Hammett Plot for Reactions of 62-68 Under Flooding Conditions.....	155
Scheme 5.44: Synthesis of Electronically Differentiated Benzoquinone Derivatives .	156
Scheme 5.45: Hammett Plot of Electronically Differentiated BQ Derivatives.....	156
Scheme 5.46: Kinetic Isotope Effect Under Flooding Conditions in BQ	157
Scheme 5.47: Kinetic Isotope Effect for Agostic Bond Formation.....	158
Scheme 5.48: Example of a Large <i>k_{ie}</i> for Agostic Bond Formation.....	158
Scheme 5.49: Kinetic Isotope Effect for the Direct Coupling between Benzene and Bromoanisole	159
Scheme 5.50: Kinetic Isotope Effect in the Oxidative Functionalization of Benzene .	159
Scheme 5.51: [BzqPdOAc] ₂ Catalyzed H/D Exchange without BQ.....	159
Scheme 5.52: Benzoquinone Catalyzed Reductive Elimination of 84	160
Scheme 5.53: <i>In Situ</i> Formation of the Bisaryl Complex through Transmetallation ...	160
Scheme 5.54: Reductive Elimination Studies from the Pd-Bisaryl Complex with and without BQ.....	161
Scheme 5.55: Mechanism for the Pd-Mediated Oxidative Cross-Coupling Reaction .	161
Scheme 5.56: Oxidative Coupling of Benzo[<i>h</i>]quinoline (33) and 1,3-Dimethoxybenzene	162
Scheme 5.57: Proposed Mechanism for the Formation of the Two Isomers Formed in Scheme 5.56.....	163
Scheme 5.58: Synthesis of BzqPd Carboxylate Complexes 90-92	164

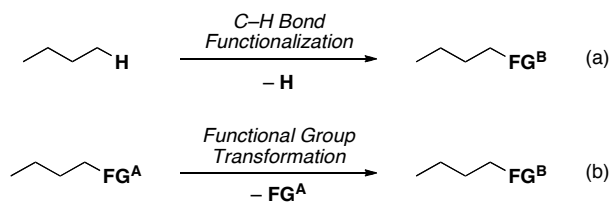
Scheme 5.59: Effect of Changing the Benzoquinone on the Regioselectivity.....	169
Scheme 5.60: Selectivity Hammett Plot for the Quinone Ligand	170
Scheme 5.61: Effect of the Benzoquinone Ligand with Carbonate Anions.....	171
Scheme 5.62: Selectivity Hammett Plot for the Electronics of the Quinone Ligand with Carbonate Anions.....	172
Scheme 5.63: Shi's Example of Amide Directed Oxidative Cross-Coupling of C–H Bonds	173
Scheme 5.64: Buckwald's Cu-Free Conditions	173
Scheme 5.65: Pd-Mediated Oxidative Cross-Coupling of Ferrocenyl Oxazolines and Benzene.....	174
Scheme 5.66: Tunable Selectivity Dependant on the Oxidant Employed.....	174
Scheme 5.67: Intramolecular Oxidative Cross-Coupling to Form an sp^3 – sp^2 C–C Bond	175

Chapter 1

Introduction

Carbon-hydrogen bonds are ubiquitous in organic chemistry; however, despite their pervasiveness, they are rarely considered synthons within the scope of synthetic organic chemistry. This is because it can be quite challenging to selectively transform an unactivated C–H bond into a new functional group (Scheme 1.1a). Therefore, when synthesizing both simple and complex organic molecules, the typical approach for the installation of a desired functionality is through functional group manipulations (*i.e.*, exchanging one functional group for another) (Scheme 1.1b).^{1,2} However, the requirement of pre-functionalized starting materials in these reactions decreases both the step and the atom economy of such syntheses, because **FG^A** must be first installed and then lost as a byproduct in the installation of **FG^B**.^{3, 4} In contrast, direct C–H bond functionalization would allow for the formation of **FG^B** in a single step with H⁺ being the only byproduct.⁵⁻¹⁰

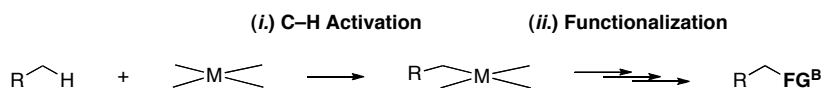
Scheme 1.1 C–H Bond Functionalization (a) and Traditional Functional Group Transformations (b)



One of the main goals within the Sanford Laboratory is to take on the challenge of developing selective methodologies for the functionalization of unactivated C–H bonds.¹¹ Achieving this would revolutionize retrosynthetic analysis to include unactivated C–H bonds as synthons for other functional groups. Our approach is to utilize transition metal

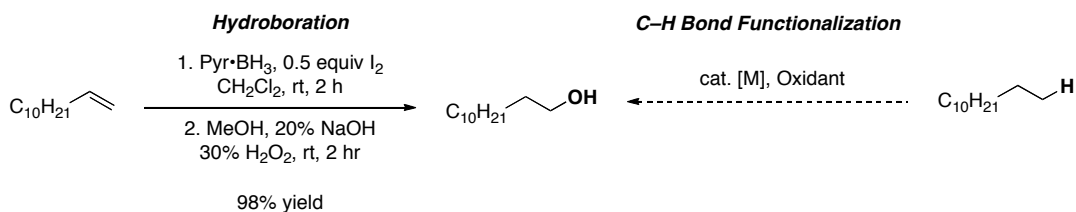
catalysts that are known to activate C–H bonds to form C–[M] bonds (Scheme 1.2). Then, the resulting C–[M] bonds can undergo functionalization reactions to install a diverse array of **FG^B**. Once developed, these methodologies would increase both the step and atom economy of the synthesis of complex organic molecules, and they have the potential to greatly expedite structure-activity relationship (SAR) studies of pharmaceutical candidates.

Scheme 1.2 Transition Metal Mediated C–H Bond Functionalization



As discussed above, C–H bond functionalization reactions can greatly increase the step and atom economy for the installation of functional groups into organic molecules. For example, hydroboration is a widely used and powerful reaction for the addition of H–OH across an alkene.¹² However, this method does not directly add H₂O across an olefin. Instead, a two step protocol involving (1) H–BH₂ addition across the alkene and then (2) oxidation of the resulting C–B bond with H₂O₂ is required to install the requisite OH functional group (Scheme 1.3). A similar transformation could be accomplished via a selective C–H bond oxygenation reaction in one step from a simple alkane (Scheme 1.3).¹¹ This is only one example of many where C–H bond functionalization methodology would expedite the synthesis of organic molecules.

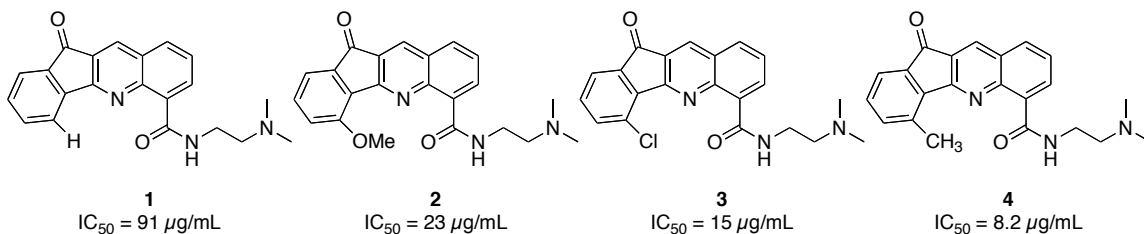
Scheme 1.3 Hydroboration vs. C–H Bond Oxidation¹³



When developing a new pharmaceutical, medicinal chemists perform SAR studies on the drug candidates to determine the effect of various substitutions on the efficacy against the target disease.¹⁴ Small differences in the scaffold of a drug molecule can have

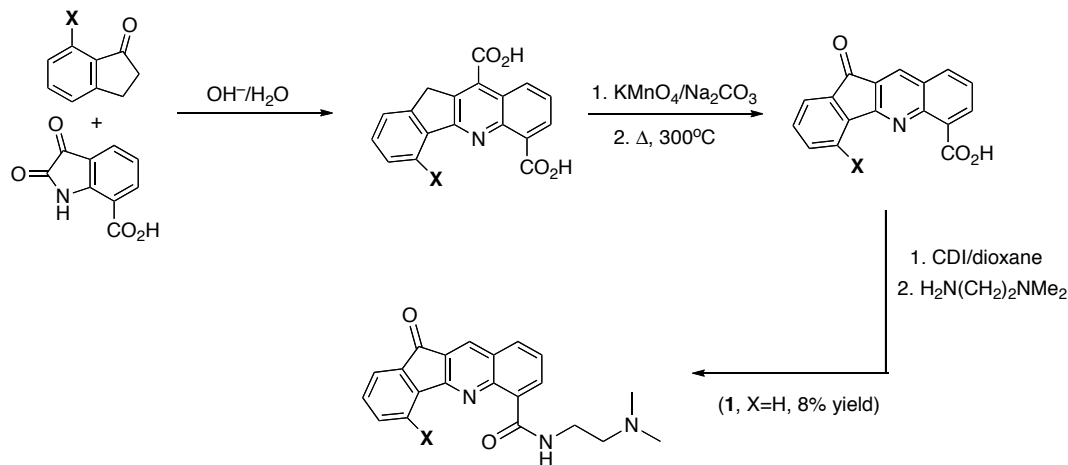
a significant affect on its biological activity. For example, indeno-quinoline-6-carboxamide (**1**) is a colon cancer drug candidate whose cytotoxicity varies significantly with substitution at the 4-position (Scheme 1.4).¹⁵

Scheme 1.4 IC₅₀ of Four Derivatives of Indeno-Quinoline-6-Carboxamide¹⁵

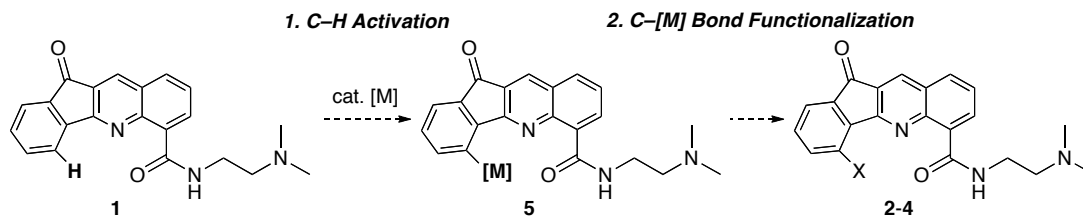


As shown in Scheme 1.5, the synthesis of each molecule in the SAR study above required at least five steps and afforded the drug candidates in low overall yield (for X = H, 8% yield was obtained over 5 steps).¹⁵ In contrast, a C–H bond functionalization reaction could allow for the late stage derivatization of **1** to form **2-4** through intermediate **5** (Scheme 1.6). Such a reaction would greatly decrease the time required for the synthesis of potential drug candidates and therefore has the potential to greatly accelerate the discovery of new pharmaceutical agents.

Scheme 1.5 Synthesis of Indeno-Quinoline-6-Carboxamides (**1-4**)¹⁵



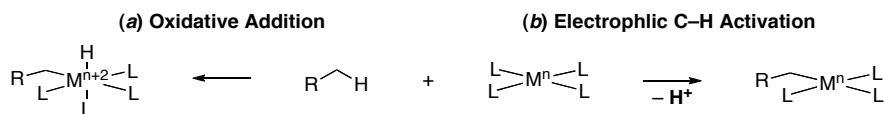
Scheme 1.6 Alternative Approach for Synthesis of 2-4 from 1



There are three key challenges in developing a selective C–H bond functionalization methodology: (1) C–H bonds are thermodynamically strong and kinetically inert, (2) as C–H bonds are ubiquitous in organic molecules, a synthetically useful methodology must selectively functionalize a single C–H bond in a molecule, and finally, (3) the reactions must allow for the incorporation of a diverse array of functionalities under similar reaction conditions.^{7, 11}

C–H bonds are thermodynamically strong and kinetically inert (Challenge 1).⁷ Nevertheless, transition metals are known to activate C–H bonds to form C–[M] bonds. These reactions can proceed by either oxidative addition or electrophilic metallation manifolds form either C–[M]–H or C–[M] plus 1 equiv of H⁺, respectively (Scheme 1.7). Since the C–H bond reacts directly with the metal center in both mechanisms, less hindered C–H bonds typically undergo C–H activation at faster rates. The mechanism of oxidative addition is direct insertion of the metal into the C–H sigma bond, therefore the oxidation state of the metal increases by two (Scheme 1.7(a)). Metals that activate C–H bonds by oxidative addition include Zr^{II}, Ru⁰, Rh^I, Ir^I, and Pt^{IV}.⁷

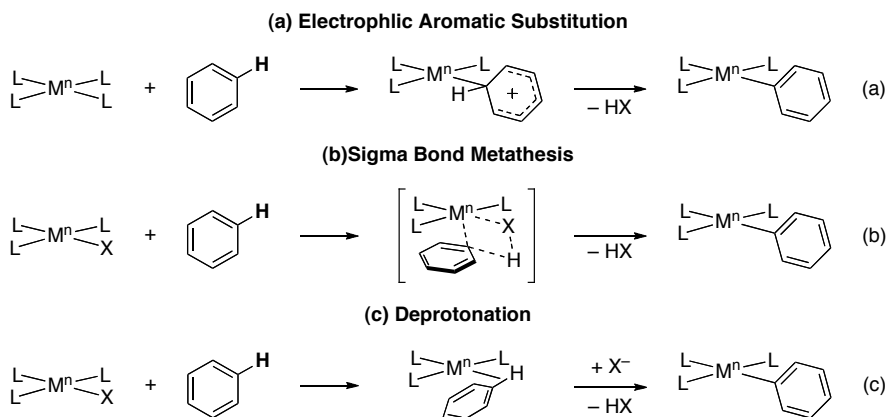
Scheme 1.7 Mechanisms of C–H Activation to Form of a C–[M] Bonds⁷



There is no oxidation state change in an electrophilic metallation of a C–H bond.⁷ Instead, an X-type ligand on the metal is replaced with a covalently bound carbon (Scheme 1.7b). Transition metals that are known to promote electrophilic C–H activation include Pd^{II}, Pt^{II}, and Rh^{III}. The activation of an aromatic C–H bond by a transition metal can proceed through (a) an electrophilic aromatic substitution mechanism (via an

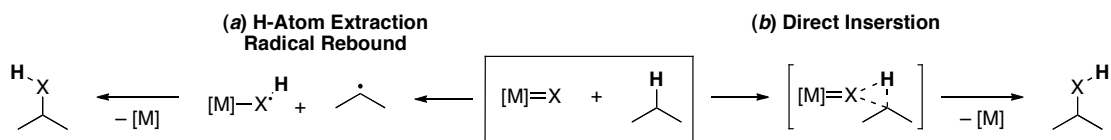
Wheland intermediate), (b) a sigma bond metathesis, or (c) the deprotonation of an agostic bond by either an internal (X-type ligand) or external base (Scheme 1.8). The C–H activation of sp^3 C–H bonds can only proceed through path b or c, as there is no π -system to nucleophilically attack the metal (Scheme 1.8).⁷

Scheme 1.8 Possible Mechanisms of Electrophilic C–H Activation⁷



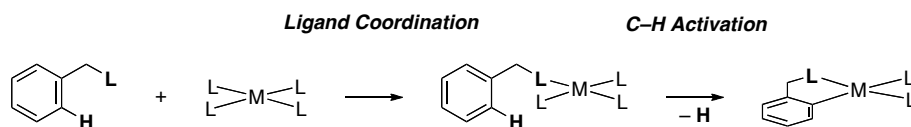
Finally, transition metals are also known to activate C–H bonds indirectly, without the direct formation of a C–[M] bond.⁷ As seen in Scheme 1.9, an activated metal complex ($[M]=X$) can abstract an electron or a hydrogen from a C–H bond forming a $C\cdot$ or C^+ . These highly reactive intermediates can then which then undergoes a subsequent functionalization or can directly insert into the C–H bond. Metals that are known to catalyze through these indirect C–H functionalization reactions include Fe^{III} , Mn^{III} , Ru^{IV} , and Rh^{II} . In these reactions, the weakest C–H bonds are often selectively functionalized; therefore, C–H bonds which are benzylic, allylic, 3° , and adjacent to a heteroatom are typically most reactive.⁷

Scheme 1.9 Indirect Activation of a C–H Bond⁷

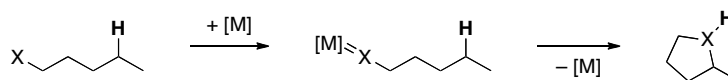


Thus, the high kinetic barriers for the functionalization of C–H bonds associated with Challenge 1 can be addressed by the utilization of metal catalysts that can either undergo C–H activation to form a [M]–C bond or indirectly activate the C–H bond.⁷ However, as there are many different C–H bonds within most organic molecules, an approach for the regioselective C–H activation of a specific C–H bond must be identified (Challenge 2). For example, for **1** to undergo metal-catalyzed functionalization reactions to afford **2-4** only the C–H bond *ortho* to the pyridine ring must undergo C–H activation (Scheme 1.6, page 4). The challenge of regioselective C–H activation can be addressed by incorporating a ligand directing group into the substrate undergoing functionalization.^{7, 16, 17} The ligand can bind to the catalyst, direct the C–H activation to a proximal C–H bond, and thereby form the requisite C–[M] bond with high levels of regioselectivity. Such transformations are known as cyclometallation reactions. Typically, cyclometallation reactions at most transition metals proceed to form five membered rings compared to both larger or smaller ring sizes, though this can be dependent upon the type of C–H bonds undergoing activation.¹⁸ Important, regioselective indirect C–H activation can also be achieved using a similar strategy, where the X of the [M]=X bond is tethered to the C–H bond that is to be functionalized.⁶

Scheme 1.10 Ligand Directed C–H Activation



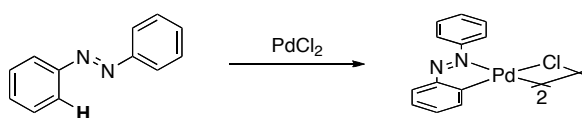
Scheme 1.11 Intramolecular Indirect C–H Activation



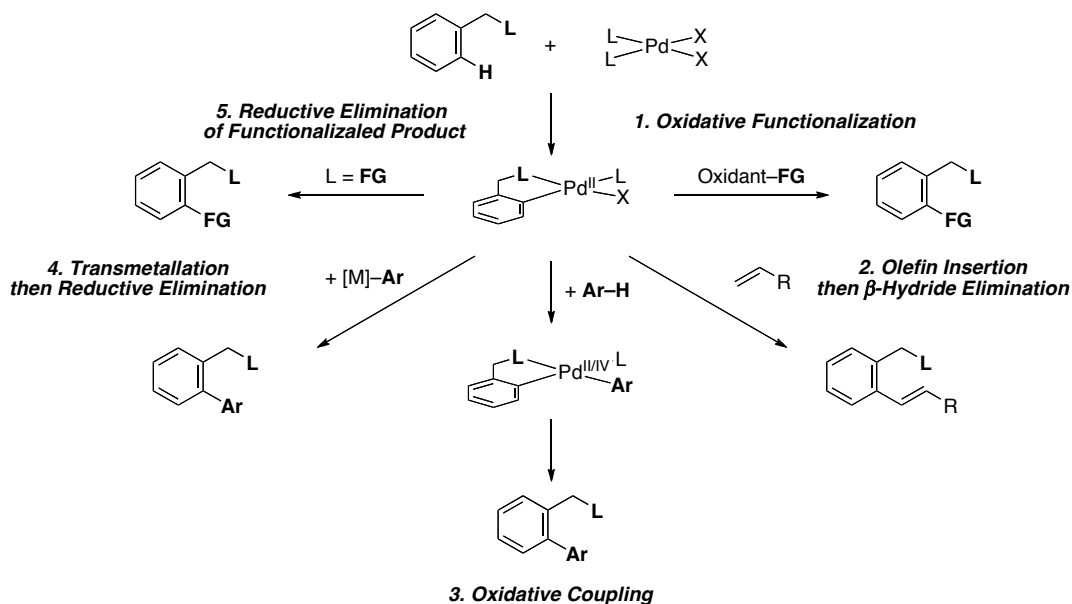
Our group chose to pursue methodologies that employ ligand directed electrophilic C–H activation with a Pd catalyst. In 1965, Cope demonstrated that PdCl₂ selectively activates the C–H bond adjacent to the azo-group in azobenzene, forming the palladacycle (Scheme 1.12).¹⁹ Since then, a wide variety of directing groups have been

shown to promote the stoichiometric activation of both sp^2 and sp^3 C–H bonds at Pd^{II} .^{6, 20} One of the advantages of C–H activation at Pd^{II} is that it forms a square planer metal complex that is coordinatively unsaturated. Thus, this species can participate in a diverse array of subsequent reactions including: oxidations to Pd^{IV} , insertion, C–H activations, transmetalation, and/or reduction to Pd^0 . As seen in Scheme 1.13, these subsequent reactions can lead to the installation of a variety of functional groups – affording the diverse functionalization that was Challenge 3.⁶

Scheme 1.12 Cyclopalladation of Azobenzene¹⁹



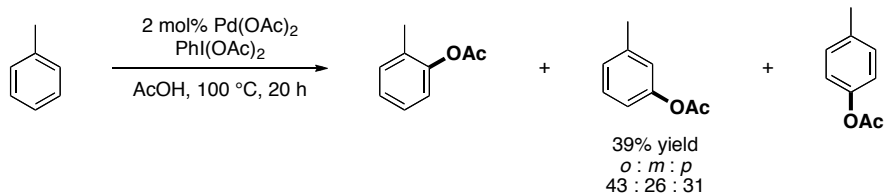
Scheme 1.13 Examples of Functionalization Reactions



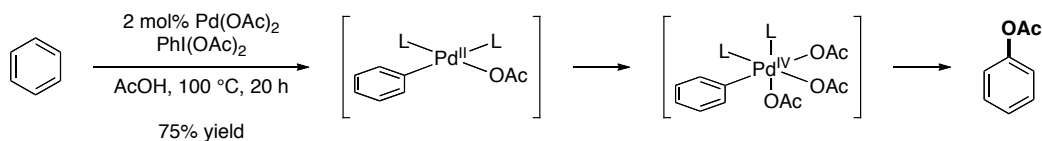
The two-functionalization pathways that will be described herein are the oxidative functionalization (path 1) and the oxidative coupling reaction (path 3). However, other groups have demonstrated the oxidative Heck reaction (path 2), transmetalation/reductive elimination (path 4), and reductive functionalization (path 5).⁶

When reacted with strong oxidants, Pd^{II} complexes are known to form Pd^{IV} intermediates.^{21, 22} Yet, prior to our work, there were limited examples of selective Pd^{II/IV}-catalyzed oxidative functionalizations of C–H bonds. Crabtree demonstrated the acetoxylation of Ar–H bonds with PhI(OAc)₂ in the presence of a substoichiometric amount of Pd(OAc)₂.²³ However, these reactions were not regioselective, affording a mixture of isomers when substituted arenes were employed as the substrate (Scheme 1.14). Importantly, a Pd^{II}/Pd^{IV} catalytic cycle was proposed for these reactions (Scheme 1.15). We initially sought to exploit this approach to develop a Pd^{II}/Pd^{IV} catalyzed ligand-directed C–H acetoxylation reaction.

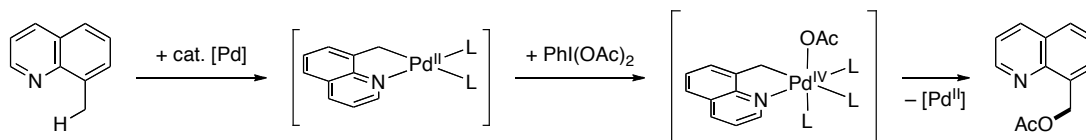
Scheme 1.14 Pd-Catalyzed Acetoxylation of Toluene²³



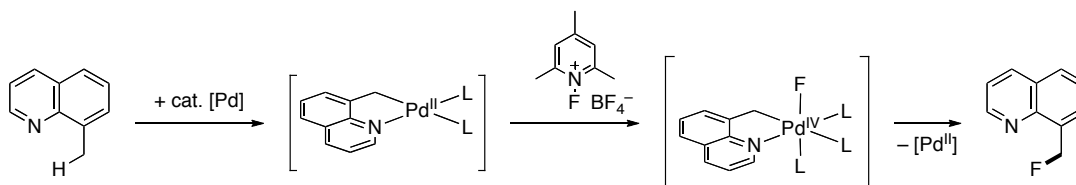
Scheme 1.15 Proposed Mechanism for Pd-Catalyzed Acetoxylation of Benzene²³



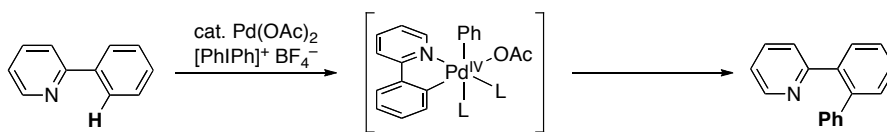
My initial research goal, upon joining the Sanford Laboratory, was to develop the Pd-catalyzed ligand-directed oxidative functionalization of sp³ C–H bonds to form new C–O bonds. As detailed in Chapter 2, we found that quinoline and pyridine ligands effectively direct the C–H activation of sp³ C–H bonds at Pd(OAc)₂.^{11, 24} PhI(OAc)₂ then oxidizes the cyclometallated Pd^{II} intermediate to Pd^{IV}, and finally, C–O bond-forming reductive elimination affords the desired acetoxyated product and regenerates the Pd^{II} catalyst. Additionally, running the reactions in alcohol solvents (MeOH, EtOH, or *i*-PrOH) allows for the formation of ether products, where a molecule of solvent is incorporated rather than an acetoxy group.

Scheme 1.16 Pd-Catalyzed Acetoxylation of sp^3 C–H bonds^{11, 24}

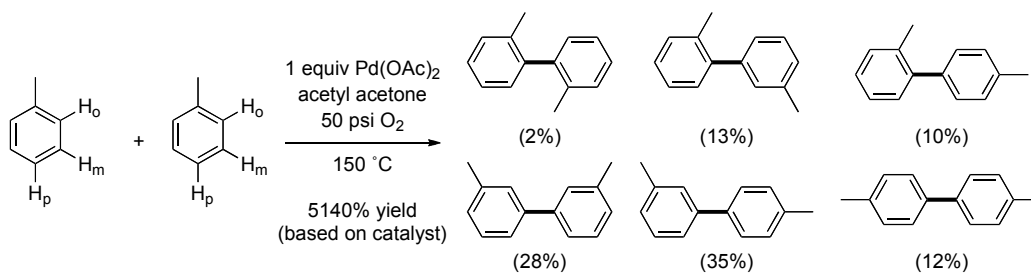
In our quest to incorporate a variety of functional groups, coworkers in the Sanford Laboratory developed conditions for analogous chlorinations, brominations, and iodinations of C–H bonds, which proceed through Pd^{II}/Pd^{IV} catalytic cycles.^{11, 25, 26} Waseem Anani and I sought to develop related transformations for the construction of C–F bonds (Chapter 3).²⁷ Importantly, carbon-fluorine bond-forming reductive elimination does not occur from Pd^{II} complexes; however, the potential of C–F bond formation from Pd^{IV} had not previously been studied. We found that *N*-fluoropyridinium salts were effective electrophilic fluorine oxidants to promote the desired Pd-catalyzed C–F bond-forming reactions at both sp^2 and sp^3 carbon centers. Subsequent work by our group and others has provided strong evidence supporting a Pd^{II/IV} mechanism for this process.

Scheme 1.17 Pd-Catalyzed Fluorination of C–H Bonds²⁷

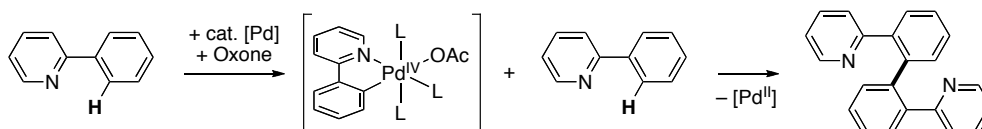
Aryl-aryl bonds are found throughout organic chemistry. Our group and others have demonstrated Pd^{II/IV}-catalyzed C–H bond activation/arylation using [Ph₂I]BF₄ as the oxidant (Scheme 1.18).^{28, 29} These, and other direct C–H functionalization reactions couple a C–H bond with a C–FG bond.^{30, 31} An even more atom and step economical process would couple two C–H bonds together to form the new C–C bond, via an oxidative coupling reaction.

Scheme 1.18 Pd-Catalyzed Direct Arylation of C–H Bonds²⁸

Palladium-mediated oxidative coupling reactions have been known since the 1960's (Scheme 1.13, path 3).³² However, similar to the acetoxylation of arenes developed by Crabtree, these reactions were not regioselective and often formed a complex mixture of all possible regioisomers (Scheme 1.19).³³ Chapters 4 and 5 will discuss our efforts to develop and determine the mechanism of regioselective Pd-catalyzed oxidative coupling reactions.³⁴⁻³⁶

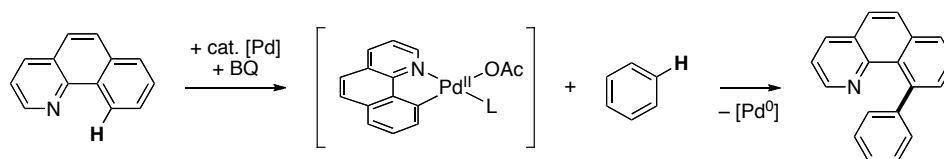
Scheme 1.19 Pd-Catalyzed Oxidative Coupling of Toluene³³

In our oxidative functionalization reactions of 2-arylpyridines, for the formation of C–OAc, C–F, C–Cl, C–Br, and C–I bonds, we often saw trace amounts of the oxidatively homocoupled substrates. Chapter 4 discusses our development of a high yielding and highly regioselective oxidative homocoupling of 2-arylpyridine derivatives (Scheme 1.20).³⁵ Through extensive mechanistic studies, we determined that the reaction was proceeding through two sequential C–H activation steps, the first at Pd^{II} followed by a second unprecedented C–H activation reaction at a Pd^{IV} intermediate.

Scheme 1.20 Pd-Catalyzed Oxidative Homocoupling of 2-Arylpyridines³⁵

Once conditions were developed for the oxidative homocoupling of 2-arylpyridines, we were interested in developing regioselective oxidative cross-coupling reactions where a new C–C' bond could be formed from two different C–H bonds (Scheme 1.21). Chapter 5 discusses our development of a new Pd-catalyzed, regioselective, oxidative cross-coupling of C–H bonds.³⁶ We have determined that these reactions proceed via two sequential C–H activation steps at Pd^{II}. The first is a ligand directed cyclometallation while the second is an undirected C–H activation. Then, benzoquinone promotes reductive elimination to form the new C–C' bond and release Pd⁰. Finally, Pd⁰ is reoxidized to Pd^{II} by Ag^I to regenerate the active catalyst. Importantly, the regioselectivity of the second, undirected C–H activation appears to be predominantly determined by the steric interactions at the metal center. Intriguingly, this selectivity can be tuned by changing the ancillary ligands: the benzoquinone and the carboxylate.

Scheme 1.21 Pd-Catalyzed Oxidative Cross-Coupling³⁶



In conclusion, one of the over-arching goals of the research in the Sanford lab is to develop methodologies for the regioselective and diverse functionalization of C–H bonds. This thesis describes my efforts at the discovery, optimization, and mechanistic study of Pd-catalyzed methodologies for C–H activation reactions that result in the formation of new sp³ C–O, C–F, C–C, and C–C' bonds.

1.1 References

- (1) Smith, M. B.; March, J. In *March's Advanced Organic Chemistry: Reactions, Mechanisms, and Structure, 5th Edition*. Section Title: Physical Organic Chemistry; 2000; , pp 1824.
- (2) Corey, E. J.; Cheng, X. In *The Logic of Chemical Synthesis*. Section Title: General Organic Chemistry; 1995; , pp 436.
- (3) Trost, B. M. *Acc. Chem. Res.* **2002**, *35*, 695-705.
- (4) Wender, P. A.; Verma, V. A.; Paxton, T. J.; Pillow, T. H. *Acc. Chem. Res.* **2008**, *41*, 40-49.
- (5) Godula, K.; Sames, D. *Science* **2006**, *312*, 67-72.
- (6) Dick, A. R.; Sanford, M. S. *Tetrahedron* **2006**, *62*, 2439-2463.
- (7) Shilov, A. E.; Shul'pin, G. B. *Chem. Rev.* **1997**, *97*, 2879-2932.
- (8) Crabtree, R. H. *J. Organomet. Chem.* **2004**, *689*, 4083-4091.
- (9) Kakiuchi, F.; Chatani, N. *Adv. Synth. Catal.* **2003**, *345*, 1077-1101.
- (10) Labinger, J. A.; Bercaw, J. E. *Nature* **2002**, *417*, 507-514.
- (11) Dick, A. R.; Hull, K. L.; Sanford, M. S. *J. Am. Chem. Soc.* **2004**, *126*, 2300-2301.
- (12) Clay, J. M. *Name React. Funct. Group Transform* **2007**, 183-188.
- (13) Clay, J. M.; Vedejs, E. *J. Am. Chem. Soc.* **2005**, *127*, 5766-5767.
- (14) Patani, G. A.; LaVoie, E. J. *Chem. Rev.* **1996**, *96*, 3147-3176.
- (15) Deady, L. W.; Desneves, J.; Kaye, A. J.; Thompson, M.; Finlay, G. J.; Baguley, B. C.; Denny, W. A. *Bioorg. Med. Chem.* **1999**, *7*, 2801-2809.
- (16) Sezen, B.; Sames, D. In *Handbook of C-H Transformations* Dyker, G., Ed.; Wiley VCH: Weinheim, 2005; p 3.
- (17) Ritleng, V.; Sirlin, C.; Pfeffer, M. *Chem. Rev.* **2002**, *102*, 1731-1769.
- (18) Omae, I. *Coord. Chem. Rev.* **2004**, *248*, 995-1023.
- (19) Cope, A. C.; Siekman, R. W. *J. Am. Chem. Soc.* **1965**, *87*, 3272-3273.
- (20) Dupont, J.; Consorti, C. S.; Spencer, J. *Chem. Rev.* **2005**, *105*, 2527-2571.

- (21) Canty, A. J. *Acc. Chem. Res.* **1992**, *25*, 83-90.
- (22) Canty, A. J. In *Handbook of Organopalladium Chemistry for Organic Synthesis*; Negishi, E.-i., de Meijere, A., Eds.; Wiley-Interscience: New York, 2002; pp 189-211.
- (23) Yoneyama, T.; Crabtree, R. H. *J. Mol. Catal. A* **1996**, *108*, 35-40.
- (24) Desai, L. V.; Hull, K. L.; Sanford, M. S. *J. Am. Chem. Soc.* **2004**, *126*, 9542-9543.
- (25) Kalyani, D.; Dick, A. R.; Anani, W. Q.; Sanford, M. S. *Org. Lett.* **2006**, *8*, 2523-2526.
- (26) Kalyani, D.; Dick, A. R.; Anani, W. Q.; Sanford, M. S. *Tetrahedron* **2006**, *62*, 11483-11498.
- (27) Hull, K. L.; Anani, W. Q.; Sanford, M. S. *J. Am. Chem. Soc.* **2006**, *128*, 7134-7135.
- (28) Kalyani, D.; Deprez, N. R.; Desai, L. V.; Sanford, M. S. *J. Am. Chem. Soc.* **2005**, *127*, 7330-7331.
- (29) Deprez, N. R.; Kalyani, D.; Krause, A.; Sanford, M. S. *J. Am. Chem. Soc.* **2006**, *128*, 4972-4973.
- (30) Campeau, L.; Fagnou, K. *Chem. Commun.* **2006**, 1253-1264.
- (31) Satoh, T.; Miura, M. *Chem. Lett.* **2007**, *36*, 200-205.
- (32) van Helden, R.; Verberg, G. *Rec. des Trav. Chim. des Pays-Bas* **1965**, *84*, 1263-1273.
- (33) Unger, M. O.; Fouty, R. A. *J. Org. Chem.* **1969**, *34*, 18-21.
- (34) Hassan, J.; Sevignon, M.; Gozzi, C.; Schulz, E.; Lemaire, M. *Chem. Rev.* **2002**, *102*, 1359-1469.
- (35) Hull, K. L.; Lanni, E. L.; Sanford, M. S. *J. Am. Chem. Soc.* **2006**, *128*, 14047-14049.
- (36) Hull, K. L.; Sanford, M. S. *J. Am. Chem. Soc.* **2007**, *129*, 11904-11905.

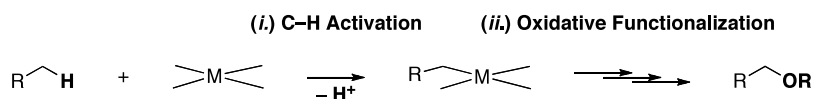
Chapter 2

Palladium-Catalyzed Regio and Chemoselective Oxidation of sp^3 C–H Bonds

3.1 Background and Significance

The regio-, chemo-, and stereoselective oxygenation of alkane C–H bonds for the functionalization of both bulk and fine chemicals is a significant challenge facing both organic and organometallic chemists.¹ Our group was interested in developing a transition metal-catalyzed approach to the regioselective oxygenation of sp^3 C–H bonds via oxidative functionalization reactions (Scheme 2.1).² In particular, our efforts focused on developing Pd- and/or Pt-based catalysts for these transformations, as these metals are known to promote electrophilic activation of both activated and unactivated sp^3 C–H bonds.^{3,4}

Scheme 2.1 Transition Metal-Catalyzed Approach for sp^3 C–H Bond Oxygenation

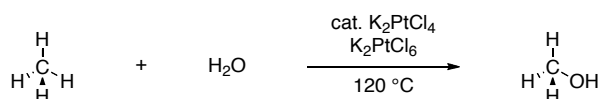


Unlike sp^2 C–H bonds, sp^3 C–H bonds are especially challenging substrates for C–H activation reactions, as they do not have available lone pairs or π -electrons that can enhance the reactivity of the bond towards C–H activation.⁵ The bond dissociation energies for methane, ethane, *iso*-propane, and *tert*-butane C–H bonds are 105.1, 98.2, 95.1, and 93.1 kcal/mol, respectively; hence, sp^3 C–H bonds are not prone to homolytic cleavage.⁶ However, in electrophilic C–H activation, the homolytic BDE's do not provide good estimates for reactivity, rather, the acidity of a C–H bond is a better indicator.⁵

However, the pK_a of ethane is estimated to be 50 and that of *tert*-butane is 71, indicating that alkanes are relatively unreactive for electrophilic C–H activation.⁶

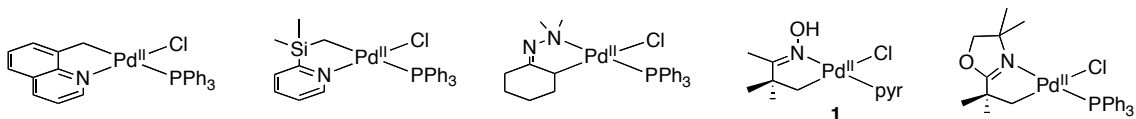
Despite these challenges, selective sp^3 C–H bond oxidation reactions are known. In an early example of platinum-catalyzed C–H bond oxidation, Shilov demonstrated that K_2PtCl_4 catalyzes the oxidation of methane to methanol using Pt^{IV} as a terminal oxidant (Scheme 2.2).⁷ This fundamental work demonstrated the viability of alkane C–H bond oxidation. However, it is not practical, as it required a stoichiometric quantity of a very costly Pt oxidant. As such, many chemists have sought to develop more general approaches for the oxidation of methane to methanol derivatives that utilize less expensive oxidants.⁸

Scheme 2.2 Oxidation of Methane to Methanol with a Pt-Catalyst⁷



Methane only has one type of C–H bond; however, most complex organic molecules contain many different C–H bonds that could potentially be oxidized. Therefore, controlling the regioselectivity of C–H activation can be extremely challenging. However, palladium and platinum are well known to undergo cyclometallation reactions in which a ligand directs C–H activation selectively to a proximal C–H bond.⁹⁻¹¹ As summarized in Scheme 2.3, this directed C–H activation pathway is often highly selective, even in the presence of multiple different C–H bonds of comparable strength and acidity.¹²⁻¹⁶

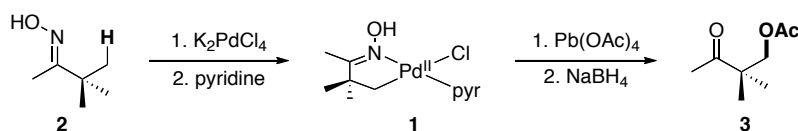
Scheme 2.3 Examples of Palladacycles Formed through sp^3 C–H Bond Activation¹²⁻¹⁶



Palladacycles like those in Scheme 2.3 have been utilized as intermediates in stoichiometric C–H bond oxidation reactions. For example, Baldwin demonstrated a four-

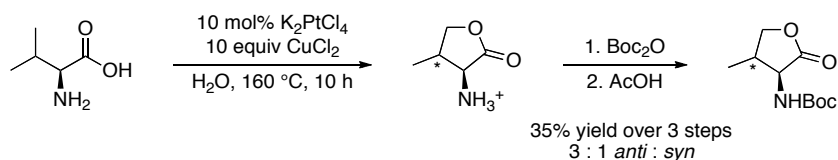
step synthetic sequence for the selective mono-acetoxylation of pinacalone oxime (**2**) (Scheme 2.4).¹⁶⁻¹⁸ First, oxime-directed C–H activation as used to form a 5-membered palladacyclic dimer, which was reacted with pyridine to form **1**. This species was then oxidized with Pb(OAc)₄, and the resulting oxime product was reduced with NaBH₄ to afford the desired functionalized product **3**. This sequence nicely demonstrates the viability of Pd-mediated oxidative functionalization reactions. However, it is fundamentally limited by the requirement for a stoichiometric amount of the Pd salt, as well as by the requirement for a toxic Pb-based oxidant.

Scheme 2.4 Pd-Mediated Oxygenation of an sp³ C–H Bond.¹⁷



Recently, there has been further progress in the development of selective Pt-catalyzed oxidative functionalization reactions of sp³ C–H bonds.¹⁹ Sames demonstrated the C–H oxygenation of amino acids to generate lactones using a Pt-based catalyst in conjunction with CuCl₂ as the terminal oxidant (Scheme 2.5). The proposed mechanism of this reaction involves a Pt^{II/IV} catalytic cycle that is initiated by chelation of the amine and carboxylic acid to the Pt^{II}, which serves to direct the activation to the proximal C–H bond. However, these reactions were limited by the requirement for expensive Pt catalysts and high temperatures (160 °C) as well as by the low yields (15-35%) and modest substrate scope.

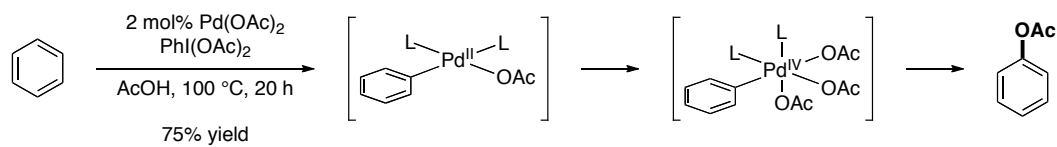
Scheme 2.5 Pt-Catalyzed Oxidative-Cyclization of Amino Acids.



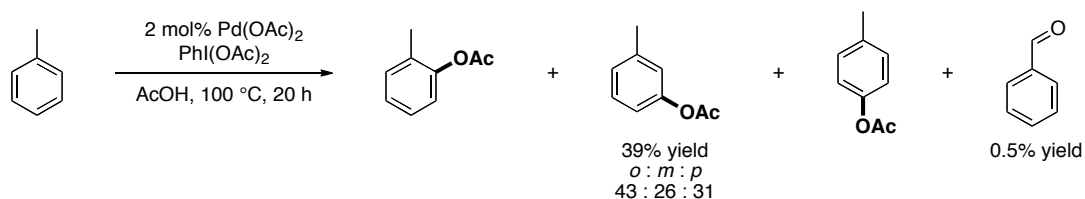
We wanted to develop a more general approach to the regioselective oxidative functionalization of sp³ C–H bonds that utilized relatively inexpensive Pd-based catalysts

in place of Pt. Therefore, we were interested in new ways to functionalize the Pd–C bond that forms upon cyclopalladation (Scheme 2.3). Palladium catalysts are known to promote the C–H activation of benzene. For example, Crabtree has reported that in the presence of the strong oxidant $\text{PhI}(\text{OAc})_2$, $\text{Pd}(\text{OAc})_2$ catalyzes C–H oxygenation of benzene to generate phenyl acetate.²⁰ This reaction proceeded in good yield (78% based on oxidant) and with high levels of chemoselectivity (only 2.9% over-oxidized products were formed) (Scheme 2.6). Crabtree proposed a $\text{Pd}^{\text{II}}/\text{Pd}^{\text{IV}}$ catalytic cycle for this reaction, in which C–H activation occurred at Pd^{II} , then $\text{PhI}(\text{OAc})_2$ oxidized the Pd^{II} intermediate to Pd^{IV} , and lastly, C–OAc bond-forming reductive elimination released the product and regenerated the Pd^{II} catalyst. However, sp^3 C–H bonds did not undergo facile functionalization in this system. For example, when toluene was subjected to the reaction conditions, aromatic C–H activation products were the major organic species formed. Benzaldehyde, a product of benzylic activation, was observed in only 0.5% yield (Scheme 2.7). Finally, this reaction showed very little regioselectivity; for example, toluene reacted to form a 46 : 26 : 31 mixture of the *ortho* : *meta* : *para* isomers of the acetoxyated product.

Scheme 2.6 Pd-Catalyzed Acetoxylation of Benzene²⁰



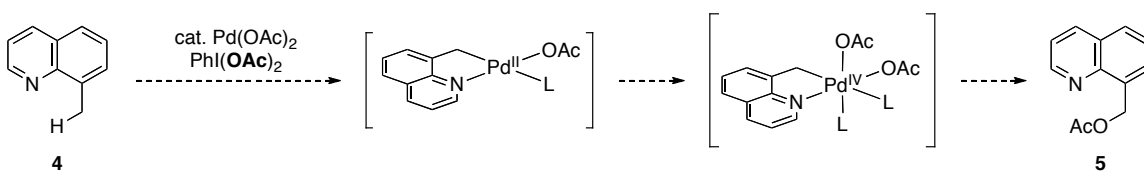
Scheme 2.7 Pd-Catalyzed Acetoxylation of Toluene²⁰



In summary, when we started this project, it was known that Pd^{II} could promote stoichiometric cyclopalladation of sp^3 C–H bonds. Further, the resulting palladacycles were susceptible to oxidative cleavage to afford a new sp^3 C–OAc bonds with super-

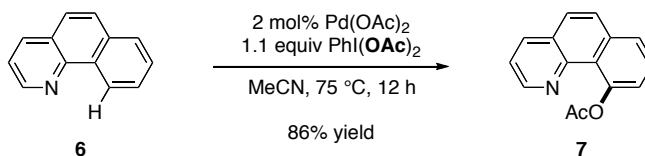
stoichiometric quantities of toxic lead tetraacetate (Scheme 2.4).¹⁶⁻¹⁸ Crabtree had demonstrated that substoichiometric quantities of Pd(OAc)₂ could promote the Pd^{II/IV}-catalyzed acetoxylation of benzene with PhI(OAc)₂.²⁰ However, these reactions proceeded with low levels of regioselectivity and did not promote the functionalization of sp³ C–H bonds. As such, we hypothesized that regioselective Pd-catalyzed C–H acetoxylation could be accomplished by combining ligand-directed C–H activation with Pd^{II/IV}-catalyzed oxidative functionalization using PhI(OAc)₂ as the terminal oxidant (Scheme 2.8).

Scheme 2.8 Proposed Pd-Catalyzed Acetoxylation of 8-Methylquinoline.

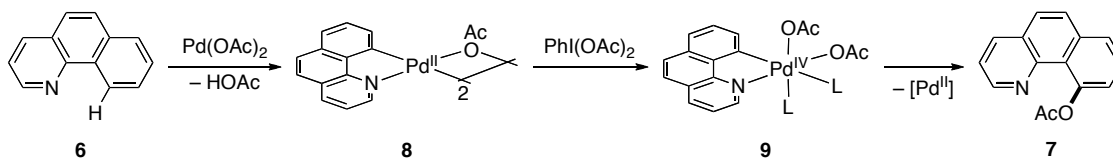


Preliminary results by Allison Dick, a fellow graduate student in the Sanford Lab, suggested that this approach to sp³ C–H bond functionalization could be promising. She found that Pd(OAc)₂ (2 mol %) in conjunction with PhI(OAc)₂ (1.1 equiv) catalyzes the selective oxidative functionalization of an sp² C–H bond of benzo[*h*]quinoline (6) to give 7 in 86% yield (Scheme 2.9).³ The proposed mechanism for this reaction involved C–H activation proximal to the pyridine-directing group, followed by oxidation of [BzqPdOAc]₂ (8) to form Pd^{IV} complex 9, and finally, reductive elimination to form the new C–OAc bond of 7 and regenerate the Pd^{II} catalyst (Scheme 2.10).

Scheme 2.9 Palladium-Catalyzed Acetoxylation of Benzo[*h*]quinoline³



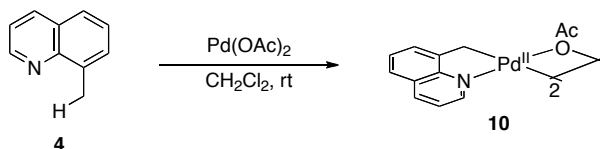
Scheme 2.10 Proposed Mechanism for the Pd-Catalyzed Regioselective Acetoxylation Reaction of Benzo[*h*]quinoline^{3, 21}



3.2 Methodology Development and Synthetic Scope

Our efforts towards the selective oxidative functionalization of sp³ C–H bonds began with 8-methylquinoline (4) as the substrate. Importantly, 4 is known to undergo stoichiometric cyclopalladation with Pd(OAc)₂ at a benzylic C–H bond to afford palladacycle 10 (Scheme 2.11).^{22, 23} In the proposed catalytic reaction sequence, this initial cyclopalladation would be followed by oxidation of 10 to Pd^{IV} with PhI(OAc)₂. Finally, C–OAc bond forming reductive elimination would release the desired acetoxy product (5) and regenerate the Pd^{II} catalyst.

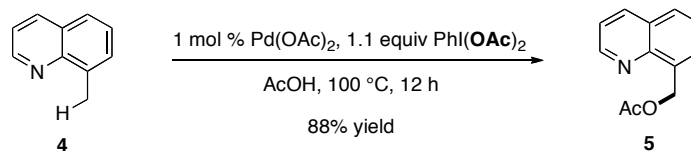
Scheme 2.11 Cyclopalladation of 8-Methylquinoline with Palladium Acetate.²²



Upon reaction optimization, we were pleased to find that 1 mol % of Pd(OAc)₂ catalyzes the acetoxylation of 8-methylquinoline (4) in the presence of PhI(OAc)₂. When the reaction was run in acetic acid (AcOH) at 100 °C, 5 could be isolated in 88% yield (Scheme 2.12).³ The methyl group of 8-methylquinoline (4) is benzylic, and such positions are often susceptible to further oxidation reactions to generate aldehydes and carboxylic acids. However, in this transformation > 1% of over-oxidized products were observed (as determined by GC and GCMS analysis of the crude reaction mixtures). This is presumably due to the fact that the relative rate of a second benzylic C–H activation is slow due to the steric hindrance associated with the newly installed OAc substituent.

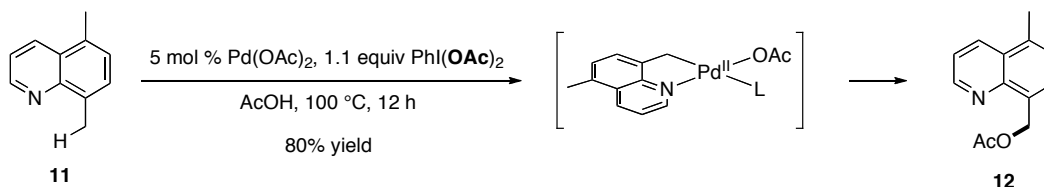
Importantly, control reactions run in the absence of the Pd catalyst or the $\text{PhI}(\text{OAc})_2$ oxidant did not afford any product **5**.

Scheme 2.12 Palladium-Catalyzed Acetoxylation of 8-Methylquinoline.

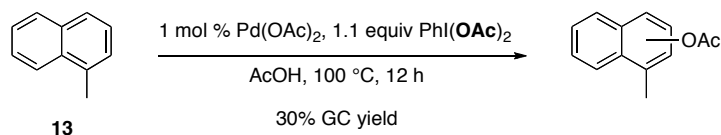


Next, we wanted to probe the role of the directing group in this reaction, in order to determine whether the quinoline nitrogen was directing the C–H activation or if the benzylic C–H bonds reacting selectively without the requirement of the ligand. When 5,8-dimethylquinoline (**11**) was subjected to analogous acetoxylation reaction conditions, the methyl group at the 5-position was unaffected, while the 8-methyl underwent selective acetoxylation, affording **12** in 80% yield (Scheme 2.13). The regioselectivity of this acetoxylation was determined by ^1H NMR spectroscopy using nOe analysis, as a 2.4% nOe was observed between the H3 and the unfunctionalized 5-methyl substituent. This result confirms that the nitrogen of the quinoline is critical in directing oxidative functionalization of the proximal sp^3 C–H bond. Additionally, as shown in Scheme 2.14, 1-methyl naphthalene (**13**), which lacks a directing group entirely, underwent unselective oxidation under our standard reaction conditions, resulting in a mixture of regioisomeric oxidized products in low yield (30% as determined by GC).

Scheme 2.13 Pd-Catalyzed Acetoxylation of 5,8-Dimethylquinoline.

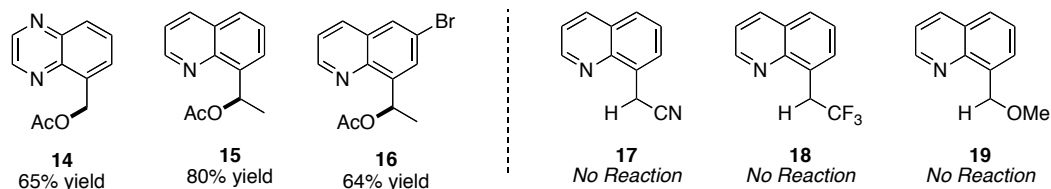


Scheme 2.14 Pd-Catalyzed Acetoxylation of 1-Methylnaphthalene.



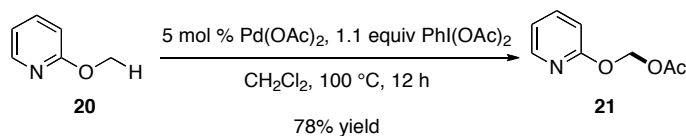
The scope of this Pd-catalyzed benzylic sp³ acetoxylation reaction was expanded to a number of other related substrates, including 5-methylquinoxaline, 8-ethylquinoline, and 6-bromo-8-ethylquinoline (Scheme 2.15). Interestingly, products **15** and **16** were formed by selective acetoxylation of secondary (versus primary) C–H bonds. This is presumably due to the preference to form 5-membered versus 6-membered palladacycles in cyclopalladation reactions. However, intriguingly, other secondary C–H bonds with adjacent cyano (**17**), chloro (**18**), or methoxy (**19**) groups did not undergo the desired Pd-catalyzed acetoxylation reaction under our standard conditions. Stoichiometric cyclopalladation also did not occur with these substrates, suggesting that catalytic turnover is limited by a slow C–H activation step in these systems.

Scheme 2.15 Substrate Scope for Pd-Catalyzed Acetoxylation of Benzylic C–H Bonds.



Next, we wanted to expand the substrate scope of these reactions to the oxidative functionalization of non-benzylic sp³ C–H bonds.⁴ We noted that adjacent heteroatoms are known to activate C–H bonds towards stoichiometric cyclometallation reactions. Gratifyingly, 2-methoxypyridine (**20**) underwent successful ligand-directed acetoxylation using 5 mol % of Pd(OAc)₂ and 1.1 equiv of PhI(OAc)₂ in CH₂Cl₂ at 100 °C, to afford the mixed acetal product **21** in 78% yield (Scheme 2.16).

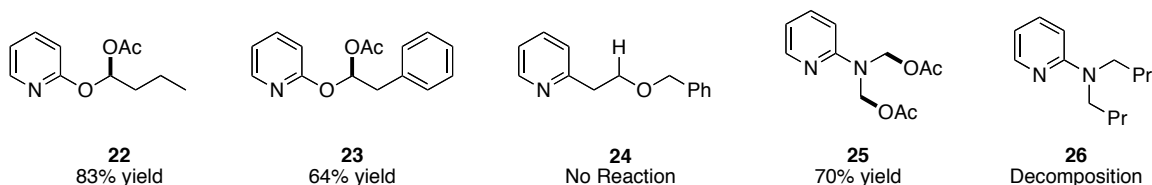
Scheme 2.16 Pd-Catalyzed Acetoxylation of 2-Methoxypyridine.



Other heteroatom-activated substrates were also reactive towards Pd-catalyzed C–H acetoxylation under the same reaction conditions (Scheme 2.17). Interestingly, the secondary C–H bonds of 2-butoxy- and 2-phenethoxy-pyridine both underwent acetoxylation to afford **22** and **23** in good yields (83% and 64%). However, 2-(2-phenoxyethyl)-pyridine (**24**), where the oxygen is not adjacent to the pyridine-directing group, did not react under a variety of reaction conditions. This result suggested that the role of the oxygen is not simply to activate the sp³ C–H bond towards cyclometallation. Instead, the oxygen substituent appears to enhance the reactivity of the pyridine-directing group. One possible explanation is that a more electron rich pyridine serves as a better ligand for the Pd catalyst, thereby increasing the concentration of the coordinated complex and thus the likelihood for the substrate to undergo C–H activation.

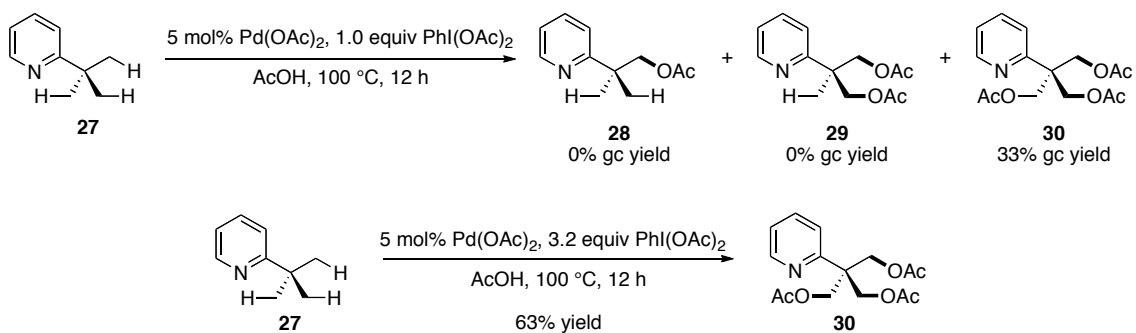
Interestingly, although 2-dimethylaminopyridine underwent the acetoxylation reaction to afford the functionalized product **25** in good 70% isolated yield, 2-dibutylaminopyridine (**26**) was a poor substrate for this transformation. Under our standard reaction conditions, **26** appeared to undergo decomposition to a mixture of unidentified products. In this case, we hypothesize that the background reaction between the highly electron-rich pyridine ring and the oxidant is faster than Pd-catalyzed C–H activation of a secondary C–H bond.

Scheme 2.17 Heteroatom Activated Substrates for the Pd-Catalyzed Acetoxylation Reaction.

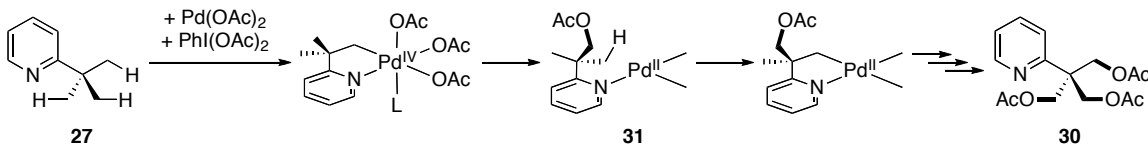


Finally, we wanted to expand the Pd-catalyzed acetoxylation reaction to unactivated C–H bonds that are not adjacent to either a phenyl ring or a heteroatom. When 2-*t*-butylpyridine (**27**) was subjected to 1 equiv of PhI(OAc)₂ and 5 mol % Pd(OAc)₂ in AcOH at 100 °C, 33% of the triacetoxylated product (**30**) was formed. In this case, the remainder of the organic material was the starting material (**27**) (66%), and neither the mono- (**28**) nor the di-acetoxylated (**29**) product were observed (Scheme 2.18). The reaction could be driven to completion by using 3.2 equiv of PhI(OAc)₂, and under these conditions, the triacetoxylated product **30** was isolated in 63% yield. We hypothesize that the exclusive formation of **30** is due to the fact that intramolecular C–H activation of the mono-acetoxyated product is faster than ligand substitution at intermediate **31** (Scheme 2.19). In other words, after C–O bond-forming reductive elimination, there is a primary C–H bond in direct proximity to the Pd-catalyst, which can undergo rapid activation and subsequent acetoxylation.

Scheme 2.18 Pd-Catalyzed Acetoxylation of 2-*tert*-Butylpyridine.



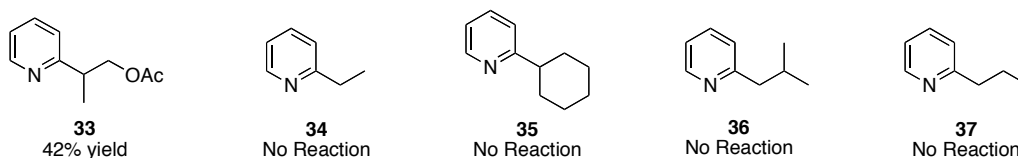
Scheme 2.19 Rationale for Formation of the Triacetoxyated Product.



Next, we sought to expand the Pd-catalyzed acetoxylation reaction to unactivated C–H bonds in other pyridine-based substrates. Interestingly, 2-*i*-propylpyridine (**32**) underwent the oxidative functionalization reaction to afford the mono-acetoxyated

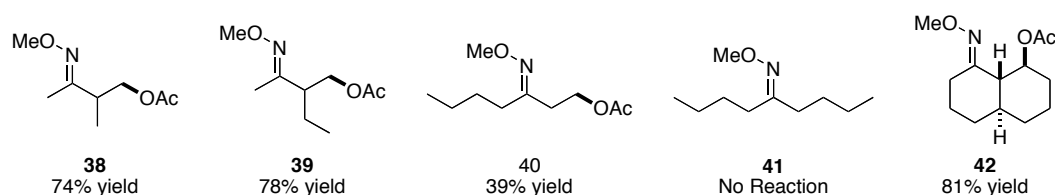
product (**33**) selectively in a moderate 42% isolated yield (Scheme 2.20). However, a variety of other substrates, including 2-ethyl- (**34**), 2-cyclohexyl- (**35**), 2-*i*-butyl- (**36**), and 2-propylpyridine (**37**), were unreactive under many different reaction conditions. We hypothesized that 2-ethylpyridine (**34**) was unreactive due to the lack of a Thorpe-Ingold effect of additional methyl groups present in 2-*i*-propylpyridine (**27**) and 2-*t*-butylpyridine (**32**).⁶ Such substitution changes the conformation of the chain, such that the terminal methyl is more likely to be proximal to the Pd catalyst. Cyclopalladation of the unactivated, secondary C–H bonds of **35** is likely to be slow due to the increased steric hindrance associated with a 2° versus a 1° carbon center, and we hypothesize that ligand exchange simply out-competes this process in this system.⁵ The activation of the less hindered 1° C–H bonds of **36** would require the formation of a six-membered palladacycle, which is known to be less favorable than the formation of analogous 5-membered palladacycles.¹¹ Finally, likely **37** suffers from both a lack of the Thorpe-Ingold effect and the requirement for formation of a less favorable 6-membered palladacycle to achieve 1° C–H bond activation.^{5, 11}

Scheme 2.20 Substrate Scope for the Pd-Catalyzed Acetoxylation Reaction of Unactivated C–H Bonds



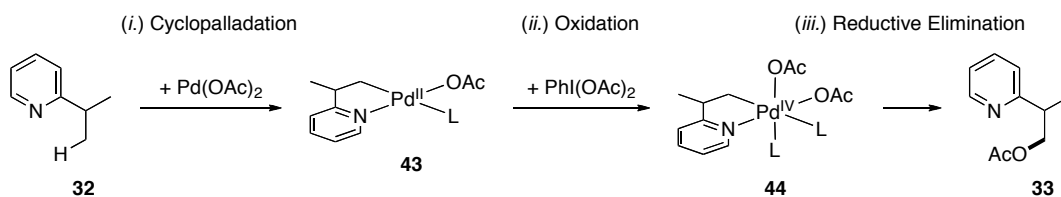
Concurrent with my efforts to functionalize unactivated sp^3 C–H bonds, Lopa Desai, a fellow graduate student in the Sanford Lab, developed the Pd-catalyzed acetoxylation of a series of related substrates containing oxime ether-based directing groups (Scheme 2.21).⁴ She demonstrated that a variety of unactivated 1° C–H bonds underwent efficient acetoxylation under similar reaction conditions using $\text{PhI}(\text{OAc})_2$ as the oxidant. She also demonstrated that a secondary sp^3 C–H bond of *trans*-decalone could undergo acetoxylation under these conditions. The observed reactivity of the 2° C–H bond of decalone (versus the lack of reactivity of **35**, **37**, and **41**) is likely due to the high rigidity of this system.

Scheme 2.21 Pd-Catalyzed Acetoxylation of Oxime Ethers.



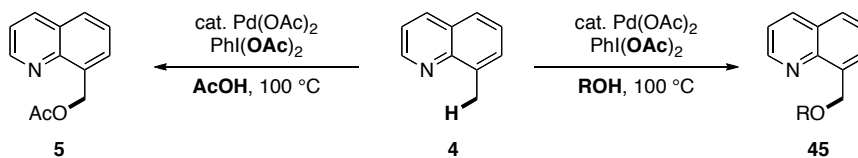
The proposed mechanism for all of these Pd-catalyzed sp^3 C–H bond acetoxylation reactions is exemplified in Scheme 2.22 using 2-*i*-propyl pyridine as the substrate. This mechanism involves (i) cyclopalladation of the sp^3 C–H bond, then (ii) oxidation of **43** to the Pd^{IV} intermediate **44** with $PhI(OAc)_2$, and finally, (iii) reductive elimination to form the new C–OAc bond of **33** and regenerate the catalyst.

Scheme 2.22 Proposed Mechanism for the Pd-Catalyzed Acetoxylation Reaction.



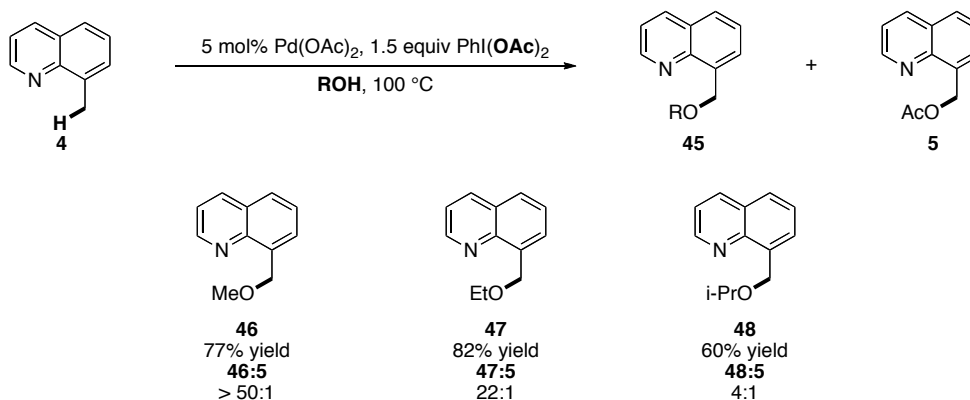
Generally, when the Pd-catalyzed acetoxylation reactions were run in AcOH or CH_2Cl_2 , a C–H bond was oxidatively functionalized to generate a C–OAc bond. Interestingly, in the functionalization of 8-methylquinoline (**4**), we found that when the solvent was changed from acetic acid to an alcohol, ether products (**45**) could be obtained (Scheme 2.23).³ Importantly, the acetoxyated product **5** was stable under the etherification reaction conditions; therefore, the ethers were not simply forming through an S_N2 reaction between **5** and the solvent (ROH). Instead, these results suggested that the C–OR bond was formed through reductive elimination from a Pd^{IV} intermediate.

Scheme 2.23 Palladium-Catalyzed Oxidative Functionalization: Acetoxylation vs. Etherification



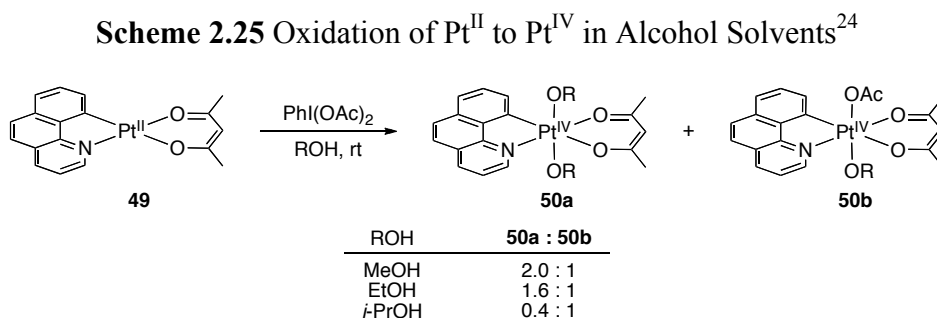
With the assistance of Waseem Anani, an undergraduate researcher in the Sanford Lab, we demonstrated that methyl (**46**), ethyl (**47**), and *i*-propyl (**48**) ethers could all be formed in the Pd-catalyzed etherification reaction when run in methanol, ethanol, and *i*-propanol, respectively (Scheme 2.24).²⁴ In the case of MeOH, only the methyl ether product (**46**) was observed; however, as the size of the alkoxy group increased, there was a concomitant increase in formation of acetoxyated side product **5**. Further, the ratio of ether to ester decreased from 22 : 1 to 4 : 1 upon moving from EtOH to *i*-PrOH. This result suggests that the etherification and acetoxylation reactions are competing pathways and that increasing the size of the alcohol slows etherification relative to acetoxylation.

Scheme 2.24 Pd-Catalyzed Oxidative Etherification of C–H Bonds.

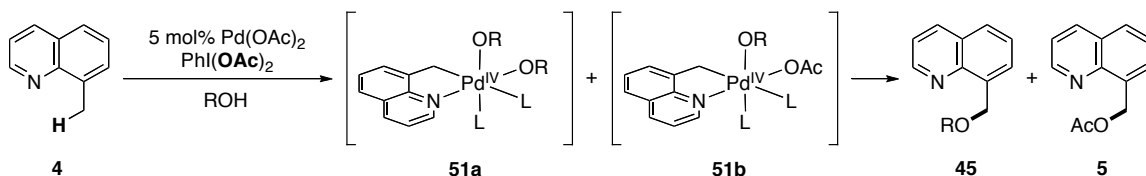


Allison Dick studied the oxidation of a Pt-model system for the proposed Pd^{IV} intermediate in alcohol solvents.²⁴ She found that oxidation of the Pt^{II} model complex **49** with PhI(OAc)_2 in ROH afforded both the bis-alkoxide Pt^{IV} product **50a** along with the mixed alkoxy/acetoxo Pt^{IV} complex **50b**. Interestingly, significantly more of the mixed complex **50b** was observed with the more sterically bulky alkoxide ligands OEt and O-*i*-

Pr (Scheme 2.25). If similar Pd^{IV} complexes (**51a** and **51b**) were formed in the catalytic reactions, then increased formation of the mixed alkoxy/acetoxo complex **51b** relative to **51a** in EtOH and *i*-PrOH would explain the higher yields of the acetoxyated product in these solvents (Scheme 2.26).



Scheme 2.26 Possible Pd^{IV} Intermediates in the Pd-Catalyzed Etherification Reaction.



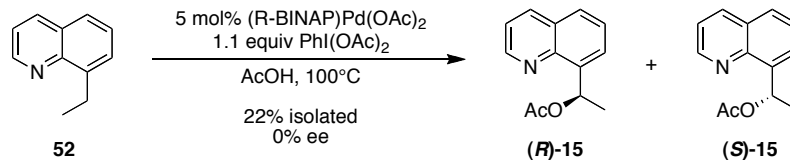
Unfortunately, the Pd-catalyzed etherification reactions were not found to be general for the oxidative functionalization of sp³ C–H bonds. Neither the heteroatom activated substrates **20** and **22-25** nor the unactivated substrates **27** and **32** afforded any C–H oxidation products when the reactions were run in alcohol solvents (as determined by GCMS). We believe that in these cases the oxidant may be decomposing prior the oxidative etherification reaction. These reactions presumably generate PhI(OR)₂ *in situ*, and this species is known to be quite unstable.²⁵ Since cyclopalladation is relatively slow for the less activated C–H bonds, oxidant decomposition at the elevated temperatures of this transformation is likely to be competitive.

3.3 Developing Reaction Conditions for Asymmetric Catalysis

We have demonstrated that activated secondary C–H bonds can undergo efficient Pd-catalyzed acetoxylation. As such, we were next interested in developing conditions

for asymmetric catalysis in these systems. Our initial attempt to achieve Pd-catalyzed asymmetric C–H acetoxylation involved the addition of (*R*)-BINAP as a chiral ligand to our standard reaction conditions: 8-ethylquinoline (150 mg, 0.94 mmol, 1 equiv), ((*R*)-BINAP)Pd(OAc)₂ (41 mg, 0.05 mmol, 5 mol %), PhI(OAc)₂ (341 mg, mmol, 1.1 equiv), in AcOH (8 mL) at 100 °C for 12 hours. This transformation proceeded in 22% isolated yield, indicating that the (*R*)-BINAP did not completely shut down catalysis; however, optical rotation and chiral HPLC analysis showed that the product was formed in 0% ee (Scheme 2.27).

Scheme 2.27 Initial Attempt Towards the Pd-Catalyzed Asymmetric Acetoxylation Reaction.

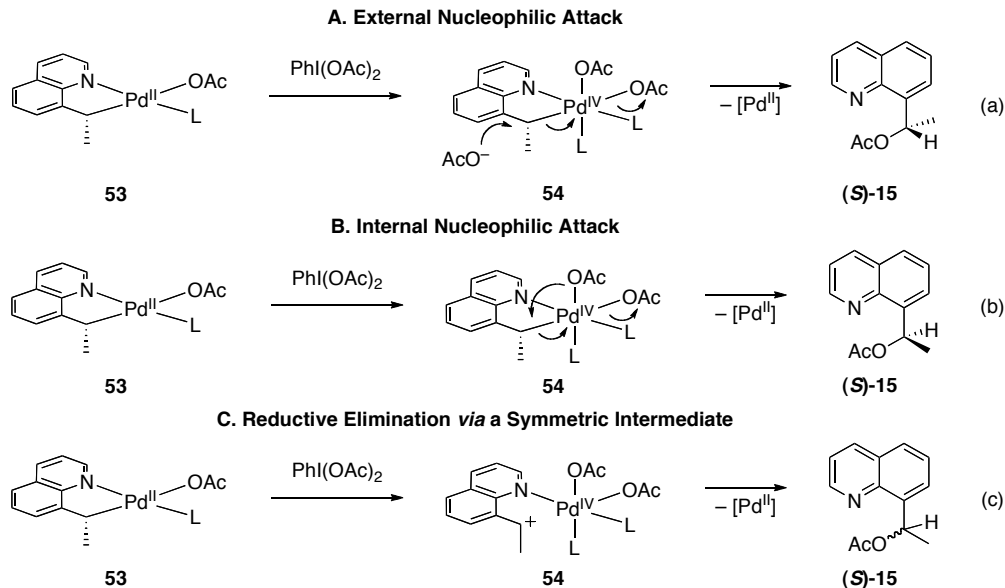


It is important to note that the product **15** does not racemize under the reaction conditions. For example, when a pure enantiomer of **15** was heated in AcOH at 100 °C with Pd(OAc)₂ and PhI(OAc)₂ for 12 h, there was no change in the % *ee* of this compound (as determined by chiral HPLC analysis). As such, there are at least two possible explanations for the formation of racemic product in this system: (1) there was no asymmetric induction in the C–H activation step or (2) the non-racemic stereogenic center that formed upon C–H activation center underwent racemization during the reductive elimination step of the catalytic cycle. If the poor results were due to an absence of asymmetric induction, then a screen of chiral ligands might be an effective means to develop a selective asymmetric catalyst. However, if, instead, the stereocenter racemized upon reductive elimination, then all chiral ligands would be expected to provide similar poor results. Therefore, we felt that it was critical to develop reaction conditions that maintained the integrity of the newly created stereocenter before pursuing asymmetric catalysis any further.

There are three possible mechanisms for C–O bond-forming reductive elimination from Pd^{IV} intermediate **54** (Scheme 2.28). Mechanism A involves nucleophilic attack of

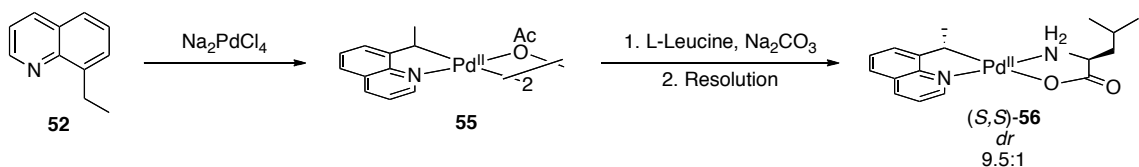
an external acetate onto the Pd–C bond, which would lead to overall inversion of stereochemistry. The second possible pathway, mechanism B, entails internal nucleophilic attack by acetate, which would afford the C–OAc bond with overall retention of stereochemistry. The final possibility, mechanism C, involves formation of a symmetrical carbocation intermediate, followed by trapping with acetate. This would result in loss of the stereochemical information and therefore result in a racemic product. However, it is important to note that formation of a racemic product would not necessarily imply that mechanism C is occurring, as a racemic product would also form if both mechanism A and mechanism B were taking place competitively.

Scheme 2.28 Three Possible Mechanisms for the Reductive Elimination from **54**.



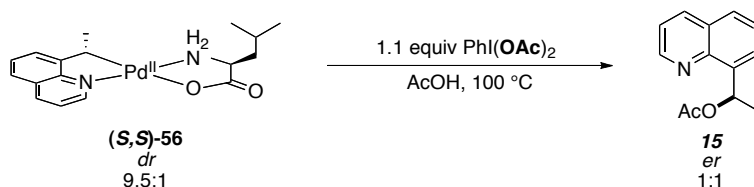
Based on these considerations, we sought to examine C–O bond-formation with $\text{PhI}(\text{OAc})_2$ at a stereochemically enriched cyclopalladated complex. Importantly, Pfeffer has demonstrated that 8-ethylquinoline palladacycles can be resolved using L-leucine as a chiral auxiliary through rapid recrystallization of the mixture of diastereomers (Scheme 2.29).²⁶ The less soluble component of this mixture was shown by X-ray crystallography to be the (*S,S*)-diastereomer (*S,S*)-**56**. Furthermore, the diastereomeric ratio of these mixtures can readily be assayed by ^1H NMR spectroscopy in CDCl_3 .

Scheme 2.29 Resolution of the Two Diastereomeric 8-Ethylquinoline Palladacycles.



Palladacycle **56** was resolved to a 9.5 : 1 mixture of diastereomers using the literature procedure.²⁶ When this complex was subjected to the oxidation conditions employed in our catalytic reactions (1.1 equiv of $\text{PhI}(\text{OAc})_2$ in AcOH at 100 °C), all of the stereochemical information was lost, and the acetoxyated organic product was obtained in 0% ee (Scheme 2.30). Importantly, the product was analyzed via chiral HPLC on a Chiral-Cel AS column, and an eluent ratio of 90% hexanes/10% *i*-PrOH afforded baseline separation of the two enantiomers.

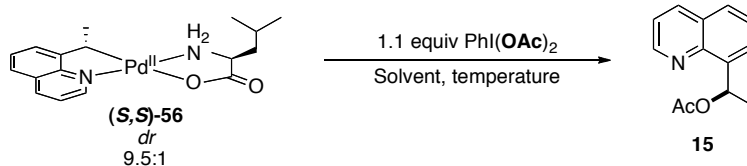
Scheme 2.30 Oxidation of the Resolved Palladacycle Under the Catalytic Conditions.



Since racemization occurred under our standard catalytic reaction conditions, we next sought to develop oxidation conditions that would minimize the loss of the chiral information during the oxidation and reductive elimination steps. A screen of solvents and temperature revealed that the use of polar solvents (*e.g.*, AcOH and CH_2Cl_2) tended to result in racemization of the stereocenter, while the use of more non-polar solvents (*e.g.*, toluene and dioxane) did not (Table 2.1). Lower temperatures also minimized the racemization in CH_2Cl_2 . Notably, when the reaction was carried in toluene, minimal loss of stereochemistry was observed at room temperature or at 100 °C (the temperature typically required to promote catalytic sp^3 C–H functionalization). The major implication of these results is that the development of Pd-catalyzed asymmetric acetoxylation reactions should be performed in toluene or dioxane. Importantly, the Pd-catalyzed

acetoxylation reaction affords similar yields of the functionalized product when run in aromatic solvents versus in AcOH.

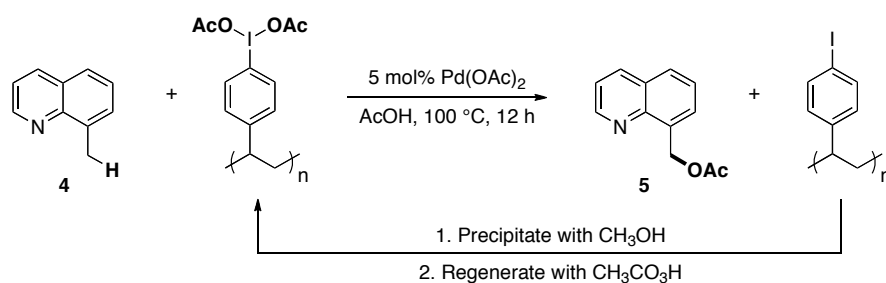
Table 2.1 Developing Conditions which Minimize Racemization



Entry	Solvent	Temperature	% de Complex	% ee Product
1	AcOH	Rt	80%	17%
2	CH ₂ Cl ₂	Rt	80%	41%
3	Benzene	Rt	80%	73%
4	Toluene	Rt	80%	71%
5	Dioxane	Rt	80%	75%
6	Toluene	100 °C	80%	70%

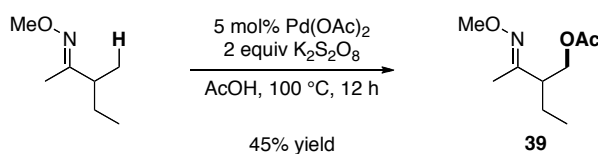
3.4 Subsequent Examples

After our pioneering work on the regio- and chemoselective Pd-catalyzed acetoxylation of C–H bonds, there have been a number of other examples of sp³ C–H bond oxygenation reactions that are believed to proceed through Pd^{II}/Pd^{IV} catalytic cycles. One of the main concerns within the Sanford laboratory is to develop greener reagents to promote our reactions. In the acetoxylation reactions that we developed, for every new C–OAc bond formed, an equivalent of iodobenzene is also released. To alleviate this concern, Dr. Eric Kalberer and Salena Whitfield developed a polymer-immobilized oxidant for the Pd-catalyzed acetoxylation of both sp³ and sp² C–H bonds.²⁷ They found that poly-4-(diacetoxyiodo)styrene (PS–I(OAc)₂) was an effective oxidant for the acetoxylation of 8-methylquinoline. Additionally, this oxidant could be recycled through five iterations with no significant loss in activity. They were able to achieve comparable yields with the PS–I(OAc)₂ (versus PhI(OAc)₂) for acetoxylation of a variety of sp³ C–H bonds.

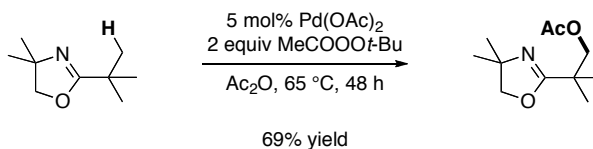
Table 2.2 Acetoxylation of 8-Methylquinoline with Recyclable Oxidant PS-I(OAc)₂²⁷

Trial	Yield 5	Yield PS-I(OAc) ₂
1	72%	85%
2	77%	81%
3	82%	84%
4	76%	81%
5	75%	86%

Two groups have also developed conditions for the acetoxylation of sp³ C–H bonds using peroxide-based oxidants in place of PhI(OAc)₂. Lopa Desai demonstrated that Oxone[®] and K₂S₂O₈ are effective oxidants for the Pd-catalyzed acetoxylation of sp² and sp³ C–H bonds (Scheme 2.31).²⁸ The AcOH solvent served as the source of acetate in the products, and when the solvent was switched to MeOH, the corresponding ether could also be formed in good yield. However, interestingly, pyridines were not effective directing groups for these reactions, as they were oxidized to the *N*-oxide by the peroxide or underwent oxidative dimerization (see Chapter 4 of this thesis for more details on this reaction). Yu reported that under similar conditions (using MeCOOO*t*-Bu as the oxidant and Ac₂O as the solvent) sp³ C–H bonds proximal to oxazoline directing groups could be efficiently acetoxyated (Scheme 2.32).²⁹

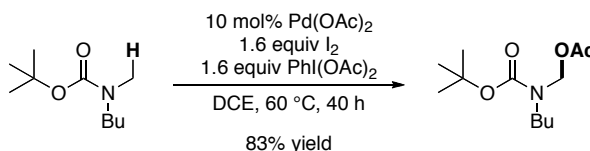
Scheme 2.31 Acetoxylation of an sp³ C–H Bond with K₂S₂O₈²⁸

Scheme 2.32 Acetoxylation of an sp^3 Bond with $\text{MeCOOO}t\text{-Bu}$ as the Oxidant²⁹



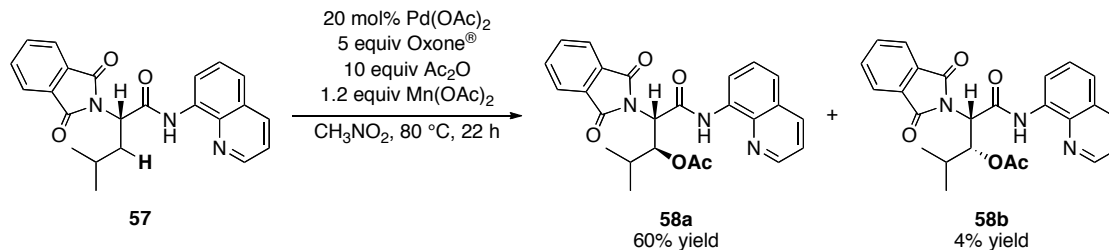
Yu has also demonstrated that Boc-protected *N*-methyl amines can undergo C–H acetoxylation using a combination of I_2 and $\text{PhI}(\text{OAc})_2$ (Scheme 2.33).³⁰ He proposes that IOAc is generated *in situ* and acts as the terminal oxidant in this system. This hypothesis is based on the fact that the use of $\text{PhI}(\text{OAc})_2$ or peroxide-based oxidants did not afford any of the desired acetoxyated product in this system. Importantly, similar to the chemistry described above, primary C–H bonds were selectively functionalized over secondary C–H bonds in this system.

Scheme 2.33 Pd-Catalyzed Acetoxylation of Boc Protected *N*-Methyl Amines.³⁰



Corey demonstrated the first example of the selective C–H acetoxylation of an unactivated secondary C–H bond of leucine derivative **57** (Scheme 2.34).³¹ In this system, Oxone[®] was used as the oxidant in conjunction with $\text{Mn}(\text{OAc})_2$. Interestingly, no products arising from C–H activation were observed in the absence of the manganese additive. The authors propose that the $\text{Mn}(\text{OAc})_2$ is being oxidized to $\text{Mn}_3\text{O}(\text{OAc})_7$ by the Oxone[®] and that this Lewis acid serves to increase the electrophilicity of the Pd-catalyst and promote 2° C–H bond activation. By using a chelating directing group, the secondary C–H bond of the leucine derivative was selectively acetoxyated to afford the major diastereomer **58a** in 60% yield.

Scheme 2.34 Pd-Catalyzed Acetoxylation of Secondary C–H Bonds.³¹



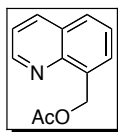
Pd-catalyzed oxidative functionalization for the formation of C–O bonds is a powerful new tool for organic synthesis. This approach allows for a single C–H bond to be both regio- and chemoselectively oxidized into a C–O bond. Importantly, only the C–H bond proximal to the directing group is functionalized, and no over-oxidation products are observed. We and others have demonstrated the applicability of this method to a wide variety of substrates containing directing groups including quinolines, pyridines, oxime ethers, oxazolines, carbamates, and amines. This general approach, using a Pd^{II}/Pd^{IV} catalytic cycle for the oxidative functionalization of sp³ C–H bonds has now been applied to the formation of sp³ C–C, C–Cl, and C–F bonds.^{32–34} Finally, as this methodology is still in the early stages of development, we expect the scope, application, and synthetic utility to continue to expand.

3.5 Conclusions

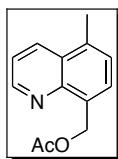
In conclusion, we have developed the first method for the Pd-catalyzed acetoxylation of sp³ C–H bonds.^{3,4} Quinoline and pyridine derivatives were shown to be effective directing groups for this reaction, and they promoted C–H activation at proximal C–H bonds in a variety of different molecules. PhI(OAc)₂ was effective at oxidizing the Pd^{II} to Pd^{IV}, while the subsequent reductive elimination afforded a new sp³ C–OAc bond. Additionally, we have demonstrated that changing the solvent from acetic acid to an alcohol afforded ethereal products rather than esters. Finally, we have developed conditions that prevent racemization upon reductive elimination. This advance should allow the screening of ligands towards the development of an asymmetric variant of this reaction.

Future work on this methodology should focus on developing general conditions for the C–H activation of secondary C–H bonds. This may be achieved by utilizing chelating ligands, Lewis acid promoters (such as $\text{Mn}(\text{OAc})_2$), and/or by rigorously screening additional solvents to expand this methodology. Additionally, crystallizing the intermediates formed upon C–H activation of secondary C–H bonds should allow for chiral ligands to be designed to maximize the interactions between the catalyst and the substrate. Ideally, this approach to ligand design will accelerate the identification of a catalyst that promotes highly enantioselective C–H activation/oxidative functionalization reactions.

3.6 Experimental Procedure

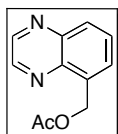
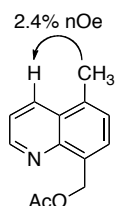


8-Methylquinoline (**4**) (162 μL , 1.4 mmol), $\text{PhI}(\text{OAc})_2$ (433.3 mg, 1.3 mmol), and $\text{Pd}(\text{OAc})_2$ (2.66 mg, 0.012 mmol) were combined in AcOH (10 mL) in a 20 mL vial. The vial was sealed with a Teflon lined cap, and the reaction mixture was heated at 100 $^\circ\text{C}$ for 22 hr. The solvent was removed under vacuum, and the resulting oil was purified by chromatography on silica gel ($R_f = 0.2$ in 80% hexanes/20% ethyl acetate). The product (**5**) was obtained as a white solid (211 mg, 88% yield). ^1H NMR (CDCl_3): δ 8.93 (dd, $J = 4.4$ Hz, 2.0 Hz, 1H), 8.14 (dd, $J = 8.4$ Hz, 2 Hz, 1H), 7.75 (m, 2H), 7.55 (dd, $J = 8.2$ Hz, 7.4 Hz, 1H), 7.44 (dd, $J = 8.6$ Hz, 4.2 Hz, 1H), 5.86 (s, 2H), 2.16 (s, 3H). ^{13}C NMR (CDCl_3): δ 171.12, 150.02, 146.24, 136.34, 134.31, 128.88, 128.25, 126.31, 121.41, 62.88, 21.26. Anal. Calcd for $\text{C}_{12}\text{H}_{11}\text{NO}_2$: C, 71.63, H, 5.51, N, 6.96; Found: C, 71.79, H, 5.91, N, 6.65.



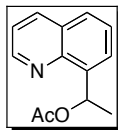
5,8-Dimethyl-quinoline (**11**) (186 mg, 1.186 mmol), $\text{PhI}(\text{OAc})_2$ (419 mg, 1.3 mmol), $\text{Pd}(\text{OAc})_2$ (10.6 mg, 0.047 mmol) were combined in $\text{CH}_3\text{CO}_2\text{H}$ (10 mL) in a 20 mL vial. The vial was sealed with a Teflon lined cap, and the reaction mixture was heated at 100 °C for 20 hr. The solvent was removed under vacuum, and the resulting oil was purified by chromatography on silica gel ($R_f = 0.05$ in 90% hexanes/10% ethyl acetate). The product (**12**) was obtained as a white solid (231 mg, 80% yield). ^1H NMR (CDCl_3): δ 8.95 (dd, $J = 4.2$ Hz, 1.4 Hz, 1H), 8.32 (dd, $J = 8.4$ Hz, 2 Hz, 1H), 7.65 (d, $J = 6.8$ Hz, 1H), 7.45 (dd, $J = 8.4$ Hz, 4.0 Hz, 1H), 7.36 (d, $J = 6.8$ Hz, 1H), 5.81 (s, 2H), 2.57 (s, 3H), 2.13 (s, 3H). ^{13}C NMR (CDCl_3): δ 171.27, 149.62, 146.63, 135.28, 133.79, 132.37, 128.98, 127.73, 126.76, 121.04, 63.13, 21.37, 18.84. Anal. Calcd for $\text{C}_{13}\text{H}_{13}\text{NO}_2$: C, 72.54, H, 6.09, N, 6.51; Found: C, 72.34, H, 6.40, N, 6.40.

nOe confirmation of regiochemistry of oxidation:

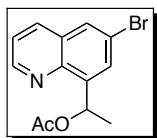


5-Methylquinoxaline (105 μL , 1.2 mmol, 1 equiv), $\text{PhI}(\text{OAc})_2$ (420 mg, 1.3 mmol, 1.1 equiv), and $\text{Pd}(\text{OAc})_2$ (5.3 mg, 0.02 mmol, 0.02 equiv) were combined in AcOH (10 mL) in a 20 mL vial. The vial was sealed with a Teflon lined cap, and the reaction was heated at 100 °C for 17 h. The reaction mixture was diluted with CH_2Cl_2 and extracted with water (3 x 50 mL) and brine (1 x 50 mL). The organic layer was dried over MgSO_4 , filtered, and concentrated. The resulting oil was purified by chromatography on silica gel ($R_f = 0.18$ in 80% hexanes/20% ethyl acetate). The product (**14**) was obtained as a yellow solid (158 mg, 65% yield). mp = 86-88 °C. ^1H NMR (399.96 Hz) (CDCl_3): δ 8.87 (s, 2H), 8.09 (d, $J = 8.3$ Hz, 1H), 7.84-7.75 (multiple peaks, 2H), 5.80 (s, 2H), 2.10 (s, 3H). ^{13}C NMR (100.57 Hz) (CDCl_3): δ 170.85, 145.03, 144.32, 142.83, 141.12, 134.71, 129.71,

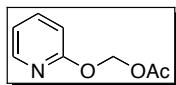
129.70, 129.40, 61.85, 21.03. IR (KBr): 2927, 1739 cm⁻¹. HRMS electrospray (m/z): [M + Na] calcd for C₁₁H₁₀N₂O₂, 202.0742; found, 202.0738.



8-Ethylquinoline (187 mg, 1.2 mmol, 1 equiv), PhI(OAc)₂ (419 mg, 1.3 mmol, 1.1 equiv), and Pd(OAc)₂ (2.7 mg, 0.03 mmol, 0.01 equiv) were combined in AcOH (10 mL) in a 20 mL vial. The vial was sealed with a Teflon lined cap, and the reaction was heated at 100 °C for 17 h. The reaction mixture was diluted with CH₂Cl₂ and extracted with water (3 x 50 mL) and brine (1 x 50 mL). The organic layer was dried over MgSO₄, filtered, and concentrated. The resulting oil was purified by chromatography on silica gel (R_f = 0.18 in 80% hexanes/20% ethyl acetate). The product (**15**) was obtained as a yellow solid (206 mg, 79% yield).

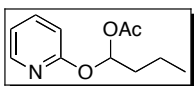


6-Bromo-8-ethylquinoline (142 mg, 0.6 mmol, 1 equiv), PhI(OAc)₂ (213 mg, 0.66 mmol, 1.1 equiv), and Pd(OAc)₂ (6.7 mg, 0.03 mmol, 0.05 equiv) were combined in AcOH (10 mL) in a 20 mL vial. The vial was sealed with a Teflon lined cap, and the reaction was heated at 100 °C for 17 h. The reaction mixture was diluted with CH₂Cl₂ and extracted with water (3 x 50 mL) and brine (1 x 50 mL). The organic layer was dried over MgSO₄, filtered, and concentrated. The resulting oil was purified by chromatography on silica gel (R_f = 0.18 in 80% hexanes/20% ethyl acetate). The product (**16**) was obtained as a yellow solid (113 mg, 64% yield).

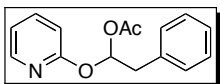


2-Methoxypyridine (**20**) (173 μL, 1.8 mmol, 1 equiv), PhI(OAc)₂ (638 mg, 1.98 mmol, 1.1 equiv), and Pd(OAc)₂ (21 mg, 0.09 mmol, 0.05 equiv) were combined in CH₂Cl₂ (15 mL) in a 20 mL vial. The vial was sealed with a Teflon lined cap, and the mixture was

stirred at 100 °C for 12 h. The reaction was concentrated under vacuum and the resulting brown oil was dissolved in ethyl acetate (250 mL) and pyridine (1 mL) and filtered through a plug of silica gel. The resulting solution was concentrated and dried under vacuum. The remaining brown solid was washed and sonicated with hexanes (5 x 10 mL), and the hexanes washes were combined, concentrated, and dried under vacuum. The product **21** was obtained as a yellow oil (201 mg, 66% yield). ¹H NMR (CDCl₃): δ 8.21 (ddd, J = 5.0, 1.9, 0.8 Hz, 1H) 7.63 (ddd, J = 8.3, 7.1, 1.9 Hz, 1H), 6.98 (ddd, 7.1, 5.0, 0.9 Hz, 1H), 6.83 (ddd, 8.2, 0.9, 0.8 Hz, 1H), 6.11 (s, 2H), 2.12 (s, 3H). ¹³C NMR: δ 170.24, 161.62, 146.84, 139.21, 118.37, 111.41, 81.36, 20.98. Anal. Calcd C₈H₉NO₃: C, 57.48, H, 5.43, N, 8.38; Found: C, 57.63, H, 5.53, N, 8.16.

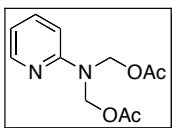


2-Butoxypyridine (92 μL, 1.2 mmol, 1 equiv), PhI(OAc)₂ (425 mg, 1.32 mmol, 1.1 equiv), and Pd(OAc)₂ (13 mg, 0.06 mmol, 0.05 equiv) were combined in CH₂Cl₂ (10 mL) in a 20 mL vial. The vial was sealed with a Teflon lined cap, and the reaction was stirred at 100 °C for 12 h. The reaction diluted with CH₂Cl₂ (40 mL), and this solution was washed with 10% pyridine in H₂O (3 x 50 mL) and saturated NaCl (1 x 50 mL), and was then dried with MgSO₄ and concentrated in vacuo. The resulting oil was sonicated and washed with pentane (5 x 5 mL), and the pentane washes were combined and dried under vacuum. The product **22** was obtained as a yellow oil (104 mg, 83% yield). ¹H NMR (CDCl₃): δ 8.16 (ddd, J = 4.9, 2.0, 0.7 Hz, 1H), 7.59 (ddd, J = 8.2, 7.1, 2.0 Hz, 1H), 7.18 (t, 5.6 Hz, 1H), 6.92 (ddd, J = 7.1, 4.9, 0.9 Hz, 1H), 6.75 (ddd, J = 8.4, 0.91, 0.73 Hz), 2.03 (s, 3H), 1.89 (m, 2H), 1.49 (m, 2H), 0.96 (t, 7.4 Hz, 3H). ¹³C NMR: δ 169.72, 161.83, 147.10, 138.93, 117.96, 111.11, 92.42, 35.86, 21.09, 17.06, 13.82. Anal. Calcd C₁₁H₁₅NO₃: C, 63.14, H, 7.23, N, 6.69; Found: C, 63.01, H, 7.22, N, 6.30.

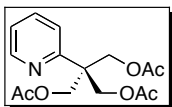


2-Phenethoxypyridine (120 mg, 0.6 mmol, 1 equiv), PhI(OAc)₂ (213 mg, 0.66 mmol, 1.1 equiv), and Pd(OAc)₂ (7 mg, 0.03 mmol, 0.05 equiv) were combined in CH₂Cl₂ (10 mL)

in a 20 mL vial. The vial was sealed with a Teflon lined cap, and the reaction was stirred at 100 °C for 12 h. The reaction diluted with CH₂Cl₂ (40 mL), and this solution was washed with 10% pyridine in H₂O (3 x 50 mL) and saturated NaCl (1 x 50 mL), and was then dried with MgSO₄ and concentrated in vacuo. The resulting oil was sonicated and washed with pentane (5 x 5 mL), and the pentane washes were combined and dried under vacuum. The product **23** was obtained as a yellow oil (74 mg, 48% yield).

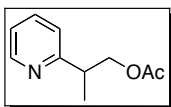


2-Dimethylaminopyridine (149 μL, 1.2 mmol, 1 equiv), PhI(OAc)₂ (811 mg, 2.52 mmol, 2.1 equiv), and Pd(OAc)₂ (13 mg, 0.06 mmol, 0.05 equiv) were combined in CH₂Cl₂ (10 mL) in a 20 mL vial. The vial was sealed with a Teflon lined cap, and the reaction was stirred at 100 °C for 12 h. The reaction diluted with CH₂Cl₂ (40 mL), and this solution was washed with 5% pyridine in H₂O (3 x 50 mL) and saturated NaCl (1 x 50 mL), and was then dried with MgSO₄ and concentrated in vacuo. The resulting oil was sonicated and washed with pentane (5 x 5 mL), and the pentane washes were combined and concentrated under vacuum. The product **25** was obtained as a yellow/brown oil (203 mg, 70% yield). ¹H NMR (CDCl₃): δ 8.29 (ddd, J = 4.8, 2.0, 1.1 Hz, 1H), 7.58 (ddd, J = 8.4, 7.3, 1.8 Hz, 1H), 6.87-6.84 (multiple peaks, 2H), 5.75 (s, 4H), 2.05 (s, 6H). ¹³C NMR: δ 171.23, 155.53, 148.12, 138.05, 116.43, 107.77, 74.17, 21.09. Anal. Calcd C₁₁H₁₄N₂O₄: C, 55.46, H, 5.92, N, 11.76; Found: C, 55.57, H, 6.15, N, 11.83.

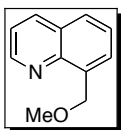


2-*tert*-Butylpyridine (**27**) (135 mg, 1.00 mmol, 1 equiv), PhI(OAc)₂ (1.03 g, 3.2 mmol, 3.2 equiv), and Pd(OAc)₂ (11 mg, 0.05 mmol, 0.05 equiv) were combined in AcOH (8 mL) in a 20 mL vial. The vial was sealed with a Teflon lined cap, and the reaction was stirred at 100 °C for 12 h. The reaction was concentrated, and the resulting oil was dissolved in CH₂Cl₂ (50 mL). This solution was washed with 5% pyridine in H₂O (3 x 50

mL) and saturated NaCl (1 x 50 mL), and then dried with MgSO₄ and concentrated in vacuo. The resulting oil was sonicated and washed with pentane (5 x 5 mL), and the pentane washes were combined and concentrated under vacuum. The product **30** was obtained as a pale yellow oil (198 mg, 63% yield). ¹H NMR (CDCl₃): δ 8.52 (ddd, J = 4.7, 1.8, 0.92 Hz, 1H), 7.62 (td, J = 7.7, 2.0 Hz, 1H), 7.23 (dd, 8.0, 0.92 Hz, 1H), 7.15 (ddd, J = 7.4, 4.8, 1.1 Hz, 1H), 4.50 (s, 6H), 1.93 (s, 9H). ¹³C NMR: δ 170.39, 157.89, 149.15, 136.11, 122.18, 121.27, 64.17, 47.76, 20.58. Anal. Calcd C₁₅H₁₉NO₆: C, 58.25, H, 6.19, N, 4.53; Found: C, 58.55, H, 6.48, N, 4.26.

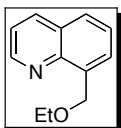


2-*iso*-Propylpyridine (**32**) (100 mg, 0.83 mmol, 1 equiv), PhI(OAc)₂ (399 mg, 1.24 mmol, 1.5 equiv), and Pd(OAc)₂ (9 mg, 0.04 mmol, 0.05 equiv) were combined in CH₂Cl₂ (8 mL) in a 20 mL vial. The vial was sealed with a Teflon lined cap, and the reaction was stirred at 100 °C for 12 h. The reaction was diluted with CH₂Cl₂ (40 mL), and this solution was washed with 5% pyridine in H₂O (3 x 50 mL) and saturated NaCl (1 x 50 mL) and was then dried with MgSO₄ and concentrated under vacuum. The resulting oil was chromatographed on silica gel with (R_f = 0.3 in 80% hexanes: 20% ethyl acetate). The product **33** was obtained as a yellow oil (68 mg, 42% yield). ¹H NMR (CDCl₃): δ 8.55 (ddd, J = 5.7, 1.7, 0.9 Hz, 1H), 7.61 (td, J = 7.6, 1.7 Hz, 1H), 7.17-7.12 (multiple peaks, 2H), 4.36 (dd, J = 10.6, 7.4 Hz, 1H), 4.27 (dd, J = 10.6, 7.6 Hz, 1H), 3.24 (m, 1H), 1.98 (s, 3H), 1.32 (d, J = 7.2 Hz, 3H). ¹³C NMR: δ 170.9, 162.38, 149.35, 136.35, 122.14, 121.67, 68.37, 40.96, 20.87, 17.11. Anal. Calcd C₁₀H₁₃NO₂: C, 67.02, H, 7.31, N, 7.82; Found: C, 66.86, H, 7.33, N, 6.92.

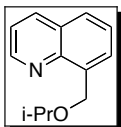


8-Methylquinoline (**4**) (162 μL, 1.2 mmol), PhI(OAc)₂ (419 mg, 1.3 mmol), and Pd(OAc)₂ (5.3 mg, 0.023 mmol) were combined in MeOH (10 mL) in a 20 mL vial. The vial was sealed with a Teflon lined cap, and the reaction mixture was heated at 100 °C for 18 h. The solvent was removed under vacuum, and the resulting oil was purified by chromatography on silica gel (R_f = 0.1 in 90% hexanes/10% ethyl acetate). The product

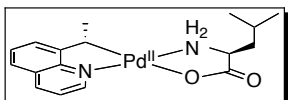
(**46**) was obtained as a yellow oil (167 mg, 80% yield). ^1H NMR (CDCl_3): δ 8.93 (dd, $J = 4.4$ Hz, 2.0 Hz, 1H), 8.15 (dd, $J = 8.2$ Hz, 1.8 Hz, 1H), 7.83 (dd, $J = 7.0$ Hz, 1.0 Hz, 1H), 7.75 (d, $J = 8$ Hz, 1H), 7.55 (t, $J = 7.8$ Hz, 1H), 7.41 (dd, $J = 8.2$ Hz, 4.2 Hz, 1H), 5.20 (s, 2H), 3.60 (s, 3H). ^{13}C NMR (CDCl_3): δ 149.66, 145.98, 136.43, 128.18, 127.62, 127.26, 126.49, 121.14, 70.87, 59.00. Anal. Calcd for $\text{C}_{11}\text{H}_{11}\text{NO}$: C, 76.28, H, 6.40, N, 8.09; Found: C, 76.30, H, 6.16, N, 8.10.



8-Methylquinoline (**4**) (61 μL , 1.2 mmol, 1 equiv), $\text{PhI}(\text{OAc})_2$ (501 mg, 2.5 mmol, 2.1 equiv), and $\text{Pd}(\text{OAc})_2$ (5 mg, 0.023 mmol, 0.05 equiv) were combined in EtOH (3.75 mL) in a 20 mL vial. The vial was sealed with a Teflon lined cap, and the reaction mixture was heated at 100 $^\circ\text{C}$ for 18 h. The solvent was removed under vacuum, and the resulting oil was purified by chromatography on silica gel ($R_f = 0.1$ in 90% hexanes/10% ethyl acetate). The product (**47**) was obtained as a yellow oil (68 mg, 82% yield).



8-Methylquinoline (**4**) (136 μL , 1.0 mmol, 1 equiv), $\text{PhI}(\text{OAc})_2$ (1127 mg, 3.5 mmol, 3.5 equiv), and $\text{Pd}(\text{OAc})_2$ (11.2 mg, 0.05 mmol, 0.05 equiv) were combined in *i*-PrOH (7.6 mL) in a 20 mL vial. The vial was sealed with a Teflon lined cap, and the reaction mixture was heated at 100 $^\circ\text{C}$ for 18 h. The solvent was removed under vacuum, and the resulting oil was purified by chromatography on silica gel ($R_f = 0.1$ in 90% hexanes/10% ethyl acetate). The product (**48**) was obtained as a yellow oil (105 mg, 60% yield).



Complex 56 was synthesized and resolved according to the procedure developed by Pfeffer.²⁶

Scheme 2.30: (*S,S*)-**56** (80% *de*) (75 mg, 0.19 mmol, 1 equiv) and $\text{PhI}(\text{OAc})_2$ (124 mg, 0.38 mmol, 2 equiv) were stirred in AcOH (2 mL) at 100 °C for 1 hour. The product **15** was isolated by column chromatography. When analyzed by chiral HPLC (Chiral Cel AS column, 10% *i*-PrOH in hexanes) the **15** had a 0% *ee*.

Table 2.2: (*S,S*)-**56** (12 mg, 0.03 mmol, 1 equiv) and $\text{PhI}(\text{OAc})_2$ (12 mg, 0.04 mmol, 1.1 equiv) were stirred in *Solvent* (1 mL) at X °C for 12 hour. The product **15** was isolated by column chromatography. When analyzed by chiral HPLC (Chiral Cel AS column, 10% *i*-PrOH in hexanes) to determine the % *ee*.

3.7 References

- (1) Stahl, S.; Labinger, J. A.; Bercaw, J. E. *Angew. Chem., Int. Ed* **1998**, *37*, 2181-2192.
- (2) Dick, A. R.; Sanford, M. S. *Tetrahedron* **2006**, *62*, 2439-2463.
- (3) Dick, A. R.; Hull, K. L.; Sanford, M. S. *J. Am. Chem. Soc.* **2004**, *126*, 2300-2301.
- (4) Desai, L. V.; Hull, K. L.; Sanford, M. S. *J. Am. Chem. Soc.* **2004**, *126*, 9542-9543.
- (5) Shilov, A. E.; Shul'pin, G. B. *Chem. Rev.* **1997**, *97*, 2879-2932.
- (6) Anslyn, E. V.; Dougherty, D. A. In *Modern Physical Organic Chemistry*; University Science Books: Sausalito, CA, 2006.
- (7) Kushch, L. A.; Lavrushko, V. V.; Misharin, Y. S.; Moravskii, A. P.; Shilov, A. E. *Nouv. J. Chim.* **1983**, *7*, 729-733.
- (8) Bhalla, G.; Mironov, O.; Jones, C. J.; Tenn, W. J., III; Nakamura, S.; Periana, R. A. In *Handbook of C-H Transformations* Dyker, G., ed. Wiley-VCH: Weinheim, 2005, 529.
- (9) Trend, R. M.; Ramtohl, Y. K.; Stoltz, B. M. *J. Am. Chem. Soc.* **2005**, *127*, 17778-17788.
- (10) Constable, A. G.; McDonald, W. S.; Sawkins, L. C.; Shaw, B. L. *J. Chem. Soc., Dalton Trans.* **1980**, 1992-2000.
- (11) Omae, I. *Coord. Chem. Rev.* **2004**, *248*, 995-1023.
- (12) Ryabov, A. D. *J. Organomet. Chem.* **1984**, *268*, 91-96.

- (13) Fuchita, Y.; Nakashima, M.; Hiraki, K.; Kawatani, M.; Ohnuma, K. *J. Chem. Soc., Dalton Trans.* **1988**, 785-789.
- (14) Cardenas, D. J.; Echavarren, A. M.; Vegas, A. *Organometallics* **1994**, *13*, 882-889.
- (15) Balavoine, G.; Clinet, J. C. *J. Organomet. Chem.* **1990**, *390*, C84-C88.
- (16) Baldwin, J. E.; Jones, R. H.; Najera, C.; Yus, M. *Tetrahedron* **1985**, *41*, 699-711.
- (17) Baldwin, J. E.; Najera, C.; Yus, M. *J. Chem. Soc., Chem. Commun.* **1985**, 126-127.
- (18) Carr, K.; Saxton, H. M.; Sutherland, J. K. *J. Chem. Soc. Perkin Trans. I* **1988**, 1599-1601.
- (19) Dangel, B. D.; Johnson, J. A.; Sames, D. *J. Am. Chem. Soc.* **2001**, *123*, 8149-8150.
- (20) Yoneyama, T.; Crabtree, R. H. *J. Mol. Catal. A* **1996**, *108*, 35-40.
- (21) Dick, A. R.; Kampf, J. W.; Sanford, M. S. *J. Am. Chem. Soc.* **2005**, *127*, 12790-12791.
- (22) Deeming, A. J.; Rothwell, I. P. *J. Organomet. Chem.* **1981**, *205*, 117-131.
- (23) Evans, P.; Hogg, P.; Grigg, R.; Nurnabi, M.; Hinsley, J.; Sridharan, V.; Suganthan, S.; Korn, S.; Collard, S.; Muir, J. E. *Tetrahedron* **2005**, *61*, 9696-9704.
- (24) Dick, A. R.; Kampf, J. W.; Sanford, M. S. *Organometallics* **2005**, *24*, 482-485.
- (25) Schardt, B. C.; Hill, C. L. *Inorg. Chem.* **1983**, *22*, 1563-1565.
- (26) Spencer, J.; Maassarani, F.; Pfeffer, M.; DeCian, A.; Fischer, J. *Tetrahedron: Asymmetry* **1994**, *5*, 321-324.
- (27) Kalberer, E. W.; Whitfield, S. R.; Sanford, M. S. *J. Mol. Catal. A* **2006**, *251*, 108-113.
- (28) Desai, L. V.; Malik, H. A.; Sanford, M. S. *Org. Lett.* **2006**, *8*, 1141-1144.
- (29) Giri, R.; Liang, J.; Lei, J.; Li, J.; Wang, D.; Chen, X.; Naggar, I. C.; Guo, C.; Foxman, B. M.; Yu, J. *Angew. Chem., Int. Ed.* **2005**, *44*, 7420-7424.
- (30) Wang, D.; Hao, X.; Wu, D.; Yu, J. *Org. Lett.* **2006**, *8*, 3387-3390.
- (31) Reddy, B. V. S.; Reddy, L. R.; Corey, E. J. *Org. Lett.* **2006**, *8*, 3391-3394.
- (32) Kalyani, D.; Dick, A. R.; Anani, W. Q.; Sanford, M. S. *Tetrahedron* **2006**, *62*, 11483-11498.
- (33) Hull, K. L.; Anani, W. Q.; Sanford, M. S. *J. Am. Chem. Soc.* **2006**, *128*, 7134-7135.

(34) Kalyani, D.; Deprez, N. R.; Desai, L. V.; Sanford, M. S. *J. Am. Chem. Soc.* **2005**, *127*, 7330-7331.

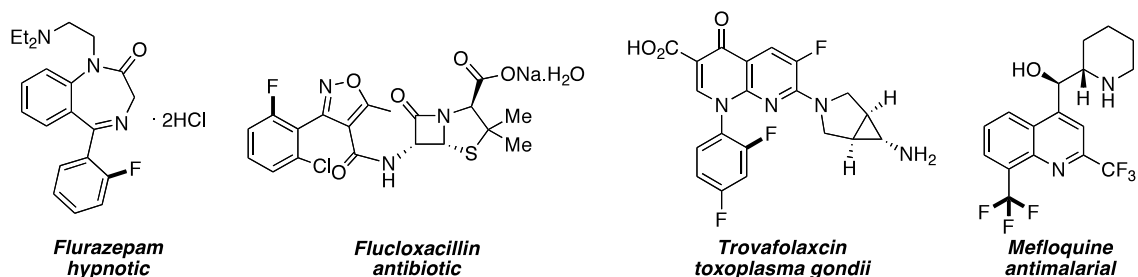
Chapter 3

Palladium-Catalyzed Oxidative Fluorination of C–H Bonds

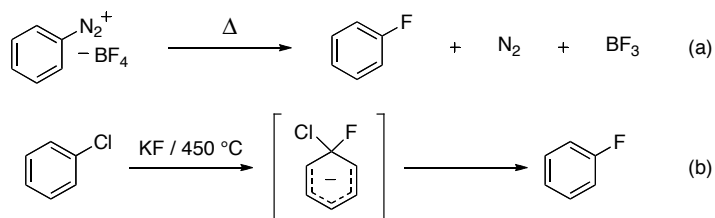
3.1 Background and Significance

The substitution of hydrogen for fluorine in organic molecules can have profound effects on their biological activity, metabolism, solubility, hydrophobicity, and bulk properties.^{1, 2} Therefore, molecules containing C–F bonds are important targets for pharmaceuticals, agrochemicals, imaging agents, fine chemicals, and organic materials. Indeed, a recent report has suggested that the probability of success of a drug candidate increases by almost ten-fold if it contains a C–F bond. Furthermore, approximately 20% of pharmaceuticals currently on the market contain C–F bonds.³ Despite their widespread utility, C–F bonds are often quite difficult to incorporate into organic molecules.^{4, 5} Relatively few synthetic methods have been developed for the construction of the C–F linkage, and most of the known methods require harsh conditions, such as the commonly used Balz-Schiemann reaction and the Halex process (Scheme 3.2).

Scheme 3.1 Examples of pharmaceuticals containing C–F bonds.

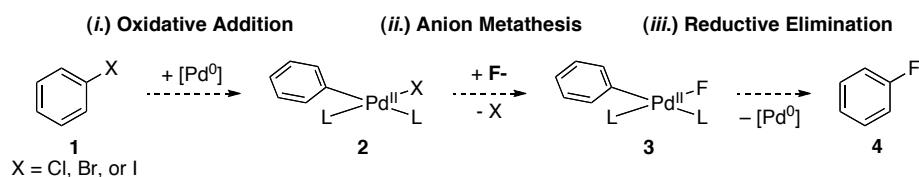


Scheme 3.2 Examples of (a) the Balz-Schiemann Reaction and (b) the Halex Process.



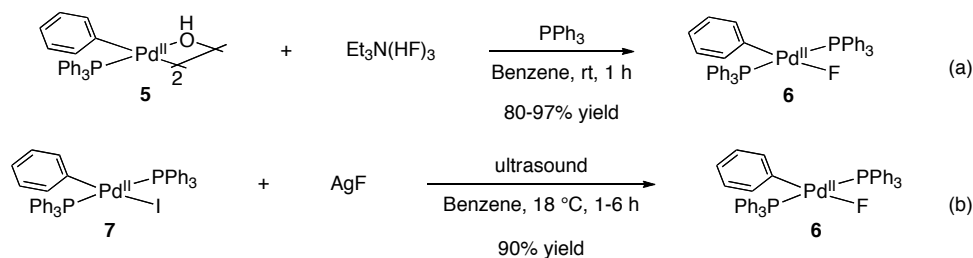
Palladium-catalyzed approaches for C–F bond formation would be extremely valuable, as they could be used for the installation of a C–F bond at a late stage in a multistep synthesis.⁶⁻⁸ Previous efforts towards developing Pd-catalyzed fluorination reactions have focused on the conversion of Ar–X (X = Cl, Br, I) to Ar–F via a Pd^{II}/Pd⁰ catalytic cycle.⁶ The proposed mechanism for such a transformation is shown in Scheme 3.3 and involves (i) oxidative addition of the Pd⁰ into the Ar–X bond of **1**, (ii) anion metathesis, exchanging X[–] for F[–] to form **3**, and (iii) C–F bond-forming reductive elimination to release the desired product **4**.

Scheme 3.3 Proposed Pd^{II}/Pd⁰ Catalytic Cycle for C–F Bond Formation⁶



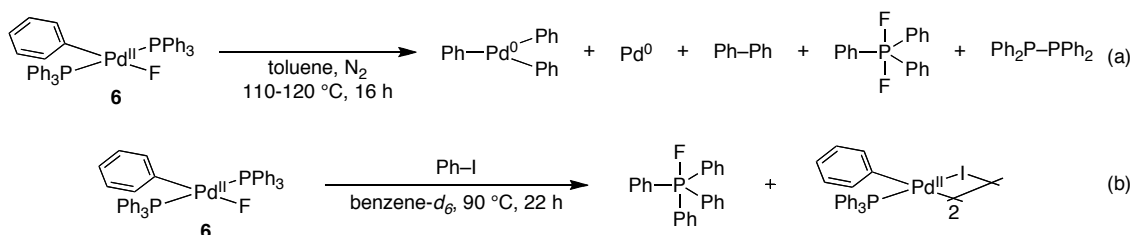
The first two steps of this proposed catalytic cycle have significant precedent in the literature.⁹ The oxidative addition of aryl halides at Pd⁰ is a well-known reaction in both stoichiometric and catalytic manifolds. There are relatively few examples of stable Pd^{II} fluoride complexes; however, Grushin has demonstrated that treatment of Pd^{II} hydroxide complex **5** with Et₃N•(HF)₃ or Pd^{II} iodide complex **7** with AgF successfully forms Pd^{II}–F adduct **6** (Scheme 3.4).¹⁰⁻¹⁴

Scheme 3.4 Synthesis of Pd^{II} Fluoride Complexes^{11, 12}



The key to completing the catalytic cycle shown in Scheme 3.3 involves developing conditions to promote Ar–F reductive elimination from Pd^{II}.^{6, 15, 16} The oxidative addition of Ar–F to Pd⁰ complexes is precedented; however, Grushin has suggested that the microscopic reverse of this reaction is thermodynamically allowed yet kinetically disfavored. Rather than Ar–F bond formation, complexes of general structure **6** are prone to competing P–F or P–C coupling processes to form a variety of side products (Scheme 3.5 a and b). Even when a bidentate phosphine was used to enforce a *cis*-relationship between the Pd–Ar and Pd–F bonds, only P–F bond formation was observed.

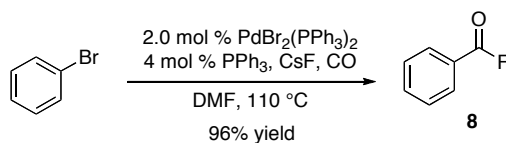
Scheme 3.5 Attempts to Reductively Eliminate Ar–F from Pd^{II}¹⁵



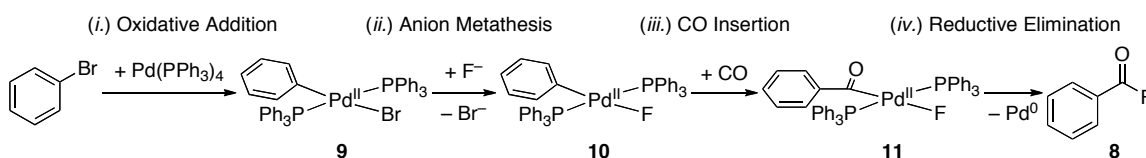
The only reported example of C–F bond-forming reductive elimination from Pd^{II} involves the formation of sp² C–F bonds of acyl fluorides. In 1992, Kiji demonstrated the Pd-catalyzed reaction between aryl bromides, CO, and CsF to afford acyl fluoride products (Scheme 3.6).¹⁷ This catalytic transformation is general to a wide variety of both electron rich and electron poor aryl bromides, and even benzyl bromide reacted to afford the corresponding acyl fluoride in 13% yield. Grushin later studied a stoichiometric version of this reaction and demonstrated that it proceeds by a mechanism involving (i) oxidative addition into the Ar–Br bond, (ii) anion metathesis to form the Pd–F bond of

10, (iii) CO insertion into the Pd–Ar bond to afford **11**, and lastly, (iv) C–F bond-forming reductive elimination to form the acid fluoride (**8**).¹¹

Scheme 3.6 Pd-Catalyzed Acyl Fluoride Formation¹⁷

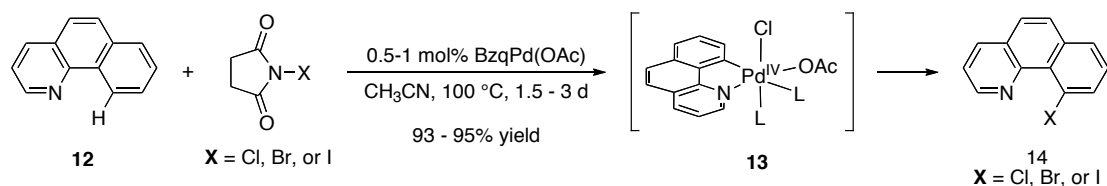


Scheme 3.7 Mechanism for the Pd-Mediated Acid Fluoride Formation¹¹



Carbon-halogen bond-forming reductive elimination is known to be slow at Pd^{II}.¹⁸ Additionally, it is often thermodynamically disfavored unless sterically bulky phosphine ligands are employed. C–F bond formation from Pd^{II} is proposed to be thermodynamically possible; however, reductive elimination to generate P–C or P–F bonds is kinetically favored over C–F coupling, with the exception of the formation of acyl fluorides.⁶ Previously, the Sanford lab had demonstrated that the Pd-catalyzed formation of carbon–halogen (halogen = Cl, Br, I) bonds was possible through a proposed Pd^{II}/Pd^{IV} catalytic cycle (Scheme 3.8).^{19–21} When [Pd^{II}–Ar] intermediates reacted with electrophilic halogenating reagents, such as *N*-halosuccinimides, [X–Pd^{IV}–Ar] (similar to **13**) intermediates were accessed (X = Cl, Br, I). C–X bond-forming reductive elimination from this highly unstable intermediate is then highly thermodynamically favorable and kinetically rapid, even in the absence of sterically bulky ancillary ligands. Based on this precedent, we hypothesized that a similar strategy, using appropriate electrophilic fluorine sources, might allow for a Pd-catalyzed oxidative C–H functionalization to form C–F bonds.²²

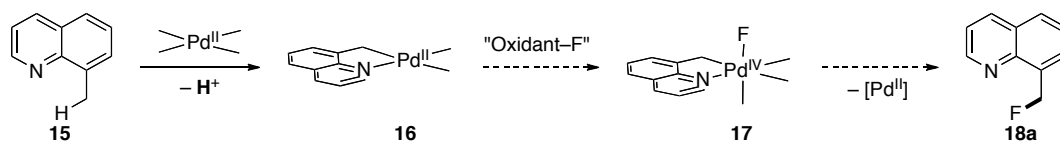
Scheme 3.8 Pd-Catalyzed Halogenation of C–H Bonds²¹



3.2 Methodology Development and Synthetic Scope

Our goal was to develop a Pd^{II/IV}-catalyzed method for the regioselective incorporation of fluorine atoms into organic molecules using commercially available, electrophilic fluorine sources (*i.e.* Selectfluor[®], *N*-fluoropyridinium salts, or iodotoluene difluoride).²² The proposed mechanism for this reaction would involve oxidation of a [Pd^{II}–alkyl] or [Pd^{II}–aryl] intermediate (for example, **16**, in Scheme 3.9) to a Pd^{IV} species (**17**), followed by subsequent C–F bond-forming reductive elimination to afford the fluorinated product. As discussed above, it is known that reductive elimination to form C–F bonds from Pd^{II} is slow; however, we reasoned that the C–F bond-formation at Pd^{IV} might be more facile from the higher energy Pd^{IV} intermediate.⁶

Scheme 3.9 Proposed Pd-Catalyzed Oxidative Fluorination of C–H Bonds



With the help of an undergraduate researcher, Waseem Anani, we began by developing conditions for the fluorination of a benzylic C–H bond of 8-methylquinoline (**15**). Compound **15** is known to undergo rapid cyclometallation at Pd(OAc)₂ to form **16**; furthermore, we had previously demonstrated that it is an excellent substrate for Pd-catalyzed C–H acetoxylation reactions that proceed through a similar mechanistic manifold (Chapter 2). Initially, we screened the reaction of **15** with a variety of different commercially available electrophilic fluorine sources (1.5 equiv) in the presence of 10 mol % of Pd(OAc)₂ in benzene at 110 °C for 13 h. A conventional oil bath was used to heat these reactions. We were pleased to find that that our desired product (**18a**) was

formed in modest (0-36%) yields, along with significant quantities of both **18b** and **18c**. Running the reaction for longer times and at higher temperatures increased the yield of **18b** and concomitantly decreased the yield of the desired product **18a**. The best conditions for the Pd-catalyzed oxidative fluorination reactions employed *N*-fluoro-2,4,6-trimethylpyridinium tetrafluoroborate which afforded the product **18** in 36% yield. Importantly, when this reaction was run in the absence of Pd^{II} salts, none of products **18a-c** were observed. Based on these promising initial results, we sought to minimize the reaction time by running the reaction in the microwave reactor.

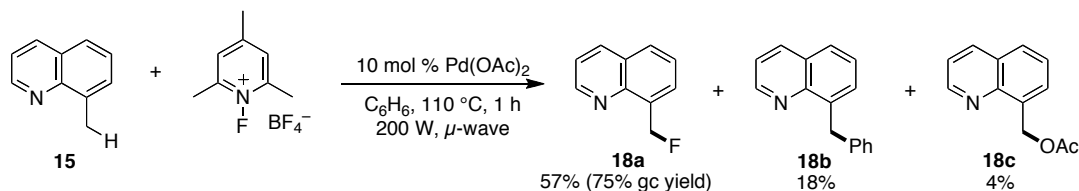
Table 3.1 Oxidant Screening for the Fluorination of Benzylic C–H Bonds

Entry	"F ⁺ " Source	yield 18a + 18b + 18c (yield 18a) Thermal	yield 18a + 18b + 18c (yield 18a) μ -wave
1		25% (0%)	37% (15%)
2		82% (36%)	97% (75%)
3		24% (22%)	19% (16%)
4		25% (12%)	8% (3%)
5		19% (9%)	9% (3%)

Microwave reactors have been shown to decrease the reaction time required for many transformations and, in some cases, dramatically improve the yields of organic transformations.²³ These results are generally attributed to more uniform and rapid heating in microwave reactors versus conventional oil baths. Gratifyingly, the Pd-catalyzed oxidative fluorination reactions proceeded in shorter reaction times and afforded increased yields of **18a** upon heating via microwave irradiation. Using 200 W of microwave irradiation, the reactions were generally complete within 1 hour at 110 °C (versus 13 hours at 110 °C in an oil bath). Additionally, when *N*-fluoro-2,4,6-

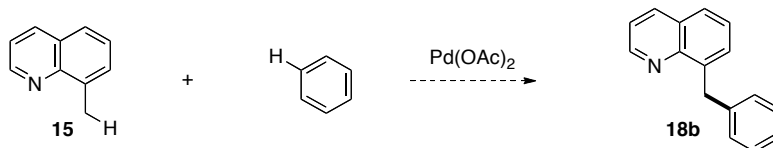
trimethylpyridinium tetrafluoroborate was used as the “F⁺” source, **18a** was formed in dramatically improved 75% GC yield (57% isolated yield). In this system, the balance of the material was 3% of unfunctionalized 8-methylquinoline, 18% of the phenylated product **18b**, and 4% of the acetoxyated product **18c**.

Scheme 3.10 Optimized Conditions for Benzylic C–H Bond Fluorination



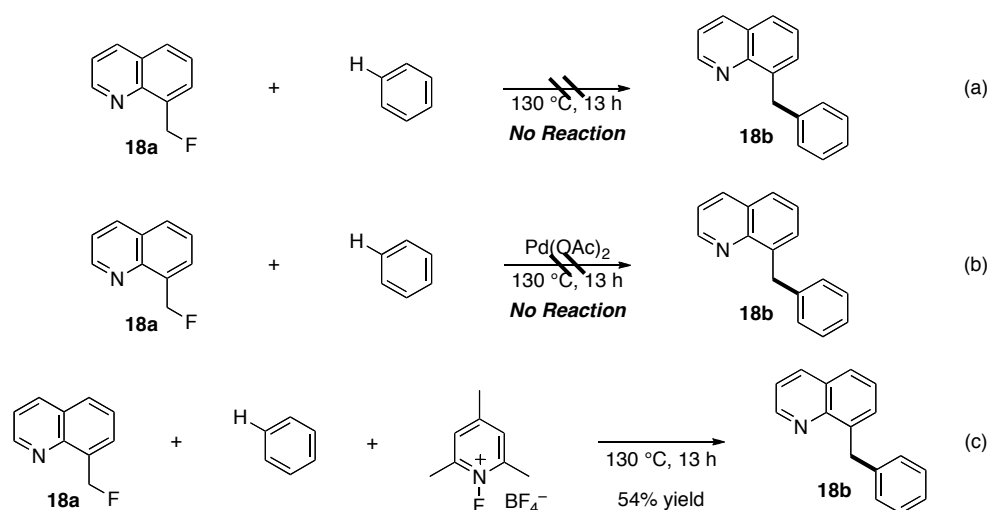
Initially, we hypothesized that the phenylation product, **18b**, was being formed through a Pd-catalyzed oxidative coupling reaction between the 8-methylquinoline (**15**) and the solvent benzene (Scheme 3.11).²⁴ An oxidative coupling reaction involves the formation of a new C–C bond from two C–H bonds. However, when the reaction was run for longer times, we observed an increase in the yield of product **18b** with a concurrent loss of **18a**. This result provided initial evidence that **18b** was, in fact, being formed from **18a**.

Scheme 3.11 Pd-Mediated Oxidative Coupling between 8-Methylquinone and Benzene



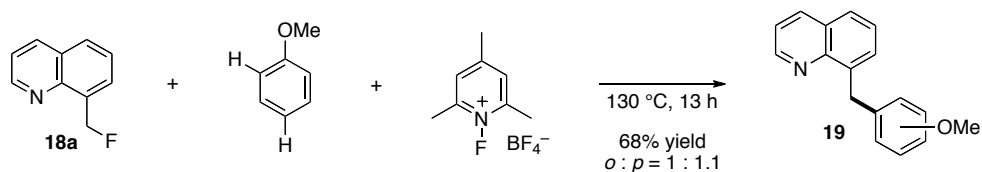
Next, we ran a series of control reactions to determine the origin of **18b**. First, we demonstrated that product **18a** does not react to form **18b** when heated at 130 °C in benzene (Scheme 3.12a). Next, we showed that **18a** also does not react to form **18b** upon thermolysis in benzene in the presence of Pd(OAc)₂ (Scheme 3.12b). Finally, we found that **18a** is transformed into **18b** in 54% yield in benzene at 110 °C in the presence of the *N*-fluoropyridinium oxidant (Scheme 3.12c). Together, these experiments indicate that **18a** is being converted into **18b** in the presence of the *N*-fluoro-2,4,6-trimethylpyridinium tetrafluoroborate and that the Pd-catalyst is not required for the transformation.

Scheme 3.12 Determining the Origin of **18b**

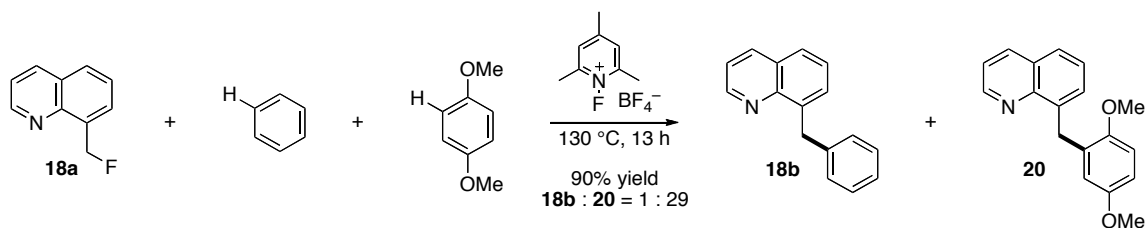


Although the mechanism for the conversion of **18a** to **18b** has not been fully elucidated, preliminary experiments suggest that it may involve an electrophilic aromatic substitution (EAS). For example, when **18a** was reacted with anisole (in place of benzene) and *N*-fluoro-2,4,6-trimethylpyridinium tetrafluoroborate, the arylated product **19** was formed as a 1 : 1.1 mixture of *ortho* and *para* isomers, as would be expected for an EAS reaction (Scheme 3.13). Additionally, a competition study between benzene and 1,4-dimethoxybenzene showed that these arenes are incorporated in a 1 : 29 ratio (**18b** : **20**), respectively (Scheme 3.14). This result demonstrates that electron-rich arenes react preferentially and suggests that there is a significant build up of positive charge in the transition state.

Scheme 3.13 Reaction Between **18a** and Anisole



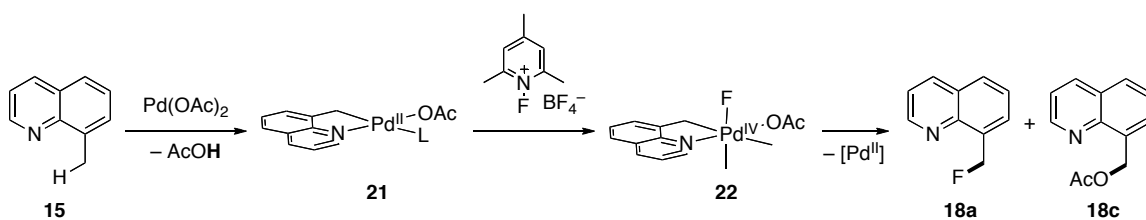
Scheme 3.14 Competition Between Benzene and 1,4-Dimethoxybenzene



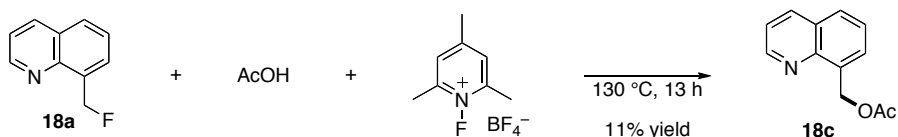
The acetoxyated product **18c** could be formed through either Pd-catalyzed or non-Pd-catalyzed reactions. The only source of acetate (OAc) in the reaction is the $\text{Pd}(\text{OAc})_2$ catalyst; therefore, the maximum theoretical yield of **18c** is 20%. One explanation for the formation of **18c** is competitive C–OAc bond-forming reductive elimination from a Pd^{IV} intermediate like **22** in Scheme 3.15. Upon cyclometalation/oxidation with the initial catalyst, there are both F and AcO ligands on the Pd^{IV} intermediate, and the ratio of **18a** to **18c** formed from intermediate **22** will depend on their relative rates of reductive elimination (Scheme 3.15). Importantly, it is known that the more nucleophilic X-type ligand typically undergoes faster reductive elimination from high oxidation state metals.²⁵⁻²⁷

A second possible pathway to **18c** would involve the reaction between **18a** and AcOH (which is generated upon C–H activation). Importantly, the control reaction of **18a** with 2 equiv of AcOH in the presence of 1.5 equiv of *N*-fluoro-2,4,6-trimethylpyridinium tetrafluoroborate did afford small amounts (11%) of **18c** (Scheme 3.16). Interestingly, when a similar reaction was run without oxidant, **18c** was not formed. This suggests that this reaction may occur by oxidant-promoted generation of a carbocation intermediate, which is then trapped with AcOH.

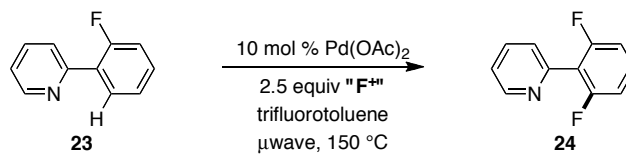
Scheme 3.15 Competing C–F and C–OAc Bond Forming Reductive Elimination.

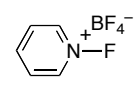
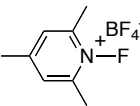
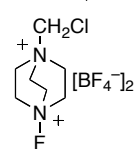
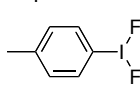
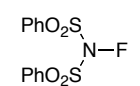


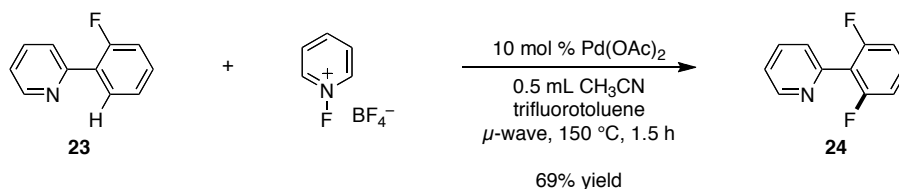
Scheme 3.16 Reaction of **18a** and AcOH in the Presence of *N*-Fluoro-2,4,6-Trimethylpyridinium Tetrafluoroborate.



The optimized conditions for Pd-catalyzed oxidative fluorination are shown in Scheme 3.10, page 51. However, these conditions were not effective for the fluorination of sp^2 C–H bonds. In order to develop conditions for the fluorination of aryl C–H bonds, we undertook an additional oxidant screening. These studies focused on the Pd(OAc)₂-catalyzed reaction between **23** and 2.5 equiv of an electrophilic fluorinating reagent. As shown in Table 3.2, the related oxidant, *N*-fluoropyridinium tetrafluoroborate, was the most effective for our desired transformation, providing fluorinated product **24** in 76% yield. The optimized conditions are shown in Scheme 3.17 and involve 10 mol % of Pd(OAc)₂, 2.5 equiv of *N*-fluoropyridinium tetrafluoroborate in trifluorotoluene with 50 μ L MeCN at 150 °C under 250 W of μ -wave irradiation. Interestingly, neither the arylated nor the acetoxyated products, analogous to **18b** and **18c**, were observed in the sp^2 C–H bond fluorination reactions.

Table 3.2 Oxidant Screening for the Fluorination of Aryl C–H Bonds


Entry	"F ⁺ " Source	Yield a
1		76%
2		6%
3		33%
4		0%
5		58%

Scheme 3.17 Optimized Conditions for the Fluorination of **23**

Next, we aimed to expand the substrate scope for both the benzylic and aryl C–H bond fluorination reactions. As shown in Table 3.3, entry 1, the benzylic fluorination reactions were tolerant of other benzylic C–H bonds in the molecule, and the 5-methyl group of product **25** was not fluorinated under the reaction conditions. The reactions were also tolerant of aryl C–Br bonds (Table 3.3 entry 3), functional groups that are often not stable in Pd^{II}/Pd⁰ catalytic cycles.

The oxidative fluorination reaction was also demonstrated with a diverse array of aromatic C–H bonds (Table 3.3 entries 4–12). This transformation was tolerant of a variety of functional groups, including benzylic methyl substituents (**25** and **28**), ethers (**29** and **34**), trifluoromethyl groups (**30** and **31**), as well as non-enolizable ketones (**35**)

and esters (**33**). Interestingly, Table 3.3, entry 5 demonstrates that, when given the choice between a benzylic and an aromatic C–H bond, the aromatic C–H bond is selectively functionalized. In the substrate that forms **28**, this selectivity could also potentially be attributed due to the preference for forming a 5-membered over a 6-membered palladacyclic intermediate. However, when a only a 6-membered palladacycle can form, as in Table 3.3, entry 12, the reaction still proceeds to afford the fluorinated product **35**, albeit in a moderate yield.

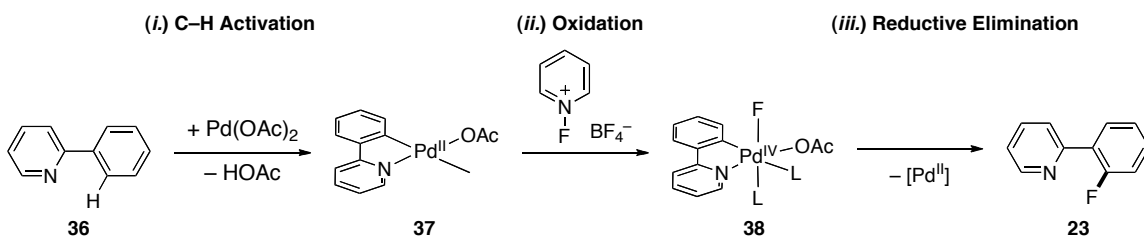
As discussed above, the proposed mechanism for this transformation is shown in Scheme 3.18. It involves: (i) initial ligand-directed C–H activation to form **37**, (ii) oxidation to a Pd^{IV} intermediate (**38**) that contains both a Pd–C and Pd–F bond, and (iii) reductive elimination to afford the new C–F bond of **39** and regenerate the Pd^{II} catalyst. It is important to note that an alternative mechanism involving direct oxidative cleavage of the Pd^{II}–C bond is also possible (Scheme 3.19). However, subsequent to this work, our group and others have shown that Pd^{IV}–F intermediates similar to **38** can be isolated and further that they undergo C–F bond-forming reductive elimination under conditions analogous to our catalytic reaction (*vide infra*).

Table 3.3 Substrate Scope for the Pd-Catalyzed Oxidative Fluorination Reaction

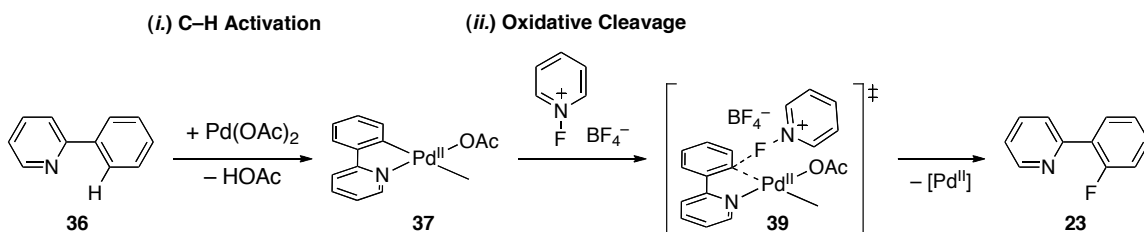
Entry	Oxidant	Product	isolated Yield	Entry	Oxidant	Product	isolated Yield
1			57% ^a	7			75% ^b
2			49% ^a	8			59% ^b
3			53% ^a	9			50% ^b
4			62% ^b	10			54% ^b
5			52% ^b	11			60% ^b
6			33% ^b	12			60% ^b

^a Conditions: 7-10 mol% Pd(OAc)₂, 1.5-2 equiv *N*-fluoro-2,4,6-trimethylpyridinium tetrafluoroborate, benzene, microwave (1-4 h, 100-110 °C, 200-250 W). ^b Conditions: 10 mol% Pd(OAc)₂, 2.5-4.5 equiv *N*-fluoropyridinium tetrafluoroborate, 0.12-0.5 mL CH₃CN, CF₃C₆H₅, microwave (1.5-2 h, 150 °C, 300 W).

Scheme 3.18 Proposed Mechanism for the Oxidative Fluorination Reaction



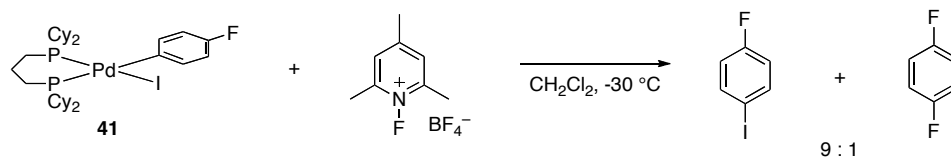
Scheme 3.19 Direct Oxidative Cleavage Mechanism for the Pd-Catalyzed Fluorination Reactions



3.3 Subsequent Examples

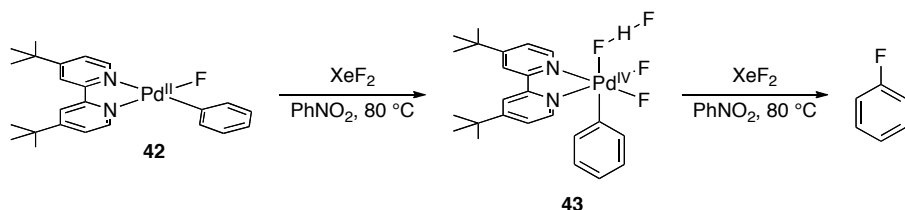
After our initial report of Pd-catalyzed oxidative fluorination reactions, our groups and others have provided evidence for a Pd^{II}/Pd^{IV} catalytic cycle occurring in these reactions. Vigalok has shown **41** reacts with XeF₂ and *N*-fluoro-2,4,6-trimethylpyridinium tetrafluoroborate to afford Ar-X (X = I or F) bonds.²⁸ Importantly, the Ar-I forms preferentially over the Ar-F bond. The formation of the Ar-I implies an oxidation to Pd^{IV}, as a direct oxidative cleavage mechanism could only afford the Ar-F bond; however, no Pd^{IV} intermediate was observed in this system.

Scheme 3.20 Oxidative of a Ar-Pd^{II}-I with an *N*-fluoro-pyridinium salt²⁸

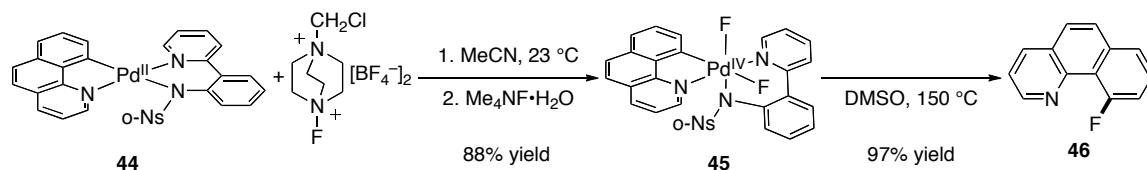


More recently, several groups have reported isolation of Pd^{IV} aryl fluoride intermediates analogous to **38** in our catalytic cycle (Scheme 3.18). For example, Nick Ball, a fellow graduate student in the Sanford laboratory, has isolated the Pd^{IV} complex **43** and has shown that this species reacts to form an Ar-F bond.²⁹ Similarly, Ritter has demonstrated the isolation of Pd^{IV} aryl fluoride **45**, and shown that it undergoes C-F bond-forming reductive elimination.³⁰

Scheme 3.21 Oxidation to an Isolable Pd^{IV} Aryl Fluoride and Reductive Elimination to Afford the new C–F Bond²⁹

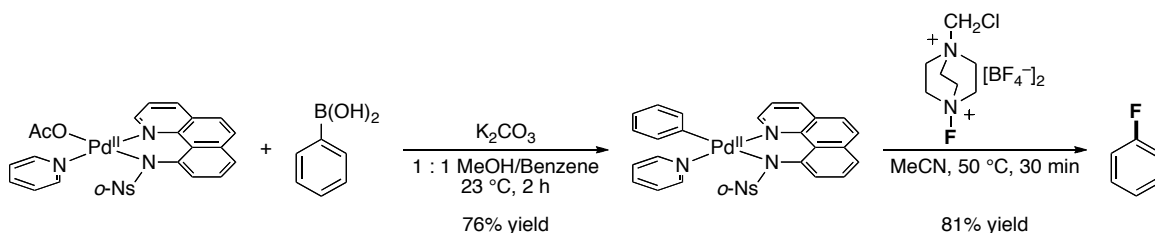


Scheme 3.22 Ritter's Example of C–F Bond Forming Reductive Elimination from Pd^{IV}³⁰



Ritter has also demonstrated that aryl boronic acids can be converted into aryl fluorides using stoichiometric quantities of [Pd^{II}] and Selectfluor as the electrophilic fluorine source.³¹ In these reactions, a transmetalation forms the Pd–C bond (versus C–H activation in our transformation), which then undergoes an oxidative fluorination reaction to afford the new C–F bond.

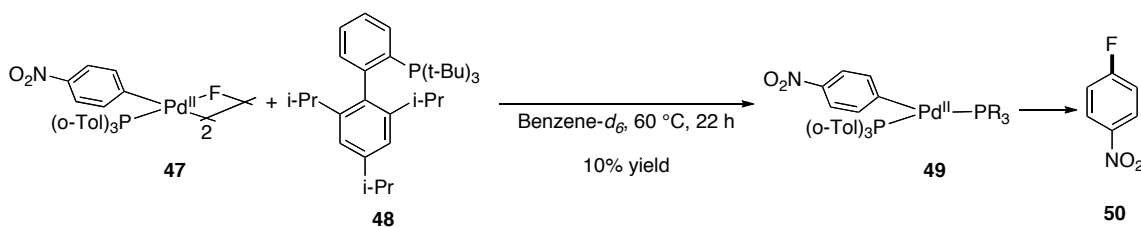
Scheme 3.23 Stoichiometric Oxidative Fluorination of Aryl Boronic Acids³¹



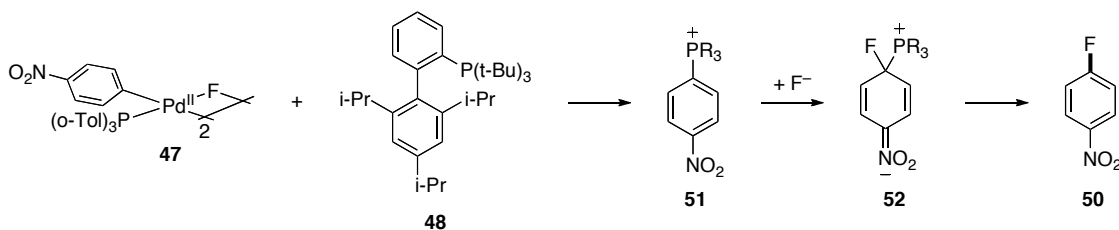
Efforts towards Pd^{II/0}-catalyzed fluorination of aryl halides using nucleophilic F⁻ sources have also continued. Yandulov has performed extensive computational experiments probing the reductive elimination of Ar–F bond from Pd^{II}.³² His results support Grushin's earlier reports that reductive elimination of a C–F bond is disfavored kinetically relative to the formation of either a P–F or a P–C bond. However, he did find computationally that reductive elimination may be possible from a trigonal complex,

rather than a square planar species. Indeed, the complex **49** (generated *in situ* by treatment of **47** with $\text{P}(\text{C}_6\text{H}_4\text{-2-Trip})(t\text{-Bu})_2$ (**48**) resulted in formation of low yields (~10%) of Ar-F **50** (Scheme 3.24). However, while the observed product could be formed by C-F bond-forming reductive elimination from Pd^{II} (as proposed by Yandulov), it could also be accessed via a pathway involving C-P bond-forming reductive elimination to generate $[\text{Ar-PR}_3]^+$ **51**, followed by a nucleophilic aromatic substitution *via* a Meisenheimer intermediate (Scheme 3.25).³³ As of yet, neither mechanism has been definitively confirmed in this system.

Scheme 3.24 Proposed Reductive Elimination of an Ar-F Bond From Pd^{II}



Scheme 3.25 Grushin's Proposed Mechanism for the Formation of the Ar-F



Grushin has also continued to seek conditions for the $\text{Pd}^{\text{II/0}}$ -mediated fluorination reactions using nucleophilic fluoride sources.^{34, 35} As phosphine ligands have proven problematic due to their propensity to form P-F and P-C bonds, he has explored the use of both *N*-heterocyclic carbene and nitrogen-based ligands. However, Ar-F bond-forming reductive elimination from Pd^{II} was not observed in any of these systems.

3.4 Conclusions

In conclusion, we have developed the first Pd-catalyzed reaction for the formation of aryl and benzylic C-F bonds.²² Unlike previous attempts with nucleophilic fluorine sources, electrophilic fluorine sources can be used to form the new C-F bonds from Pd^{II} -aryl intermediates. Using a substrate containing a ligand directing group and a Pd^{II}

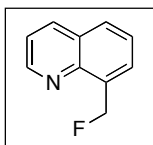
catalyst, first a cyclopalladation event can occur to form a Pd^{II}-C bond, then a subsequent reaction between the oxidant and the Pd^{II} intermediate can lead to the formation of the new C-F bond. Evidence by our group and others suggest that a Pd^{IV} mechanism is plausible, as Pd^{IV} fluorides have been isolated and shown to undergo C-F bond-forming reductive elimination under conditions analogous to our reaction.

3.5 Experimental Procedure

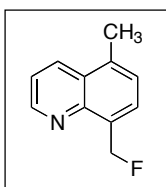
General Procedures: NMR spectra were obtained on a Varian Inova 500 (499.90 MHz for ¹H; 125.70 MHz for ¹³C) or a Varian Inova 400 (399.96 MHz for ¹H; 100.57 MHz for ¹³C; 376.34 MHz for ¹⁹F) spectrometer. ¹H and ¹³C NMR chemical shifts are reported in parts per million (ppm) relative to TMS, with the residual solvent peak used as an internal reference; ¹⁹F NMR are referenced based on the residual solvent peak in the ¹H NMR. Multiplicities are reported as follows: singlet (s), doublet (d), doublet of doublets (dd), doublet of doublet of doublets (ddd), doublet of triplets (dt), doublet of quartets (dq), triplet (t), triplet of doublets (td), quartet (q), quartet of doublets (qd), and multiplet (m).

Materials and Methods: Substrates **1**, **11**, and **2-phenylpyridine** were obtained from commercial sources and used as received. Quinoline substrates were prepared through the reaction of substituted 2-methylanilines and glycerol according to a literature procedure.³⁶ Non-commercially available 2-arylpyridine substrates were prepared by Suzuki cross coupling of the respective aryl boronic acid and 2-bromopyridine or 2-bromo-6-methoxypyridine.³⁷ The fluorinating reagents *N*-fluoro-2,4,6-trimethylpyridinium (**2**) and *N*-fluoropyridinium tetrafluoroborate (**3**) were obtained from TCI America and Aldrich and used as received. Iodotoluene difluoride, *N*-fluorobenzenesulfonimide, and Selectfluor® were obtained from Aldrich and used without further purification. Pd(OAc)₂ was obtained from Pressure Chemical or Frontier Scientific and used as received. Microwave heating was carried out using a CEM Discovery microwave reactor. The microwave reactions were run in closed reaction vessels with magnetic stirring and with the temperature controlled via IR detection. Flash chromatography was performed on EM Science silica gel 60 (0.040-0.063 mm particle

size, 230-400 mesh) and thin layer chromatography was performed on Merck TLC plates pre-coated with silica gel 60 F₂₅₄. HPLC was performed on a Varian ProStar 210 HPLC using Waters μ Porasil® 10 μ m silica (19 x 300 mm) columns. Control reactions (in the absence of Pd catalyst) were run for each substrate, and generally showed none the desired fluorinated product under our standard reaction conditions.

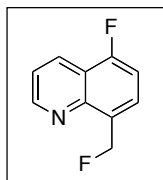
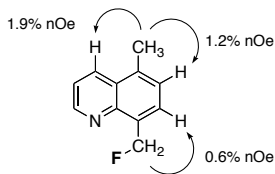


8-Methylquinoline (**15**) (95.2 μ L, 0.69 mmol, 1 equiv), *N*-fluoro-2,4,6-trimethylpyridinium tetrafluoroborate (242.6 mg, 1.07 mmol, 1.5 equiv) and Pd(OAc)₂ (15.6 mg, 0.069 mmol, 10 mol %) were combined in benzene (4.5 mL) in an 80 mL microwave reaction vessel equipped with a Teflon stirbar. The reaction mixture was heated in the microwave at 110 °C for 1 h (250 W, 110 °C, 1 h, 10 min ramp). The resulting pale yellow/brown suspension was cooled to room temperature, naphthalene was added as an internal standard, and the reaction was analyzed by gas chromatography (which showed 65% GC yield). The reaction was then diluted with methanol (10 mL) and methylene chloride (10 mL) and filtered through a plug of Na₂CO₃ (~2 g) and Celite (0.5 g), and the plug was washed with copious methylene chloride (3 x 50 mL). The resulting solution was evaporated to dryness, and the brown solid was purified by chromatography on silica gel (R_f = 0.1 in 95% hexanes/5% ethyl acetate). Product **18a** was isolated as a pale yellow oil (66.1 mg, 59% yield). Note: GC-MS of the crude reaction mixture also showed unreacted starting material (5% GC yield), as well as traces of the acetoxylated product **18c** (6% GC yield)²¹ and the phenylated product **18b** (2% GC yield).³⁸ ¹H NMR (400 MHz, CDCl₃): δ 8.94 (dd, J = 4.0, 2.0 Hz, 1H), 8.18 (dd, J = 8.4, 2.0 Hz, 1H), 7.85-7.80 (multiple peaks, 2H), 7.58 (t, J = 3.4 Hz, 1H), 7.45 (dd, 8.4, J = 4.4 Hz, 1H), 6.15 (d, ² J_{HF} = 47.6 Hz, 2H); ¹⁹F NMR (376 MHz, CDCl₃): δ -219.3 (t, ² J_{FH} = 47.2 Hz); ¹³C NMR (100 MHz, CDCl₃): δ 149.53, 145.11 (d, J_{CF} = 3.8 Hz), 135.83, 134.36 (d, J_{CF} = 16.7 Hz), 127.91 (d, J_{CF} = 2.3 Hz), 127.63, 127.04 (d, J_{CF} = 9.8 Hz), 125.94, 121.05, 81.50 (d, J_{CF} = 164.7 Hz). HRMS EI (m/z): [M^+] calcd for C₁₀H₈NF, 161.0641; found, 161.063. Anal. Calcd for C₁₀H₈NF: C, 74.52, H, 5.00, N, 8.69; Found: C, 74.67, H, 5.10, N, 8.53.



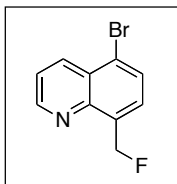
5,8-Dimethylquinoline (105.7 mg, 0.669 mmol, 1 equiv), *N*-fluoro-2,4,6-trimethylpyridinium tetrafluoroborate (237.9 mg, 1.05 mmol, 1.6 equiv) and Pd(OAc)₂ (15.6 mg, 0.069 mmol, 10 mol %) were combined in benzene (4.5 mL) in an 80 mL microwave reaction vessel equipped with a Teflon stirbar. The reaction mixture was heated in the microwave at 110 °C for 1 h (250 W, 110 °C, 1 h, 10 min ramp). The resulting yellow suspension was cooled to room temperature, naphthalene was added as an internal standard, and the reaction was analyzed by gas chromatography (which showed ~57% GC yield). The reaction was then diluted with acetonitrile (10 mL), filtered through a plug of Na₂CO₃ (2.5 mg) and Celite (0.5 mg), and the plug was washed with copious acetonitrile (3 x 50 mL). The resulting solution was evaporated to dryness, and the brown solid was purified by chromatography on silica gel (*R*_f = 0.07 in 90% toluene/10% hexanes). Product **25** was obtained as a yellow oil (67 mg, 57% yield). Note: GC-MS analysis of the crude reaction mixture also showed unreacted material (~4% GC yield), as well as traces of the corresponding acetoxyated product (~5% GC yield), the corresponding phenylated product (~2% GC yield), and the corresponding difluorinated product (~4% GC yield). ¹H NMR (400 MHz, acetone-*d*₆): δ 8.90 (dd, *J* = 4.0, 1.6 Hz, 1H), 8.43 (dd, *J* = 8.6, 1.8 Hz, 1H), 7.70 (d, *J* = 7.2 Hz, 1H), 7.54 (dd, *J* = 8.4, 4.0 Hz, 1H), 7.44 (d, *J* = 7.2 Hz, 1H), 6.06 (d, ²*J*_{HF} = 48.0 Hz, 2H), 2.67 (s); ¹⁹F NMR (376 MHz, acetone-*d*₆): δ -217.03 (t, *J*_{FH} = 48.0 Hz); ¹³C NMR (100 MHz, acetone-*d*₆): δ 149.43, 145.70 (d, *J*_{CF} = 3.6), 135.45 (d, *J*_{CF} = 2.2), 132.78 (d, *J*_{CF} = 16.1), 132.54, 127.31 (d, *J*_{CF} = 8.8), 127.17, 126.4, 121.11, 81.12 (d, *J*_{CF} = 161.9), 17.70. HRMS EI (*m/z*): [*M*⁺] calcd for C₁₁H₁₀NF, 175.0797; found, 175.0789. Anal. Calcd for C₁₁H₁₀NF: C, 75.41, H, 5.75, N, 7.99; Found: C, 75.20, H, 5.93, N, 7.73.

nOe conformation of regiochemistry of oxidation:

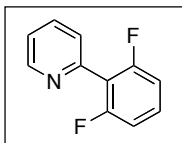


5-Fluoro-8-methylquinoline (100 mg, 0.62 mmol, 1 equiv), *N*-fluoro-2,4,6-trimethylpyridinium tetrafluoroborate (211.0 mg, 0.93 mmol, 1.5 equiv) and Pd(OAc)₂ (9.7 mg, 0.043 mmol, 7.0 mol %) were combined in benzene (2.0 mL) in a 10 mL microwave reaction vessel equipped with a Teflon stirbar. The reaction mixture was heated in the microwave at 100 °C for 4 h (200 W, 100 °C, 4 h, 10 min ramp). The resulting yellow suspension was cooled to room temperature, naphthalene was added as an internal standard, and the reaction was analyzed by gas chromatography (which showed ~54% GC yield). The reaction was then diluted with acetonitrile (10 mL), filtered through a plug of Na₂CO₃ (2.5 mg) and Celite (0.5 mg), and the plug was washed with copious acetonitrile (3 x 50 mL). The resulting solution was evaporated to dryness, and the brown solid was purified by chromatography on silica gel (*R*_f = 0.07 in 70% toluene/30% hexanes). Product **26** was obtained as an off-white crystalline solid (54 mg, 49% yield). Mp = 52.8-54.7 °C. Note: GC-MS analysis of the crude reaction mixture also showed traces of the corresponding acetoxyated product (~7% GC yield), the corresponding phenylated product (~25% GC yield), and the corresponding difluorinated product (~6% GC yield). ¹H NMR (500 MHz, acetone-*d*₆): δ 9.00 (dd, *J* = 4.3, 1.8 Hz, 1H), 8.49 (dd, *J* = 8.3, 1.8 Hz, 1H), 7.84 (m, 1H), 7.66 (dd, *J* = 8.5, 4.0 Hz, 1H), 7.39 (dd, *J* = 10.0, 8.0 Hz, 1H), 6.03 (d, ²*J*_{HF} = 47.5 Hz); ¹⁹F NMR (376 MHz, acetone-*d*₆): δ -123.65 - -123.75 (m), -215.83 (td, *J* = 48.0, 5.1); ¹³C NMR (125 MHz, acetone-*d*₆): δ 158.75 (dd, *J*_{CF} = 254.3, 6.4 Hz), 152.07, 147.06 (d, *J*_{CF} = 3.6), 132.03 (dd, *J*_{CF} = 16.3,

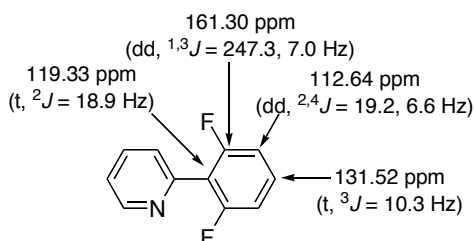
4.9 Hz), 129.97 (d, $J_{CF} = 4.5$ Hz), 129.01 (t, $J_{CF} = 9.43$ Hz), 122.92 (d, $J_{CF} = 2.8$ Hz), 119.45 (d, $J_{CF} = 16.2$ Hz), 110.70 (d, $J_{CF} = 20.24$ Hz), 81.51 (dt, $J_{CF} = 163.87$, 4.8 Hz). HRMS EI (m/z): [M^+] calcd for $C_{10}H_7NF_2$, 179.0547; found, 179.0552. Anal. Calcd for $C_{10}H_7NF_2$: C, 67.04, H, 3.94, N, 7.82; Found: C, 67.49, H, 4.27, N, 7.46.



5-Bromo-8-methylquinoline (100 mg, 0.45 mmol, 1 equiv), N-fluoro-2,4,6-trimethylpyridinium tetrafluoroborate (204.3 mg, 0.90 mmol, 2 equiv), and $Pd(OAc)_2$ (10.1 mg, 0.045 mmol, 10 mol %) were combined in benzene (10 mL) in an 80 mL microwave reaction vessel equipped with a Teflon stirbar. The vessel was sealed with a Teflon lined cap, and the reaction mixture was heated in the microwave at 110 °C for 4 h (250 W, 110 °C, 4 h, 10 min ramp). The resulting yellow suspension was cooled to room temperature, then diluted with CH_2Cl_2 (50 mL) and washed three times with water. The organic layer was then dried over magnesium sulfate and concentrated. The resulting brown solid was purified by chromatography on silica gel ($R_f = 0.15$ in 80% toluene/20% hexanes). Product **27** was isolated as a white crystalline solid (57 mg, 53% yield). Mp = 67.9-69.4 °C. Note: GC-MS analysis of the crude reaction mixture also showed 52% GC yield of **27**, along with traces of the corresponding difluorinated product (~6% GC yield), acetoxyated product (~6% GC yield), and the corresponding phenylated product (~14% GC yield). 1H NMR (400 MHz, acetone- d_6): δ 8.97 (dd, $J = 4.0, 1.6$ Hz, 1H), 8.56 (dd, $J = 8.6, 1.4$ Hz, 1H), 7.96 (d, $J = 7.6$ Hz, 1H), 7.75 (dd, $J = 7.8, 1.0$ Hz, 1H), 7.70 (dd, $J = 8.4, 4.2$ Hz, 1H), 6.16 (dd, $J = 47.6, 0.8$ Hz, 2H); ^{19}F NMR (376 MHz, acetone- d_6): δ -223.09 (t, $^2J_{FH} = 47.8$ Hz); ^{13}C NMR (100 MHz, acetone- d_6): δ 151.74, 146.73 (d, $J_{CF} = 3.7$ Hz), 136.23 (d, $J_{CF} = 16.94$ Hz), 136.06, 131.12, 128.45 (d, $J_{CF} = 11.1$ Hz), 127.91, 123.94, 122.34 (d, $J_{CF} = 2.9$ Hz), 81.80 (d, $J_{CF} = 165.0$ Hz). HRMS EI (m/z): [M^+] calcd for $C_{10}H_7BrNF$, 238.9746; found, 238.9756.

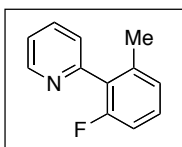


2-(2-Fluorophenyl)-pyridine (100 mg, 0.58 mmol, 1 equiv), *N*-fluoropyridinium tetrafluoroborate (267 mg, 1.44 mmol, 2.5 equiv), and Pd(OAc)₂ (13 mg, 0.058 mmol, 10 mol %) were combined in trifluorotoluene (26.2 mL) and acetonitrile (0.5 mL) in an 80 mL microwave reaction vessel equipped with a Teflon stirbar. The reaction mixture was heated in the microwave to 150 °C for 1.5 h (300W, 150 °C, 1.5 h, 20 min ramp). The light brown suspension was cooled to room temperature, methylnaphthalene was added as an internal standard, and the reaction was analyzed by gas chromatography (which showed 82% GC yield). The reaction mixture was then diluted with acetonitrile (20 mL) and filtered through a plug of Na₂CO₃ (~2 g) and Celite (~0.5 g) and the plug was washed with an additional 100 mL of acetonitrile. The solvent was removed under vacuum, and the resulting brown solid was purified by chromatography on silica gel (*R*_f = 0.2 in 80% hexanes/20% ethyl acetate). Product **24** was isolated as a pale yellow oil (75.6 mg, 69% yield). ¹H NMR (400 MHz, CDCl₃): δ 8.76 (ddd, *J* = 4.9, 1.9, 0.9 Hz, 1H), 7.78 (td, *J* = 7.7, 1.9 Hz, 1H), 7.52-7.48 (m, 1H), 7.37-7.28 (multiple peaks, 2H), 7.03-6.96 (m, 2H); ¹⁹F NMR (376 MHz, CDCl₃): δ -114.78 - -114.88 (m); ¹³C NMR (100 MHz, acetone-*d*₆): δ 161.30 (dd, *J*_{CF} = 247.25, 7.0 Hz), 150.68, 150.34, 137.25, 131.52 (t, *J*_{CF} = 10.3 Hz), 126.70, 124.06, 119.33 (t, *J*_{CF} = 18.88 Hz), 112.64 (dd, *J*_{CF} = 19.2, 6.6 Hz). HRMS EI (*m/z*): [*M*⁺] calcd for C₁₁H₇NF₂, 191.0457; found, 191.0546. Anal. Calcd for C₁₁H₇NF₂: C, 69.11, H, 3.69, N, 7.33; Found: C, 69.07, H, 3.84, N, 7.17.



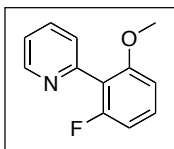
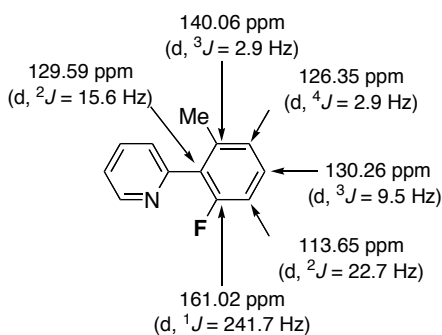
2-Phenylpyridine (**36**) (82.5 μL, 0.58 mmol, 1 equiv), *N*-fluoropyridinium tetrafluoroborate (480.9 mg, 2.60 mmol, 4.5 equiv), and Pd(OAc)₂ (13 mg, 0.058 mmol, 10 mol %) were combined in trifluorotoluene (26.2 mL) and acetonitrile (0.5 mL) in an

80 mL microwave reaction vessel equipped with a Teflon stirbar. The reaction mixture was heated in the microwave to 150 °C for 1.5 h (150 °C, 20 min ramp, 300 W maximum). The resulting light brown suspension was cooled to room temperature, methylnaphthalene was added as an internal standard, and the reaction was analyzed by gas chromatography (which showed 57% GC yield). The reaction mixture was then diluted with acetonitrile (20 mL) and filtered through a plug of Na₂CO₃ (~2 g) and Celite (~0.5 g) and the plug was washed with an additional 100 mL of acetonitrile. The solvent was removed under vacuum, and the resulting brown solid was purified by chromatography on silica gel (R_f = 0.2 in 80% hexanes/20% ethyl acetate). Product **24** was isolated as a pale yellow oil (69.0 mg, 62% yield). For characterization data, see previous entry (above).



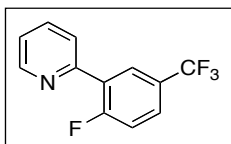
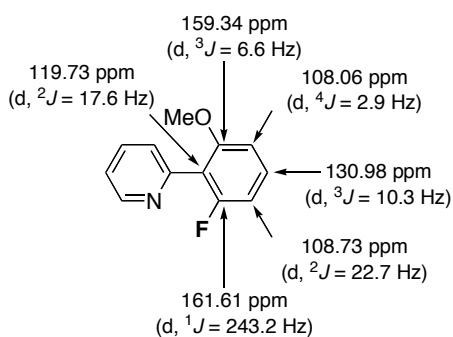
2-(2-Methylphenyl)-pyridine (97.8 mg, 0.58 mmol, 1 equiv), *N*-fluoropyridinium tetrafluoroborate (300 mg, 1.62 mmol, 2.8 equiv), and Pd(OAc)₂ (13 mg, 0.058 mmol, 10 mol%) were combined in trifluorotoluene (26.2 mL) and acetonitrile (0.25 mL) in an 80 mL microwave reaction vessel equipped with a Teflon stirbar. The reaction mixture was heated in the microwave to 150 °C for 1.5 h (150 °C, 20 min ramp, 300 W maximum). The resulting light brown suspension was cooled to room temperature, methylnaphthalene was added as an internal standard, and the reaction was analyzed by gas chromatography (which showed ~72% GC yield). The reaction mixture was then diluted with acetonitrile (20 mL) and filtered through a plug of Na₂CO₃ (~2 g) and Celite (~0.5 g) and the plug was washed with an additional 100 mL of acetonitrile, 10 mL of methylene chloride, and 10 mL of methanol. The solvent was removed under vacuum, and the resulting brown solid was purified by chromatography on silica gel (R_f = 0.2 in 80% hexanes/20% ethyl acetate). Product **28** was isolated as a pale yellow oil (56 mg, 52% yield). ¹H NMR (400 MHz, acetone-*d*₆): δ 8.71 (ddd, *J* = 4.8, 1.7, 1.0 Hz, 1H), 7.88 (td, *J* = 7.7, 1.9 Hz, 1H), 7.42 (dd, *J* = 8.0, 1.2 Hz, 1H), 7.37 (ddd, *J* = 7.6, 4.9, 1.2 Hz, 1H), 7.34-7.29 (m, 1H), 7.14 (d, *J* = 7.6 Hz, 1H), 7.05 (t, *J* = 9.2 Hz, 1H), 2.18 (s, 3 H);

^{19}F NMR (376 MHz, acetone- d_6): δ -113.79 (dd, $J = 8.8, 6.3$); ^{13}C NMR (100 MHz, acetone- d_6): δ 161.02 (d, $J_{\text{C-F}} = 241.7$ Hz), 155.14 (d, $J_{\text{CF}} = 1.1$ Hz), 150.45, 140.06 (d, $J = 2.9$ Hz), 137.11, 130.26 (s, $J_{\text{CF}} = 9.5$ Hz), 129.59 (d, $J_{\text{CF}} = 15.6$ Hz), 126.87 (d, $J_{\text{CF}} = 2.9$ Hz), 126.35 (d, $J_{\text{CF}} = 1.5$ Hz), 123.38, 113.65 (d, $J_{\text{CF}} = 22.7$ Hz). HRMS EI (m/z): $[\text{M}-\text{H}^+]$ calcd for $\text{C}_{12}\text{H}_{10}\text{FN}$, 186.0719; found, 186.0714. Anal. Calcd for $\text{C}_{12}\text{H}_{10}\text{FN}$: C, 76.99, H, 5.38, N, 7.48; Found: C, 76.90, H, 5.62, N, 7.32.



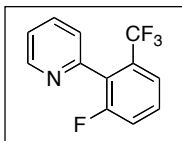
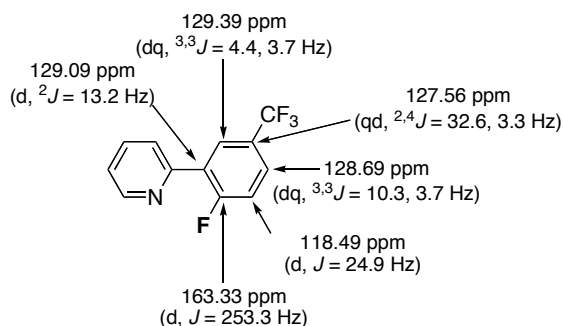
2-(2-Methoxyphenyl)-pyridine (107 mg, 0.578 mmol, 1 equiv), *N*-fluoropyridinium tetrafluoroborate (267 mg, 1.44 mmol, 2.5 equiv), and $\text{Pd}(\text{OAc})_2$ (13 mg, 0.0578 mmol, 10 mol %) were combined in trifluorotoluene (26 mL) and acetonitrile (0.25 mL) in an 80 mL microwave reaction vessel equipped with a Teflon stirbar. The reaction mixture was heated in the microwave at 150 °C for 2 h (150 °C, 2 h, 20 min ramp, 300 W maximum). The resulting light brown suspension was cooled to room temperature, methylnaphthalene was added as an internal standard, and the reaction was analyzed by gas chromatography (which showed ~35% GC yield). The reaction mixture was then diluted with acetonitrile (20 mL) and filtered through a plug of Na_2CO_3 (~2 g) and Celite (~0.5 g) and the plug was washed with an additional 100 mL of acetonitrile, 10 mL of methylene chloride, and 10 mL of methanol. The solvent was removed under vacuum, and the resulting brown solid was purified by chromatography on silica gel ($R_f = 0.21$ in 50% hexanes/50% ethyl acetate). Product **29** was isolated as a clear oil (39 mg, 33%

yield). ^1H NMR (400 MHz, acetone- d_6): δ 8.66 (ddd, $J = 4.7, 1.5, 1.1\text{ Hz}$, 1H), 7.83 (td, $J = 7.7, 1.9\text{ Hz}$, 1H), 7.44-7.37 (multiple peaks, 2H), 7.33 (ddd, $J = 7.6, 4.8, 1.2\text{ Hz}$, 1H), 6.95 (d, $J = 8.4\text{ Hz}$, 1H), 6.83 (td, $J = 8.8, 0.8\text{ Hz}$, 1H), 3.77 (s, 3H). ^{19}F NMR (376 MHz, acetone- d_6): δ -117.19 (dd, $J_{\text{FH}} = 9.2, 6.6\text{ Hz}$). ^{13}C NMR (100 MHz, acetone- d_6): 161.61 (d, $^1J_{\text{CF}} = 243.2\text{ Hz}$), 159.34 (d, $J_{\text{CF}} = 6.6\text{ Hz}$), 152.97, 150.24, 136.60, 130.98 (d, $^3J_{\text{CF}} = 10.3\text{ Hz}$), 126.92, 123.22, 119.73 (d, $^2J_{\text{CF}} = 17.6\text{ Hz}$), 108.73 (d, $J_{\text{CF}} = 22.7\text{ Hz}$), 108.06 (d, $^4J_{\text{CF}} = 2.9\text{ Hz}$), 56.53. HRMS EI (m/z): $[\text{M}^+]$ calcd for $\text{C}_{12}\text{H}_{10}\text{FNO}$, 203.0746; found, 203.0737. Anal. Calcd for $\text{C}_{12}\text{H}_{10}\text{FNO}$: C, 70.93, H, 4.96, N, 6.89; Found: C, 70.53, H, 5.21, N, 6.46.



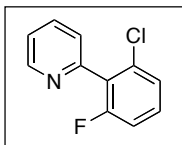
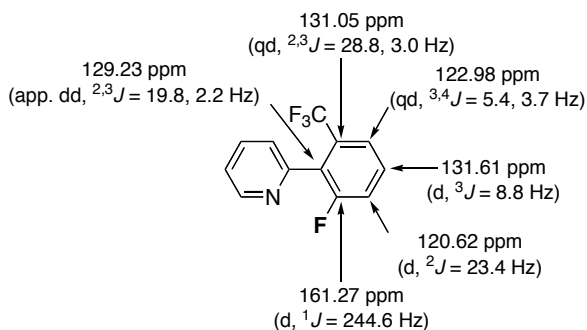
2-(3-Trifluoromethylphenyl)-pyridine (129 mg, 0.58 mmol, 1 equiv), *N*-fluoropyridinium tetrafluoroborate (300 mg, 1.6 mmol, 2.8 equiv), and $\text{Pd}(\text{OAc})_2$ (13 mg, 0.058 mmol, 10 mol %) were combined in trifluorotoluene (26.2 mL) and acetonitrile (0.25 mL) in an 80 mL microwave reaction vessel equipped with a Teflon stirbar. The reaction mixture was heated in the microwave at 150 °C for 2 h (150 °C, 2 h, 20 min ramp, 300 W maximum). The resulting light brown suspension was cooled to room temperature, methylnaphthalene was added as an internal standard, and the reaction was analyzed by gas chromatography (which showed ~88% GC yield). The reaction mixture was then diluted with acetonitrile (20 mL) and filtered through a plug of Na_2CO_3 (~2 g) and Celite (~0.5 g) and the plug was washed with an additional 100 mL of acetonitrile, 10 mL of

methylene chloride, and 10 mL of methanol. The solvent was removed under vacuum, and the resulting brown solid was purified by chromatography on silica gel ($R_f = 0.17$ in 90% hexanes/10% ethyl acetate). Product **30** was isolated as a clear oil (105 mg, 75% yield). The regioselectivity of this reaction was confirmed through COSY and HMQC experiments as well as ^{13}C NMR coupling constant analysis. ^1H NMR (400 MHz, acetone- d_6): δ 8.76 (dt, $J = 4.8, 1.4$ Hz, 1H), 8.44 (dd, $J = 7.0, 2.2$ Hz, 1H), 7.96-7.90 (multiple peaks, 2H), 7.83 (dddd, $J = 8.7, 4.4, 2.6, 0.7$ Hz, 1H), 7.51 (dd, $J = 11.1, 8.7$ Hz, 1H), 7.46-7.40 (m, 1H); ^{19}F NMR (376 MHz, acetone- d_6): δ -62.61 (d, $J = 1.1$ Hz), -112.40 - -112.51 (m); ^{13}C NMR (100 MHz, acetone- d_6): δ 163.33 (d, $J_{\text{CF}} = 253.5$ Hz), 152.09 (d, $J_{\text{CF}} = 2.6$ Hz), 151.04, 137.85, 129.39 (dq, $J = 4.4, 3.7$), 129.09 (d, $J_{\text{CF}} = 13.2$ Hz), 128.69 (dq, $J_{\text{CF}} = 10.3, 3.7$ Hz), 127.56 (qd, $J_{\text{CF}} = 32.6, 3.3$ Hz), 125.33 (d, $J_{\text{CF}} = 11.0$ Hz), 125.07 (q, $J_{\text{CF}} = 269.6$ Hz), 124.43, 118.49 (d, $J_{\text{CF}} = 24.9$ Hz). HRMS EI (m/z): $[\text{M}^+]$ calcd for $\text{C}_{12}\text{H}_7\text{F}_4\text{N}$, 241.0515; found, 241.0503. Anal. Calcd for $\text{C}_{12}\text{H}_7\text{F}_4\text{N}$: C, 59.76, H, 2.93, N, 5.81; Found: C, 60.22, H, 3.03, N, 5.55.



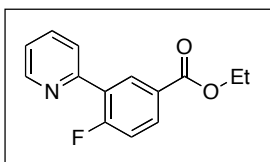
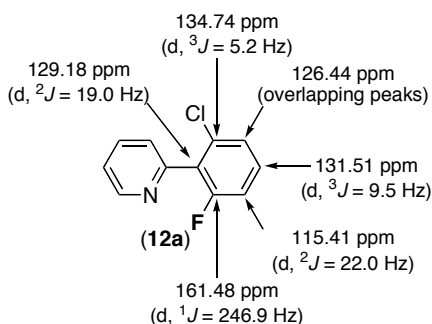
2-(2-Trifluoromethylphenyl)-pyridine (129 mg, 0.59 mmol, 1 equiv), N-Fluoropyridinium tetrafluoroborate (300 mg, 1.6 mmol, 2.8 equiv), and $\text{Pd}(\text{OAc})_2$ (13 mg, 0.0578 mmol, 10 mol %) were combined in trifluorotoluene (26.2 mL) and acetonitrile (0.25 mL) in an 80 mL microwave reaction vessel equipped with a Teflon stirbar. The reaction mixture was heated in the microwave at 150 °C for 2 h (150 °C, 20

min ramp, 300 W maximum). The resulting light brown suspension was cooled to room temperature, methylnaphthalene was added as an internal standard, and the reaction was analyzed by gas chromatography (which showed ~62% GC yield). The reaction mixture was then diluted with acetonitrile (20 mL) and filtered through a plug of Na₂CO₃ (~2 g) and Celite (~0.5 g) and the plug was washed with an additional 100 mL of acetonitrile and 10 mL of methanol. The solvent was removed under vacuum, and the resulting brown solid was purified by chromatography on silica gel (R_f = 0.08 in 90% hexanes/10% ethyl acetate). Product **31** was isolated as a clear oil (77 mg, 55% yield). ¹H NMR (400 MHz, acetone-*d*₆): δ 8.70 (ddd, *J* = 4.8, 1.6, 1.0 Hz, 1H), 7.91 (td, *J* = 7.7, 1.7 Hz, 1H), 7.76-7.68 (multiple peaks, 2H), 7.60-7.45 (m, 1H), 7.50 (d, *J* = 8.0 Hz, 1H), 7.45 (ddd, *J* = 7.7, 4.9, 1.1 Hz, 1H); ¹⁹F NMR (376 MHz, acetone-*d*₆): δ -57.85 (s), -114.50 - -114.58 (m); ¹³C NMR (100 MHz, acetone-*d*₆): δ 161.27 (d, *J*_{CF} = 244.6 Hz), 152.56, 150.27, 137.01, 131.61 (d, *J*_{CF} = 8.8 Hz), 131.05 (qd, *J*_{CF} = 28.8, 3.0 Hz), 129.23 (app. dd, *J*_{CF} = 19.8, 2.2 Hz), 126.05, 124.51 (qd, *J*_{CF} = 271.95, 3.7 Hz), 124.18, 122.98 (dq, *J*_{CF} = 5.4, 3.7 Hz), 120.62 (d, *J*_{CF} = 23.4 Hz). HRMS EI (*m/z*): [M⁺] calcd for C₁₂H₇F₄N, 241.0515; found, 241.0517.

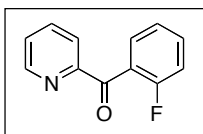
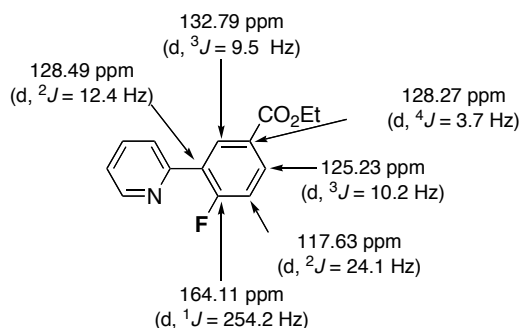


2-(2-Chlorophenyl)-pyridine (107 mg, 0.578 mmol, 1 equiv), *N*-fluoropyridinium tetrafluoroborate (333 mg, 1.8 mmol, 3.1 equiv), and Pd(OAc)₂ (13 mg, 0.0578 mmol,

10 mol %) were combined in trifluorotoluene (26 mL) and acetonitrile (0.25 mL) in an 80 mL microwave reaction vessel equipped with a Teflon stirbar. The reaction mixture was heated in the microwave to 150 °C for 2 h (150 °C, 2 h, 20 min ramp, 300 W maximum). The resulting light brown suspension was cooled to room temperature, methylnaphthalene was added as an internal standard, and the reaction was analyzed by gas chromatography (which showed ~66% GC yield). The reaction mixture was then diluted with acetonitrile (20 mL) and filtered through a plug of Na₂CO₃ (~2 g) and Celite (~0.5 g) and the plug was washed with an additional 100 mL of acetonitrile, 10 mL of methylene chloride, and 10 mL of methanol. The solvent was removed under vacuum, and the resulting brown solid was purified by chromatography on silica gel (*R_f* = 0.32 in 80% hexanes/20% ethyl acetate). Product **32** was isolated as a pale yellow oil (59 mg, 50% yield). ¹H NMR (400 MHz, acetone-*d*₆): δ 8.72 (ddd, *J* = 4.9, 1.8, 1Hz, 1H), 7.93 (td, *J* = 7.7, 1.8 Hz, 1H), 7.56-7.46 (multiple peaks, 2H), 7.44 (ddd, *J* = 7.6, 5.0, 1.0 Hz, 1H), 7.41 (d, *J* = 8.0 Hz, 1H), 7.26 (td, *J* = 8.7, 0.8, 1H); ¹⁹F NMR (376 MHz, acetone-*d*₆): δ -118.51 (ddd, *J_{FH}* = 9.7, 5.9, 1.5 Hz); ¹³C NMR (100 MHz, acetone-*d*₆): δ 161.48 (d, *J_{CF}* = 246.9 Hz), 153.07, 150.56, 137.26, 134.74 (*J_{CF}* = 5.2Hz), 131.51 (d, *J_{CF}* = 9.5 Hz), 129.18 (d, *J_{CF}* = 19.0 Hz), 126.44, 124.40, 124.14, 115.41 (*J_{CF}* = 22.0 Hz). HRMS EI (*m/z*): [M⁺] calcd for C₁₁H₇ClFN, 207.0251; found, 207.0252.

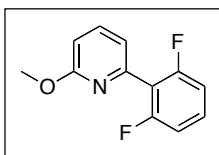
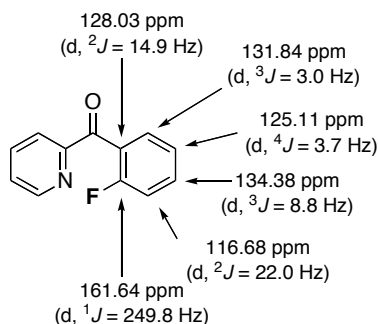


Ethyl 3-(pyridin-2-yl)benzoate (131.4 mg, 0.58 mmol, 1 equiv), N-Fluoropyridinium tetrafluoroborate (333 mg, 1.8 mmol, 3.1 equiv), and Pd(OAc)₂ (13 mg, 0.058 mmol, 10 mol %) were combined in trifluorotoluene (26.2 mL) and acetonitrile (0.25 mL) in an 80 mL microwave reaction vessel equipped with a Teflon stirbar. The reaction mixture was heated in the microwave at 150 °C for 2 h (150 °C, 2 h, 20 min ramp, 300 W maximum). The resulting yellow suspension was cooled to room temperature, methyl-naphthalene was added as an internal standard, and the reaction was analyzed by gas chromatography (which showed ~84% GC yield). The reaction mixture was then diluted with acetonitrile (20 mL) and filtered through a plug of Na₂CO₃ (~2 g) and Celite (~0.5 g) and the plug was washed with an additional 100 mL of acetonitrile and 10 mL of methanol. The solvent was removed under vacuum, and the resulting brown solid was dried onto silica gel and purified by chromatography on silica gel (R_f = 0.27 in 90% hexanes/10% ethyl acetate). Product **33** was isolated as a white crystalline solid (77 mg, 54% yield). Note: the sample obtained from column chromatography was contaminated with traces (6% by GC analysis) of the starting material. Samples for microanalysis were obtained after further purification by HPLC (90% hexanes/ 10% ethyl acetate, 20 mL/min, Waters μ-porasil 19.1 mm). The regioselectivity of this reaction was confirmed through COSY and HMQC experiments as well as ¹³C NMR coupling constant analysis. Mp = 36.5-37.8 °C. ¹H NMR (400 MHz, acetone-*d*₆): δ 8.78-8.73 (multiple peaks, 2H), 8.11 (ddd, *J* = 8.5, 4.9, 2.3 Hz, 1H), 7.96-7.86 (multiple peaks, 2H), 4.39 (q, *J* = 7.2Hz, 2H), 1.38 (t, *J* = 7.2Hz, 3H); ¹⁹F NMR (376 MHz, acetone-*d*₆): δ -111.86 - -111.93 (m); ¹³C NMR (100 MHz, acetone-*d*₆): δ 137.97, 164.11 (d, *J*_{CF} = 254.2Hz), 152.82 (d, *J*_{CF} = 2.9 Hz), 150.99, 137.70, 133.71 (d, *J*_{CF} = 4.4 Hz), 123.79 (d, *J*_{CF} = 9.5 Hz), 128.49 (d, *J*_{CF} = 12.4 Hz), 128.27 (d, *J*_{CF} = 3.7 Hz), 125.23 (d, *J*_{CF} = 10.2Hz), 124.12, 117.63 (d, *J*_{CF} = 24.1Hz), 33.97, 13.20. IR (KBr): 1713 cm⁻¹. Anal. Calcd for C₁₄H₁₂FNO₂: C, 68.56, H, 4.93, N, 5.71; Found: C, 68.78, H, 5.14, N, 5.68.



2-Benzoylpyridine (105.9 mg, 0.58 mmol, 1 equiv), N-Fluoropyridinium tetrafluoroborate (350 mg, 1.8 mmol, 3.3 equiv), and Pd(OAc)₂ (13 mg, 0.058 mmol, 10 mol %) were combined in trifluorotoluene (26.2 mL) and acetonitrile (0.125 mL) in an 80 mL microwave reaction vessel equipped with a Teflon stirbar. The reaction mixture was heated in the microwave at 150 °C for 2 h (150 °C, 20 min ramp, 2 h, 300 W maximum). The resulting yellow suspension was cooled to room temperature, methylnaphthalene was added as an internal standard, and the reaction was analyzed by gas chromatography (which showed ~80% GC yield). The reaction mixture was then diluted with acetonitrile (20 mL) and filtered through a plug of Na₂CO₃ (~2 g) and Celite (~0.5 g) and the plug was washed with an additional 100 mL of acetonitrile and 10 mL of methanol. The solvent was removed under vacuum, and the resulting brown solid was dried onto silica gel and purified by chromatography on silica gel (R_f = 0.12 in 80% hexanes/20% ethyl acetate). Product **35** was isolated as a white solid (55 mg, 48% yield). Mp = 35.3-36.5 °C. ¹H NMR (400 MHz, acetone-*d*₆): δ 8.65 (dt, *J* = 3.7, 0.9 Hz, 1H), 8.10-8.05 (multiple peaks, 2H), 7.70-7.62 (multiple peaks, 3H), 7.36 (td, *J* = 6.0, 0.8 Hz, 1H), 7.24 (ddd, *J* = 8.4, 6.8, 0.4 Hz, 1H); ¹⁹F NMR (376 MHz, acetone-*d*₆): δ -111.60 (ddd, *J* = 10.1, 6.9, 5.0 Hz); ¹³C NMR (100 MHz, acetone-*d*₆): δ 194.06, 161.64 (d, *J*_{CF} = 249.8 Hz), 155.33, 150.06, 138.21, 134.38 (d, *J*_{CF} = 8.8 Hz), 131.84 (d, *J*_{CF} = 3.0 Hz), 128.22, 128.03 (d, *J* = 14.9), 125.11 (d, *J*_{CF} = 3.7 Hz), 123.70, 116.68 (d, *J*_{CF} = 22.0). IR (KBr): 1668 cm⁻¹.

HRMS EI (m/z): [M⁺] calcd for C₁₂H₉FNO, 201.0590; found, 201.0595. Anal. Calcd for C₁₂H₉FNO: C, 71.64, H, 4.01, N, 6.96; Found: C, 71.49, H, 4.01, N, 6.90.



2-Methoxy-6-phenylpyridine (107 mg, 0.58 mmol, 1 equiv), N-Fluoropyridinium tetrafluoroborate (481 mg, 2.6 mmol, 4.5 equiv), and Pd(OAc)₂ (13 mg, 0.058 mmol, 10 mol %) were combined in trifluorotoluene (26.2 mL) and acetonitrile (0.5 mL) in an 80 mL microwave reaction vessel equipped with a Teflon stirbar. The reaction mixture was heated in the microwave at 150 °C for 2 h (150 °C, 2 h, 20 min ramp, 300 W maximum). The resulting yellow suspension was cooled to room temperature, methylnaphthalene was added as an internal standard, and the reaction was analyzed by gas chromatography (which showed ~57% GC yield). The reaction mixture was then diluted with acetonitrile (20 mL) and filtered through a plug of Na₂CO₃ (~2 g) and Celite (~0.5 g) and the plug was washed with an additional 100 mL of acetonitrile and 10 mL of methanol. The solvent was removed under vacuum, and the resulting brown solid was dried onto silica gel purified by chromatography on silica gel (R_f = 0.4 in 90% hexanes/10% ethyl acetate). Product **34** was isolated as a clear oil (71 mg, 60% yield). ¹H NMR (400 MHz, acetone-*d*₆): δ 7.81 (dd, *J* = 8.2, 7.4 Hz, 1H), 7.52 (tt, *J* = 8.4, 6.4 Hz, 1H), 7.18-7.09 (multiple peaks, 3H), 6.83 (dd, *J* = 8.4, 0.8 Hz, 1H), 3.89 (s, 3H); ¹⁹F NMR (376 MHz, acetone-*d*₆): δ -115.55 - -115.64 (m); ¹³C NMR (100 MHz, acetone-*d*₆): δ 164.73, 161.36 (dd, *J*_{CF} = 247.6, 7.4 Hz), 147.46, 140.01, 131.45 (t, *J*_{CF} = 10.3 Hz), 119.72, 118.96 (t, *J* =

18.6), 112.70 (dd, $J_{CF} = 19.4, 6.2\text{Hz}$), 111.27, 53.68. HRMS EI (m/z): $[M^+]$ calcd for $C_{12}H_9F_2NO$, 221.0662; found, 221.0652. Anal. Calcd for $C_{12}H_9F_2NO$: C, 65.16, H, 4.10, N, 6.33; Found: C, 64.95, H, 4.11, N, 6.31.

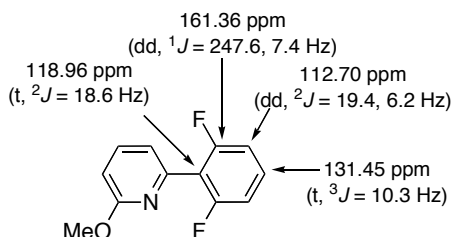


Table 3.1: All oxidant screening reactions were set up in duplicate and were analyzed by GC analysis with naphthalene as the internal standard.

Thermal Reactions: 8-Methylquinoline (6.1 μL , 0.045 mmol, 1 equiv), “F⁺” reagent (0.067 mmol, 1.5 equiv), and $\text{Pd}(\text{OAc})_2$ (1.0 mg, 0.0045 mmol, 10 mol %) were combined in benzene (0.75 mL) in a 4 mL vial. The vial was sealed with a Teflon lined cap, and the reaction heated at 110 $^\circ\text{C}$ for 13 h. After cooling, naphthalene was added as an internal standard, and the reaction mixture was diluted with CH_3CN and filtered through a plug of Na_2CO_3 and Celite. The yields of **18a**, **18b**, and **18c** were determined through GC analysis.

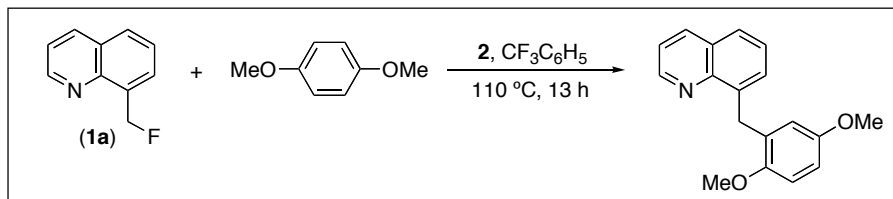
Microwave Reactions: 8-Methylquinoline (6.1 μL , 0.045 mmol, 1 equiv), “F⁺” reagent (0.067 mmol, 1.5 equiv), and $\text{Pd}(\text{OAc})_2$ (1.0 mg, 0.0045 mmol, 10 mol %) were combined in benzene (0.75 mL) in a 10 mL microwave reaction vessel. The vessel was sealed, and the redaction was heated with microwave irradiation at 110 $^\circ\text{C}$ for 1 h (250 W, 110 $^\circ\text{C}$, 1 h, 10 min ramp). After cooling, naphthalene was added as an internal standard, and the reaction mixture was diluted with CH_3CN and filtered through a plug of Na_2CO_3 and Celite. The yields of **18a**, **18b**, and **18c** were determined through GC analysis.

Table 3.2: All oxidant screening reactions were set up in duplicate and were analyzed by GC analysis with naphthalene as the internal standard. Note: these reactions were carried out on 22.5 mM scale in a 10 mL microwave reaction vessel. Furthermore, the conditions used were those that provided optimal isolated yield on 22.0 mM scale. In contrast, the larger scale reactions (from which isolated yields were determined) were carried out on 100 mM scale in an 80 mL microwave reaction vessel. We have found that these arene fluorination reactions generally do not scale particularly well between different sized microwave reaction vessels. As a result, reoptimization of the larger scale reactions was often required. Substrate **23** (8 mg, 0.045 mmol, 1 equiv), “F⁺” reagent (0.11 mmol, 2.5 equiv), and Pd(OAc)₂ (1.0 mg, 0.005 mmol, 10 mol %) were combined in trifluorotoluene (2.0 mL) and CH₃CN (0.038 mL) in a 10 mL microwave reaction vessel. The vessel was sealed, and the reaction was heated while stirring with microwave irradiation at 150 °C for 1.5 h (300 W, 150 °C, 1.5 h, 20 min ramp). After cooling, methylnaphthalene was added as an internal standard, and the reaction mixture was diluted with CH₃CN and filtered through a plug of Na₂CO₃ and Celite. The yield of **24** was determined through GC analysis.

Scheme 3.12: 8-(Fluoromethyl)quinoline (**18a**) (50 mg, 0.31 mmol, 1 equiv) and *N*-fluoro-2,4,6-trimethylpyridinium tetrafluoroborate (141 mg, 0.62 mmol, 2 equiv) were combined in benzene (5.2 mL) in a 20 mL vial. The vial was sealed with a Teflon lined cap, and the reaction was heated at 130 °C for 13 h. The reaction was diluted with 10 mL acetonitrile and filtered through ~2 g sodium carbonate and ~0.5 g Celite, washing with an additional 100 mL acetonitrile, 10 mL methylene chloride, and 10 mL methanol. The washes were concentrated, and the resulting product was purified by chromatography on silica gel ($R_f = 0.27$ in 90% hexanes/10% ethyl acetate). Product **18b** was isolated as a white solid (37 mg, 54% yield). Spectroscopic data was identical to that previously reported for this compound.³⁸

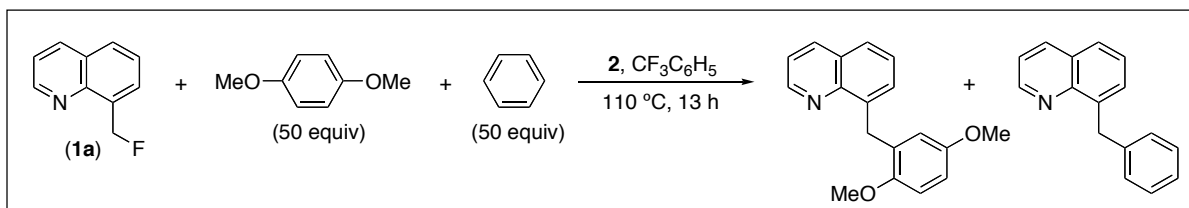
Scheme 3.13: 8-(Fluoromethyl)quinoline (**18a**) (50 mg, 0.31 mmol, 1 equiv) and *N*-fluoro-2,4,6-trimethylpyridinium tetrafluoroborate (141 mg, 0.62 mmol, 2 equiv) were

combined in anisole (5.2 mL) in a 20 mL vial. The vial was sealed with a Teflon lined cap, and the reaction was heated at 110 °C for 13 h. The reaction was diluted with 10 mL acetonitrile and filtered through ~2 g sodium carbonate and ~0.5 g Celite, washing with an additional 100 mL acetonitrile, 10 mL methylene chloride, and 10 mL methanol. The washes were concentrated, and the resulting product was purified by chromatography on silica gel ($R_f = 0.53$ in 80% hexanes/20% ethyl acetate). The product was isolated as a clear oil (53 mg, 68% yield; $o/p = 1:1.1$ by GC). The two regioisomers were separated by HPLC (90% hexanes, 10% ethyl acetate, 20 mL/min, 19.1 mm Waters μ -Porasil column). (*o*-Methoxybenzyl)quinoline: ^1H NMR (400 MHz, acetone- d_6): δ 8.90 (dd, $J = 4.2, 1.8$ Hz, 1H), 8.25 (dd, $J = 8.4, 1.6$ Hz, 1H), 7.74 (dd, $J = 8.0, 1.6$ Hz, 1H), 7.48 – 7.37 (multiple peaks, 3H), 7.15 (td, $J = 7.7, 1.5$ Hz, 1H), 7.07 (dd, $J = 7.6, 1.2$ Hz, 1H), 6.95 (d, $J = 6.95$ Hz, 1H), 6.77 (td, $J = 7.4, 1.1$ Hz, 1H), 4.63 (s, 2H), 3.79 (s, 3H); ^{13}C NMR (100 MHz, acetone- d_6): δ 158.61, 150.35, 147.84, 140.71, 137.08, 131.53, 130.43, 129.97, 129.33, 128.17, 127.21, 127.09, 122.03, 121.15, 111.32, 55.73, 31.37. (*p*-Methoxybenzyl)quinoline: ^1H NMR (400 MHz, acetone- d_6): δ 8.96 (dd, $J = 4.2, 1.8$ Hz, 1H), 8.29 (dd, $J = 8.4, 1.6$ Hz, 1H), 7.79 (dd, $J = 8.0, 1.6$ Hz, 1H), 7.57 – 7.47 (multiple peaks, 3H), 7.27 (d, $J = 8.4$ Hz, 2H), 6.81 (d, $J = 8.8$ Hz, 2H), 4.59 (s, 2H), 3.72 (s, 3H). ^{13}C NMR (100 MHz, acetone- d_6): δ 158.95, 150.49, 147.55, 141.75, 137.09, 134.67, 130.95, 130.14, 129.46, 127.29, 127.26, 122.13, 114.50, 55.44, 36.42. HRMS (EI) [M^+] for $\text{C}_{17}\text{H}_{15}\text{NO}$, 249.1154, found, 249.1163.

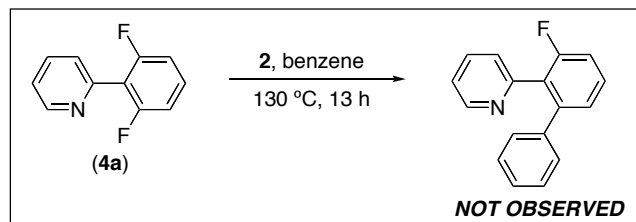


8-(Fluoromethyl)quinoline (**18a**) (50 mg, 0.31 mmol, 1 equiv), *N*-fluoro-2,4,6-trimethylpyridinium tetrafluoroborate (141 mg, 0.62 mmol, 2 equiv), and 1,4-dimethoxybenzene (857 mg, 6.2 mmol, 20 equiv) combined in trifluorotoluene (5 mL) in a 20 mL vial. The vial was sealed with a Teflon lined cap, and the reaction was heated at

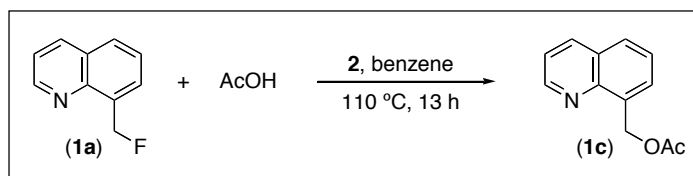
110 °C for 13 h. The reaction was diluted with 10 mL acetonitrile and filtered through ~2 g sodium carbonate and ~0.5 g Celite, washing with an additional 100 mL acetonitrile, 10 mL methylene chloride, and 10 mL methanol. The washes were concentrated, and the resulting product was purified by chromatography on silica gel ($R_f = 0.16$ in 90% hexanes/10% ethyl acetate). The product was isolated as a clear oil (49 mg, 57% yield). ^1H NMR (400 MHz, acetone- d_6): δ 8.95 (dd, $J = 4.0, 2.0$ Hz, 1H), 8.31 (dd, $J = 8.0, 1.0$ Hz, 1H), 7.80 (dd, $J = 7.4, 2.2$ Hz, 1H), 7.53-7.44 (multiple peaks, 3H), 6.91 (dd, $J = 8.0, 1.2$ Hz, 1H), 6.77-6.70 (multiple peaks, 2H), 4.62 (s, 2H), 3.79 (s, 3H), 3.63 (s, 3H); ^{13}C NMR (100 MHz, acetone- d_6): δ 154.56, 152.82, 150.37, 147.78, 140.58, 137.09, 131.70, 130.03, 129.34, 127.23, 127.15, 122.05, 118.17, 112.20, 111.77, 56.29, 55.65, 31.49. HRMS (EI): $[\text{M}^+]$ for $\text{C}_{19}\text{H}_{17}\text{NO}_2$, 279.1259, found, 279.1267.



Scheme 3.14: 8-(Fluoromethyl)quinoline (**1a**) (7.2 mg, 0.045 mmol, 1 equiv), *N*-fluoro-2,4,6-trimethylpyridinium tetrafluoroborate (15.1 mg, 0.067 mmol, 1.5 equiv), benzene (50 equiv) and *p*-dimethoxybenzene (50 equiv) were combined with trifluorotoluene (1 mL) in a 4 mL vial. The vial was sealed with a Teflon lined cap, and the reaction was heated at 130 °C for 13 h. After cooling, naphthalene was added as an internal standard, and the reaction mixture was diluted with CH_3CN and filtered through a plug of Na_2CO_3 and Celite. The yields of **1b** and the corresponding (*p*-MeO)₂C₆H₃ product were determined by GC analysis to be 3% and 87%, respectively (a 1:29 ratio).



2-(2,6-Difluoro)pyridine (**24**) (8.5 mg, 0.0445 mmol, 1 equiv) and *N*-fluoro-2,4,6-trimethylpyridinium tetrafluoroborate (15.1 mg, 0.067, 1.5 equiv) were combined in benzene (1 mL) in a 4 mL vial. The vial was sealed with a Teflon lined cap, and the reaction heated at 130 °C for 13 h. After cooling, naphthalene was added as an internal standard, and the reaction mixture was diluted with CH₃CN and filtered through a plug of Na₂CO₃ and Celite. The reaction was analyzed by GCMS and no phenylated product was observed.



Scheme 3.16: 8-(Fluoromethyl)quinoline (**1a**) (7.2 mg, 0.045 mmol, 1 equiv), *N*-fluoro-2,4,6-trimethylpyridinium tetrafluoroborate (15.1 mg, 0.067 mmol, 1.5 equiv), and AcOH (5 μL, 0.089 mmol, 2 equiv) were combined. The vial was sealed with a Teflon lined cap, and the reaction was heated at 110 °C for 13 h. After cooling, naphthalene was added as an internal standard, and the reaction mixture was diluted with CH₃CN and filtered through a plug of Na₂CO₃ and Celite. GC analysis showed that **1c** was formed in 11% yield under these conditions.

Note: Product **1c** was *not* formed under the same reaction conditions in the absence of **2**. Additionally, the reaction of **1a** with AcOH in the presence of Pd(OAc)₂ but in the absence of **2** also afforded none of product **1c**.

3.6 References

- (1) Pagliaro, M.; Ciriminna, R. *J. Mater. Chem.* **2005**, *15*, 4981-4991.
- (2) Smart, B. E. *J. Fluorine Chem.* **2001**, *109*, 3-11.
- (3) Thayer, A. M. *Chem. Eng. News* **2006**, *84*, 15-24.
- (4) Furuya, T.; Kuttruff, C. A.; Ritter, T. *Curr. Opin. Drug Discov. Devel.* **2008**, *11*, 803-819.
- (5) Shimizu, M.; Hiyama, T. *Angew. Chem., Int. Ed.* **2005**, *44*, 214-231.
- (6) Grushin, V. V. *Chem. Eur. J.* **2002**, *8*, 1006-1014.
- (7) Hartwig, J. F. *Nature* **2008**, *455*, 314-322.
- (8) Vigalok, A. *Chem. Eur. J.* **2008**, *14*, 5102-5108.
- (9) Negishi, E. I., Ed.; In *Handbook of Organopalladium Chemistry for Organic Synthesis*; Wiley-Interscience: New York, 2002; .
- (10) Flemming, J. P.; Pilon, M. C.; Borbulevitch, O. Y.; Antipin, M. Y.; Grushin, V. V. *Inorg. Chim. Acta* **1998**, *280*, 87-98.
- (11) Fraser, S. L.; Antipin, M. Y.; Khroustalyov, V. N.; Grushin, V. V. *J. Am. Chem. Soc.* **1997**, *119*, 4769-4770.
- (12) Grushin, V. V. *Chem. Rev.* **1996**, *96*, 2011-2033.
- (13) Roe, D. C.; Marshall, W. J.; Davidson, F.; Soper, P. D.; Grushin, V. V. *Organometallics* **2000**, *19*, 4575-4582.
- (14) Pilon, M. C.; Grushin, V. V. *Organometallics* **1998**, *17*, 1774-1781.
- (15) Grushin, V. V. *Organometallics* **2000**, *19*, 1888-1900.
- (16) Grushin, V. V. *Angew. Chem., Int. Ed.* **1998**, *37*, 994-996.
- (17) Okano, T.; Harada, N.; Kiji, J. *Bull. Chem. Soc. Jpn.* **1992**, *65*, 1741-1743.
- (18) Roy, A. H.; Hartwig, J. F. *Organometallics* **2004**, *23*, 1533-1541.
- (19) Kalyani, D.; Dick, A. R.; Anani, W. Q.; Sanford, M. S. *Org. Lett.* **2006**, *8*, 2523-2526.
- (20) Kalyani, D.; Dick, A. R.; Anani, W. Q.; Sanford, M. S. *Tetrahedron* **2006**, *62*, 11483-11498.
- (21) Dick, A. R.; Hull, K. L.; Sanford, M. S. *J. Am. Chem. Soc.* **2004**, *126*, 2300-2301.

- (22) Hull, K. L.; Anani, W. Q.; Sanford, M. S. *J. Am. Chem. Soc.* **2006**, *128*, 7134-7135.
- (23) Hayes, B. L. In *Microwave Synthesis: Chemistry at the Speed of Light*; CEM Publishing: Matthews, NC, 2002; .
- (24) Hassan, J.; Sevignon, M.; Gozzi, C.; Schulz, E.; Lemaire, M. *Chemical Reviews* **2002**, *102*, 1359-1469.
- (25) Culkin, D. A.; Hartwig, J. F. *Organometallics* **2004**, *23*, 3398-3416.
- (26) Hartwig, J. F. *Inorg. Chem.* **2007**, *46*, 1936-1947.
- (27) Mann, G.; Shelby, Q.; Roy, A. H.; Hartwig, J. F. *Organometallics* **2003**, *22*, 2775-2789.
- (28) Kaspi, A. W.; Yahav-Levi, A.; Goldberg, I.; Vigalok, A. *Inorg. Chem.* **2008**, *47*, 5-7.
- (29) Ball, N. D.; Sanford, M. S. *submitted*.
- (30) Furuya, T.; Ritter, T. *J. Am. Chem. Soc.* **2008**, *130*, 10060-10061.
- (31) Furuya, T.; Kaiser, H. M.; Ritter, T. *Angew. Chem., Int. Ed.* **2008**, *47*, 5993-5996, S5993/1-S5993/78.
- (32) Yandulov, D. V.; Tran, N. T. *J. Am. Chem. Soc.* **2007**, *129*, 1342-1358.
- (33) Grushin, V. V.; Marshall, W. J. *Organometallics* **2007**, *26*, 4997-5002.
- (34) Grushin, V. V.; Marshall, W. J. *Organometallics* **2008**, *27*, 4825-4828.
- (35) Grushin, V. V.; Marshall, W. J. *Organometallics* **2008**, *27*, 4825-4828.
- (36) O'Murchu, C. *Synthesis* **1989**, 880-882.
- (37) Littke, A. F.; Dai, C.; Fu, G. C. *J. Am. Chem. Soc.* **2000**, *122*, 4020-4028.
- (38) Kalyani, D.; Deprez, N. R.; Desai, L. V.; Sanford, M. S. *J. Am. Chem. Soc.* **2005**, *127*, 7330-7331.

Chapter 4

Palladium-Catalyzed Oxidative Homocoupling of 2-Phenylpyridine Derivatives

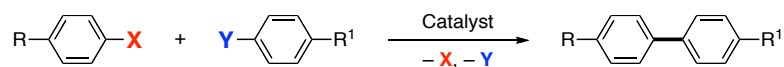
4.1 Background and Significance

Biaryl linkages are prominent functionalities found throughout natural products, pharmaceuticals, and organic materials.¹ Palladium-catalyzed methods for carbon–carbon bond formation have found widespread use in organic synthesis.^{2–4} These methods can be broken into three different categories: traditional cross-coupling reactions, direct arylation, and C–H/C–H oxidative coupling.¹ These three methods are discussed in more detail below. However, it is important to note that from the perspectives of operational simplicity, availability of starting materials, and atom economy,^{5, 6} the most attractive approach to biaryls would be the direct oxidative coupling of two C–H bonds to form a new C–C bond.

Traditional metal-catalyzed methodologies for C–C bond formation couple two prefunctionalized carbon bonds (C–X and C–Y) together to form a new C–C bond (Scheme 4.1).¹ These transformations are widely studied and applied to the synthesis of a wide variety of organic molecules.^{3, 4, 7} A significant advantage of such procedures is that the regioselectivity is determined by the location of the X and Y in the prefunctionalized starting material, thereby limiting the formation of undesired regioisomers. However, there are two significant drawbacks. First, these reactions require two prefunctionalized starting materials. These requisite functionalities often take several synthetic steps to install, decreasing the overall step economy of the transformation. Secondly, the reactions are not atom economical – the two functional groups that were installed over several synthetic steps are both subsequently lost as stoichiometric byproducts.⁶ These

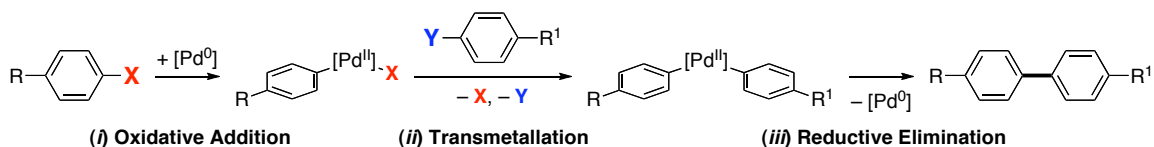
byproducts are often corrosive, toxic, and/or require purification steps to remove from the desired product.

Scheme 4.1 Ar–Ar Bond Formation via Metal-Catalyzed Cross-Coupling.



Palladium-based catalysts have found widespread use in cross-coupling reactions.¹ In these transformations, Ar–X is generally an aryl halide, while the Ar–Y is a transmetallating reagent, and a general mechanism is shown in Scheme 4.2.⁴ The aryl halide (Ar–X) acts as the oxidant, to oxidize the Pd⁰ to Pd^{II}, then transmetallation takes place to form a bisaryl Pd^{II}-intermediate, and finally reductive elimination occurs to form the new C–C bond. The starting materials employed determine the regioselectivity of the final product. No external oxidant is required, as one of the two coupling partners acts as the oxidant in the catalytic cycle. Consequently, these reactions often require air-free reaction conditions. Examples of palladium-catalyzed cross-couplings include the Stille, Suzuki, Kumada, Negishi, and Hiyama reactions, which differ mainly in the transmetallating agent employed (Ar–SnR₃, Ar–B(OR)₂, Ar–MgX, Ar–ZnX, and Ar–SiR₃, respectively).^{1,4}

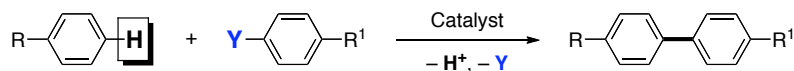
Scheme 4.2 General Mechanism for Pd-Catalyzed Cross-Coupling Reactions.⁸



Recently, there has been significant research on direct C–H arylation reactions, which form a new C–C bond from a C–H bond and a C–Y bond (Scheme 4.2).^{1,9-11} This approach increases both the step and atom economy of the coupling reaction, in that one of the coupling partners is now a C–H bond, which is ubiquitous in nature and does not require installation prior to the coupling step.¹² Additionally, one of the stoichiometric byproducts has now been reduced to an equivalent of H⁺, thereby increasing the overall

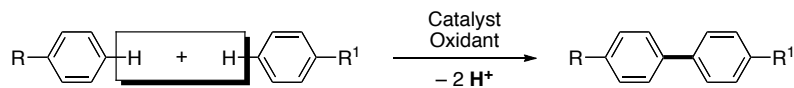
atom economy of the reaction.⁶ However, the coupling partner (Ar–Y) still requires prefunctionalization; furthermore, an equivalent of Y is lost upon the direct coupling reaction, reducing the “greenness” of this approach to C–C bond formation.

Scheme 4.3 Direct Arylation of a C–H Bond.



Transition metal-mediated oxidative coupling forms a new C–C bond directly from two C–H bonds.^{1, 13-15} This approach requires no prefunctionalization at the carbon undergoing the bond formation and reduces the stoichiometric byproducts to two equivalents of H⁺, thereby making it exceptionally atom and step economical (Scheme 4.4).^{6, 12} However, there are three significant challenges associated with such oxidative cross-coupling reactions. First, in order to develop a practical methodology for the formation of a single regioisomeric product, both C–H activations must be selective for a single C–H bond on each substrate. Second, as neither substrate serves to oxidize the Pd-catalyst, an appropriate stoichiometric oxidant must be identified. Finally, as C–H activation is often slow, the arene(s) undergoing the oxidative coupling must often be used in large excess.

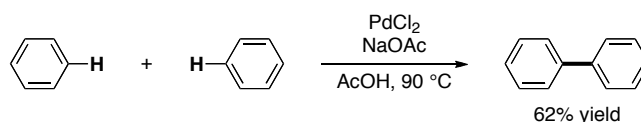
Scheme 4.4 Transition-Metal Catalyzed C–H Oxidative Coupling.



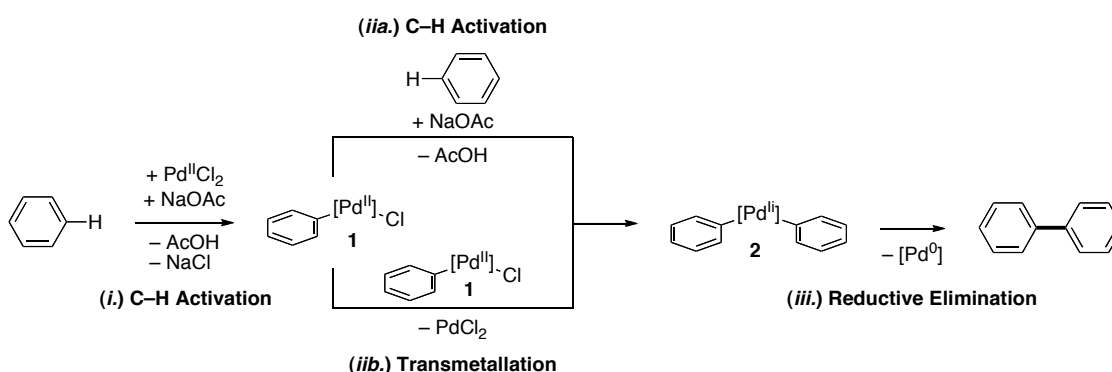
Palladium-mediated oxidative coupling has been known since 1965 when van Helden demonstrated that stoichiometric amounts of PdCl₂ promoted the oxidative coupling of two molecules of benzene to form biphenyl (Scheme 4.5).¹⁶ This reaction was found to be first order when benzene and NaOAc were in large excess; therefore, the initial C–H activation to form **1** was proposed to be the rate determining step (Scheme 4.6, step *i*). This was followed by either a second C–H activation of benzene (step *ii**a*) or a transmetalation with a second equivalent of **1** (step *ii**b*) to generate the Pd(Ar)₂ (**2**) and

finally, (step *iii*) C–C bond-forming reductive elimination affords the new Ar–Ar bond of biphenyl.

Scheme 4.5 The First Example of Pd-Mediated Oxidative Coupling.¹⁶

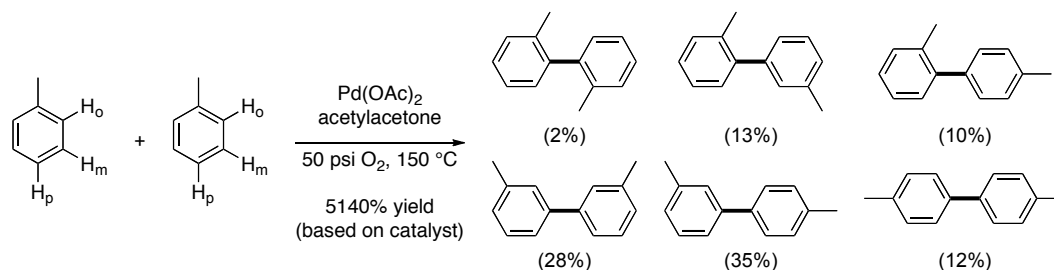


Scheme 4.6 Two Likely Mechanisms for the Pd-Mediated Oxidative Coupling of Benzene.



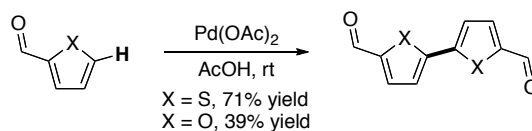
In the oxidative homocoupling of benzene, regioselectivity is not a challenge, as all the C–H bonds are equivalent. However, the palladium-catalyzed oxidative homocoupling of substituted arenes, such as toluene, affords bi-tolyl as a mixture of all possible regioisomers (Scheme 4.7).^{17–20} Three approaches have been pursued to develop regioselective palladium-catalyzed oxidative homocoupling reactions: (1) exploit the inherent reactivity of activated heterocycles as the coupling partner, as they are known to undergo electrophilic palladation regioselectively at the more electron rich carbon, (2) utilize ligands on the Pd-catalyst to prevent C–H activation from occurring adjacent to sterically large functional substituents on the arene, or (3) employ substrates that contain coordinating ligands that can direct the functionalization to a proximal C–H bond. These approaches are discussed in more detail below.

Scheme 4.7 Palladium-Catalyzed Oxidative Homocoupling of Toluene.¹⁸

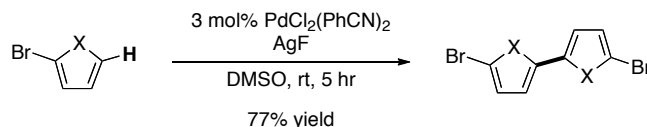


Heteroaromatics are also known to participate in highly regioselective Pd-promoted oxidative dimerization reactions (Scheme 4.8).²¹⁻²⁴ For example, in 1984, Itahara showed that thiophenes and furans undergo Pd(OAc)_2 -mediated oxidative homocoupling at the most nucleophilic carbon of the molecules.²⁵ The reaction required stoichiometric quantities of palladium salts and often required a large excess of thiophene relative to catalyst; however, more recent studies have shown that the Pd loading can be lowered to 0.1-3 mol % by adding copper, iron, or silver salts as oxidants.^{21, 23, 26, 27} Interestingly, when silver fluoride is used as the oxidant, Ag^{I} reacts selectively over an Ar-Br bond to reoxidize the Pd^0 to Pd^{II} . Furthermore, a large excess of the thiophene substrate was not required in this system, making it a practical route to thiophene dimers (Scheme 4.9).^{26, 27}

Scheme 4.8 Oxidative Dimerization of Thiophenes and Furans.²⁵



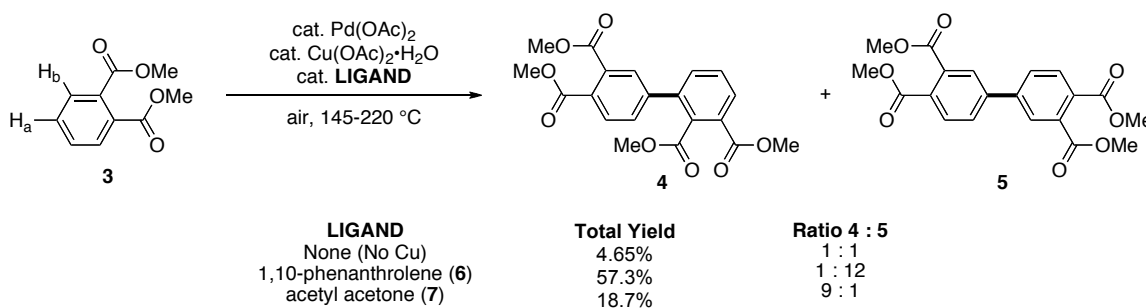
Scheme 4.9 Selective Reoxidation of Pd^0 with AgF .^{26, 27}



A second approach to controlling the regioselectivity of Pd-catalyzed oxidative homocoupling reactions involves modification of the catalyst in order to influence the

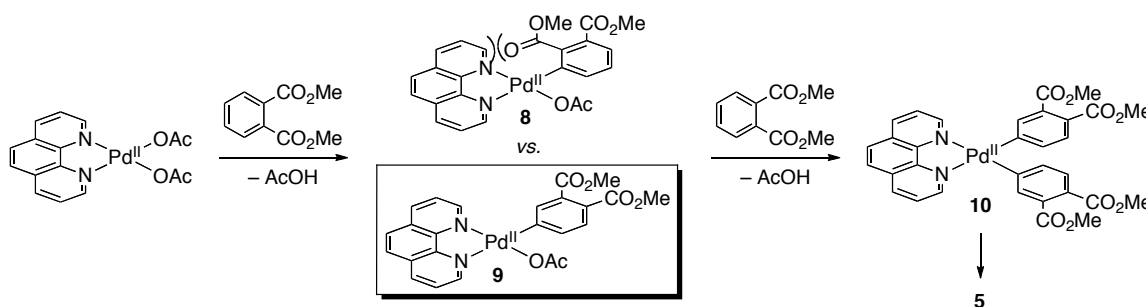
regioselectivity of C–H activation (Scheme 4.10). For example, in the absence of a ligand, Pd(OAc)₂ catalyzes the dimerization of dimethyl phthalate (**3**) to form a 1 : 1 mixture of **4** and **5**.²⁸⁻³⁰ However, the addition of 1,10-phenanthroline (phen) (**6**) changes the catalyst such that **5** is formed with good selectivity. Interestingly, the selectivity can be reversed to favor **4** upon the addition of acetyl acetone (acac) (**7**).

Scheme 4.10 Ligand Effects on the Regioselectivity of the Oxidative Coupling of Dimethyl Phthalate (**3**).^{28, 29}



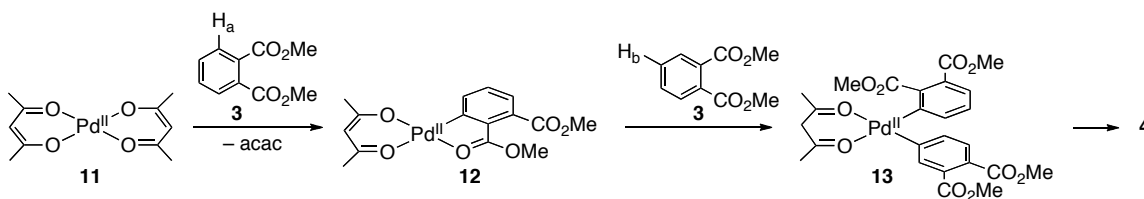
The role of the bidentate phen ligand in this reaction is believed to involve binding to the Pd, taking up two coordination sites, and increasing the steric environment at the metal center. This is proposed to limit coordination of the ester (Scheme 4.11), and thereby prevent ester-directed C–H activation at the *ortho*-position. Instead, the less sterically hindered C–H bond is activated with good selectivity to form intermediate **9**. This example demonstrates how catalyst design can be used to control the regioselectivity of Pd-mediated oxidative homocoupling reactions through producing a sterically hindered catalyst which prevents C–H activation adjacent to a bulky functional group.

Scheme 4.11 C–H Activation of Dimethyl Phthalate with (phen)Pd(OAc)₂.²⁸⁻³⁰



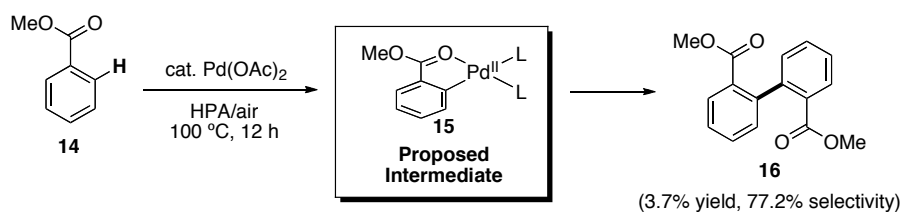
The final approach that has been utilized for the regioselective oxidative homocoupling of arenes is to incorporate a ligand into the substrate that can direct the C–H activation. For example, as seen in Scheme 4.10, when acac (**7**) is added to the oxidative homocoupling reaction of dimethyl phthalate (**3**), the regioselectivity is reversed, favoring **4**.^{29, 30} The ester group on **3** is believed to act as a directing group, promoting the first C–H activation to occur at H_b and to form intermediate **12** (Scheme 4.12). Importantly, in this transformation, the second C–H activation (to form **13** is not directed), as there are not enough open sites at the Pd to allow ester coordination. Therefore, this second reaction is sterically controlled and occurs selectively at H_a.

Scheme 4.12 C–H Activation of Dimethyl Phthalate with Pd(acac)₂.^{29, 30}



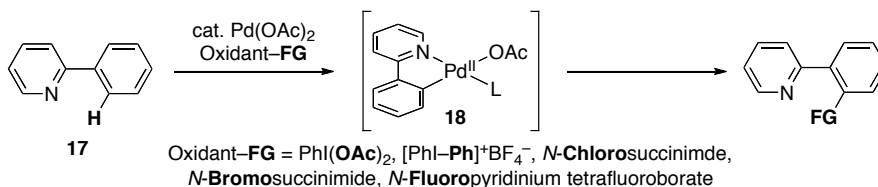
A second example, in which there are two ligand directed C–H activations, is the Pd(OAc)₂-catalyzed oxidative homocoupling of methylbenzoate (**14**), which proceeds with moderate selectivity for formation of the 2,2'-biaryl (Scheme 4.13).³¹ It is proposed that the ester can coordinate to the [Pd^{II}] and direct the C–H activation; however, the poor ligating ability of an ester to Pd explains the moderate regioselectivity observed. Similar to the oxidative coupling of dimethyl phthalate (**3**), the addition of acetylacetonone (**7**) promotes the formation of the 2,3' or 2,4' isomers.³² Ligand **7** is believed to promote an initial ligand-directed C–H activation while inhibiting a second.

Scheme 4.13 The Regioselective Oxidative Coupling of Methylbenzoate



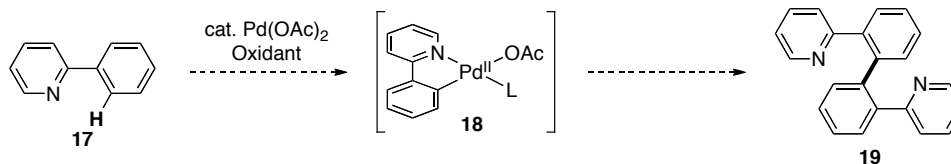
Previously, our group has demonstrated that in the presence of a palladium catalyst and an oxidant, 2-arylpyridine derivatives undergo highly regioselective C–H activation/oxidative functionalization reactions to afford exclusively *ortho*-derivatized products (Scheme 4.14).³³⁻⁴¹ The basic nitrogen of 2-phenylpyridine (**17**) directs the C–H activation to occur selectively at the *ortho* position, forming the key cyclometallated intermediate **18**.⁴²

Scheme 4.14 Pyridine-Directed *ortho*-Selective Oxidative C–H Functionalization.



We hypothesized that the use of a pyridine-directing group, which is more basic than an ester and thus a better ligand for Pd^{II}, should improve the regioselectivity of Pd-catalyzed ligand-directed oxidative homocoupling reactions (Scheme 4.15). Additionally, as 2-arylpyridines undergo facile C–H activation, a large excess of the substrate relative to the catalyst should not be required, increasing the efficiency of the transformation.⁴²⁻⁴⁴ Hence, we sought to identify conditions that would allow for the oxidative homocoupling of 2-arylpyridine derivatives.⁴⁵

Scheme 4.15 Proposed Oxidative Homocoupling of 2-Phenylpyridine.

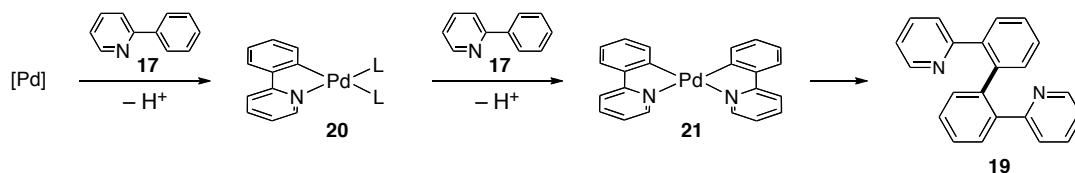


4.2 Methodology Development and Synthetic Scope

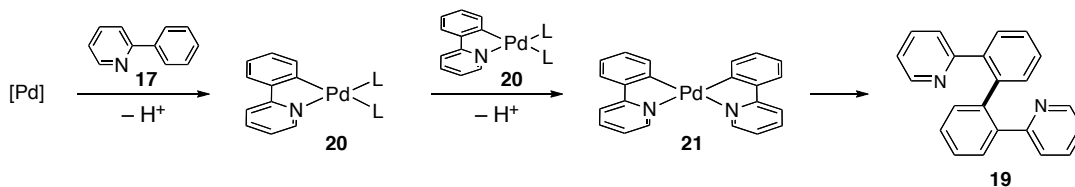
There are two key challenges for the development of an efficient, regioselective oxidative homocoupling reaction that uses substoichiometric quantities of a palladium catalyst. First, an appropriate stoichiometric oxidant must be identified. Second,

conditions must be developed that allow for either two regioselective C–H activation events to occur at a single metal center (Scheme 4.16) or for transmetalation between two cyclopalladated intermediates to form the requisite biaryl-palladium complex (Scheme 4.17).

Scheme 4.16 Oxidative Homocoupling via Two C–H Activations.



Scheme 4.17 Oxidative Homocoupling via a C–H activation Followed by a Transmetalation.

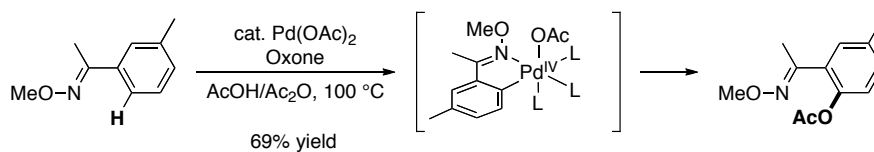


Trace amounts of the oxidative homocoupled 2-arylpyridines had been observed in our previous oxidative functionalization reactions; however, the major product in those reactions always contained the electrophilic functional group derived from the oxidant. The first hint that oxidative coupling could be induced to occur in preference to oxidative functionalization was obtained by Lopa Desai, during the development of Pd-catalyzed ligand-directed C–H acetoxylation reactions with Oxone[®] as the terminal oxidant in AcOH (Scheme 4.18).⁴⁶ Oxone[®] is an environmentally benign, inexpensive peroxide-based oxidant that allows the oxidative functionalization of molecules to be “greener” than when employing oxidants such as PhI(OAc)₂. Oxone[®] lacks a transferable functional group; therefore, the solvent (AcOH) is typically incorporated into the functionalized products.

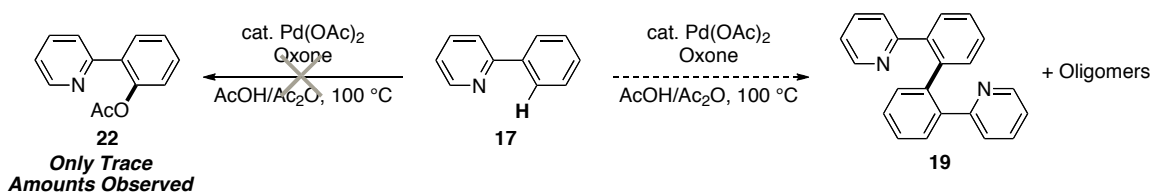
Oxime ethers, amides, and isoxazolines were effective directing groups for this transformation, and underwent directed C–H acetoxylation in high yields. However, more basic ligands, such as quinoxalines and pyridines only afforded small amounts of the desired C–OAc product.^{33, 47} We hypothesized that the oxidative coupling of the 2-

phenylpyridine (**17**) might be out-competing the C–O bond formation in this system (Scheme 4.19).

Scheme 4.18 Palladium-Catalyzed Acetoxylation Utilizing Oxone[®] as the Oxidant.

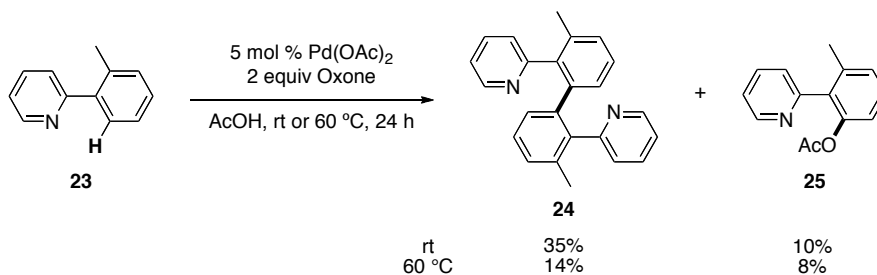


Scheme 4.19 Possible Oxidative Homocoupling of 2-Phenylpyridine.



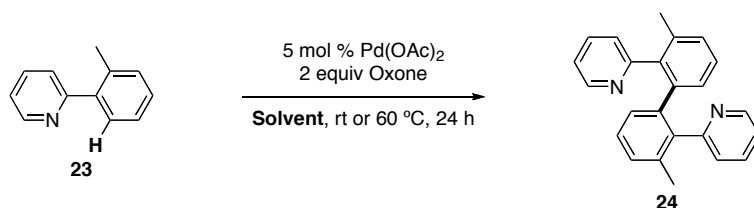
To probe this hypothesis, our initial investigations focused on the Pd-catalyzed reactions of Oxone with 2-(*o*-tolyl)pyridine (**23**). Importantly, this substrate has only a single C–H bond *ortho* to the directing group that can undergo C–H activation; therefore, the oxidative dimerization product should not be susceptible to forming regioisomeric or further oligomerized side products. Using conditions similar to those in Scheme 4.18 (5 mol % of Pd(OAc)₂, 1.1 equiv of Oxone[®] in AcOH at rt or 60 °C), we found that small amounts of the desired homocoupled product (**24**), along with some of the acetoxyated product (**25**) were formed in this reaction. Interestingly, the yield of the desired product increased as the temperature was decreased (Scheme 4.20).

Scheme 4.20 Initial Result on the Oxidative Homocoupling of 2-(*o*-Tolyl)pyridine.



The reaction shown in Scheme 4.15 was optimized through systematic variation of the solvent, oxidant, and palladium catalyst. A wide variety of solvents were screened to determine their effect on the oxidative homocoupling reaction (Table 4.1). It was found that running the reaction in *i*-propanol (entry 1) or methanol (entry 2) at room temperature led to the highest yield of **24**. The ether product, resulting from reductive elimination of the C–OR bond from Pd, was also observed in these reactions. However, this side-product could be minimized through the use of *iso*-propanol as the solvent, presumably due to the poorer ligating abilities of this sterically bulky alcohol.

Table 4.1 Solvent Screen for the Pd-Catalyzed Oxidative Coupling of 2-(*o*-Tolyl)pyridine.



Entry	Solvent	% Yield (GC) RT ^a	% Yield (GC) 60 °C ^a
1	<i>i</i> -PrOH	76%	69% ^b
2	MeOH	71% ^b	63% ^b
3	Dichloroethane	60%	16%
4	AcOH	35% ^b	14% ^b
5	DMF	32%	40%
6	CH ₃ NO ₂	30%	48%
7	Trifluoroethanol	19%	13% ^b
8	DMSO	2%	1%

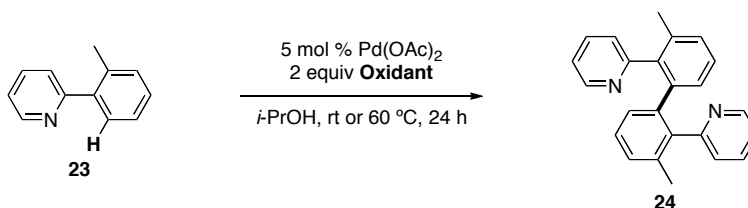
^a % Yield determined based on methyl naphthalene as an internal standard

^b The corresponding *o*-OR (OR = *Oi*-Pr, OMe, OCH₂CF₃, OAc) was also observed by GC and GCMS

A screen of different oxidants revealed that the reaction is highly sensitive to the nature of this reagent (Table 4.2). For example, while the potassium peroxide salts Oxone[®] (entry 1) and K₂S₂O₈ (entry 2) afforded the homocoupled product **24** in good yields, other peroxide-based oxidants such as H₂O₂•urea (entry 4) did not afford any of the desired product. As expected, oxidants that contain electrophilic functional groups, such as PhI(OAc)₂ (entry 3), afforded predominantly the product of functional group

transfer, rather than **24**.³⁵ Finally, oxidants that have been shown to promote other oxidative homocoupling reactions, such as AgF, Cu(OAc)₂, and air, (entries 6, 8, and 10) did not afford any of the desired product.^{26, 27, 29, 48} The latter results suggested that this reaction may proceed through a different mechanism than the Pd^{II}/Pd⁰ pathway proposed in previously reported oxidative couplings.

Table 4.2 Oxidant Screening for the Oxidative Homocoupling of 2-(*o*-Tolyl)pyridine.



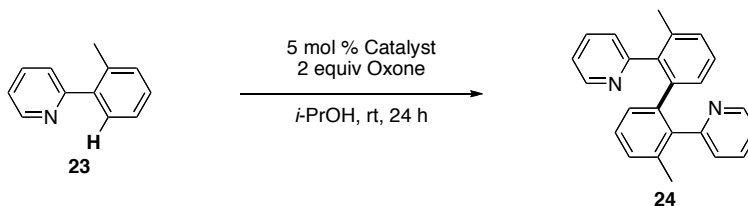
Entry	Oxidant	% Yield (GC) RT ^a	% Yield (GC) 60 °C ^a
1	Oxone	78% ^b	65% ^b
2	K ₂ S ₂ O ₈	57% ^b	37% ^b
3	PhI(OAc) ₂	7% ^b	0% ^b
4	H ₂ O ₂ •urea	0%	0% ^b
5	Benzoquinone	0%	0%
6	AgF	0%	0%
7	AgOAc	0%	0%
8	Cu(OAc) ₂	0%	0%
9	CuCl ₂	0%	0%
10	air	0%	0%

^a % Yield determined based on 1-methyl naphthalene as an internal standard

^b The corresponding *o*-*Oi*-Pr product was also observed by GC and GCMS

Finally, a wide variety of Pd(II) salts were screened for their catalytic activity, as shown in Table 4.3. Catalysts with either acetate or trifluoroacetate ligands were the most effective at this transformation (entries 1-3). Catalysts containing bidentate ligands, such as bipyridine (bipy) (entry 7), and those that are insoluble in *i*-PrOH, such as PdBr₂ (entry 8), did not afford significant amounts of the homocoupled product **24**.

Table 4.3 Catalyst Screen for the Pd-Catalyzed Oxidative Coupling of 2-(*o*-Tolyl)pyridine.



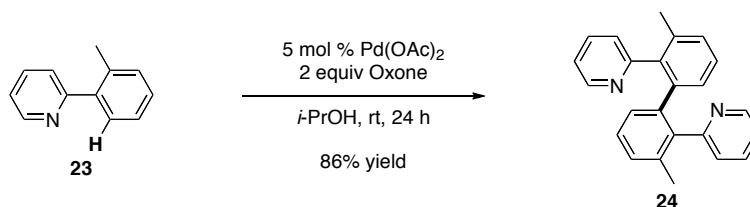
Entry	Catalyst	% Yield (GC) ^a
1	Pd(OAc) ₂	71% ^b
2	Pd(TFA) ₂	60% ^b
3	(IMes)Pd(OAc) ₂	41%
4	PdCl ₂	23%
5	PdCl ₂ (MeCN) ₂	15%
6	PdCl ₂ (PhCN) ₂	8%
7	Pd(bipy)Cl ₂	1%
8	PdBr ₂	0%

^a % Yield determined based on methyl naphthalene as an internal standard

^b The corresponding *o*-OMe product was also observed by GC and GCMS (see ref. 3)

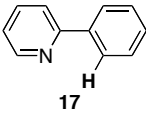
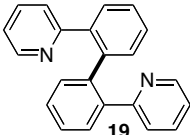
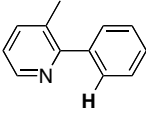
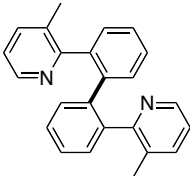
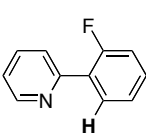
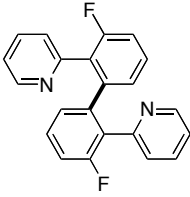
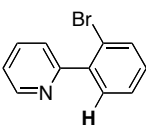
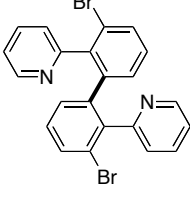
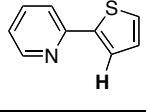
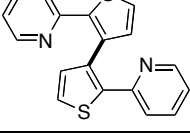
Based on the studies above, the optimized conditions for oxidative coupling of 2-(*o*-tolyl)pyridine (**23**) were determined to be 5 mol % of Pd(OAc)₂, 2 equiv of Oxone[®] in *i*-PrOH at room temperature, which afforded **24** in 86% isolated yield (Scheme 4.21). With the help of Erica Lanni, a first year graduate student who was rotating in our laboratory, the scope of this homocoupling was then investigated using a wide variety of 2-arylpyridine derivatives. As summarized in Table 4.4, the reactions were all highly regioselective, forming exclusively the coupled product with the new C–C bond *ortho* to the directing groups. Interestingly, in the reaction of 2-(α -thiophenyl)pyridine, the ligand-directed C–H activation was faster than electrophilic palladation, as the β,β' isomer was formed exclusively (Table 4.4, entry 5).⁴⁹ This is in notable contrast to other Pd-promoted thiophene oxidative coupling reactions.^{21, 23-25, 27, 50}

Scheme 4.21 Optimized Conditions for the Oxidative Coupling of 2-(*o*-Tolyl)pyridine.



When 2-phenylpyridine (**17**) was subjected to the standard oxidative coupling conditions, the desired dimer **19** was formed in only modest (41%) yield, along with higher oligomers (Table 4.4, entry 1). This undesired oligomerization could be attenuated by placing substituents at the 3-position of the pyridine or the *ortho* position of the aryl ring (Scheme 4.21 and Table 4.4, entries 2-4). The reaction was demonstrated to be tolerant of a variety of functionalities, including OMe, F, Cl, Br, CF₃, as well as benzylic Me groups (Table 4.4, entries 2-4 and Table 4.5). Importantly, the stability of the *ortho*-Br substituent in Table 4.4, entry 4 suggests that the reaction is not proceeding through either an Ullman-type radical coupling or a Pd^{II}/Pd⁰ pathway.¹ In an Ullman coupling mechanism, radical formation should occur faster on an Ar–Br than an Ar–H, while a Pd⁰ intermediate should undergo rapid oxidative addition into the Ar–Br.

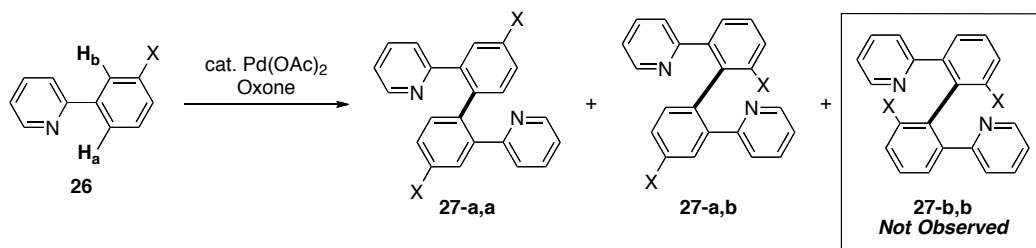
Table 4.4 Substrate Scope of the Oxidative Coupling Reactions.

Entry	Substrate	Product	Yield
1			41%
2			86%
3			82%
4			67%
5			44%

As seen in Table 4.5, substrates containing *meta*-substitution on the aryl ring (**26**) reacted to form two regioisomeric dimers, **27-a,a** and **27-a,b** (Scheme 4.22). The two regioisomers result from selective C–H activation *ortho* to the ligand at either H_a or H_b. The symmetrical isomer (**27-a,a**) results from two C–H activations at H_a, while the unsymmetrical isomer (**27-a,b**) is formed from both H_a and H_b being activated. A third possible isomer (**27-b,b**), which would be the product of both substrates undergoing C–H activation at H_b, was not observed. As shown in Table 4.5, the regioisomers were formed in approximately a 1:1 ratio, which varied slightly based on the nature of the *meta* functional group. The observation of the a,b-isomers was quite surprising, as it is in contrast to our previous work, where H_a was shown to undergo functionalization with very high selectivity (> 20:1 for most functional groups) (Scheme 4.23).^{39, 43, 44, 47, 51} This

lack of regioselectivity suggested that a novel mechanism might be occurring in these oxidative homocoupling reactions.

Scheme 4.22 The Oxidative Coupling of *meta*-Substituted 2-Arylpyridine Derivatives.



Scheme 4.23 High Regioselectivity in the Palladium-Catalyzed Acetoxylation of 2-(*m*-MeO-Phenyl)pyridine.

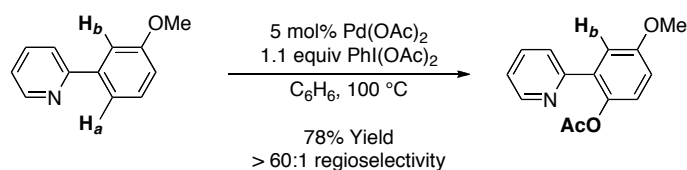
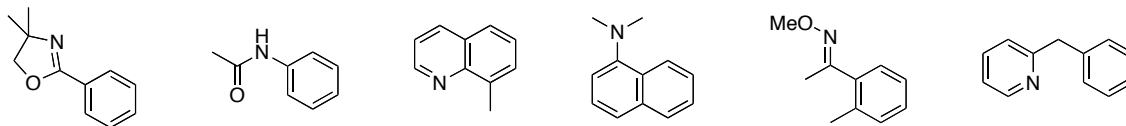


Table 4.5 Oxidative Coupling of *meta*-Substituted 2-Arylpyridines.

Entry	Substrate	<i>a,a</i> -isomer	<i>a,b</i> -isomer	% Yield <i>a,a</i> : <i>a,b</i>
1				76% 1 : 1.3
2				44% 1.7 : 1
3				58% 1.1 : 1

Despite their reactivity in other oxidative functionalization reactions, initial efforts to use other directing groups (*e.g.*, oxime ethers and amides) as well as substrates that would form 6-membered palladacycles or those which would oxidatively couple at sp^3 carbon centers were unsuccessful (Scheme 4.24).^{34, 38, 39, 46, 47, 52, 53} In order to better understand this new methodology, so that the reaction can ultimately be expanded to other substrates, we initiated studies to determine the mechanistic pathway of this transformation.

Scheme 4.24 Substrates that were not Oxidatively Coupled Under Our Reaction Conditions.



4.3 Mechanistic Investigations

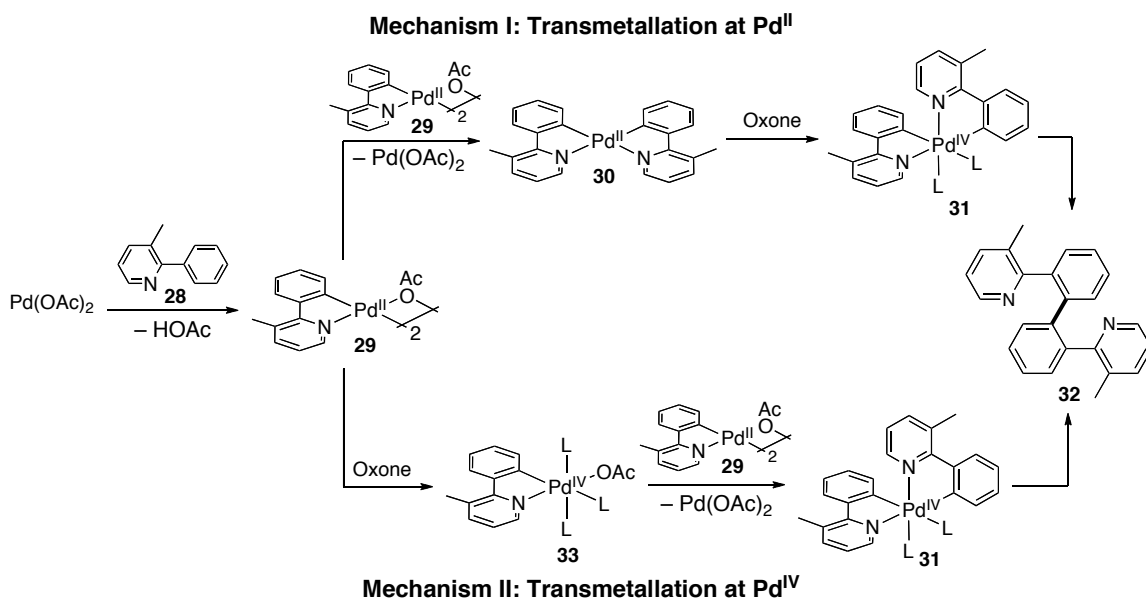
Several results from the reaction optimization and substrate scope studies suggested that a novel mechanism might be occurring in these oxidative homocoupling reactions. The oxidant screenings revealed that strong oxidants were required, as no product was formed in the absence of oxidant or in the presence of weak oxidants (Table 4.2). Importantly, if a Pd^{II}/Pd^0 mechanism were operating in this system, one turnover should occur without the presence of oxidant; furthermore, relatively weak oxidants, such as benzoquinone or air, should promote catalytic turnover. Based on these two pieces of data, we hypothesized that a $Pd^{II/IV}$ mechanism might be operating in this system.

Additionally, the regioselectivity of the oxidative homocoupling reaction on *meta*-substituted 2-arylpyridine derivatives did not reflect what was typically found in ligand-directed C–H activation/oxidative functionalization reactions at Pd^{II} (Scheme 4.22). It is known that stoichiometric C–H activation at Pd^{II} using $Pd(OAc)_2$ occurs with high selectivity for the less sterically hindered C–H bond. As such, the observed activation of

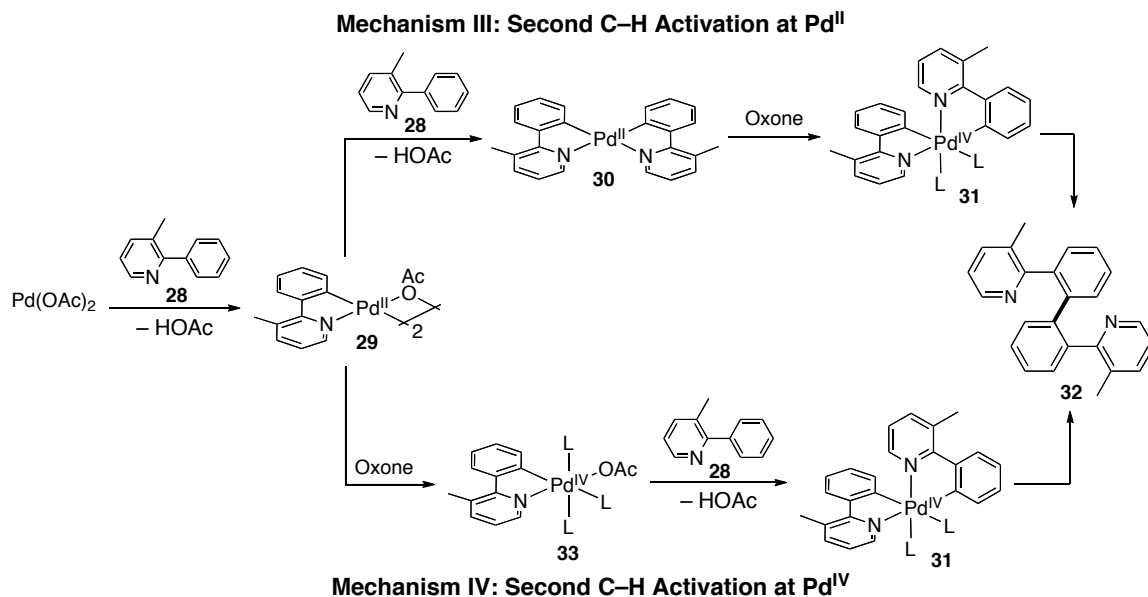
the more hindered C–H bond (H_b) suggested that a different mechanism of C–H activation was occurring and/or that the reactive intermediate was substantially less selective.^{43, 44, 51}

These observations lead us to propose four potential Pd^{II}/Pd^{IV} mechanisms for the Pd-catalyzed oxidative homocoupling reaction (Scheme 4.25 and Scheme 4.26). The first step in each mechanism is the cyclopalladation of **28** to form **29**, which is known to be facile under the reaction conditions. Additionally, under similar reaction conditions the preformed cyclometallated Pd^{II} intermediate (**29**) does lead to formation of the C–C coupled product (*vide infra*). Mechanisms I and II then involve transmetalation, either at Pd^{II} (**29**) or at a transient Pd^{IV} (**33**) species, followed by oxidation/reductive elimination or reductive elimination, respectively, to form the new C–C bond of **32**. Transmetalation reactions between Pd centers are well precedented and are proposed to occur in many oxidative coupling reactions (see Scheme 4.17, page 91).^{1, 4} Conversely, as shown in Scheme 4.26, the reaction could proceed through mechanisms III or IV, which involve two sequential C–H activation steps, both at Pd^{II} or one at Pd^{II} and a second at Pd^{IV}, followed by C–C coupling to afford **32**.

Scheme 4.25 Possible Transmetalation Mechanisms for Pd-Mediated Oxidative Homocoupling.

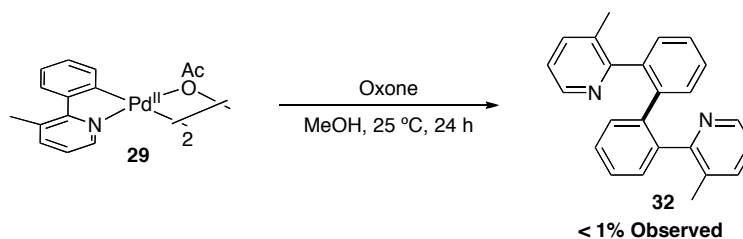


Scheme 4.26 Possible Sequential C–H Activation Mechanisms for Pd-Mediated Oxidative Homocoupling.

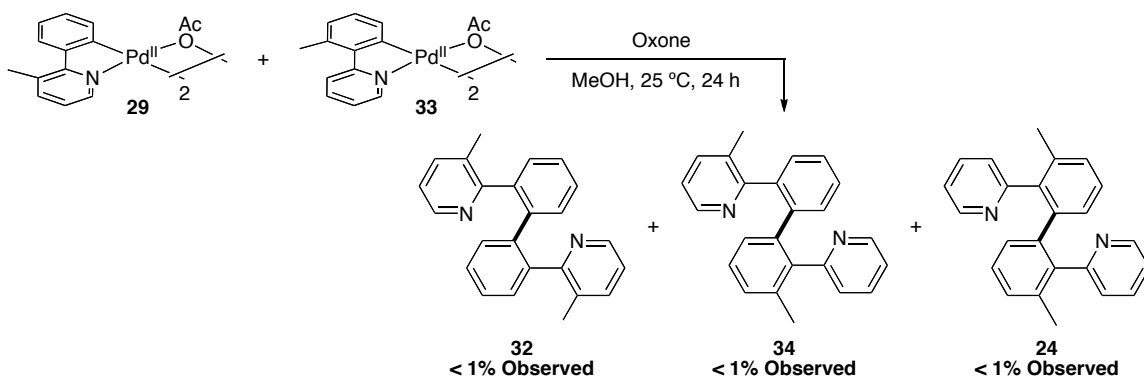


Our initial mechanistic experiments focused on determining if the product was being formed through a transmetalation mechanism. Mechanisms I and II require transmetalation between the cyclometallated 3-methyl-2-phenyl-pyridine intermediate **29** and either Pd^{II} intermediate **29** or Pd^{IV} intermediate **33**, preceding the C–C bond formation. If these mechanisms were operating, we reasoned that the cyclopalladated complex should react in the presence of Oxone[®] to afford **32**. However, less than 1% of product was observed when the cyclopalladated species **29** was subjected to 2 equiv Oxone[®] (Scheme 4.27). Additionally, if the reaction was going through a disproportionation to form the key bisaryl-Pd intermediate, a crossover experiment between two different cyclopalladated species should afford a mixture of all three possible coupled products **32**, **34**, and **24**. However, as shown in Scheme 4.28, less than 1% yield of **32**, **34**, or **24** was obtained when a crossover experiment between two different cyclopalladated species was performed.

Scheme 4.27 Stoichiometric Oxidation of Cyclopalladated Complex **29**.

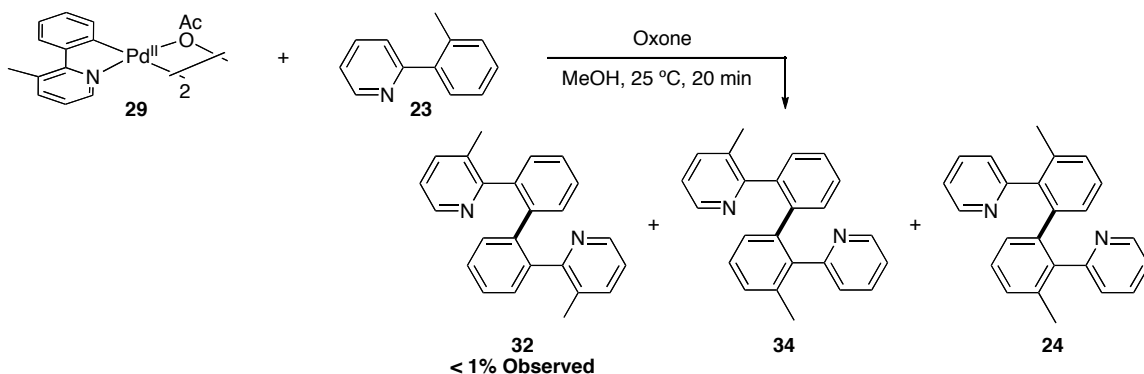


Scheme 4.28 Crossover Experiments Between **29** and **33**.



The experiments in Scheme 4.27 and Scheme 4.28 are dissimilar from our reaction conditions because they do not contain any free substrate. Therefore, in order to definitively rule out a transmetallation mechanism, we needed to carry out a crossover experiment with cyclopalladated 3-methyl-2-phenylpyridine complex **29** and Oxone[®] in the presence of 2-(*o*-tolyl)pyridine **23** (Scheme 4.29). If transmetallation were occurring, one would expect that all three possible coupled products would be formed. Product **32** would form through transmetallation between two molecules of **29** forming two equivalents of Pd(OAc)₂, which could then undergo cyclopalladation of the free 2-(*o*-tolyl)pyridine. Products **34** and **24** would then form through similar transmetallation processes. However, when this reaction was conducted, only **34** and **24** were observed. This result suggests strongly that the reaction is not proceeding through a disproportionation and therefore either mechanism III or IV are likely to be occurring (Scheme 4.29).

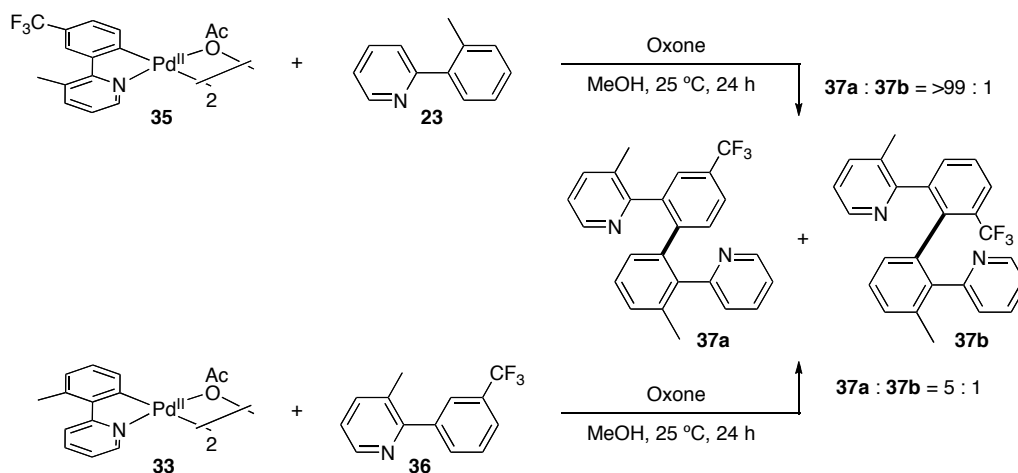
Scheme 4.29 Crossover Experiments Between **29** and Free 2-*o*-tolylpyridine **23**.



The oxidative coupling of *meta*-substituted 2-arylpyridine derivatives (**26**) afforded the dimeric products as a mixture of two of the three possible regioisomers (Scheme 4.22, page 98). Importantly, the isomer (**27-b,b**), resulting from both C–H activation events taking place at H_b, was not observed. This lack of selectivity provides further support for a pathway with two discreet C–H activations steps, as in mechanisms III and IV. Thus, we wanted to distinguish whether the first or second C–H activation was responsible for the low selectivity.

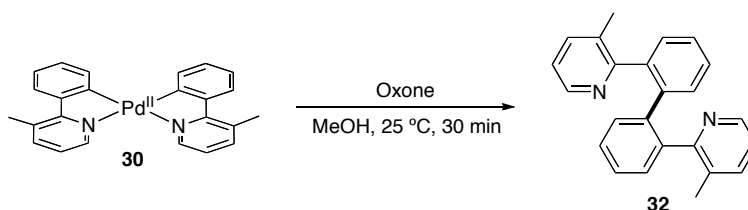
In order to determine the selectivity of each C–H activation event, two stoichiometric reactions were studied, as shown in Scheme 4.30. Complex **35**, which was synthesized as a single regioisomer by cyclometalation with Pd(OAc)₂, reacted with 2-*o*-tolylpyridine (**23**) to afford **37a** as the only observable heterodimer. On the other hand, **33** reacted with 3-methyl-2-(*m*-trifluoromethylphenyl)pyridine (**36**) to afford a 5 : 1 mixture of heterodimers (**37a** : **37b**). This data indicates that the two C–H activation events are discreet and occur with vastly different degrees of selectivity. The second C–H activation occurs with decreased selectivity relative to the first. Again, this evidence suggests that neither mechanism I nor II is occurring, as these would involve transmetalation from a common cyclopalladated intermediate, with defined regioselectivity.

Scheme 4.30 Regioselectivity of the C–H Activation.



Next, we needed to determine whether the second C–H activation was occurring at Pd^{II} (mechanism III) or Pd^{IV} (mechanism IV) (Scheme 4.26). Initially, we were interested in studying the oxidation of **30** under the reaction conditions, as if mechanism III were a catalytic intermediate then dimer **32** should be formed directly. When complex **30**, which was synthesized independently by Allison Dick, was subjected to the reaction conditions with Oxone[®], product **32** was formed cleanly, indicating that **30** provides a viable pathway to the observed product (Scheme 4.31).⁵⁴

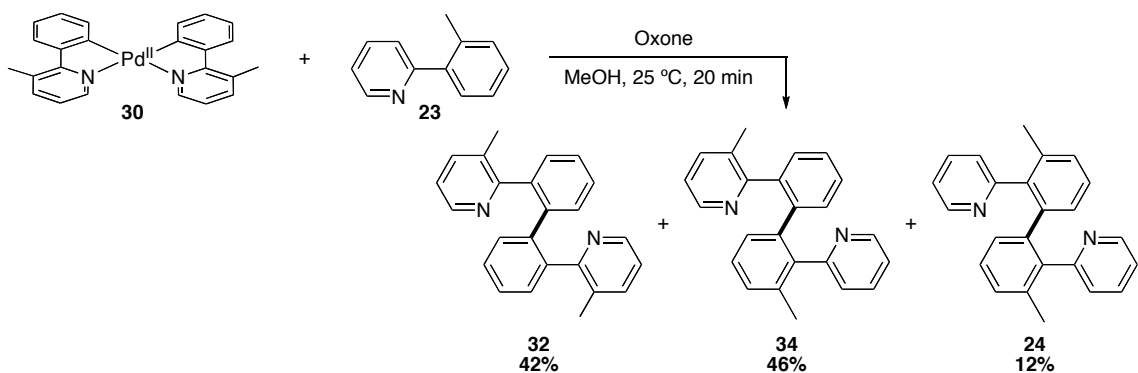
Scheme 4.31 Oxidation of Intermediate **30**.



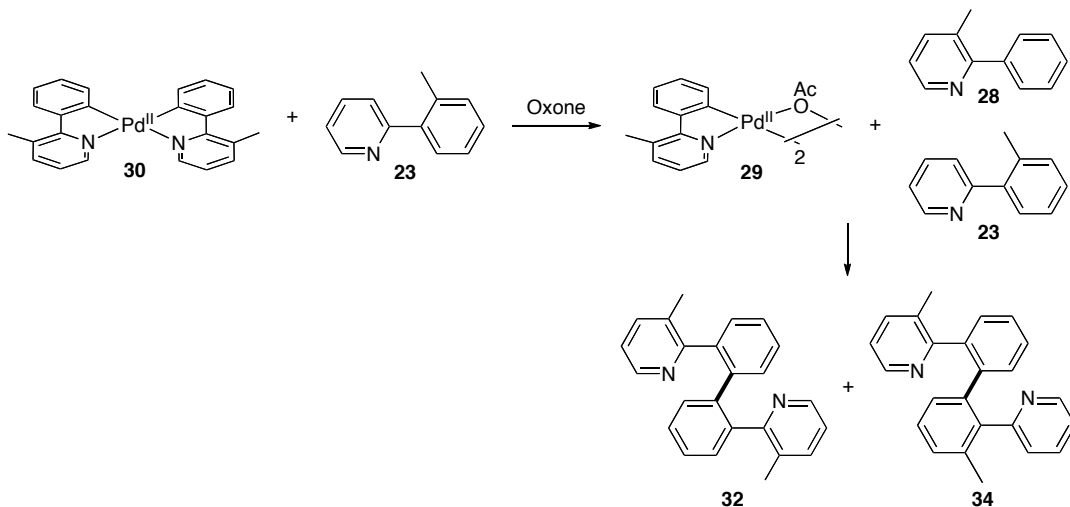
This initial result suggested **30** might be an intermediate in our catalytic cycle. However, when the experiment was run in the presence of free 2-*o*-tolylpyridine, a 42 : 46 : 12 mixture of **32** : **34** : **24** was observed (Scheme 4.32). The crossover product **34** would not be expected if intermediate **30** underwent direct oxidation/reductive elimination to form the dimer. Instead, it appears that the bis-cyclometallated dimer is undergoing an initial protonation by the moderately acidic Oxone[®] (a 0.06 M solution of

Oxone[®] in water has a pH of 1.84), to form **29** and free 3-methyl-2-phenylpyridine (**28**) (Scheme 4.33). Then **29** could react with either **28** or **23** to afford **32** and **34**, respectively. In addition, after the first oxidative coupling reaction with the cyclopalladated ligand, the resulting [Pd^{II}] could catalyze the oxidative homo- and cross-coupling of the free substrates in the reaction (**28** and **23**), providing an additional pathway to **32**, **34**, and **24**. As the protonation of **30** would form **29**, an intermediate common to both mechanisms III and IV, this experiment did not allow us to distinguish between the two possible pathways (Scheme 4.26, page 101).

Scheme 4.32 Reaction of **30** with Oxone[®] in the Presence of Free Substrate **23**



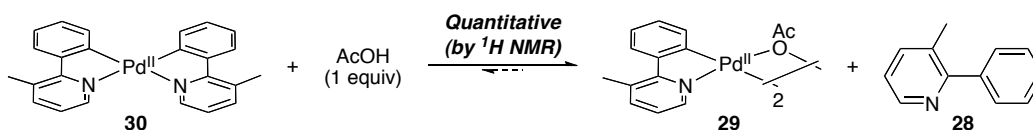
Scheme 4.33 Explanation for the Formation of the Crossover Product **34** in Scheme 4.32



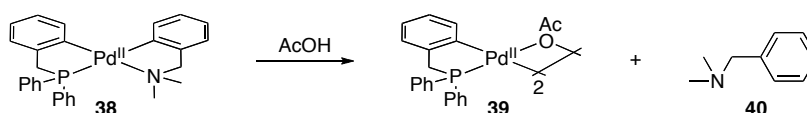
The bis-cyclometallated Pd^{II} complex **30** is not stable under the reaction conditions; however, it could still be an intermediate formed transiently prior to

oxidation/reductive elimination. Therefore, we needed to design a different experiment to determine whether mechanism III or IV was operative (Scheme 4.26, page 101). We reasoned that if **30** were forming transiently under the reaction conditions, it should be in equilibrium with the cyclopalladated complex **29**. To study this equilibrium, **30** was subjected to 1 equivalent of AcOH, which would be present in the catalytic reaction after C–H activation. One of the Pd–C bonds was quantitatively protonated, forming an equivalent of cyclometallated **29** and free substrate **28**. This experiment clearly established that the equilibrium between **30** and **29** lies far to the right in our system (Scheme 4.34). As seen in Scheme 4.35, this is consistent with prior studies by Ryabov, who showed that **38** also reacts instantaneously with AcOH to form the cyclopalladated palladium acetate dimer (**39**) and free benzyl amine (**40**).^{49, 55} Therefore, if mechanism III were operative, there would have to be a rapid equilibrium between **29** and the transient intermediate **30**, followed by trapping of the **30** with Oxone[®] to afford **32**.

Scheme 4.34 Reaction of **30** with AcOH.



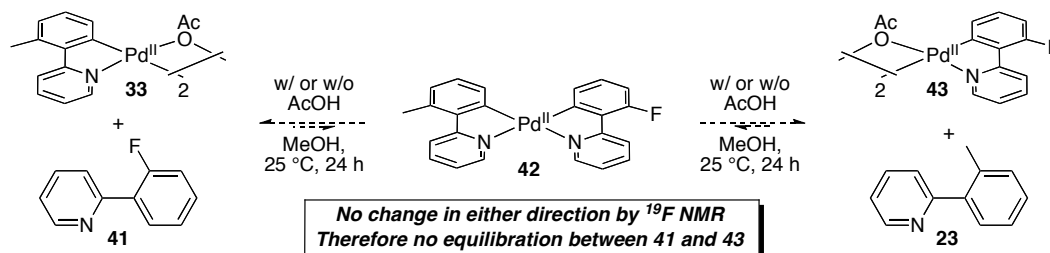
Scheme 4.35 Facile Protonation of Complex **38**



If mechanism III were operative, **30** would be a short-lived, unobservable intermediate under the reaction conditions. The accessibility of intermediate **30** can be probed by studying the equilibration between cyclometallated intermediates (**33** and **42**) and a free, differentially substituted aryl pyridine (**41** or **23** in Scheme 4.36). If **42** formed fleetingly in the reaction between **33** and **41**, it should be immediately protonated by AcOH to form **43** and **23**. Consequently, there should be equilibration between the two cyclopalladated species. However, attempts to approach this equilibrium from either side resulted in no observable reaction at rt after 24 hours. No evidence of equilibration was

observed until the reaction was heated above 100 °C or run in neat AcOH. This result shows that **42** is not forming under the reaction conditions (at rt), and thus provides significant evidence that mechanism III is not operative in this system.

Scheme 4.36 Probing Equilibration between **41** and **43** via the Transient Intermediate **42**.



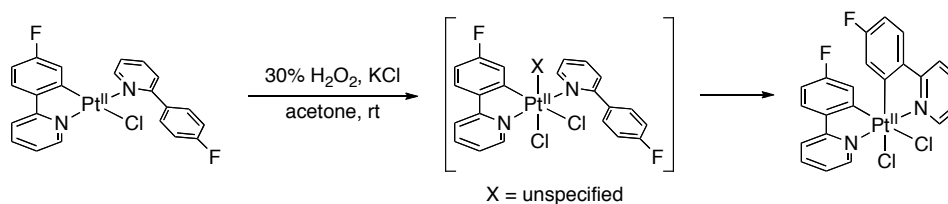
Mechanism IV (Scheme 4.26, page 101), involves first a C–H activation at Pd^{II} followed by an unprecedented C–H activation at Pd^{IV}. It is the only reaction pathway that is consistent with all of the experimental results. A strong oxidant is required to oxidize Pd^{II} to Pd^{IV}, there is no transmetalation from one Pd species to another, and the formation of the bis-cyclopalladated Pd^{II} is not required. Finally, the second C–H activation occurs at Pd^{IV}, which is consistent with its lack of regioselectivity. Pd^{IV} is more electrophilic than Pd^{II}; therefore, it is expected to be more reactive, and as reactivity increases, selectivity often decreases. Importantly, the differences in reactivity between Pd^{II} and Pd^{IV} towards C–H activation have not been assessed previously, as this was the first report suggesting such a mechanism.

4.4 Subsequent Work

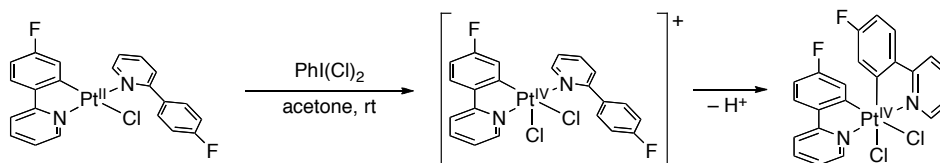
Although direct observation of C–H activation at Pd^{IV} remains unprecedented, there are examples of C–H activation at Pt^{IV}. Platinum, being directly below palladium on the periodic table, has similar reactivity and forms more stable, high oxidation complexes than Pd; for these reasons, Pt^{IV} is often used as a model system for Pd^{IV} complexes. Subsequent to this work, the cycloplatination of 2-phenylpyridine derivatives was demonstrated at Pt^{IV} (Scheme 4.37).^{56, 57} The authors propose that initial oxidation from Pt^{II} to Pt^{IV} occurs with H₂O₂ or PhICl₂ followed by spontaneous C–H activation. This is supported by the fact that similar complexes, lacking a ligand that can be

cyclometallated, undergo oxidation to Pt^{IV} in a similar fashion to form a trichloride Pt^{IV} complex. The authors propose that the C–H activation occurs spontaneously due to the cationic nature of the metal directly following oxidation and the increased electrophilicity of the Pt^{IV} relative to Pt^{II} (Scheme 4.38). Further, they propose that the cycloplatination of the pendant 2-(*p*-fluorophenyl)pyridine is faster than the association of a Cl^- anion.⁵⁷

Scheme 4.37 C–H Activation at Pt^{IV} .⁵⁶

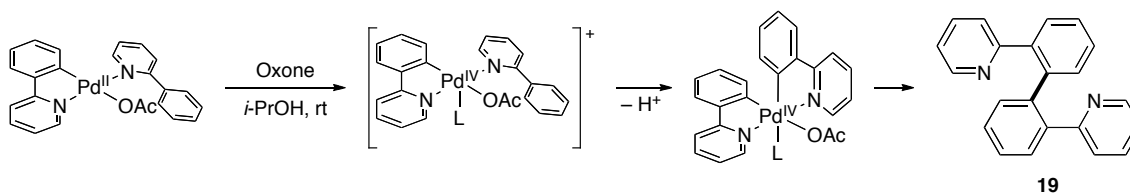


Scheme 4.38 C–H Activation at a Cationic Pt^{IV} is Faster than Ligand Association of Cl^- .⁵⁷



A similar mechanism for the second C–H activation could be occurring in our oxidative homocoupling reactions. The 2-arylpiperidine could be bound to the Pd^{II} intermediate, and, upon oxidation, the cyclopalladation at the cationic Pd^{IV} could be faster than association of the *i*-PrO⁻ ligand. Finally, C–C bond-forming reductive elimination from this intermediate would afford **19** (Scheme 4.39).

Scheme 4.39 Possible Mechanism for the Second C–H Activation at Pd^{IV} .



4.5 Conclusions

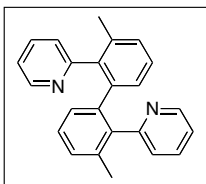
We have demonstrated that palladium can catalyze the oxidative homocoupling of 2-arylpyridine derivatives with excellent selectivity for functionalization *ortho* to the directing group. Additionally, we have provided significant evidence that the reaction is occurring through an unprecedented mechanism involving two sequential C–H activation steps: first, a cyclopalladation at Pd^{II}, followed by oxidation to Pd^{IV}, and a second cyclopalladation at Pd^{IV}.

4.6 Experimental Procedure

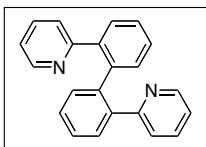
General Procedures: NMR spectra were obtained on a Varian Inova 500 (499.90 MHz for ¹H; 125.70 MHz for ¹³C), a Varian Inova 400 (399.96 MHz for ¹H; 100.57 MHz for ¹³C; 376.34 MHz for ¹⁹F), or a Varian Mercury 300 (300.07 MHz for ¹H; 75.45 MHz for ¹³C NMR; 282.35 MHz for ¹⁹F) spectrometer. ¹H and ¹³C NMR chemical shifts are reported in parts per million (ppm) relative to TMS, with the residual solvent peak used as an internal reference; ¹⁹F NMR are referenced based on the residual solvent peak in the ¹H NMR spectrum. Multiplicities are reported as follows: singlet (s), doublet (d), doublet of doublets (dd), doublet of doublet of doublets (ddd), doublet of triplets (dt), doublet of quartets (dq), triplet (t), triplet of doublets (td), quartet (q), quartet of doublets (qd), and multiplet (m). Unless otherwise indicated, the ¹H and ¹³C NMR spectra were recorded at room temperature.

Materials and Methods: 2-Phenylpyridine was obtained from commercial sources and used as received. 2-*o*-Bromophenylpyridine was prepared by palladium-catalyzed *ortho*-bromination of 2-phenylpyridine.³⁸ The remainder of the arylpyridine/heteroarylpyridine substrates were prepared by Suzuki cross coupling between 2-bromopyridine or 2-bromo-3-methylpyridine and the corresponding boronic acid.⁵⁸ Oxone was obtained from Acros and used without further purification. Pd(OAc)₂ was obtained from Pressure Chemical or Frontier Scientific and used as received. Solvents were obtained from Fisher Scientific and used without purification. Flash chromatography was performed on EM Science

silica gel 60 (0.040-0.063 mm particle size, 230-400 mesh) and thin layer chromatography was performed on Merck TLC plates pre-coated with silica gel 60 F₂₅₄. Gas chromatographs were obtained on a Shimadzu 17A using a Restek Rtx®-5 (Crossbond 5% diphenyl – 95% dimethyl polysiloxane; 15 m, 0.25 mmID, 0.25 mmID, 0.25 μm df) column, the method injects the sample at 100 °C and ramps at 15 °C/min to 270 °C and holds for 20 min.



Product 24. 2-*o*-Tolylpyridine (**23**) (100 mg, 0.59 mmol, 1 equiv), Oxone (710 mg, 1.15 mmol, 2.0 equiv) and Pd(OAc)₂ (6.5 mg, 0.029 mmol, 5.0 mol %) were combined in *i*-PrOH (5.0 mL) in a 20 mL scintillation vial equipped with a Teflon stirbar. The reaction mixture was stirred at room temperature for 17 h. GC analysis of the crude reaction mixture showed a >100 : 1 ratio of **24** to 2-*o*-tolylpyridine as well as traces of the *o*-isopropylether product. The resulting pale yellow suspension was diluted with ethyl acetate (100 mL) and washed three times with 10% Na₂SO₃ and one time with brine. The organic layer was dried over MgSO₄ and concentrated, and the resulting orange oil was purified by chromatography on silica gel (R_f = 0.4 in 50% hexanes/50% ethyl acetate). Product **24** was isolated as a white solid (85 mg, 86% yield, mp = 152.4-154.5 °C). ¹H NMR (400 MHz, DMSO-*d*₆, 60 °C): δ 8.53 (ddd, *J* = 4.8, 1.6, 0.8 Hz, 2H), 7.63 (td, *J* = 7.7, 1.7 Hz, 2H), 7.37 (d, *J* = 7.6 Hz, 2H), 7.16 (ddd, *J* = 7.6, 5.1, 1.1 Hz, 2H), 7.06 (d, *J* = 7.6 Hz, 2H), 6.94 (t, *J* = 7.8 Hz, 2H), 6.68 (d, *J* = 7.2 Hz, 2H), 1.99 (s, 6H); ¹³C NMR (75 MHz, 59 °C, DMSO-*d*₆): δ 158.55, 148.28, 139.63, 139.57, 135.30, 135.18, 128.14, 128.04, 126.01, 125.13, 121.08, 19.79. HRMS ESI with Formic Acid (*m/z*): [M+H]⁺ calcd for C₂₄H₂₁N₂, 337.1705; found, 337.1695.



Product 19. 2-Phenylpyridine (**17**) (82 μ L, 0.57 mmol, 1 equiv), Oxone (390 mg, 0.63 mmol, 1.1 equiv) and Pd(OAc)₂ (6.5 mg, 0.029 mmol, 5.0 mol %) were combined in MeOH (5.0 mL) in a 20 mL scintillation vial equipped with a Teflon stirbar. The reaction mixture was stirred at room temperature for 17 h. GC analysis of the crude reaction mixture showed an \sim 2.4 : 1 ratio of **19** to 2-phenylpyridine as well as traces of the *o*-methylether product. The resulting pale yellow suspension was diluted with ethyl acetate (100 mL) and washed three times with 10% Na₂SO₃ and one time with brine. The organic layer was dried over MgSO₄ and concentrated, and the resulting orange oil was purified by chromatography on silica gel (R_f = 0.1 in 50% hexanes/50% ethyl acetate). Product **19** was isolated as a white solid (36 mg, 41% yield, mp = 136-136.5 °C). Note: electrospray mass spectrometry of the crude reaction mixture showed the presence of further oligomers of 2-phenylpyridine (predominantly $n = 3$ and $n = 4$). ¹H NMR (400 MHz, acetone-*d*₆): δ 8.38 (ddd, $J = 4.8, 1.6, 0.8$ Hz, 2H), 7.60 (dd, $J = 3.5, 1.4$ Hz, 2H), 7.47 (td, $J = 7.7, 1.9$ Hz, 2H), 7.37 (td, $J = 7.6, 1.2$ Hz, 2H), 7.27 (td, $J = 7.6, 1.5$ Hz, 2H), 7.18 (dt, $J = 8.0, 1.1$ Hz, 2H), 7.12–7.05 (multiple peaks, 4H); ¹³C NMR (100 MHz, acetone-*d*₆): δ 159.70, 149.88, 141.48, 141.06, 136.19, 132.22, 131.07, 128.71, 127.95, 125.29, 122.17. HRMS ESI with Formic Acid (m/z): [M+H]⁺ calcd for C₂₂H₁₇N₂, 309.1392; found, 309.1385.

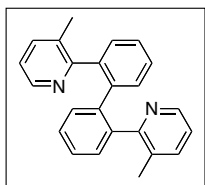


Table 4.4, **entry 2.** 3-Methyl-2-phenylpyridine (95 mg, 0.58 mmol, 1 equiv), Oxone (710 mg, 1.15 mmol, 2.0 equiv) and Pd(OAc)₂ (6.5 mg, 0.029 mmol, 5.0 mol %) were combined in MeOH (5.0 mL) in a 20 mL scintillation vial equipped with a Teflon stirbar. The reaction mixture stirred at room temperature for 17 h. GC analysis of the crude reaction mixture showed a >100 : 1 ratio of dimer to 2-phenyl-3-methylpyridine as well as traces of the *o*-methylether product. The resulting pale yellow suspension was diluted with ethyl acetate (100 mL) and washed three times with 10% Na₂SO₃ and one time with brine. The organic layer was dried over MgSO₄ and concentrated, and the resulting

orange oil was purified by chromatography on silica gel ($R_f = 0.07$ in 50% hexanes/50% ethyl acetate). It was isolated as a white solid (83 mg, 86% yield, mp = 178.4-179.3 °C). ^1H NMR (400 MHz, DMSO- d_6 , 59 °C): δ 8.17 (d, $J = 4.5$ Hz, 2H), 7.48 (d, $J = 7.2$ Hz, 2H), 7.26–7.06 (multiple peaks, 10H), 1.92 (s, 6H); ^{13}C NMR (75 MHz, DMSO- d_6 , 59 °C): δ 158.27, 145.34, 139.25, 139.13, 137.24, 131.23, 131.19, 129.40, 126.37, 125.87, 121.48, 18.78. HRMS ESI with Formic Acid (m/z): $[\text{M}+\text{H}]^+$ calcd for $\text{C}_{24}\text{H}_{21}\text{N}_2$, 337.1705; found, 337.1691.

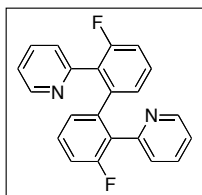


Table 4.4, **entry 3**. 2-(*o*-Fluorophenyl)pyridine (100 mg, 0.58 mmol, 1 equiv), Oxone (710 mg, 1.15 mmol, 2.0 equiv) and Pd(OAc) $_2$ (6.5 mg, 0.029 mmol, 5.0 mol %) were combined in MeNO $_2$ (5.0 mL) in a 20 mL scintillation vial equipped with a Teflon stirbar. The reaction mixture stirred at 60 °C for 17 h. GC analysis of the crude reaction mixture showed a >100 : 1 ratio of dimer to 2-*o*-fluorophenylpyridine. The resulting pale yellow suspension was diluted with ethyl acetate (100 mL) and washed three times with 10% Na $_2$ SO $_3$ and one time with brine. The organic layer was dried over MgSO $_4$ and concentrated, and the resulting orange oil. was purified by chromatography on silica gel ($R_f = 0.4$ in 50% hexanes/50% ethyl acetate). The product was isolated as a white solid (82 mg, 82% yield, mp = 126.5-127.2 °C). ^1H NMR (300 MHz, acetone- d_6): δ 8.49 (ddd, $J = 5.1, 1.8, 0.9$ Hz, 2H), 7.65 (td, $J = 7.5, 1.5$ Hz, 2H), 7.50 (dd, $J = 7.8, 1.2$ Hz, 2H), 7.22-7.05 (multiple peaks, 6H), 6.80 (dd, $J = 7.4, 1.4$ Hz, 2H); ^{13}C NMR (75 MHz, acetone- d_6): δ 160.96 (d, $J_{\text{CF}} = 234.9$ Hz), 154.64, 149.86, 142.77 (t, $J_{\text{CF}} = 2.9$ Hz), 136.51, 129.61 (d, $J_{\text{CF}} = 8.8$ Hz), 129.45 (d, $J_{\text{CF}} = 15.4$ Hz), 127.79 (d, $J_{\text{CF}} = 3.6$ Hz), 127.00 (d, $J_{\text{CF}} = 2.1$ Hz), 123.01, 115.14 (d, $J_{\text{CF}} = 22.7$ Hz); ^{19}F NMR (282 MHz, acetone- d_6): δ -117.78 (dd, $J = 9.3, 5.9$ Hz). HRMS ESI with Formic Acid (m/z): $[\text{M}+\text{H}]^+$ calcd for $\text{C}_{22}\text{H}_{15}\text{F}_2\text{N}_2$, 345.1203; found, 345.1190.

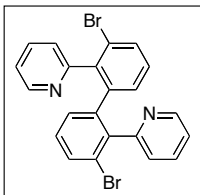


Table 4.4, **entry 2**. 2-(2-Bromophenyl)pyridine (135 mg, 0.58 mmol, 1 equiv), Oxone (710 mg, 1.15 mmol, 2.0 equiv) and Pd(OAc)₂ (6.5 mg, 0.029 mmol, 5.0 mol %) were combined in MeOH (5.0 mL) in a 20 mL scintillation vial equipped with a Teflon stirbar. The reaction mixture was stirred at room temperature for 17 h. The resulting pale yellow suspension was diluted with ethyl acetate (100 mL) and washed three times with 10% Na₂SO₃ and one time with brine. The organic layer was dried over MgSO₄ and concentrated, and the resulting orange oil was purified by chromatography on silica gel (R_f = 0.56 in 50% hexanes/50% ethyl acetate). It was isolated as a white solid (91 mg, 67% yield, mp = 193.1-195.2 °C). ¹H NMR (300 MHz, DMSO-*d*₆, 50 °C): δ 8.52 (d, *J* = 4.2 Hz, 2H), 7.70 (td, *J* = 7.5, 0.9 Hz, 2H) 7.51 (dd, *J* = 7.8, 1.2 Hz, 2H), 7.44 (d, *J* = 7.5 Hz, 2H), 7.21 (ddd, *J* = 7.5, 4.8, 1.2 Hz, 2H), 7.02 (t, *J* = 7.8 Hz, 2H), 6.93 (d, *J* = 7.5, 2H); ¹³C NMR (75 MHz, DMSO-*d*₆, 50 °C): δ 157.35, 148.39, 140.81, 140.12, 135.63, 131.22, 129.71, 128.24, 125.29, 122.25, 122.15. HRMS ESI with Formic Acid (m/z): [M+H]⁺ calcd for C₂₂H₁₅Br₂N₂, 464.9602; found, 464.9592.

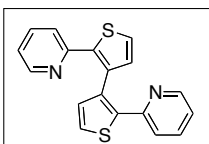


Table 4.4, **entry 2**. 2-(2-Thiophenyl)pyridine (175 mg, 1.1 mmol, 1 equiv), Oxone (1.3 g, 2.1 mmol, 1.9 equiv) and Pd(OAc)₂ (24 mg, 0.11 mmol, 10 mol %) were combined in trifluoroethanol (10 mL) in a 20 mL scintillation vial equipped with a Teflon stirbar. The reaction mixture was stirred at room temperature for 17 h. GC analysis of the crude reaction mixture showed an ~ 1.3 : 1 ratio of dimer to 2-(2-thiophenyl)pyridine. The reaction was quenched with 10% Na₂SO₃ (7 mL) and diluted with ethyl acetate (20 mL). The phases were separated, and the aqueous layer was extracted with ethyl acetate (3 x 20 mL). The combined organic layers were then washed with 10% Na₂SO₃ (3 x 20 mL) and one time with brine. The organic layer was dried over MgSO₄ and concentrated, and the

resulting oil was purified by chromatography on silica gel ($R_f = 0.26$ in 30% ethyl acetate/70% hexanes). It was isolated as a pale yellow solid (76 mg, 44% yield, mp = 171.0-171.6 °C). ^1H NMR (300 MHz, $\text{DMSO-}d_6$) δ 8.48 (ddd, $J = 4.8, 1.8, 0.9$ Hz, 2H), 7.78 (d, $J = 5.4$, 2H), 7.54 (td, $J = 7.8, 1.8$ Hz, 2H), 7.17 (ddd, 7.5, 4.8, 1.0 Hz, 2H), 7.03 (d, $J = 5.4$ Hz, 2H), 6.92 (d, $J = 8.1$ Hz, 2H). ^{13}C NMR (75 MHz, $\text{DMSO-}d_6$): δ 151.43, 149.42, 140.41, 136.78, 134.01, 130.88, 128.50, 122.29, 119.05. HRMS ESI with Formic Acid (m/z): $[\text{M}+\text{H}]^+$ calcd for $\text{C}_{18}\text{H}_{13}\text{N}_2\text{S}_2$, 321.0520; found, 321.0516.

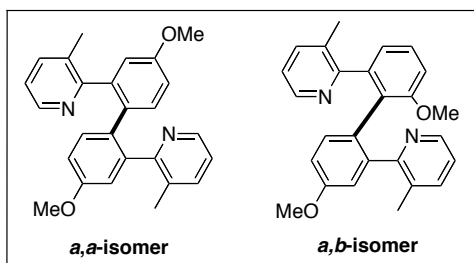


Table 4.5, **entry 1**. 3-Methyl-2-(3-methoxyphenyl)pyridine (115 mg, 0.58 mmol, 1 equiv), Oxone (710 mg, 1.15 mmol, 2.0 equiv) and $\text{Pd}(\text{OAc})_2$ (6.5 mg, 0.029 mmol, 5.0 mol %) were combined in *i*-PrOH (5.0 mL) in a 20 mL scintillation vial equipped with a Teflon stirbar. The reaction mixture was stirred at room temperature for 17 h. The resulting pale orange suspension was diluted with ethyl acetate (100 mL) and washed three times with 10% Na_2SO_3 and one time with brine. The organic layer was dried over MgSO_4 and concentrated, and the resulting orange oil was purified by chromatography on silica gel (R_f for **a,a-isomer** = 0.27 in 95% ethyl acetate/5% methanol; R_f for **a,b-isomer** = 0.04 in 95% ethyl acetate/5% methanol). Products **a,a-** and **a,b-isomers** were isolated as white solids (87 mg, 76% combined yield, ratio of **a,a** : **a,b** = 1 : 1.3).

Characterization data for a,a: mp = 61.2-62.6 °C. ^1H NMR (400 MHz, $\text{DMSO-}d_6$, 50 °C): δ 8.20 (d, $J = 4.2$ Hz, 2H), 7.49 (d, $J = 7.5$ Hz, 2H), 7.11 (dd, $J = 7.7, 4.7$ Hz, 2H), 6.93 (d, $J = 8.7$ Hz, 2H), 6.72-6.64 (multiple peaks, 4H), 3.69 (s, 6H), 1.97 (s, 6H); ^{13}C NMR (100 MHz, $\text{DMSO-}d_6$, 50 °C): δ 158.41, 156.96, 145.50, 140.47, 137.35, 132.39, 131.28, 128.06, 121.69, 114.60, 112.46, 54.85, 18.94. HRMS ESI with Formic Acid (m/z): $[\text{M}+\text{H}]^+$ calcd for $\text{C}_{26}\text{H}_{25}\text{N}_2\text{O}_2$, 397.1916; found, 397.1919.

Characterization data for a,b: mp: begins to sublime at 158 °C and then decomposes at 202.8-206.8 °C. ¹H NMR (400 MHz, DMSO-*d*₆, 48 °C): δ 8.20 (d, *J* = 3.6 Hz, 1H), 8.00 (d, *J* = 4.5 Hz, 1H), 7.51 (d, *J* = 7.8 Hz, 1H), 7.41 (d, *J* = 7.5 Hz, 1H), 7.20–7.12 (multiple peaks, 2H), 7.09–7.01 (multiple peaks, 2H), 6.79 (d, *J* = 8.1 Hz, 1H), 6.72 (dd, *J* = 8.4, 2.8 Hz, 1H), 6.66–6.64 (multiple peaks, 2H), 3.69 (s, 3H), 3.41 (s, 3H), 1.97 (s, 3H), 1.92 (s, 3H); ¹³C NMR (75 MHz, DMSO, 55 °C): δ 158.48, 158.12, 156.85, 156.52, 144.97, 144.74, 141.15, 140.74, 137.28, 137.12, 134.12, 131.50, 131.00, 128.54, 127.44, 126.87, 121.50, 121.35, 121.23, 114.36, 111.64, 109.66, 54.80, 54.69, 19.05, 18.72. HRMS ESI with Formic Acid (*m/z*): [M+H]⁺ calcd for C₂₆H₂₅N₂O₂, 397.1916; found, 397.1913.

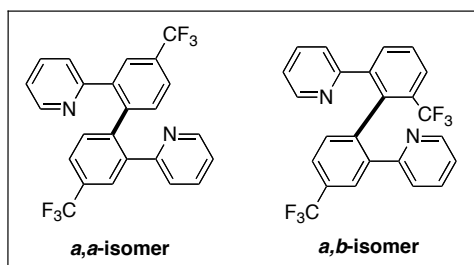


Table 4.5, **entry 2.** 2-(*m*-Trifluoromethylphenyl)pyridine (129 mg, 0.58 mmol, 1 equiv), Oxone (710 mg, 1.1 mmol, 2 equiv) and Pd(OAc)₂ (6.5 mg, 0.029 mmol, 5 mol %) were combined in MeOH (5 mL) in a 25 mL round bottom flask equipped with a Teflon stirbar. The reaction mixture was stirred at room temperature for 17 h. GC analysis of the crude reaction mixture showed an ~1.3 :1 ratio of **a,a** + **a,b** : 2-(*m*-trifluoromethylphenyl)pyridine and an ~2.5 : 1 ratio of **a,a** + **a,b** : the *o*-methylether product. The reaction was quenched with 10% Na₂SO₃ (15 mL) and diluted with ethyl acetate (15 mL). The phases were separated, and the aqueous layer was extracted with ethyl acetate (3 x 15 mL). The combined organic layers were then washed with 10% Na₂SO₃ (3 x 15 mL) and one time with brine. The organic layer was dried over MgSO₄ and concentrated, and the resulting oil was purified by chromatography on silica gel (*R_f* for **a,a** = 0.6 in 50% ethyl acetate/ 50% hexanes; *R_f* for **a,b** = 0.2 in 50% ethyl acetate/50% methanol). Product **a,a** was isolated as a white solid and **a,b** was isolated as white semi-solid (58 mg, 44% combined yield, ratio of **7-a** : **7-b** = 1.7 : 1).

Characterization data for a,a: mp = 132.5-135.8 °C. ¹H NMR (400 MHz, acetone-*d*₆): δ 8.39 (ddd, *J* = 4.8, 1.8, 1.0 Hz, 2H), 7.92 (dd, *J* = 1.2, 0.4 Hz, 2H), 7.70 (ddd, *J* = 8.0, 2.0, 0.8 Hz, 2H), 7.58 (td, *J* = 7.7, 1.9 Hz, 2H), 7.40 (d, *J* = 8.0 Hz, 2H), 7.26 (dt, *J* = 7.9, 1.1 Hz, 2H), 7.20 (ddd, *J* = 7.6, 4.8, 1.2 Hz, 2H); ¹⁹F NMR (376 MHz, acetone-*d*₆): δ -62.96 (s); ¹³C NMR (100 MHz, acetone-*d*₆): δ 157.59, 150.23, 144.32, 141.78, 136.93, 133.03, 130.27 (q, *J*_{CF} = 32.2 Hz), 127.75 (q, *J*_{CF} = 4.4 Hz) 125.57 (q, *J*_{CF} = 3.7 Hz), 125.30 (q, *J*_{CF} = 269.8 Hz), 125.25, 123.16; HRMS ESI with Formic Acid (m/z): [M+H]⁺ calcd for C₂₄H₁₅F₆N₂, 445.1139; found, 445.1136.

Characterization data for a,b: ¹H NMR (400 MHz, DMSO-*d*₆, 75 °C): δ 8.35 (d, *J* = 4.0 Hz, 1H), 8.25 (d, *J* = 4.8 Hz, 1H), 7.89 (s, 1H), 7.85 (d, *J* = 7.6 Hz, 1H), 7.75-7.66 - (multiple peaks, 3H), 7.57-7.46 (multiple peaks, 3H), 7.17 (dd, *J* = 7.4, 4.6 Hz, 1H), 7.13-7.08 (multiple peaks, 2H), 6.93 (d, *J* = 8.0 Hz, 1H); ¹⁹F NMR (376 MHz, DMSO-*d*₆, 75 °C): δ -55.92 (s), -61.21 (s); ¹³C NMR (100 MHz, DMSO-*d*₆, 75 °C): δ 156.51, 155.12, 148.42, 148.06, 141.64, 140.07, 139.30, 136.77 (app. d, *J* = 1.0 Hz), 135.57, 135.23, 133.31, 132.60, 128.4 (q, *J*_{CF} = 31.9 Hz), 128.13, 127.58 (q, *J*_{CF} = 28.5 Hz), 125.8 (q, *J*_{CF} = 5.1 Hz), 125.20 (app. d, *J*_{CF} = 2.9), 123.69 (q, *J*_{CF} = 272.4 Hz), 123.68, 123.60 (q, *J*_{CF} = 274.8 Hz) 123.1 (app. d, *J*_{CF} = 2.9), 122.81, 121.78, 121.48. HRMS ESI with Formic Acid (m/z): [M+H]⁺ calcd for C₂₄H₁₅F₆N₂, 445.1139; found, 445.1140.

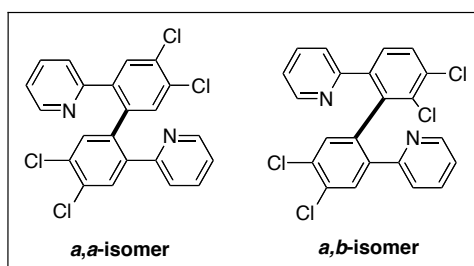
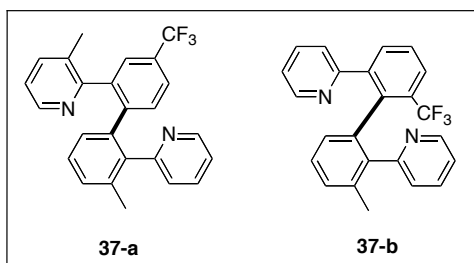


Table 4.5, **entry 3.** 2-(3,4-Dichlorophenyl)pyridine (130 mg, 0.58 mmol, 1 equiv), Oxone (710 mg, 1.15 mmol, 2.0 equiv) and Pd(OAc)₂ (6.5 mg, 0.029 mmol, 5.0 mol %) were combined in MeOH (5.0 mL) in a 20 mL scintillation vial equipped with a Teflon stirbar. The reaction mixture was stirred at room temperature for 17 h. The resulting pale orange suspension was diluted with ethyl acetate (100 mL) and washed three times with 10%

Na₂SO₃ and one time with brine. The organic layer was dried over MgSO₄ and concentrated, and the resulting orange oil was purified by chromatography on silica gel (*R_f* for **a,a** = 0.40 in 50% hexanes/50% ethyl acetate; *R_f* for **a,b** = 0.29 in 50% hexanes/50% ethyl acetate). Products **a,a** and **a,b** were isolated as white solids (75 mg, 58% combined yield, ratio of **a,a** : **a,b** = 1.1 : 1).

Characterization data for a,a. mp = 201.6-202.6 °C. ¹H NMR (400 MHz, CDCl₃): δ 8.32 (dd, *J* = 4.9, 1.7, 0.7 Hz, 2H), 7.62 (s, 2H), 7.50 (s, 2H), 7.43 (td, *J* = 7.7, 1.7 Hz, 2H), 7.10 (ddd, *J* = 7.6, 4.8, 1.2 Hz, 2H), 6.76 (d, *J* = 8.0 Hz, 2H); ¹³C NMR (100 MHz, CDCl₃): δ 155.28, 149.24, 139.41, 137.44, 135.99, 132.85, 132.69, 132.47, 131.95, 124.01, 122.12. HRMS ESI with Formic Acid (*m/z*): [M+H]⁺ calcd for C₂₂H₁₃N₂Cl₄, 444.9833; found, 444.9829.

Characterization data for a,b. mp = 155.9-157.0 °C. ¹H NMR (400 MHz, CDCl₃): δ 8.39-8.37 (multiple peaks, 2H), 7.72 (s, 1H), 7.54 (d, *J* = 8.4 Hz, 1H), 7.50–7.40 (multiple peaks, 2H), 7.41 (d, *J* = 8.4 Hz, 1H), 7.35 (s, 1H), 7.13–7.08 (multiple peaks, 2H), 7.01 (dt, *J* = 8.0, 1.0 Hz, 1H), 6.93 (d, *J* = 8.0 Hz, 1H); ¹³C NMR (100 MHz, CDCl₃): δ 156.43, 155.47, 149.12, 149.04, 140.44, 140.01, 138.53, 136.01, 136.00, 135.87, 133.54, 133.26, 132.64, 132.28, 132.22, 131.55, 129.98, 129.13, 124.22, 123.42, 122.30, 122.11. HRMS ESI with Formic Acid (*m/z*): [M+H]⁺ calcd for C₂₂H₁₃N₂Cl₄, 444.9833; found, 444.9833.



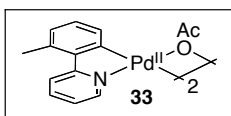
Products 37-a and 37-b. Complex **33** [400 mg, 0.6 mmol, 0.5 equiv (1 equiv based on [Pd])], Oxone (1.424 g, 2.40 mmol, 2 equiv), and substrate **36** (569 mg, 2.40 mmol, 2 equiv) were combined in MeOH (10 mL), and the mixture was stirred at room temperature for 12 h. The resulting red suspension was diluted with ethyl acetate (100 mL) and washed three times with 10% Na₂SO₃ and one time with brine. The organic

layer was dried over MgSO₄ and concentrated, and the resulting orange oil was purified by chromatography on silica gel (R_f for **37-a** = 0.23 in 20% ethyl acetate/ 80% hexanes; R_f for **37-b** = 0.15 in 75% ethyl acetate/ 25% methylene chloride).

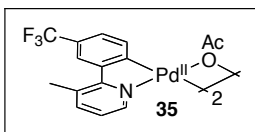
Characterization data for 37-a. mp = 45.0–50.2 °C. ¹H NMR (400 MHz, DMSO-*d*₆, 80 °C): δ 8.53 (d, *J* = 4.0 Hz, 1H), 8.26 (d, *J* = 4.0 Hz, 1H), 7.62–7.55 (multiple peaks, 2H), 7.52 (d, *J* = 1.2 Hz, 1H), 7.41 (app. d, *J* = 8.0 Hz, 2H), 7.20–7.10 (multiple peaks, 4H), 7.02 (t, *J* = 7.6 Hz, 1H), 6.78 (d, *J* = 7.6 Hz, 1H), 2.11 (s, 3H), 2.03 (s, 3H); ¹³C NMR (100 MHz, DMSO-*d*₆, 80 °C) δ 157.95, 156.58, 148.01, 145.71, 144.07, 139.96, 139.17, 137.80, 137.41 (app. d, *J* = 2.9 Hz), 135.58, 135.16, 132.07, 131.03, 128.84, 126.95, 126.64 (q, *J* = 31.5 Hz), 126.21, 125.67 (m), 125.05, 123.65 (q, *J* = 271 Hz), 122.70 (m), 121.94 (bs), 121.18, 19.56, 18.50; ¹⁹F NMR (376 MHz, DMSO-*d*₆): δ -61.03 (s). HRMS ESI with Formic Acid (m/z): [M+H]⁺ calcd for C₂₅H₂₀F₃N₂, 405.1579; found, 405.1573.

Characterization data for 37-b. ¹H NMR (400 MHz, DMSO-*d*₆, 80 °C): δ 8.40 (d, *J* = 4.8 Hz, 1H), 8.07 (d, *J* = 4.4 Hz, 1H), 7.64 (d, *J* = 7.6 Hz, 1H), 7.55-7.45 (multiple peaks, 4H), 7.40 (d, *J* = 7.6 Hz, 1H), 7.12–6.97 (multiple peaks, 5H), 1.97 (s, 3H), 1.82 (bs, 3H); ¹³C NMR (100 MHz, DMSO-*d*₆, 80 °C): δ 157.10, 156.53, 147.70, 144.90, 140.83, 138.91, 138.18, 137.13 (app. d, *J* = 2.7 Hz), 135.17, 134.67, 134.51, 132.42, 130.94, 129.14, 128.49 (q, *J* = 30.0 Hz), 127.78 (bm), 126.77, 125.23, 125.14 (app. d, *J* = 5.7 Hz), 124.63, 123.68 (q, *J* = 274 Hz), 121.50, 120.77, 19.96, 18.60; ¹⁹F NMR (376 MHz, DMSO-*d*₆, 80 °C): δ -55.27. HRMS ESI with Formic Acid (m/z): [M+H]⁺ calcd for C₂₅H₂₀F₃N₂, 405.1579; found, 405.1575.

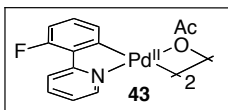
The new palladacycles **33** and **43** were synthesized according to the literature procedure for complex **29**.³⁴ The new palladacycle **35** was prepared by an alternative route based on a literature procedure.⁴⁴ They were characterized by ¹H NMR spectroscopy by breaking up the acetate-bridged dimer *in situ* with pyridine-*d*₅.



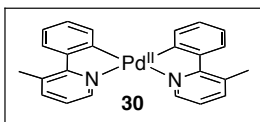
Complex 33. ^1H NMR (500 MHz, CDCl_3 with several drops of pyridine- d_5): δ 8.77 (d, J = 1.5 Hz, 1H), 8.11-8.05 (multiple peaks, 2H), 7.37 (m, 1H), 6.91 (d, J = 7.5 Hz, 1H), 6.78 (t, J = 7.0 Hz, 1H), 6.15 (d, J = 7.5 Hz, 1H), 2.66 (s, 3H), 1.77 (s, 3H).



Complex 35. ^1H NMR (500 MHz, acetone- d_6 with several drops of pyridine- d_5): δ 8.72 (bs, 1H), 8.01 (s, 1H), 7.92 (d, J = 7.5 Hz, 1H), 7.35 (d, J = 7.5 Hz, 1H), 7.23 (d, J = 8.0 Hz, 1H), 6.53 (d, J = 7.5 Hz, 1H), 2.79 (s, 3H), 1.82 (s, 3H). Complex **35** was palladated with >20:1 selectivity at the less sterically hindered position.



Complex 43. ^1H NMR (400 MHz, CD_3OD with several drops of pyridine- d_5): δ 8.12 (d, J = 8.4 Hz, 1H), 8.01 (td, J = 6.4, 1.6 Hz, 1H), 7.56 (d, J = 13.6 Hz, 1H), 7.20 (td, J = 7.6, 1.2 Hz, 1H), 6.98-6.87 (multiple peaks, 2H), 5.89 (dd, J = 7.6, 1.2 Hz, 1H), 1.90 (s, 3H); ^{19}F NMR (376 MHz, CD_3OD with several drops of pyridine- d_5): δ -113.80 (multiplet).



Complex 30 was prepared according to a literature procedure for closely related phenylpyridine complexes.⁵⁴ ^1H NMR (500 MHz, CDCl_3): δ 8.52 (dd, J = 5.5, 1.5 Hz, 2H), 8.16 (dd, J = 7.5, 1.0 Hz, 2H), 7.73 (dd, J = 7.5, 1.0 Hz, 2H), 7.60 (dd, J = 7.5, 1.0 Hz, 2H), 7.27 (td, J = 7.5, 1.5 Hz, 2H), 7.16-7.11 (multiple peaks, 4H), 2.73 (s, 6H).

Scheme 4.27: Complex **29** [4.8 mg, 0.007 mmol, 0.5 equiv (1 equiv based on [Pd])], Oxone (17.7 mg, 0.029 mmol, 2 equiv), and AcOH (0 equiv, 1 equiv or 20 equiv) were

combined in MeOH (0.5 mL), and the mixture was stirred at room temperature for 17 h. Methyl naphthalene (5 μ L), 10% aqueous Na₂SO₃ (0.5 mL), and ethyl acetate (2 mL) were then added, and the resulting biphasic mixture was stirred for 30 min. The organic layer was analyzed by gas chromatography, which revealed <1% of the oxidative coupling product **32**.

Scheme 4.28: Complex **29** [2.4 mg, 0.0035 mmol, 0.25 equiv (0.5 equiv based on [Pd])], complex **33** [2.4 mg, 0.0035 mmol, 0.25 equiv (0.5 equiv based on [Pd])], Oxone (17.7 mg, 0.029 mmol, 2 equiv), and AcOH (0 equiv, 1 equiv or 20 equiv) were combined in MeOH (0.5 mL), and the mixture was stirred at room temperature for 17 h. Methyl naphthalene (5 μ L), 10% aqueous Na₂SO₃ (0.5 mL), and ethyl acetate (2 mL) were then added, and the resulting biphasic mixture was stirred for 30 min. The organic layer was analyzed by gas chromatography, which revealed <1% of each of the oxidative coupling products **32**, **34**, or **24**.

Scheme 4.29: Complex **29** [4.8 mg, 0.07 mmol, 0.5 equiv (1 equiv based on [Pd])], 2-*o*-tolylpyridine (**23**) (4.9 mg, 0.029 mmol, 2 equiv), Oxone (17.7 mg, 0.029 mmol, 2 equiv), and AcOH (0 equiv, 1 equiv or 20 equiv) were combined in MeOH (0.5 mL), and the mixture was stirred at room temperature for 20 min. Methyl naphthalene (5 μ L), 10% aqueous Na₂SO₃ (0.5 mL), and ethyl acetate (2 mL) were then added, and the resulting biphasic mixture was stirred for 30 min. The organic layer was analyzed by gas chromatography, which revealed the presence of **34**, and **24** but showed <1% of compound **32**.

Scheme 4.30a: Complex **35** [5.8 mg, 0.07 mmol, 0.5 equiv (1 equiv based on [Pd])], 2-*o*-tolylpyridine (**23**) (4.9 mg, 0.029 mmol, 2 equiv), and Oxone (17.7 mg, 0.029 mmol, 2 equiv) were combined in MeOH (0.5 mL), and the mixture was stirred at room temperature for 30 min. 5 μ L 1-methylnaphthalene, 10% aqueous Na₂SO₃ (0.5 mL), and ethyl acetate (2 mL) were then added, and the resulting biphasic mixture was stirred for 30 min. The organic layer was analyzed by gas chromatography, which revealed the presence of **37a**, but showed <1% of compound **37b**.

Scheme 4.30b: Complex **33** [4.8 mg, 0.07 mmol, 0.5 equiv (1 equiv based on [Pd])], 3-methyl-2-(*m*-trifluoromethylphenyl)pyridine (**36**) (6.8 mg, 0.0289 mmol, 2 equiv), and oxone (17.7 mg, 0.029 mmol, 2 equiv) were combined in MeOH (0.5 mL) and the mixture was stirred at room temperature for 30 min. 5 μ l 1-methylnaphthalene, 10% aqueous Na₂SO₃ (0.5 mL) and ethyl acetate (2 mL) were then added, and the resulting biphasic mixture was stirred for 30 min. The organic layer was analyzed by gas chromatography and it shows the presence of **37a** and **37b** in a 5 : 1 ratio.

Scheme 4.31: Complex **30** (6.4 mg, 0.014 mmol, 1 equiv) and Oxone (17.6 mg, 0.28 mmol, 1 equiv) were combined in MeOH and the reaction mixture was stirred 30 min at 25 °C. 1-Methylnaphthalene (5 μ L), 10% aqueous Na₂SO₃ (0.5 mL), and ethyl acetate (2 mL) were then added, and the resulting biphasic mixture was stirred for 30 min. The organic layer was analyzed by gas chromatography and **32** was observed.

Scheme 4.32: Complex **30** (6.4 mg, 0.014 mmol, 1 equiv), 2-*o*-tolylpyridine (**23**) (4.8 equiv, 0.0289 mmol, 2 equiv), and Oxone (17.6 mg, 0.28 mmol, 1 equiv) were combined in MeOH and the reaction mixture was stirred for 30 min at 25 °C. 1-Methylnaphthalene (5 μ L), 10% aqueous Na₂SO₃ (0.5 mL), and ethyl acetate (2 mL) were then added, and the resulting biphasic mixture was stirred for 30 min. The organic layer was analyzed by gas chromatography, which revealed the presence of **32**, **34**, and **24**.

Scheme 4.34: Complex **30** (6.4 mg, 0.014 mmol, 1 equiv) was placed in an NMR tube in CD₃OD. AcOH (1.95 μ L, 1 equiv) was added. A ¹H NMR spectrum was acquired after ~10 min, which showed quantitative conversion to **29** + 2-phenyl-3-methylpyridine (**28**) by ¹H NMR. This was confirmed by comparing the spectrum to an authentic equimolar mixture **29** and 2-phenyl-3-methylpyridine (**28**).^{49, 55}

Scheme 4.36: The palladium complex [0.007 mmol, 0.5 equiv (1 equiv based on [Pd])], arylpyridine (0.014 mmol, 1 equiv), and CD₃CO₂D [0 equiv, 20 equiv (16 μ L), or in neat CD₃CO₂D] were combined in CD₃OD (0.5 mL, 0.5 mL or 0 mL respectively) in a 4 mL

vial equipped with a Teflon stirbar. The vial was fitted with a Teflon-lined cap, and the reaction mixture was stirred at room temperature, 60 °C or 100 °C for 24 h. The reaction mixture was transferred to an NMR tube, and a ^{19}F NMR spectrum was acquired. The ^{19}F NMR spectra for reaction of **33** with 2-*o*-fluoropyridine (**41**) and for the reaction of **43** with 2-*o*-tolylpyridine (**23**) at room temperature show that neither mixture has equilibrated to any appreciable extent. When the reactions were conducted in CD_3OD with 20 equiv $\text{CD}_3\text{CO}_2\text{D}$ at 100 °C or in neat $\text{CD}_3\text{CO}_2\text{D}$ at 60 °C a small amount of equilibration was observed. In neat $\text{CD}_3\text{CO}_2\text{D}$ at 100 °C a significant amount of equilibration is observed. However, these are not conditions that are relevant to the catalytic transformations.

4.7 References

- (1) Hassan, J.; Sevignon, M.; Gozzi, C.; Schulz, E.; Lemaire, M. *Chem. Rev.* **2002**, *102*, 1359-1469.
- (2) Frost, C. G. *Rodd's Chemistry of Carbon Compounds, 2nd Edition* Elsevier: Amsterdam, 2001, *5*, 315-350.
- (3) Nicolaou, K. C.; Bulger, P. G.; Sarlah, D. *Angew. Chem., Int. Ed.* **2005**, *44*, 4442-4489.
- (4) Negishi, E. I., Ed.; In *Handbook of Organopalladium Chemistry for Organic Synthesis*; Wiley-Interscience: New York, 2002.
- (5) Trost, B. M. *Science* **1991**, *254*, 1471-1477.
- (6) Trost, B. M. *Acc. Chem. Res.* **2002**, *35*, 695-705.
- (7) Schlueter, A. D.; Bo, Z. In *Handbook of Organopalladium Chemistry for Organic Synthesis*; Wiley-Interscience: New York, 2002, *1*, 825-861.
- (8) Amatore, C.; Jutand, A. In *Handbook of Organopalladium Chemistry for Organic Synthesis*; Wiley-Interscience: New York, 2002, *1*, 943-972.
- (9) Campeau, L.; Fagnou, K. *Chem. Commun.* **2006**, 1253-1264.
- (10) Satoh, T.; Miura, M. *Chem. Lett.* **2007**, *36*, 200-205.
- (11) Li, B.; Yang, S.; Shi, Z. *Synlett* **2008**, 949-957.
- (12) Wender, P. A.; Verma, V. A.; Paxton, T. J.; Pillow, T. H. *Acc. Chem. Res.* **2008**, *41*, 40-49.
- (13) Beccalli, E. M.; Broggini, G.; Martinelli, M.; Sottocornola, S. *Chem. Rev.* **2007**, *107*, 5318-5365.

- (14) Fujiwara, Y.; Jia, C. In *Handbook of Organopalladium Chemistry for Organic Synthesis*; Wiley-Interscience: New York, 2002, 2, 2859-2862.
- (15) Stahl, S. S. *Angew. Chem., Int. Ed.* **2004**, *43*, 3400-3420.
- (16) van Helden, R.; Verberg, G. *Rec. Trav. Chim. Pays-Bas* **1965**, *84*, 1263-1273.
- (17) Nakajima, R.; Hara, T.; Fac, E. *Chem. Lett.* **1972**, 523-526.
- (18) Yoshimoto, H.; Itatani, H. *Bull. Chem. Soc. Jpn.* **1973**, *46*, 2490-2492.
- (19) Mennenga, G. U.; Rudenkov, A. I.; Matveev, K. I.; Kozhevnikov, I. V. *React. Kinet. Catal. Lett.* **1976**, *5*, 401-406.
- (20) Rudenkov, A. I.; Mennenga, H.; Rachkovskaya, L. N.; Matveev, K. I.; Kozhevnikov, I. V. *Kinetika i Kataliz* **1977**, *18*, 915-920.
- (21) Kozhevnikov, I. V. *React. Kinet. Catal. Lett.* **1976**, *4*, 451-458.
- (22) Kozhevnikov, I. V. *React. Kinet. Catal. Lett.* **1976**, *5*, 415-419.
- (23) Kozhevnikov, I. V. *React. Kinet. Catal. Lett.* **1977**, *6*, 401-407.
- (24) Tarabanko, V. E.; Kozhevnikov, I. V.; Matveev, K. I. *React. Kinet. Catal. Lett.* **1978**, *8*, 77-79.
- (25) Itahara, T.; Hashimoto, M.; Yumisashi, H. *Synthesis* **1984**, 255-256.
- (26) Masui, K.; Ikegami, H.; Mori, A. *J. Am. Chem. Soc.* **2004**, *126*, 5074-5075.
- (27) Takahashi, M.; Masui, K.; Sekiguchi, H.; Kobayashi, N.; Mori, A.; Funahashi, M.; Tamaoki, N. *J. Am. Chem. Soc.* **2006**, *128*, 10930-10933.
- (28) Shiotani, A.; Shiotani, J. *Mol. Cat.* **1983**, *18*, 23.
- (29) Shiotani, A.; Itatani, H.; Inagaki, T. *J. Mol. Cat.* **1986**, *34*, 57-66.
- (30) Shiotani, A. *Z. Naturforsch. B* **1994**, *49*, 1731-1736.
- (31) Lee, S. H.; Lee, K. H.; Lee, J. S.; Jung, J. D.; Shim, J. S. *J. Mol. Catal. A* **1997**, *115*, 241-246.
- (32) Iretskii, A. V.; Sherman, S. C.; White, M. G.; Kenvin, J. C.; Schiraldi, D. A. *J. Catal.* **2000**, *193*, 49-57.
- (33) Dick, A. R.; Hull, K. L.; Sanford, M. S. *J. Am. Chem. Soc.* **2004**, *126*, 2300-2301.
- (34) Kalyani, D.; Deprez, N. R.; Desai, L. V.; Sanford, M. S. *J. Am. Chem. Soc.* **2005**, *127*, 7330-7331.
- (35) Dick, A. R.; Sanford, M. S. *Tetrahedron* **2006**, *62*, 2439-2463.
- (36) Hull, K. L.; Anani, W. Q.; Sanford, M. S. *J. Am. Chem. Soc.* **2006**, *128*, 7134-7135.
- (37) Kalberer, E. W.; Whitfield, S. R.; Sanford, M. S. *J. Mol. Catal. A* **2006**, *251*, 108-113.
- (38) Kalyani, D.; Dick, A. R.; Anani, W. Q.; Sanford, M. S. *Org. Lett.* **2006**, *8*, 2523-2526.

- (39) Kalyani, D.; Dick, A. R.; Anani, W. Q.; Sanford, M. S. *Tetrahedron* **2006**, *62*, 11483-11498.
- (40) Dick, A. R.; Remy, M. S.; Kampf, J. W.; Sanford, M. S. *Organometallics* **2007**, *26*, 1365-1370.
- (41) Desai, L. V.; Stowers, K. J.; Sanford, M. S. *J. Am. Chem. Soc.* **2008**, *130*, 13285-13293.
- (42) Kasahara, A.; Kasahara, *Bull. Chem. Soc. Jap.* **1968**, *41*, 1272.
- (43) Holton, R.; Holton, *J. Am. Chem. Soc.* **1977**, *99*, 4175.
- (44) Gutierrez, M. A.; Newkome, G. R.; Selbin, J. J. *Organomet. Chem.* **1980**, *202*, 341-350.
- (45) Hull, K. L.; Lanni, E. L.; Sanford, M. S. *J. Am. Chem. Soc.* **2006**, *128*, 14047-14049.
- (46) Desai, L. V.; Malik, H. A.; Sanford, M. S. *Org. Lett.* **2006**, *8*, 1141-1144.
- (47) Kalyani, D.; Sanford, M. S. *Org. Lett.* **2005**, *7*, 4149-4152.
- (48) Mukhopadhyay, S.; Rothenberg, G.; Lando, G.; Agbaria, K.; Kazanci, M.; Sasson, Y. *Adv. Synth. Catal.* **2001**, *343*, 455-459.
- (49) Ryabov, A. D. *Inorg. Chem.* **1987**, *26*, 1252-1260.
- (50) Rudakov, E. S.; Ignatenko, V. M. *React. Kinet. Catal. Lett.* **1983**, *22*, 75-79.
- (51) Teijido, B.; Teijido, *J. Organomet. Chem.* **2000**, *598*, 71.
- (52) Desai, L. V.; Hull, K. L.; Sanford, M. S. *J. Am. Chem. Soc.* **2004**, *126*, 9542-9543.
- (53) Giri, R.; Chen, X.; Yu, J. *Angew. Chem., Int. Ed.* **2005**, *44*, 2112-2115.
- (54) Dick, A. R.; Kampf, J. W.; Sanford, M. S. *J. Am. Chem. Soc.* **2005**, *127*, 12790-12791.
- (55) Ryabov, A. D.; Yatsimirskii, A. K.; Abicht, H. P. *Polyhedron* **1987**, *6*, 1619-1620.
- (56) Newman, C. P.; Casey-Green, K.; Clarkson, G. J.; Cave, G. W. V.; Errington, W.; Rourke, J. P. *J. Chem. Soc.; Dalton Trans.* **2007**, 3170.
- (57) Mamtora, J.; Crosby, S. H.; Newman, C. P.; Clarkson, G. J.; Rourke, J. P. *Organometallics* **2008**, *27*, 5559.
- (58) Littke, A. F.; Dai, C.; Fu, G. C. *J. Am. Chem. Soc.* **2000**, *122*, 4020-4028.

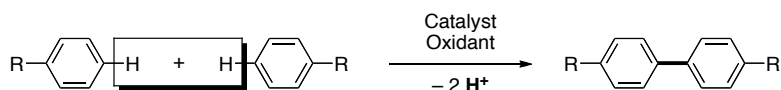
Chapter 5

Palladium-Catalyzed Oxidative Cross-Coupling of C–H Bonds

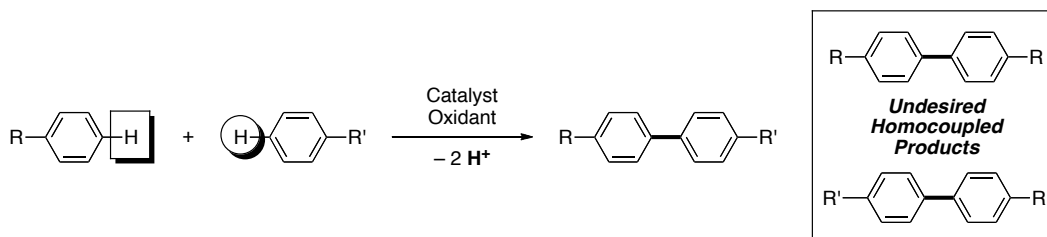
5.1 Background and Significance

Palladium-catalyzed oxidative coupling is an atom economical approach for the formation of C–C bonds.¹ A significant amount of research has been performed studying Pd-catalyzed oxidative homocoupling of Ar–H bonds to form Ar–Ar dimers (Scheme 5.1).²⁻¹⁶ However, the synthetic utility of homocoupling is limited; conversely, a more widely applicable methodology would allow for oxidative cross-coupling of two different C–H bonds to selectively form a new Ar–Ar¹ heterocoupled product (Scheme 5.2).

Scheme 5.1 Oxidative Homocoupling of C–H Bonds.



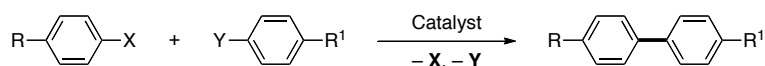
Scheme 5.2 Oxidative Cross-coupling of C–H Bonds.



As discussed in Chapter 4, traditional Pd-catalyzed cross-coupling involves reaction between two prefunctionalized starting materials to afford a new C–C¹ bond (Scheme 5.3).^{1, 17, 18} The requisite prefunctionalization assists in the selective formation

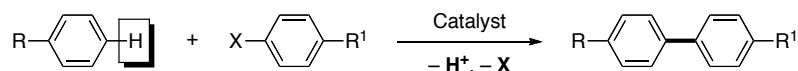
of a cross-coupled product. First, the catalyst reacts selectively at the prefunctionalized carbon-center, and thus the regioselectivity of the reaction is predetermined by the structure of the starting materials employed. Secondly, each coupling partner reacts selectively at a specific step within the catalytic cycle, thus minimizing the formation of undesired homo-coupled byproducts.

Scheme 5.3 Traditional Cross-Coupling



In contrast, direct-coupling forms a new Ar–Ar¹ bond from an Ar–X bond and an Ar¹–H bond (Scheme 5.4).^{1, 19} The regioselectivity of Ar¹–H coupling is dictated by the catalyst’s ability to selectively activate a single C–H bond within the molecule. Chemists have developed many selective direct-coupling methodologies. For example, intramolecular direct coupling reactions have been reported where the C–H bond undergoing functionalization is proximal to the prefunctionalized site. Alternatively, intermolecular direct coupling can be achieved by controlling the acidity or nucleophilicity of a C–H bond or its proximity to a directing group. Both traditional cross-coupling and direct coupling methodologies have found widespread use in the synthesis of complex organic molecules and organic materials. Despite their utility, the required sites of pre-functionalization result in significant amounts of stoichiometric by-products and render the reaction inefficient.

Scheme 5.4 Direct-Arylation of a C–H Bond

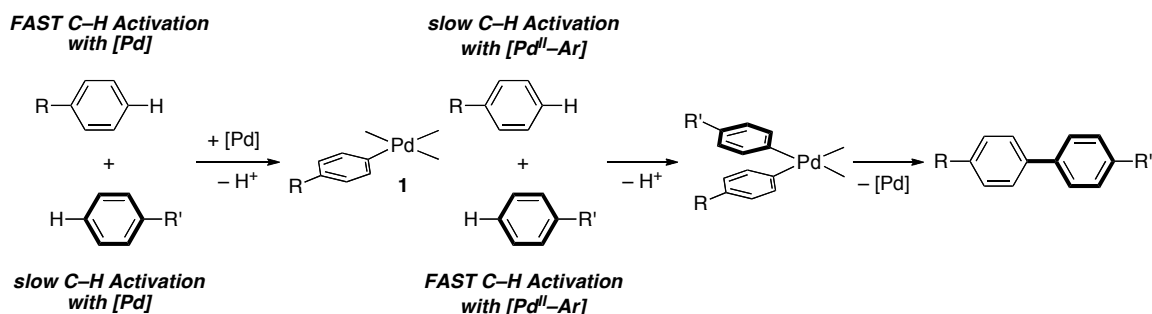


Palladium-catalyzed oxidative cross-coupling is an ideal approach for the formation of new C–C¹ bonds.¹ In such reactions, the two coupling partners are C–H bonds, therefore no pre-functionalization is required, and the only by-product from the reaction is two equivalents of H⁺ (Scheme 5.2). However, Pd-catalyzed oxidative C–H

cross-coupling has several significant challenges. First, the reaction must selectively form the cross-coupled product over either of the homo-coupled dimers. Second, in order for the reaction to be synthetically useful, it must form a single regioisomer, rather than a mixture of several regioisomers. Finally, an appropriate oxidant must be identified such that a sub-stoichiometric amount of the Pd-catalyst can be employed.

Addressing the first challenge, oxidative cross-coupled products can be formed selectively over the undesired homo-coupled products if the Pd-catalyst can promote two chemoselective, sequential C–H activation reactions (Scheme 5.5). More specifically, the transformation must proceed through a mechanism where the Pd-catalyst reacts with each arene selectively at different mechanistic steps. To achieve this, the two arenes must undergo C–H activation at significantly different rates; furthermore, these rates must be dictated by the structure and, therefore, reactivity of the catalyst. As summarized in Scheme 5.3, one arene must react exclusively with the initial catalyst to do the first C–H activation, followed by the second arene reacting discriminatingly with Pd–Ar species **1** in the second C–H activation step.

Scheme 5.5 Two Chemoselective, Sequential C–H Activations are Required for Selective Oxidative Cross-Coupling.

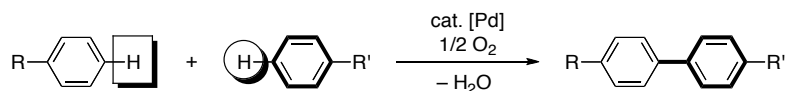


For Pd-catalyzed oxidative cross-coupling methodologies to be synthetically useful, the reactions must also form a single regioisomeric product. In order to achieve this selectivity, both C–H activations must proceed with high regioselectivity. As discussed in Chapter 4, there are several ways to control the regioselectivity of C–H activation. For intermolecular reactions, two common approaches include: (1) the use of directing groups, which promote C–H activation at a proximal C–H bond and (2) the use

of activated heterocycles or electron rich arenes, which promote palladation at the most nucleophilic position of the arene.

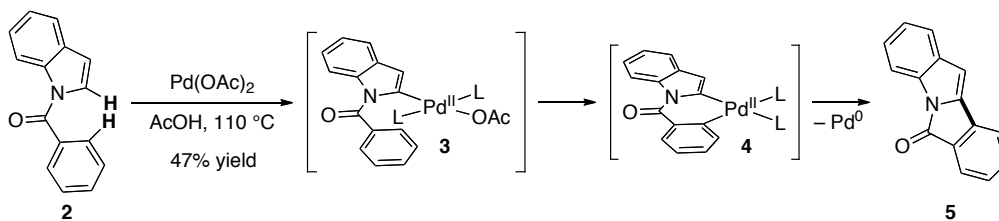
Finally, once conditions are developed that promote the Pd-mediated oxidative cross-coupling of two C–H bonds, an oxidant must be identified that can reoxidize the metal to the catalytically active species. Ideally, the oxidant would be dioxygen, as then the only byproduct for the formation of the new C–C bond would be 1 equiv of H₂O (Scheme 5.6). However, the use of O₂ as a terminal oxidant is often limited by the requirement for high pressures and high reaction temperatures. Fortunately, there are many other oxidants that are known to be active in both Pd^{II}/Pd⁰ and Pd^{II}/Pd^{IV} catalytic cycles and may be used to promote catalytic turnover in these systems, including Cu^{II}, Ag^I, O₂ with a HMPV co-oxidant, and K₂S₂O₈ (*vide infra*).²⁰⁻²⁴

Scheme 5.6 Oxygen as Oxidant for the Formation of Biaryls



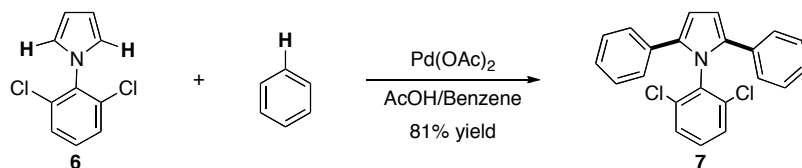
Despite these significant challenges, selective Pd-mediated oxidative cross-coupling of arenes has been known since 1979, when Itahara published the intramolecular reaction between the indole and pendant arene of **2**.²⁵ This reaction was proposed to proceed by an initial palladation at the 2-position of the indole, which then directs a second activation at the *ortho*-C–H bond on the phenyl ring, affording **3** (Scheme 5.7). Finally, reductive elimination of **4** generates the desired C–C bond of **5** and forms Pd⁰.

Scheme 5.7 The First Example of Pd-Mediated Oxidative Cross-Coupling²⁵

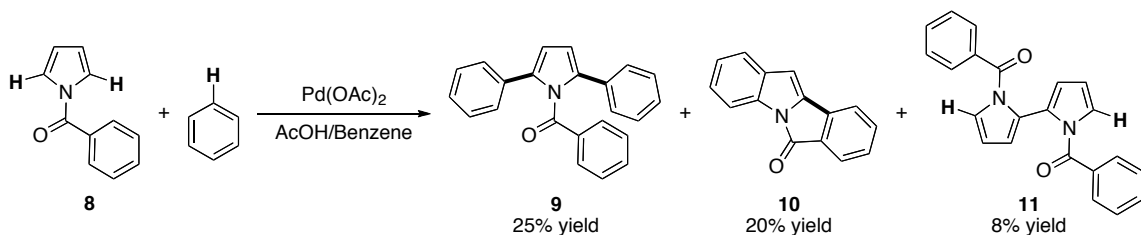


Itahara then expanded the reaction to intermolecular oxidative cross-coupling of activated heteroaromatics with arenes.^{26, 27} For example, *N*-acetyl indoles and *N*-arylpyrrole derivatives were coupled with benzene, *p*-xylene, and 1,4-dichlorobenzene. The cross coupling of *N*-(2,6-dichlorophenyl)-pyrrole (**6**) with benzene occurred to afford **7** in very good yield (81%) (Scheme 5.8). However, other reactions, such as the coupling of *N*-benzylpyrrole (**8**) and benzene, formed the desired product (**9**) in low yields along with the undesired intramolecular cross-coupled species (**10**) as well as homo-coupled bis-pyrrole adducts (**11**). Interestingly, biphenyl was not observed in any of these reactions.

Scheme 5.8 Oxidative Cross-Coupling of Activated Heterocycle **6** with Benzene^{26, 27}



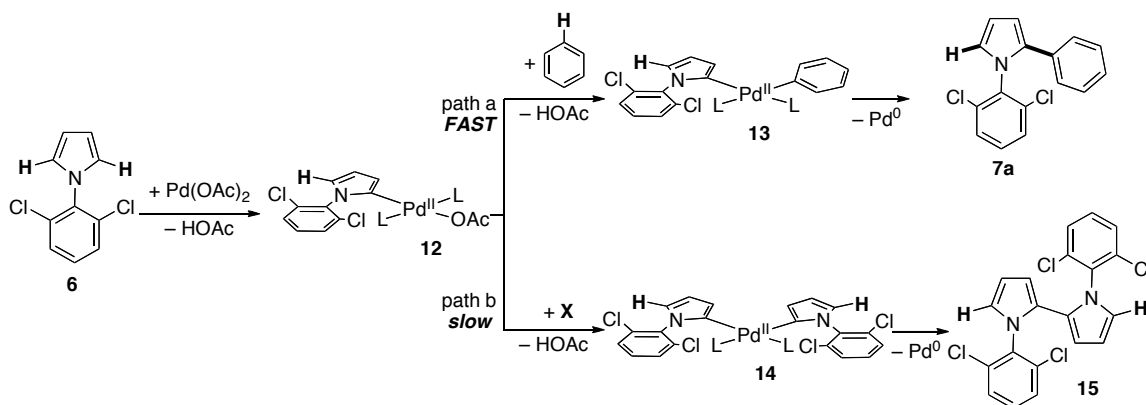
Scheme 5.9 Oxidative Coupling of *N*-Benzylpyrrole (**8**) with Benzene^{26, 27}



The selectivity for the cross-coupled product in Scheme 5.8 is due to the differing reactivity of the two arenes undergoing the cross-coupling reaction.^{26, 27} Importantly, electrophilic palladation of the nucleophilic pyrrole by Pd(OAc)₂ is faster than C–H activation of unactivated benzene; therefore, the initial C–H activation is chemoselective for **12** (Scheme 5.10). The resulting Pd-heteroaryl intermediate is much more electron rich than Pd(OAc)₂, and it is therefore likely to react more slowly with an electron rich pyrrole **16** (path b) relative to that with the electron neutral solvent molecule benzene (path a). However, this chemoselectivity was found to be extremely sensitive, as the

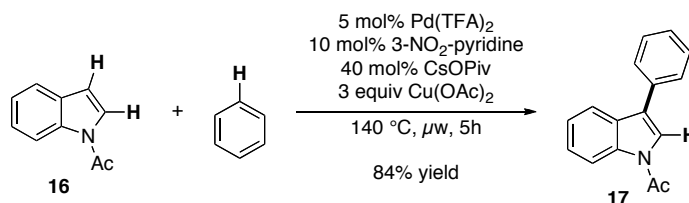
selectivity for cross-coupled : homocoupled products changed dramatically with variation of the protecting group on the pyrrole (Scheme 5.9).

Scheme 5.10 Proposed Mechanism for the Oxidative Cross Coupling of **6** and Benzene.

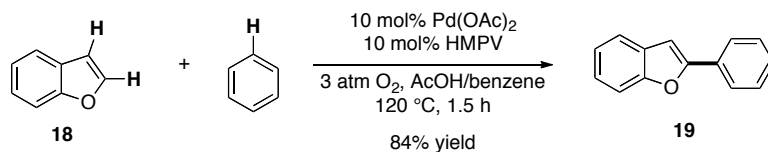


Concurrent with our efforts towards developing Pd-catalyzed oxidative cross-coupling reactions, Fagnou and DeBoef independently developed conditions for Pd-catalyzed oxidative cross-coupling between activated heterocycles and arenes.^{20, 22} In his initial report, Fagnou demonstrated that $\text{Pd}(\text{OAc})_2$ catalyzes oxidative coupling between *N*-acetyl indoles (such as **16**) and arenes, including benzene, *p*-xylene, 1,4-dimethoxybenzene, and 1,4-difluorobenzene employing stoichiometric $\text{Cu}(\text{OAc})_2$ as the oxidant.²⁰ Shortly thereafter, DeBoef reported a similar method for the oxidative coupling of benzofurans (such as **18**) or indoles with arenes, using O_2 as the terminal oxidant in the presence of $\text{H}_4\text{PMo}_{11}\text{VO}_{40}$ (HMPV) as a co-oxidant.²²

Scheme 5.11 Fagnou's Oxidative Coupling of *N*-Acetylindole with Benzene²⁰

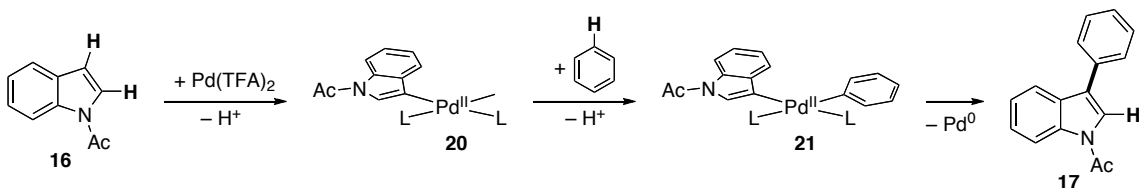


Scheme 5.12 DeBoef's Oxidative Coupling of Benzofuran with O₂ as the Terminal Oxidant²²



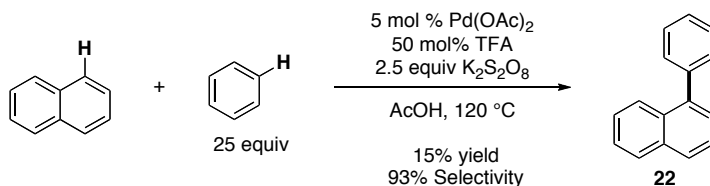
Similar mechanisms are proposed for both of these oxidative cross-coupling reactions.^{20, 22} The activated heterocycle reacts selectively with the initial electron deficient Pd-catalyst in a C–H activation step. This is followed by reaction of this electron rich [Pd] intermediate **20** with the unactivated arene (the reaction solvent), and finally reductive elimination from **21** to form the new C–C bond of **17**.

Scheme 5.13 Proposed Mechanism for the Pd-Catalyzed Cross-Coupling of Indole and Benzene²⁰



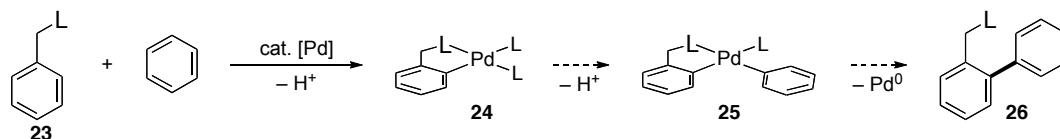
Additionally, Lu has reported the Pd-catalyzed regio- and chemoselective oxidative cross-coupling of naphthalene with arenes (Scheme 5.14).²⁴ The undesired homocoupling of naphthalene can be prevented by tuning the concentration of TFA and the naphthalene : arene ratio in the reaction mixture. These reactions give relatively low yields (15-50%) and TON's (3.1-22). In addition, the products of the oxidative coupling, like **22**, have increased reactivity towards C–H activation relative to the starting materials. Therefore, if the reactions are run for long periods of time or with increased catalyst loadings, competing oligomerization processes decrease the yield of the desired product.

Scheme 5.14 Pd-Catalyzed Oxidative Cross-Coupling of Naphthalene and Benzene²⁴



These examples all employ the relative reactivities of activated arenes and simple arenes to control the chemoselectivity of oxidative cross-coupling reactions. Previously, the Sanford group has demonstrated that substrates bearing ligand directing groups effectively control the regioselectivity of C–H activation reactions.^{28-30, 30-32} Additionally, we also demonstrated that two ligand directed C–H activations do not readily occur at Pd^{II} (Chapter 4).³³ We sought to exploit this regiocontrol for the oxidative cross-coupling of C–H bonds, and thereby couple a substrate with a directing group to a simple arene (Scheme 5.15).³⁴

Scheme 5.15 Proposed Pd-Mediated Oxidative Cross-Coupling

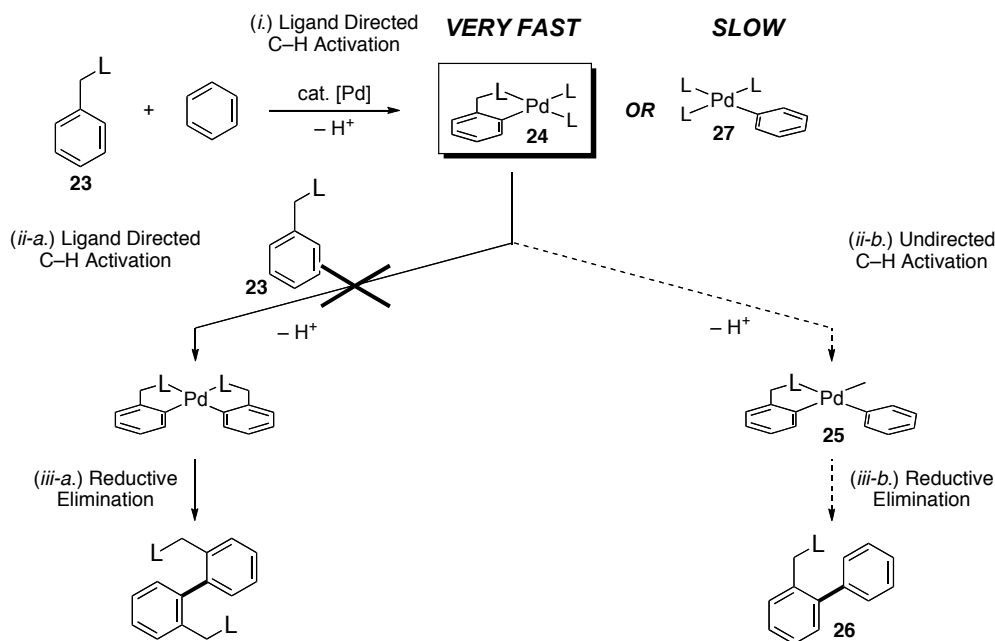


5.2 Methodology Development and Synthetic Scope

We sought to develop a Pd-catalyzed oxidative cross-coupling reaction that proceeds through two discrete chemo- and regio- selective C–H activations.³⁴ As detailed in Scheme 5.16, our approach was to couple a substrate containing a ligand-directing group (**23**) with a simple arene. Cyclopalladation of substrates containing a directing group is facile and highly regioselective.^{35, 36} Consequently, we expected that a Pd^{II} catalyst would initially react selectively with a substrate containing a ligand (**23**) over a simple arene, leading to a selective palladation process, affording **24** rather than **27** (Scheme 5.16, step *i*). Additionally, our previous studies on the mechanism of oxidative homo-coupling of 2-arylpyridine derivatives (Chapter 4) revealed that a second, ligand-directed C–H activation does not occur at Pd^{II} (step *ii-a*).^{33, 37, 38} We sought to exploit this

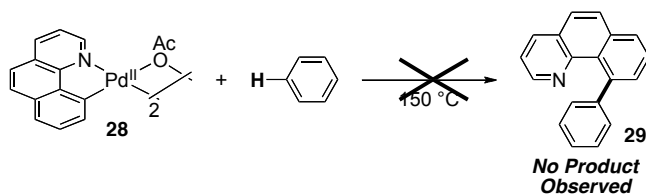
lack of reactivity, by instead promoting undirected C–H activation of a simple arene (step *ii-b*). Reductive elimination would then afford the desired cross-coupled product **26** (step *ii-c*).

Scheme 5.16 Proposed Oxidative Cross-Coupling Reaction



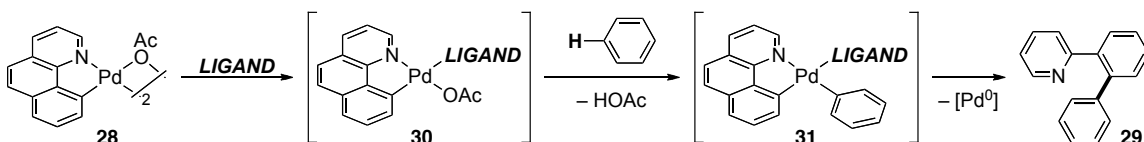
Our initial efforts focused on the stoichiometric reaction between cyclopalladated benzo[*h*]quinoline complex ($[\text{BzqPdOAc}]_2$, **28**) and benzene. Heating **28** up to 150 °C in benzene did not afford any of the desired cross-coupled product **29**. We initially hypothesized that this lack of product formation might be due to the inability of **28** to promote a second undirected C–H activation of benzene.

Scheme 5.17 Stoichiometric Reaction Between $[\text{BzqPdOAc}]_2$ (**28**) and Benzene.

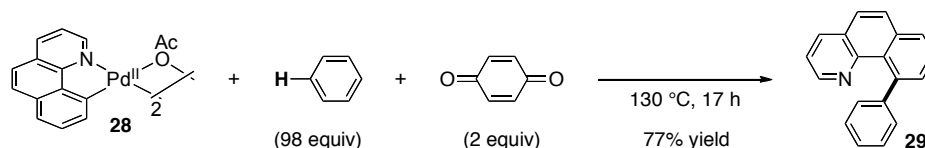


C–H activation is generally believed to be accelerated at more electrophilic Pd^{II} centers; however, the Pd atom of **28** contains a σ -aryl bond and is therefore quite electron rich. Thus, we hypothesized that adding a π -acidic ligand to the reaction might promote the second C–H activation. The π -acidic ligand could bind to the cyclometallated Pd^{II} species **28**, making it more electrophilic, and thereby promote the second C–H activation to form **31** (Scheme 5.18). We were delighted to find that benzoquinone (BQ) was an effective promoter for generating the desired oxidative cross-coupled product **29** in 77% isolated yield (Scheme 5.19).

Scheme 5.18 Addition of π -Acidic Ligands to Promote the Second C–H Activation

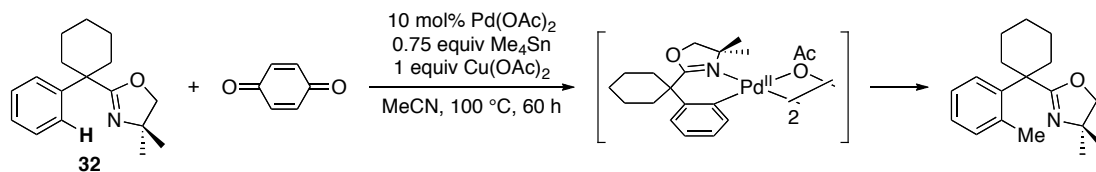


Scheme 5.19 Benzoquinone-Promoted Stoichiometric Oxidative Coupling



Benzoquinone (BQ) has previously been shown to bind to Pd^{II} complexes, and to accelerate C–H activation reactions. For example, Yu found that cyclopalladation of oxazoline substrates, like **32** (Scheme 5.20), was promoted by BQ.³⁹ This additive was also proposed to serve the additional purpose in promoting reductive elimination to form the new Ar–Me bond. The benzoquinone ligates to the Pd-catalyst, increasing its electrophilicity, and promoting C–H activation and/or reductive elimination.

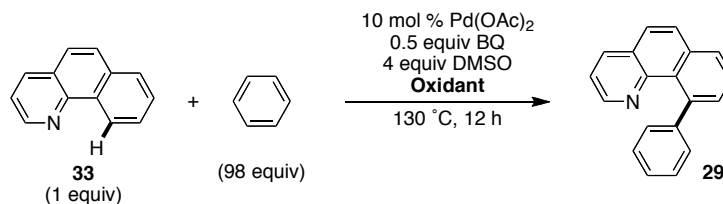
Scheme 5.20 BQ-Promoted Direct Coupling of Ar-H with Me₄Sn³⁹



After we established conditions that afforded our desired cross-coupled product stoichiometrically (Scheme 5.19), we sought to identify conditions that would render the reaction catalytic in Pd. Despite its widespread application as an oxidant for Pd⁰/Pd^{II} catalytic cycles, under our reaction conditions benzoquinone was not redox active, and only a single turnover was observed. In fact, substoichiometric amounts of BQ could be employed in the reaction, as it acted as a catalyst. Benzoquinone is readily reduced under acidic conditions; but, in the current system the addition of acids, such as AcOH (acetic acid) or PivOH (pivalic acid), inhibited formation of the desired product.⁴⁰

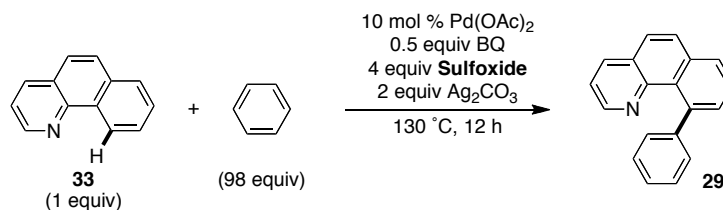
We next turned to other oxidants that are commonly employed in Pd^{II}/Pd⁰ catalytic cycles and oxidative coupling reactions. A screen of copper(II), silver(I), and peroxide salts (Table 5.1), revealed that Ag₂CO₃ was the most effective oxidant for the cross-coupling reaction. Additionally, DMSO has been employed as a co-additive with Ag₂CO₃; thus, we screened a variety of sulfoxides, and found that the use of 4 equiv of DMSO increased the yield of **29** from 74% to 89% (Table 5.2).⁴¹ The DMSO could possibly be acting as a ligand that slows catalyst decomposition or Pd⁰ aggregation, helping to solublize the Ag₂CO₃, and/or having a beneficial effect on the reaction medium by making it more polar.^{42, 43}

Table 5.1 Oxidant Screening for the Pd-Catalyzed Oxidative Cross-Coupling of Benzo[*h*]quinoline (**33**) and Benzene



Entry	Oxidant	Equiv	GC Yield
1	none	0	10%
2	benzoquinone	4	9%
3	K ₂ S ₂ O ₈	4	1%
4	Oxone	4	0%
5	CuCl ₂	4	0%
6	Cu(OAc) ₂ • H ₂ O	4	53%
7	CuO	4	8%
8	Ag(O ₂ CCF ₃)	4	0%
9	AgOTf	4	0%
10	Ag ₂ O	2	15%
11	AgOAc • H ₂ O	4	38%
12	Ag ₂ CO ₃	2	89%

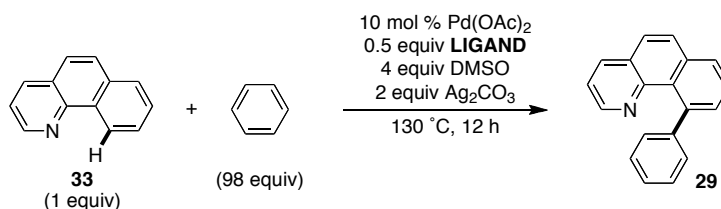
Table 5.2 Screening of Sulfoxide Additives for the Pd-Catalyzed Oxidative Coupling of Benzo[*h*]quinoline (**33**) and Benzene



Entry	Sulfoxide Derivative	GC Yield
1	none	74%
2	DMSO	89%
3	tetramethylene sulfoxide	86%
4	diphenyl sulfoxide	75%
5	dibenzyl sulfoxide	52%
6	1,2-bis(benzylsulfinyl)ethane	33%

A variety of benzoquinone derivatives and other π -acids were also screened as promoters for this reaction. As summarized in Table 5.3, benzoquinone was the most effective additive to the reaction. As the quinone became more sterically hindered or more electron deficient, the reaction afforded **29** in lower yield. Interestingly, β -nitrostyrene, which is not redox active but is known to act as π -acidic ligand for Pd, does promote the oxidative coupling reaction, albeit in low yields.

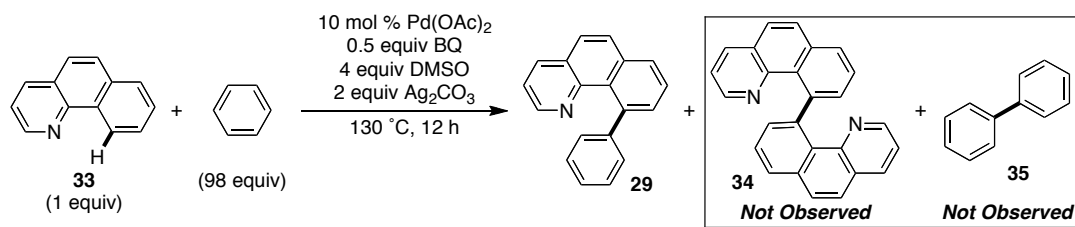
Table 5.3 Screening of Ligands and their Ability to Promote the Oxidative Coupling Reaction



Entry	Olefin Derivative	GC Yield
1	benzoquinone	89%
2	2-methylbenzoquinone	80%
3	2,6-dimethylbenzoquinone	54%
4	duroquinone	53%
5	2,6-dichlorobenzoquinone	36%
6	2,5-dichlorobenzoquinone	43%
7	tetrachlorobenzoquinone	2%
8	tetrafluorobenzoquinone	0%
9	tetracyanoethylene	0%
10	<i>trans</i> - β -nitrostyrene	15%

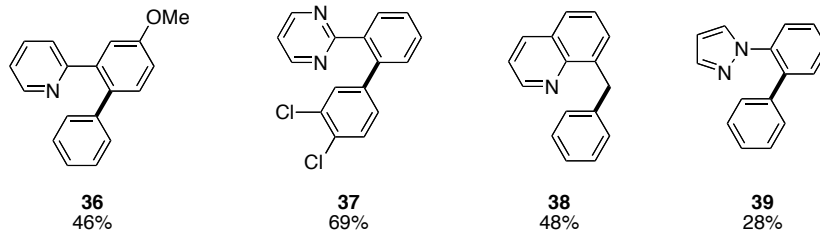
The optimized conditions for the Pd-catalyzed oxidative cross-coupling of benzo[*h*]quinoline (**33**) and benzene are shown in Scheme 5.21. In order to obtain reproducible reactivity and yields, the reaction had to be stirred vigorously, or catalyst decomposition occurred prior to the reaction's completion. Importantly, neither the benzo[*h*]quinoline–benzo[*h*]quinoline dimer (**34**) nor biphenyl (**35**) were observed in the reaction.

Scheme 5.21 The Optimized Conditions for the Oxidative Cross-Coupling of Benzo[*h*]quinoline (**33**) and Benzene

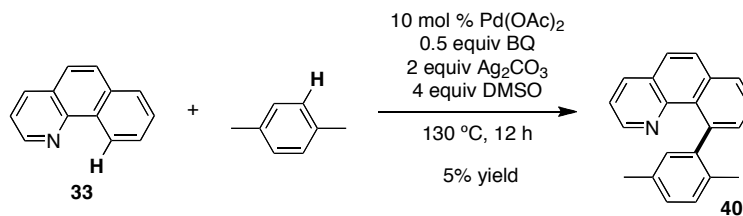
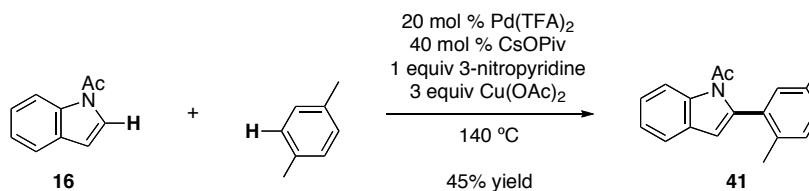


Once conditions were identified that promoted catalytic turnover in the Pd-catalyzed oxidative coupling reaction, the substrate scope was explored. Substrates containing pyridine, pyrimidine, quinoline, and pyrazole directing groups all underwent the oxidative cross-coupling reaction with simple arene coupling partners to afford **36-39** (Scheme 5.22). Perhaps the most interesting substrate is the 8-methylquinoline, which forms a new sp³-sp² C–C bond of **38**.

Scheme 5.22 Cross-Coupling Products with Other Directing Groups



Next, we explored the substrate scope of the arene coupling partner, which undergoes the second C–H activation. Our initial efforts began with *p*-xylene, which is electronically similar to benzene but has two methyl groups, which makes the aromatic C–H bonds more sterically hindered. The reaction proceeded in very low yield, affording only 5% of the desired cross-coupled product (**40**) (Scheme 5.23). This result was intriguing, because *p*-xylene was an effective coupling partner in other Pd-catalyzed oxidative coupling reactions. For instance, Fagnou reported that the coupling of *N*-acetylindole and *p*-xylene occurred in 45% yield (Scheme 5.24).²⁰

Scheme 5.23 Oxidative Coupling of Benzo[*h*]quinoline (**33**) with *p*-Xylene**Scheme 5.24** Fagnou's Oxidative Coupling of *N*-Acetylindole (**16**) and *p*-Xylene²⁰

The ineffectiveness of *p*-xylene as a coupling partner indicated that our oxidative coupling reaction is highly sensitive to the steric hindrance of the arene. Thus, we reasoned that this might be exploited to control the regioselectivity of the coupling reaction. To probe this possibility, we screened a series of 1,2-disubstituted aromatics, in which the C–H bonds are electronically equivalent but sterically different (Table 5.4, entries 1-4). We found that the reactions proceeded in good yields and that the less sterically hindered C–H bond was functionalized with high selectivity (>10:1 in most cases). Notably, even the relatively small fluoro groups of *o*-difluorobenzene hindered the functionalization at the 3-position (Table 5.4, entry 4).

Next we wanted to study our oxidative coupling reaction with 1,3-disubstituted and 1,2,3-trisubstituted arenes, where the C–H bonds were both sterically and electronically inequivalent (Table 5.4, entries 5-10). In most cases, there was very high selectivity for functionalization at the 5-position of the arene, regardless of whether that position was electron rich, as in 1,3-dimethylanisole (Table 5.4, entry 6) or electron poor, as in 1,3-dimethyl-2-nitrobenzene (Table 5.4, entry 8). The only substrates that did not show <5% of a regioisomer were 3-methylanisole and 1,3-dimethoxybenzene (Table 5.4, entries 9 and 10). In both cases, a minor regioisomer was observed in which functionalization had occurred adjacent to the methoxy group. This can be explained by the relatively small size of the methoxy group.

Mono-substituted arenes reacted with modest regioselectivity, and coupling at the *meta*- and *para*-positions was favored over the *ortho*-sites (Table 5.4, entries 11-12). Both electron rich anisole and electron poor nitrobenzene were effective substrates, affording the oxidative cross-coupled product in similar yields. The regioselectivity was affected by the electronic nature of the arene, as a statistical mixture of *meta*- to *para*-functionalized regioisomers was not formed in either the oxidative coupling of anisole or nitrobenzene. Rather the reactions showed slight preference for coupling at the more electron rich carbon (the *para*-position of anisole and the *meta* position of nitrobenzene).

A general strategy for sterically controlled regioselectivity had not previously been reported for C–H activation at Pd^{II}. One example, with similar selectivity, is the Pd-catalyzed oxidative homo-coupling of dimethyl phthalate in the presence of 1,10-phenanthroline.^{8, 44} The steric bulk of the ligand prevents cyclometallation, and promotes selective oxidative coupling at the less hindered C–H bond. Without added ligand, the two regioisomers were formed in a 1:1 ratio (Scheme 5.25). However, this approach has not been applied to oxidative coupling or functionalization of other arenes lacking a directing group. Similar steric-based selectivity has been observed in Ir- and Rh-catalyzed C–H activation/borylation reactions, where the least hindered C–H bond is borylated with extremely high selectivity for both 1,2- and 1,3-disubstituted arenes (Scheme 5.26).⁴⁵⁻⁴⁸

Scheme 5.25 Sterically Controlled Selectivity in the Pd-Catalyzed Oxidative Homocoupling of Dimethyl Phthalate^{8, 44}

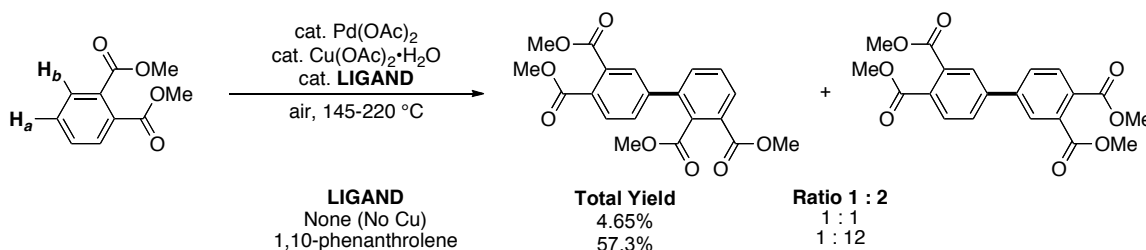
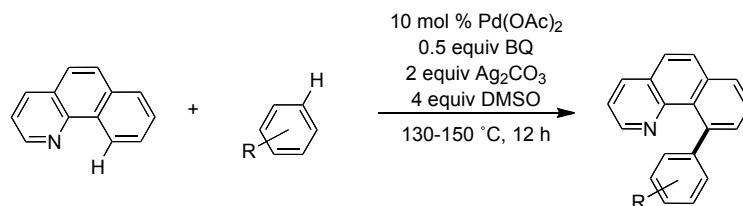
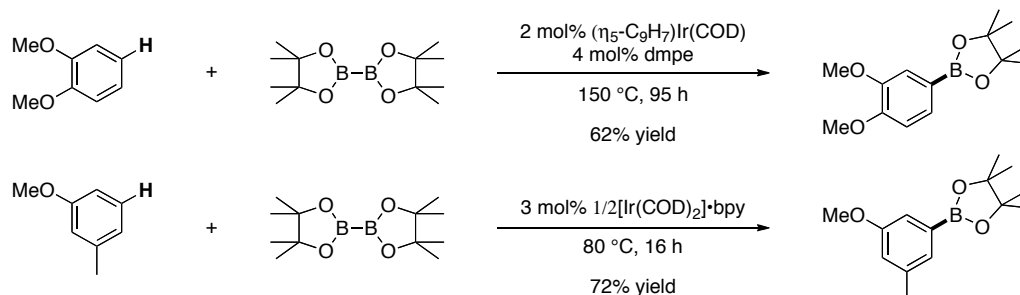


Table 5.4 Substrate Scope for the Oxidative Cross-Coupling of Benzoquinone and a Variety of 1,2- and 1,3-Disubstituted Arenes.



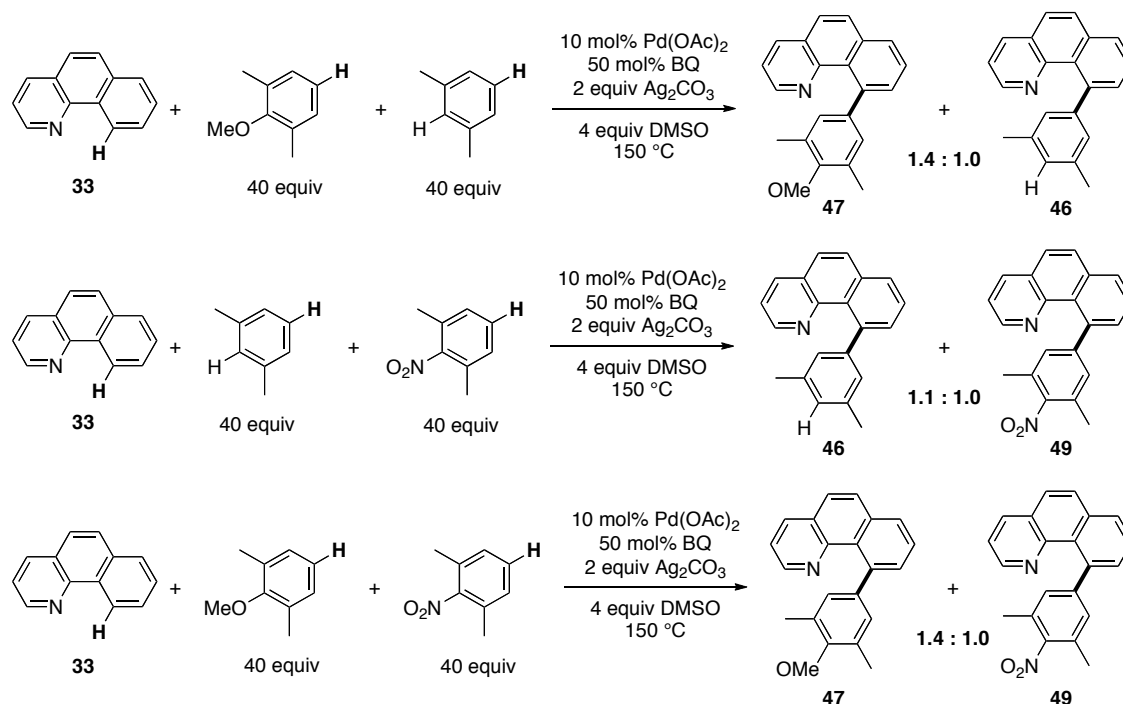
Entry	Arene	Product	Yield	Entry	Arene	Product	Yield
1			(66%)	7			(73%)
2			(94%)	8			(55%)
3			(67%)	9			(70%) 1,3,5 : 1,3,4 2.5 : 1
4			(53%) 1,2,4 : 1,2,3 10 : 1	10			(75%) 1,3,5 (a) : 1,3,4 (b) 2.7 : 1
5			(66%)	11			(80%) o:m:p 1 : 2.6 : 3.3
6			(74%)	12			(77%) o:m:p 0 : 3.5 : 1

Scheme 5.26 Sterically Controlled Selectivity in Ir-Catalyzed C–H Borylation^{46, 47}



The regioselectivity of C–H activation at Pd^{II} is often influenced by the electronic nature of the C–H bond undergoing functionalization. C–H activation reactions are known to selectively functionalize the most electron rich C–H bond through electrophilic palladation mechanisms and the most acidic C–H bonds via deprotonation mechanisms. However, many C–H activation reactions are only moderately affected by the electronics of the arene. To gain insight into the influence of the electronic nature of Ar–H on the second C–H activation, a series of competition studies were performed with the sterically identical, electronically different substrates: electron rich 1,3-dimethylanisole, electron neutral *m*-xylene, and electron deficient 1,3-dimethylnitrobenzene (Scheme 5.27). These competition studies revealed that the reactions were only mildly affected by the electronic nature of the C–H bond, where the electron rich substrate reacts slightly (1.4 times) faster than the electron poor substrate.

Scheme 5.27 Competition Studies Between Electronically Different Arene Substrates.



Our next efforts focused on investigating the mechanism of this Pd-catalyzed oxidative cross-coupling reaction. We especially wanted to gain a better understanding of the role of benzoquinone in the reaction as well as the factors contributing to the sterically controlled regioselectivity.

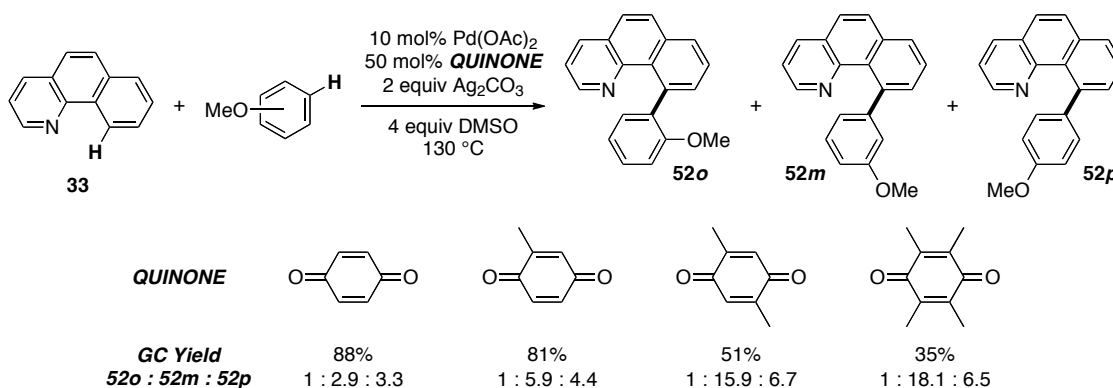
5.3 Mechanistic Investigations of Pd-Mediated Oxidative Cross-Coupling Reactions

The palladium catalyzed oxidative cross-coupling of C–H bonds is proposed to go through two discrete C–H activations steps at Pd^{II}. The regioselectivity of the first C–H activation is determined by the ligand-directing group. The selectivity of the second C–H activation is affected by both the size and electronic effects of the substituents on the arene, as well by the structure of the quinone employed in the reaction. In order to gain further insight into our Pd-catalyzed oxidative cross-coupling reaction, we undertook a variety of mechanistic studies, focusing on more clearly determining the role benzoquinone was playing in the reaction.

Benzoquinone is known to promote both C–H activation and reductive elimination reactions at Pd^{II} centers. Yu demonstrated that the cyclometallation of some oxazole derivatives only occurred in the presence of BQ (Scheme 5.20, page 135), and in his system the BQ also promoted the reductive elimination to form an sp³–sp² C–C bond.³⁹ In addition to Yu, White has also observed benzoquinone promoted reductive elimination from Pd^{II}.^{42, 43, 49}

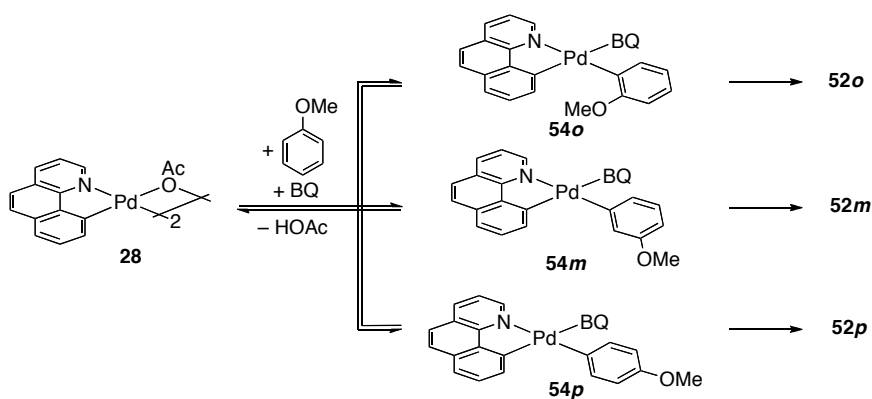
We hypothesized that the benzoquinone (BQ) was binding to the metal during the oxidative coupling reaction to either promote C–H activation or reductive elimination. If this were occurring in our reaction, we reasoned that changing the steric and/or electronic nature of the BQ might affect the regioselectivity of oxidative cross-coupling. To test this hypothesis, we studied the oxidative cross-coupling between benzo[*h*]quinoline (**33**) and anisole as a function of benzoquinone substitution. With simple benzoquinone, this reaction afforded **52** as a 1 : 2.9 : 3.3 (*o*:*m*:*p*) mixture of regioisomers. However, intriguingly, sequentially adding methyl groups to the BQ increased the regioselectivity, favoring the formation of the *meta*- and *para*- isomers over the more sterically hindered *ortho*- isomer (Scheme 5.28). Mechanistically, this strongly suggested to us that the BQ ligand is bound or in the process of binding to the Pd during a selectivity-determining step of the reaction. Additionally, this indicated that the regioselectivity in our Pd-catalyzed oxidative cross-coupling reactions can be tuned by changing the sterics and electronics of an ancillary ligand.

Scheme 5.28 Effect of Benzoquinone Structure on Selectivity.

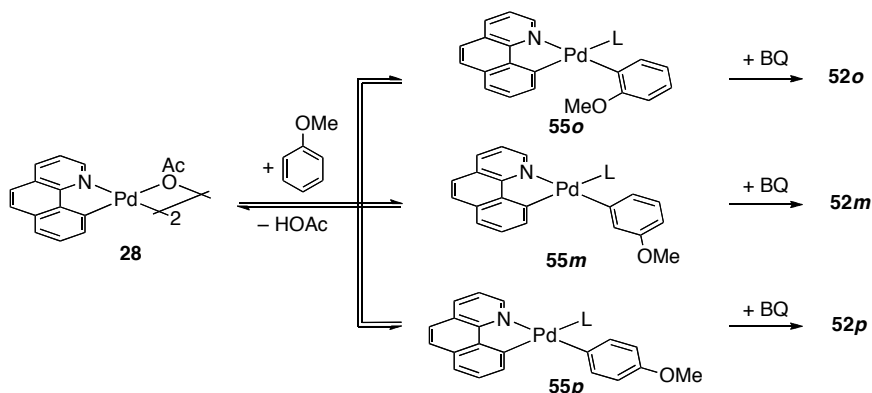


There are two mechanistic scenarios that could explain how increasing the substitution on the BQ could affect the regioselectivity of the oxidative coupling reaction between **33** and anisole. The first possibility (scenario A), as seen in Scheme 5.29, is that the benzoquinone is binding to the Pd^{II} and promoting the second C–H activation, a more hindered quinone will slow the rate of functionalization *ortho* to a functional group. Alternatively, in scenario B (Scheme 5.30) the regioselectivity of the reaction would depend on the relative rates of the BQ binding to the different Pd-biaryl intermediates if the second C–H activation to form Pd-biaryl complex **55** is rapid and reversible and the BQ binds to **55** to promote reductive elimination. Our next goal was to develop experiments that would allow us to distinguish between the two pathways.

Scheme 5.29 Scenario A, Involving a BQ Promoted C–H Activation



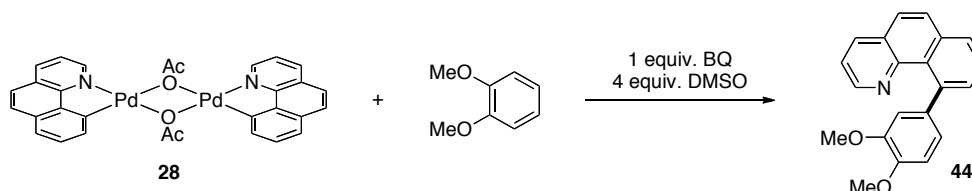
Scheme 5.30 Scenario B, Where the BQ Induces Reductive Elimination



In order to simplify the mechanistic studies, we focused only on the second C–H activation and reductive elimination steps rather than the entire catalytic cycle. With this

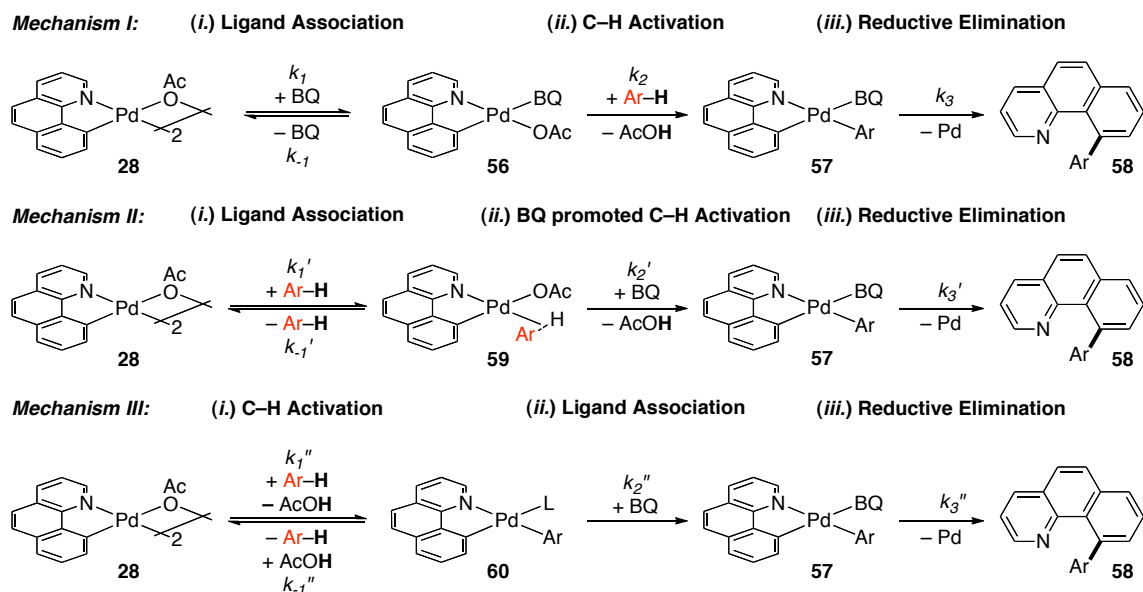
in mind, we studied the stoichiometric reaction between $[\text{BzqPdOAc}]_2$ (a putative catalytic intermediate) and 1,2-dimethoxybenzene, which affords **44** as a single regioisomer.

Scheme 5.31 Stoichiometric Oxidative Coupling Between **28** and 1,2-Dimethoxybenzene.



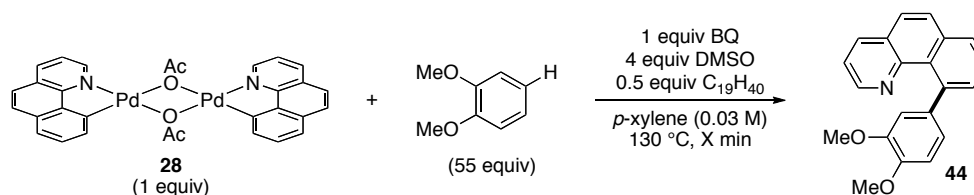
In Scheme 5.26 and 5.30 two possible mechanistic scenarios were laid out. The benzoquinone could either promote C–H activation or C–C bond forming reductive elimination. These two scenarios can be broken into three possible mechanisms for the stoichiometric Pd-mediated oxidative cross-coupling reaction between $[\text{BzqPdOAc}]_2$ (**28**) and 1,2-dimethoxybenzene, as shown in Scheme 5.32. Mechanism I is similar to that preliminarily being proposed in the catalytic cycle (Scheme 5.29); it involves first (1-i) coordination of BQ to the **28**, followed by (1-ii) C–H activation of the arene by **56**, and, finally, (1-iii) reductive elimination to form the new C–C bond. In Mechanism II, first (2-i) the arene breaks up the $[\text{BzqPdOAc}]_2$ (**28**) dimer, forming an agostic bond between the Ar–H bond and the Pd (**59**), then (2-ii) BQ coordinates to the Pd and promotes the C–H activation affording **57**, and, finally, (2-iii) reductive elimination forms the new C–C bond of **58**. In the final mechanism, mechanism III, there is (3-i) initial C–H activation forming **60**, followed by (3-ii) coordination of the BQ to the Pd (**57**), and (3-iii) BQ-induced reductive elimination to form the new C–C bond. Mechanisms 1 and 2 require BQ to promote the C–H activation and possibly the reductive elimination, while mechanism 3 only requires the BQ to catalyze the reductive elimination step of the catalytic cycle. A variety of experiments were conducted to distinguish between these three possible mechanisms.

Scheme 5.32 Three Possible Mechanisms for Pd-Mediated Oxidative Cross-Coupling



General Procedure for Kinetic Experiments. The initial rates of the reaction under each set of conditions were determined by monitoring the product formation in six identical reactions, set up simultaneously. As seen in Scheme 5.33, the standard reaction conditions were [BzqPdOAc]₂ (**28**) (6.9 mg, 0.01 mmol, 0.5 equiv (1 equiv per Pd)) weighed directly into a vial, then 0.806 mL of a standard solution containing (per aliquot) benzoquinone (BQ) (2.2 mg, 0.02 mmol, 1 equiv), DMSO (5.7 μL, 0.08 mmol, 4 equiv), nonadecane (internal standard) (2.7 mg, 0.01 mmol, 0.5 equiv), 1,2-dimethoxybenzene (0.14 mL, 1.1 mmol, 55 equiv), and *p*-xylene (0.66) was added via a 1 mL Hamilton airtight syringe. The reactions were then allowed to stir at room temperature for > 30 s and then at 130 °C for *t* min in an aluminum reaction block while stirring at the highest rpm (IKA stirplate setting of 11). After the allotted period of time ($t \approx n \cdot (\text{time to reach 10\% yield}) / 6$, ($n = 1-6$)), each reaction was taken out sequentially, cooled to 0 °C in an ice bath, then diluted with CH₂Cl₂. The reaction was then analyzed by GC twice and the yield of **44** determined by comparison to a calibration against the nonadecane internal standard. Importantly, the reactions did not progress after the work-up, a reaction analyzed immediately and 12 hours later gave the same GC yield. Additionally, under the reaction conditions none of **40**, where the *p*-xylenes is oxidatively coupled, was observed. The reported initial rate values are the average of three unique kinetic experiments.

Scheme 5.33 Standard Reaction Conditions for the Initial Rate Kinetic Experiments



Order Studies. Our initial efforts focused on determining the order of the reaction in the various reagents, as this should allow us to distinguish between the three different mechanisms outlined in Scheme 5.32.

A rate equation can be derived for the three proposed mechanisms. The equation would depend upon which step was rate determining; as such, all nine possible rate equations are shown in Scheme 5.34.

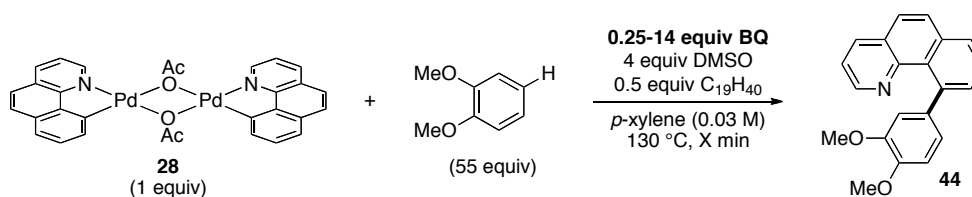
Scheme 5.34 Derived Rate Equations for the Three Mechanisms Shown in **Scheme 5.32**.

	<i>Mechanism I:</i>	<i>Mechanism II:</i>	<i>Mechanism III:</i>
Step (i.) is rds:	rate = $k_1 [\text{Pd}]^{1/2} [\text{BQ}]$	rate = $k_1' [\text{Pd}]^{1/2} [\text{Ar-H}]$	rate = $k_1'' [\text{Pd}]^{1/2} [\text{Ar-H}]$
Step (ii.) is rds:	$\text{rate} = \frac{K_{\text{eq}} k_2 [\text{Pd}]^{1/2} [\text{BQ}] [\text{Ar-H}]}{(1 + (k_2 / k_1) [\text{Ar-H}])}$	$\text{rate} = \frac{k_1' k_2' [\text{Pd}]^{1/2} [\text{BQ}] [\text{Ar-H}]}{k_1 + k_2 [\text{BQ}]}$	$\text{rate} = \frac{k_1'' k_2'' [\text{Pd}]^{1/2} [\text{BQ}] [\text{Ar-H}]}{k_1'' [\text{AcOH}] + k_2'' [\text{BQ}]}$
Step (iii.) is rds:	$\text{rate} = \frac{K_{\text{eq}} k_2 k_3 [\text{Pd}]^{1/2} [\text{BQ}] [\text{Ar-H}]}{(1 + (k_2 / k_1) [\text{Ar-H}])}$	$\text{rate} = \frac{k_1' k_2' k_3' [\text{Pd}]^{1/2} [\text{BQ}] [\text{Ar-H}]}{k_1' + k_2' [\text{BQ}]}$	$\text{rate} = \frac{k_1'' k_2'' k_3'' [\text{Pd}]^{1/2} [\text{BQ}] [\text{Ar-H}]}{k_1'' [\text{AcOH}] + k_2'' [\text{BQ}]}$

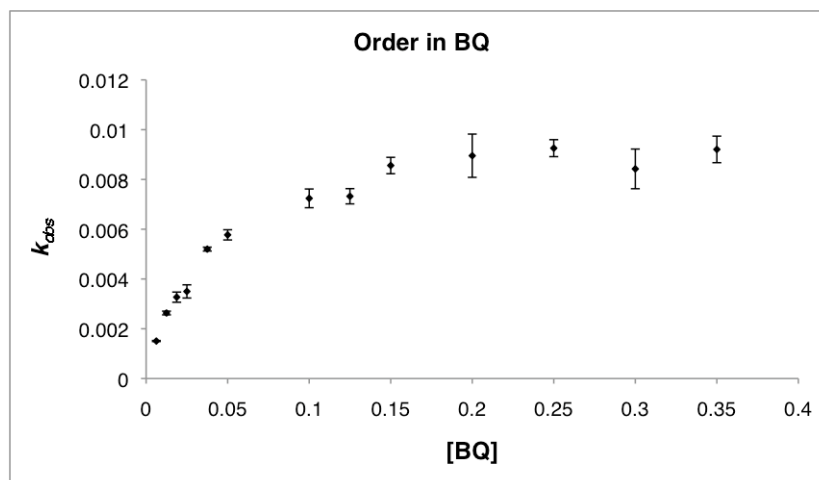
The order in benzoquinone (BQ) was determined by studying the initial rate of reactions with different [BQ] (Scheme 5.35). These kinetics experiments revealed that the reaction showed saturation kinetics in BQ (Scheme 5.36). This was initially determined by plotting k_{obs} versus [BQ], with the [BQ] varied from 0.00625-0.35 mM (0.25-14 equiv). The double reciprocal plot of this data was also consistent with saturation kinetics, as it was linear with a non-zero intercept (Scheme 5.37). This implies that there is a steady state intermediate that reacts with BQ to afford the product. If mechanism I (Scheme 5.32) was occurring, the reaction should be first order in BQ (Scheme 5.34),

however mechanisms II and III are both consistent with a steady state intermediate reacting with BQ to form the product. This data suggests that when the reactions are run with one equivalent of BQ, the second or third step is rate determining and when the reactions are run with > 5 equivalents of BQ (under saturation conditions) the first step is rate determining. This first piece of mechanistic evidence suggests strongly that Pd-mediated oxidative cross-coupling is not proceeding via mechanism I.

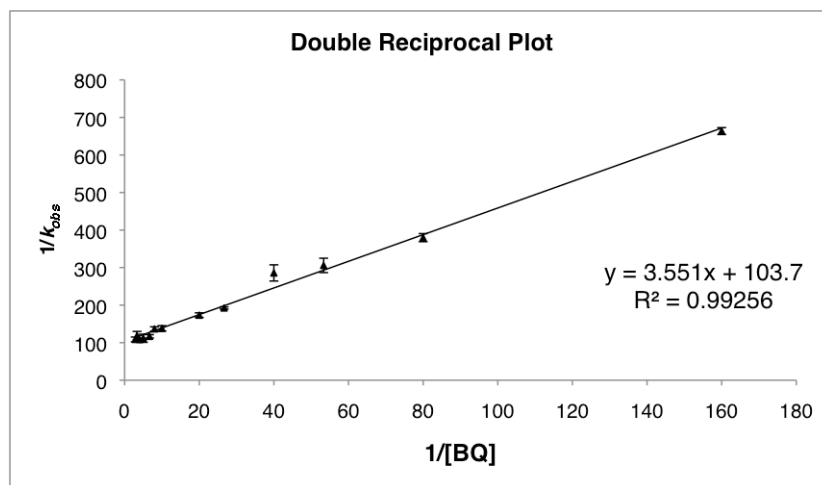
Scheme 5.35 Reaction Conditions for Determining the Order in BQ



Scheme 5.36 Order Studies in BQ.

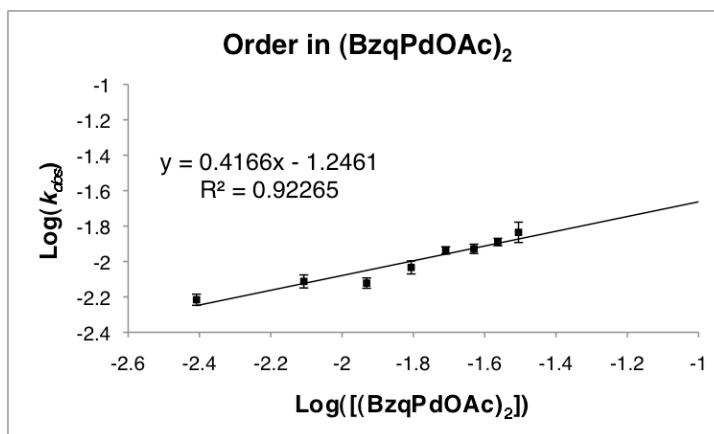
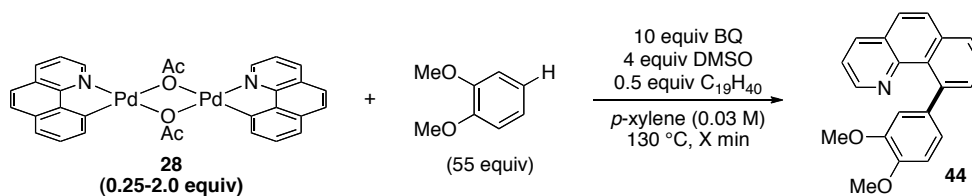


Scheme 5.37 A Linear Double Reciprocal Plot is Consistent with Saturation Kinetics.



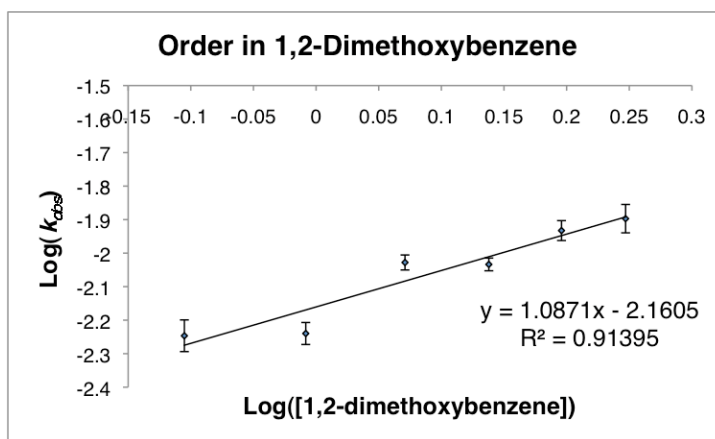
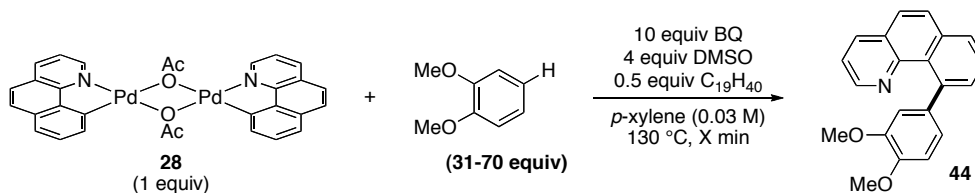
The order in the both the $[BzqPdOAc]_2$ (**28**) and 1,2-dimethoxybenzene were determined under flooding conditions in BQ. The kinetics for determining the order in $[BzqPdOAc]_2$ (**28**) were conducted using the same protocol discussed above, except with 10 equiv of BQ (21.6 mg, 0.2 mmol) where the **[28]** was varied from 0.008-0.03 M (0.25-2.0 equiv). When the $\log([28])$ is plotted against $\log(k_{obs})$ the reaction was found to be 0.42 ± 0.05 order in $[BzqPdOAc]_2$ (Scheme 5.38).

Scheme 5.38 Experiments Determining the Order in $[BzqPdOAc]_2$ (**28**)



When determining the order in 1,2-dimethoxybenzene the concentration of arene needed to change without changing the concentration of the other reagents in the reaction. 1,2-dimethoxybenzene is a co-solvent in the reaction, therefore the concentrations were kept constant by changing both the amounts of 1,2-dimethoxybenzene and *p*-xylene, such that total volume (X mL 1,2-dimethoxybenzene + Y mL *p*-xylene = 0.8 mL). Therefore, the reactions were run with [1,2-dimethoxybenzene] ranging from 0.8-1.8 M (31-70 equiv 1,2-dimethoxybenzene). The change in the solvent medium was assumed to be negligible over the range. As seen in Scheme 5.39, when the $\log([1,2\text{-dimethoxybenzene}])$ was plotted against $\log(k_{obs})$, the order in arene was determined to be 1.08 ± 0.16 .

Scheme 5.39 Determining the Order in 1,2-Dimethoxybenzene

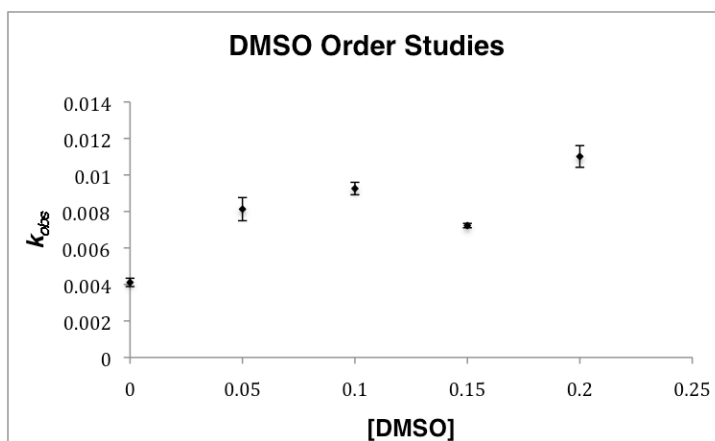
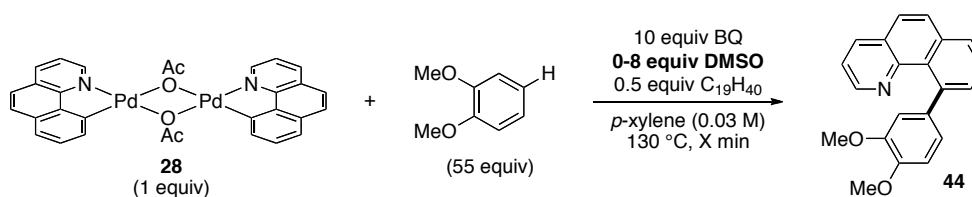


The reaction is half-order in [BzqPdOAc]₂ (**28**) and first-order in 1,2-dimethoxybenzene. The order in **28** is consistent with the dimer being broken up into the monomer and both halves of the dimer proceeding to form the product; only half of the starting Pd-complex is involved in the transition state of the rate determining step. The

first-order dependence on 1,2-dimethoxybenzene indicates that there is one equivalent of arene involved at or before the rate-determining step, which is consistent with one arene reacting with half of the $[\text{BzqPdOAc}]_2$ at or before the rate determining step. These orders and the saturation kinetics observed for BQ are consistent with both mechanism II and mechanism III; therefore, further experiments were needed to distinguish between these pathways.

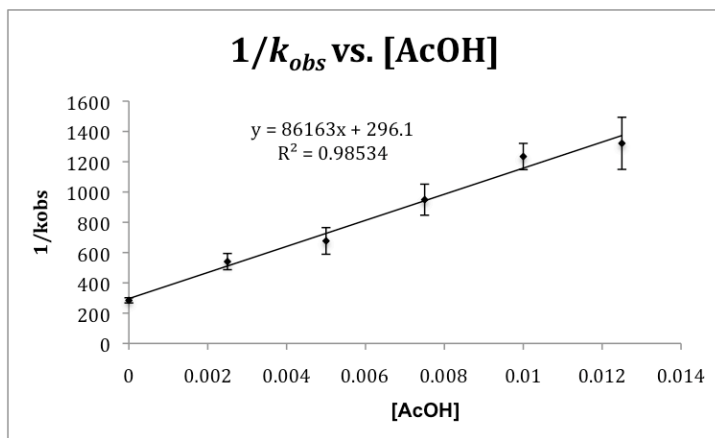
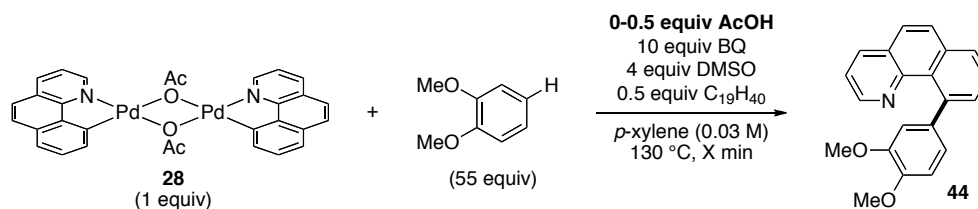
Order studies were also conducted with DMSO (an additive that enhanced the yields of the catalytic reactions) and AcOH (which is generated in the pre-equilibrium step of mechanism III). The rate dependence on DMSO was determined using the standard kinetic conditions with 10 equivalents of BQ and varying the concentration of DMSO from 0-0.2 M (0-8 equiv). As shown in Scheme 5.40, there was no clear order in DMSO (a log-log plot gave an order of 0.12 ± 0.09 with an R^2 of 0.15 suggesting no correlation); however, even small amounts of this additive did lead to a moderate rate enhancement. This may be due to an increase in the solvent polarity stabilizing the transition state or aiding in the solvation of the AcOH that is formed upon C-H activation.

Scheme 5.40 Determining the Order in DMSO



Intriguingly, the reaction was significantly inhibited by the addition of AcOH under both flooding and non-flooding conditions in BQ. There is a linear correlation between $[\text{AcOH}]$ and $1/k_{\text{obs}}$, indicating that the reaction is -1 order in AcOH, as determined by adding 0-0.5 equiv AcOH to the standard kinetic reactions, described above. Inhibition by AcOH does not necessarily imply that the reaction is proceeding through mechanism III, the AcOH could be binding to the $[\text{BzqPdOAc}]_2$ (**28**) and inhibiting the reaction. Alternatively, the addition of the polar protic solvent might have deleterious effects on the reaction, destabilizing the transition state of the rate-determining step. Likewise, it may be counteracting the beneficial effects of the DMSO additive, by tying up the hydrogen bond accepting sulfoxides.

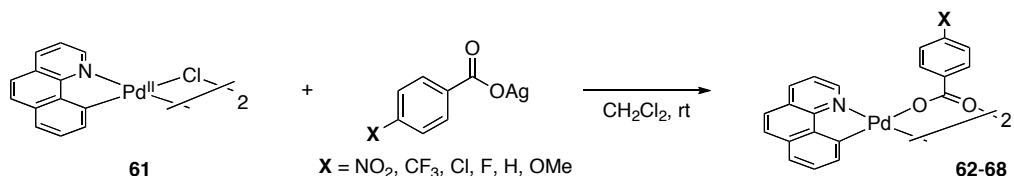
Scheme 5.41 Determining the Order in AcOH



In summary, the order studies allowed us to rule out mechanism I entirely as it would not show saturation kinetics in BQ. In addition, they provided clear evidence that the first step of mechanism II or mechanism III cannot be rate determining. The observed inhibition of the reaction by AcOH provided tentative support for mechanism III. However, additional mechanistic experiments were required to confirm whether mechanism III is operative.

Hammett Studies. Hammett studies were conducted on both the carboxylate and the benzoquinone, by substituting the acetate for *p*-substituted benzoates and using 2,5-di(*p*-X-phenyl)benzoquinone derivatives.

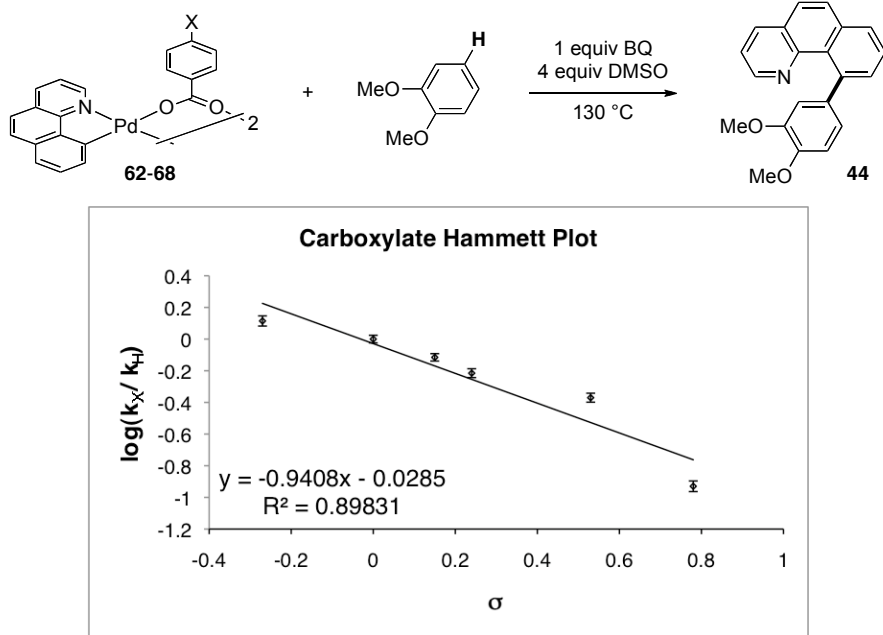
Scheme 5.42 Synthesis of [BzqPdO₂C(*Ar*)]₂ (**62-68**) Complexes.



First, the kinetics of the oxidative coupling reaction were studied with a series of Pd-dimers containing substituted benzoate ligands. These complexes (**62-68**) were prepared by the reaction of the [BzqPdCl]₂ (**61**) with AgO₂C(*p*-X-Ph) in CH₂Cl₂ (Scheme 5.42).

As shown in Scheme 5.43, a Hammett plot was constructed for the reaction of various [BzqPdO₂C(*p*-X-Ph)]₂ derivatives (**62-68**) under saturation conditions in BQ, when step (*i*) is rate determining. The kinetics of the reaction between **62-68** and 1,2-dimethoxybenzene were conducted under the standard kinetic conditions, using [BzqPdO₂C(*p*-X-Ph)]₂, 1,2-dimethoxybenzene (0.14 mL, 1.1 mmol, 55 equiv), BQ (43.2 mg, 0.4 mmol, 20 equiv) and DMSO (5.6 μL, 0.08 mmol, 4 equiv) in *p*-xylenes (0.66 mL) at 130 °C. Under saturation conditions in BQ (where step *i* should be rate determining), the Hammett ρ value was determined to be -0.94 ± 0.16 (Scheme 5.43). This implies that the reaction is moderately accelerated by electron donating groups.

Scheme 5.43 Hammett Plot for Reactions of **62-68** Under Flooding Conditions



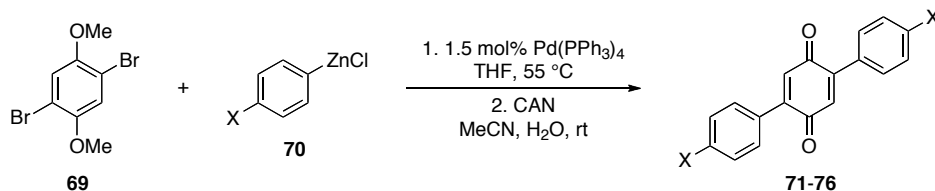
The ρ value for the first step of the reaction is -0.94 ± 0.16 , which is consistent with both mechanisms II and III. The formation of an agostic bond between the Ar–H and the Pd in step *i* of mechanism II, would be accelerated by an electron-donating group on the carboxylate. Ar–H bonds are relatively weak electron donor ligands, therefore the $[\text{BzqPd}(\text{O}_2\text{CAr})(\text{H}-\text{Ar})]$ (**59**, Scheme 5.32) would be destabilized by electron withdrawing groups, as they would increase the electrophilicity of the Pd^{II} .

Step *i* of mechanism III, C–H activation, would also be accelerated by electron-donating groups on the carboxylate. The carboxylate acts as a base, deprotonating the C–H bond. Electron donating groups increase the basicity of a carboxylate and will stabilize any δ^+ charge that builds during the transition state. The observed ρ value of -0.94 ± 0.16 is consistent with both mechanisms II and III and hence does not distinguish between the two.

A second Hammett study was conducted to investigate the influence of benzoquinone electronics on the reaction. A variety of 2,5-di(*p*-X-phenyl)benzoquinone derivatives were synthesized via a two step protocol involving (1) Negishi coupling

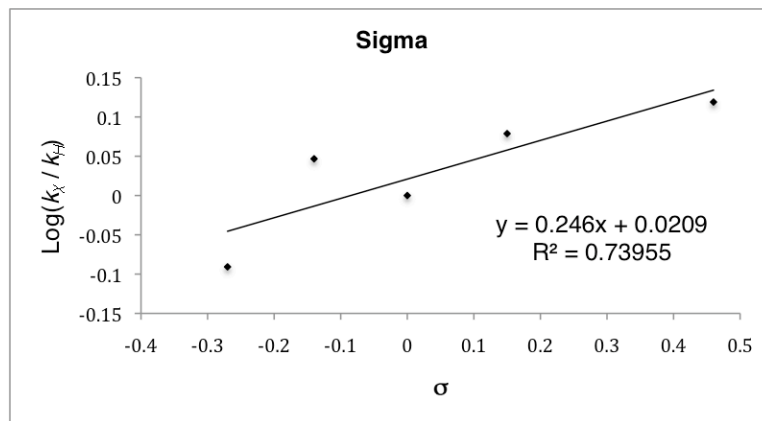
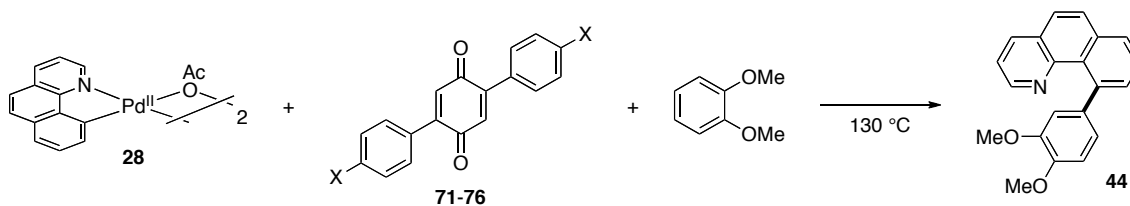
between **69** and **70** followed by (2) oxidative demethylation with ceric ammonium nitrate (CAN) (Scheme 5.44).⁵⁰

Scheme 5.44 Synthesis of Electronically Differentiated Benzoquinone Derivatives⁵⁰



Kinetics of the reaction of **28** and 1,2-dimethoxybenzene in the presence of **71-76** were conducted under the standard conditions described above: [BzqPdOAc]₂ (6.9 mg, 0.01 mmol, 1 equiv (per Pd)), 2,5-di(*p*-X-Ph)-benzoquinone **71-76** (0.02 mmol, 1 equiv), DMSO (5.7 μL, 0.08 mmol, 4 equiv), in 1,2-dimethoxybenzene (0.8 mL, 1.1 mmol, 313 equiv), in *p*-xylene at 130 °C. A Hammett plot of the data showed that $\rho = 0.25 \pm 0.08$, suggesting that the reaction is only slightly accelerated by the electron poor benzoquinone derivatives (Scheme 5.45).

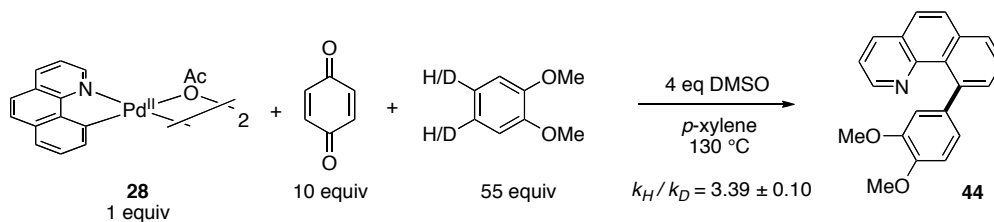
Scheme 5.45 Hammett Plot of Electronically Differentiated BQ Derivatives



The observed small ρ value of 0.25 ± 0.08 for the Hammett plot with electronically differentiated benzoquinone derivatives is consistent with both mechanism II or III operating in the reaction. Increasing the π -acidity of the ligand would make the resulting Pd complex more electrophilic, thereby increasing the rate of electrophilic C–H activation. In addition, increased electrophilicity at the Pd^{II} center is expected to accelerate the reductive elimination.

Kinetic Isotope Effect. We next determined the kinetic isotope effect associated with this reaction by determining the rate with 1,2-dimethoxybenzene and with 4,5-di-deutero-1,2-dimethoxybenzene running the reactions using the standard kinetic protocol. Under flooding conditions, with 10 equivalents of BQ (when step *i* is rate determining) the k_H/k_D is 3.39 ± 0.10 (Scheme 5.46). The moderately large *kie* is consistent with C–H bond breaking, and therefore suggests that the reaction is proceeding through mechanism III. However, there are rare examples of similar *kie* for agostic bond formation (*vide infra*).

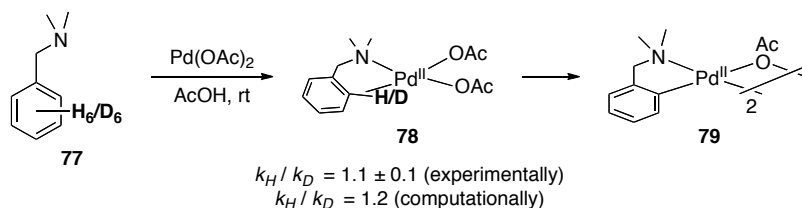
Scheme 5.46 Kinetic Isotope Effect Under Flooding Conditions in BQ.



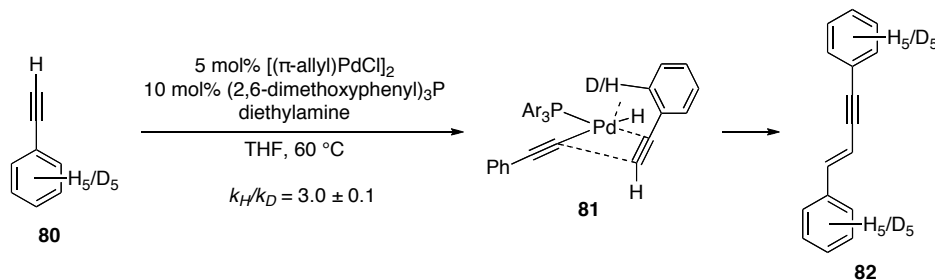
Step *i* of mechanism II is agostic bond formation. Computational studies on the cyclopalladation of benzylamines (such as **77**) suggest that agostic bond formation to give complex **78** is the rate determining step, not C–H bond cleavage. The experimental k_H/k_D for cyclometallation of benzylamine **77** was determined to be 1.1 ± 0.1 which agrees with the computationally predicted value of 1.2 for the agostic bond formation.^{51, 52} The agostic bond formation does not typically have a large *kie*; however, there is a reported example for a *kie* of 3.0 ± 0.1 for the formation of an agostic bond at Pd^{II}.⁵³ It was proposed that the agostic bond between the Pd and the C–H bond (**81**) stabilizes the transition state of the insertion into the alkyne (Scheme 5.48). Additionally, the authors

state that C–H/D bond breaking does not occur, as they observe no H/D exchange. Therefore, the observed *kie* of 3.39 ± 0.10 is possibly explained by mechanism *ii*, however the value is high for a typical agostic bond.

Scheme 5.47 Kinetic Isotope Effect for Agostic Bond Formation^{51, 52}

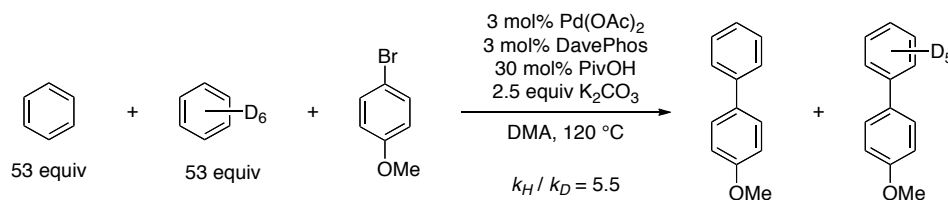


Scheme 5.48 Example of a Large *kie* for Agostic Bond Formation⁵³

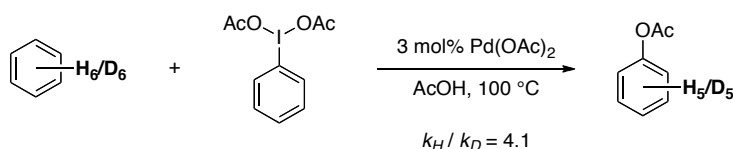


The kinetic isotope effect of 3.4 ± 0.10 can also be explained by step *i* of mechanism III where C–H bond cleavage is occurring; primary kinetic isotopes reported in the literature for Pd-mediated C–H activation range from 3–6.⁵⁴ Two examples of the *kie* when C–H activation is rate determining are the direct-coupling of benzene with bromoanisole which has an intermolecular *kie* of 5.5 in (Scheme 5.49) and the oxidative functionalization of benzene with a *kie* of 4.1 (Scheme 5.50).^{55, 56} Therefore, the *kie* of 3.4 is suggestive that mechanism III is operative in our oxidative cross coupling reactions; however, further experiments are needed to support that the reaction is not proceeding through mechanism II.

Scheme 5.49 Kinetic Isotope Effect for the Direct Coupling between Benzene and Bromoanisole⁵⁵

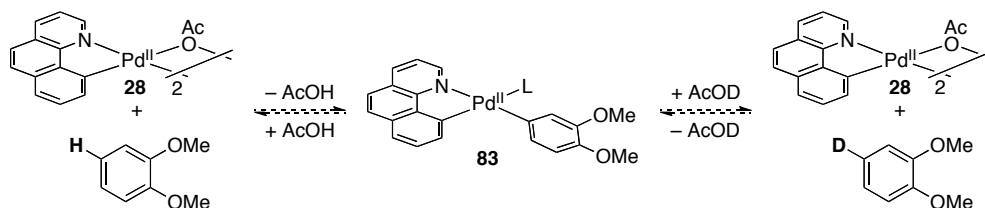


Scheme 5.50 Kinetic Isotope Effect in the Oxidative Functionalization of Benzene⁵⁶



H/D Exchange Experiments. Both the inhibition by acetic acid and the *kie* experiment suggest that operating pathway is mechanism III, which involves a rapid, reversible C–H activation reaction followed by benzoquinone promoted reductive elimination. If this were, indeed, the mechanism, then there should be observable H/D exchange between arene, 1,2-dimethoxybenzene, and added AcOD in the absence of BQ.

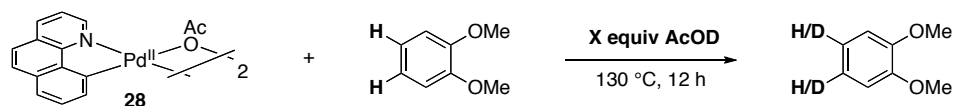
Scheme 5.51 [BzqPdOAc]₂ Catalyzed H/D Exchange without BQ



Indeed, as seen in Table 5.5, when the reactions were run without BQ in the presence of AcOD, H/D exchange was observed ([BzqPdOAc]₂ (**28**) (6.9 mg, 0.01 mmol, 1 equiv (based on Pd)), AcOD-*d*₄ (10-100 equiv), 1,2-dimethoxybenzene (0.8 mL, 1.1 mmol, 313 equiv) at 130 °C for 12 h, deuterium incorporation was monitored by ²D NMR by comparison to an internal standard). % D incorporation is the percentage of the deuterioacetic acid which has been incorporated in to the 1,2-dimethoxybenzene (mmol deuterio-1,2-dimethoxybenzene / mmol AcOD). Importantly, there was no exchange in

the control reactions without added **28**. This evidence strongly supports that mechanism III is occurring in the Pd-mediated oxidative cross-coupling reactions.

Table 5.5 H/D Exchange Studies.



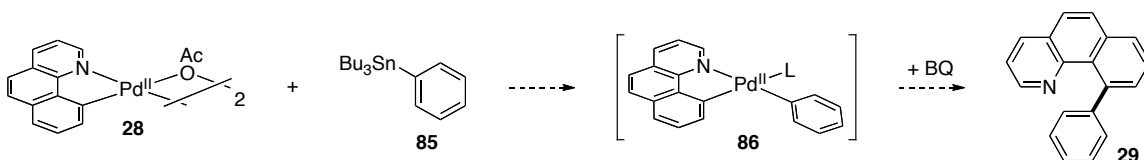
equiv AcOD	% D incorporation	TON
10	70	6.9
50	50	25
100	27	27

Reductive elimination studies from BzqPdAr. If mechanism III is operating, then reductive elimination of the Bzq–Ar bond should only occur in the presence of BQ. However, attempts to synthesize **84** independently have been unsuccessful. Although reductive elimination does not occur, the Pd–Ar bond appears to be very sensitive to protonation and, perhaps, other decomposition pathways.

Scheme 5.52 Benzoquinone Catalyzed Reductive Elimination of **84**



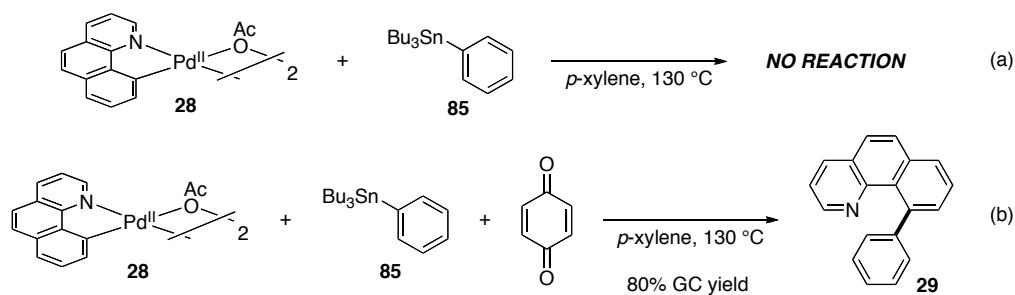
Scheme 5.53 *In Situ* Formation of the Bisaryl Complex through Transmetalation.



The Pd-bisaryl complex **86** may be made *in situ* by transmetalation with an aryl tin reagent (Scheme 5.53). When [BzqPdOAc]₂ (**28**) (6.9 mg, 0.01 mmol, 1 equiv (based on Pd)), tributylphenyltin (**85**) (6.5 μ L, 0.02 mmol, 1 equiv), and DMSO (5.7 μ L, 0.08

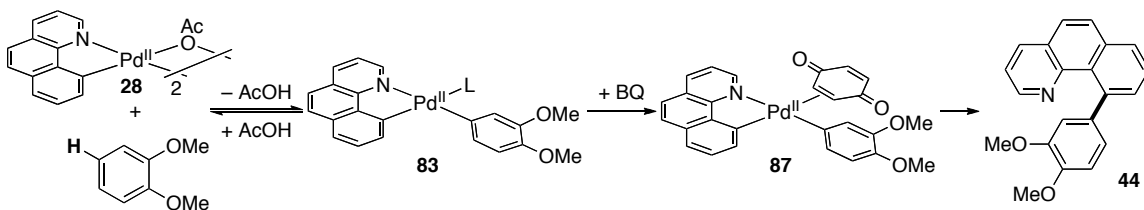
mmol, 4 equiv) were heated to 130 °C in *p*-xylene, no reductive elimination products were observed by GC analysis of the crude reaction mixture (Scheme 5.54a). However when the same reagents were heated in the presence of BQ (2.2 mg, 0.02 mmol, 1 equiv), the cross-coupled product (**29**) was formed in 80% GC yield (Scheme 5.54b). This experiment strongly supports that BQ is required for reductive elimination and that mechanism III is operative.

Scheme 5.54 Reductive Elimination Studies from the Pd-Bisaryl Complex with and without BQ.



Together these experiments suggest that the palladium-mediated oxidative coupling reaction proceeds through mechanism III, which involves a rapid, reversible C–H activation, followed by benzoquinone-catalyzed reductive elimination and formation of the new C–C bond (Scheme 5.55). Now that the mechanism of the second C–H activation was better understood, we sought to study the factors that influence the regioselectivity of the second C–H activation/oxidative coupling reaction. In particular, we hoped to develop conditions that would afford the oxidative cross-coupled products with high and potentially tunable regioselectivity.

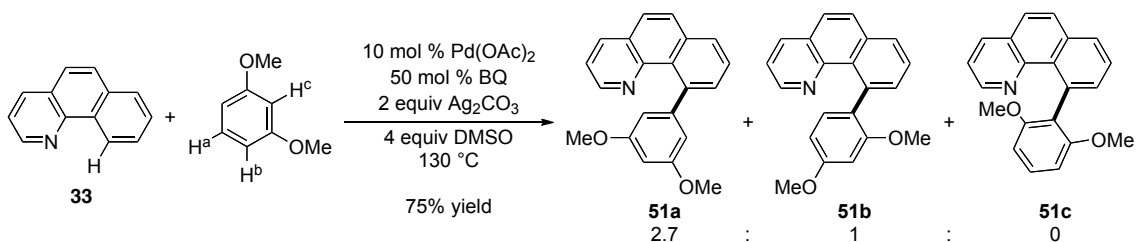
Scheme 5.55 Mechanism for the Pd-Mediated Oxidative Cross-Coupling Reaction.



5.4 Regioselectivity Studies

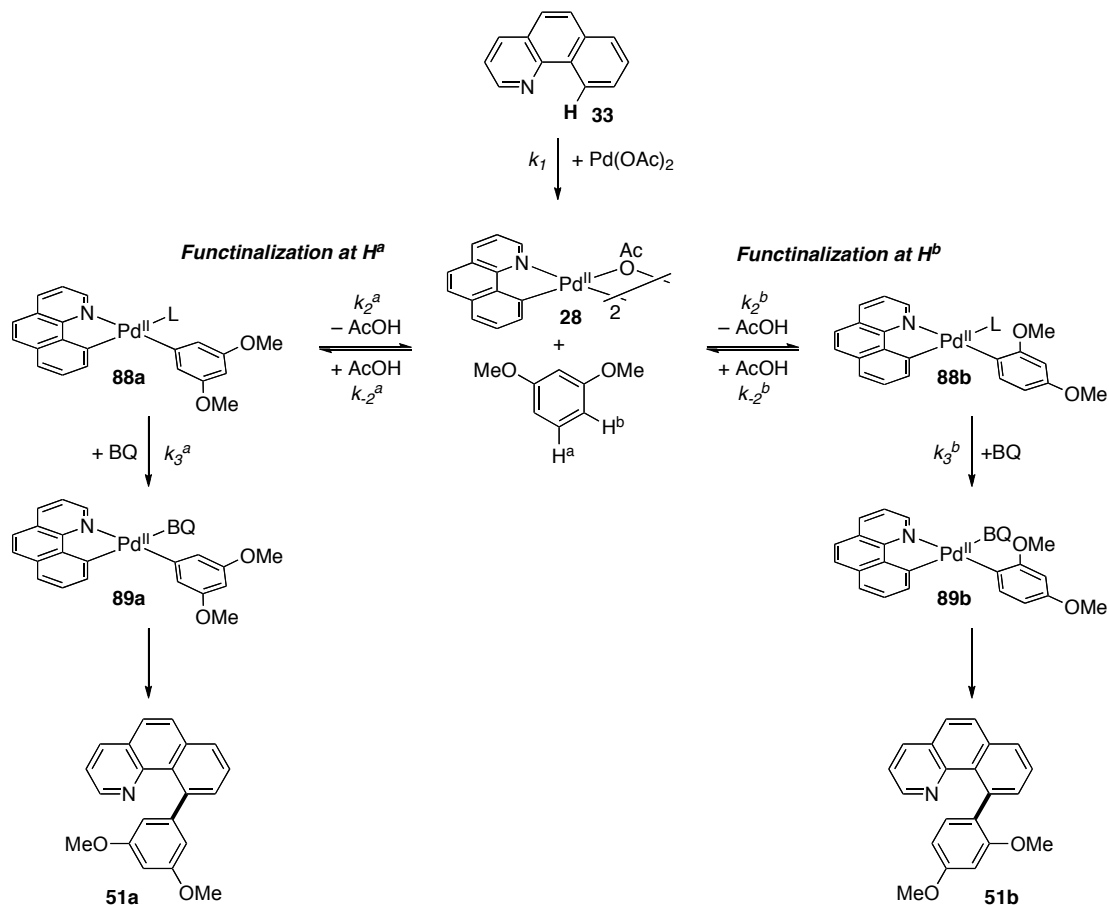
The regioselectivity observed in Pd-catalyzed oxidative cross-coupling reactions was highly dependent on the steric environment of the C–H bonds, and less hindered C–H bonds were selectively functionalized over more hindered C–H bonds. Conversely, when the adjacent functional group was relatively small (such as a MeO) the regioselectivity was diminished, and a mixture of isomers was formed (Table 5.4, page 141). For instance, the Pd-catalyzed oxidative coupling of benzo[*h*]quinoline (**33**) and 1,3-dimethoxybenzene afforded a 2.7 : 1 (**51a** : **51b**) mixture of two of the three possible regioisomers Scheme 5.56.

Scheme 5.56 Oxidative Coupling of Benzo[*h*]quinoline (**33**) and 1,3-Dimethoxybenzene.



Based on the mechanistic studies (*vide supra*) the proposed mechanism for the formation of both isomers is shown in Scheme 5.57. The mechanism involves initial cyclopalladation of the benzo[*h*]quinoline (**33**), followed by a reversible C–H activation at either the 3 or 4 position of the 1,3-dimethoxybenzene, and then BQ-promoted reductive elimination to afford the two products. The product ratio of **51a** : **51b** will be dependent on the relative rates of: (1) C–H activation at H^a vs. H^b, (2) protonation of the Pd–Ar bond of **88a** and **88b**, and (3) coordination of the BQ. We hypothesized that changing the ancillary ligands on the Pd (ie, the carboxylate and benzoquinone) might change some/all of these relative rates, and therefore allow for tuning of the regioselectivity of this reaction. Preliminary studies support this hypothesis. For example, in the oxidative coupling of benzo[*h*]quinoline (**33**) and anisole, increasing the substitution on the BQ decreased the formation of the *ortho* (**51o**) functionalized product relative to the *meta* (**51m**) or *para* (**51p**) isomers (Scheme 5.28, page 144).

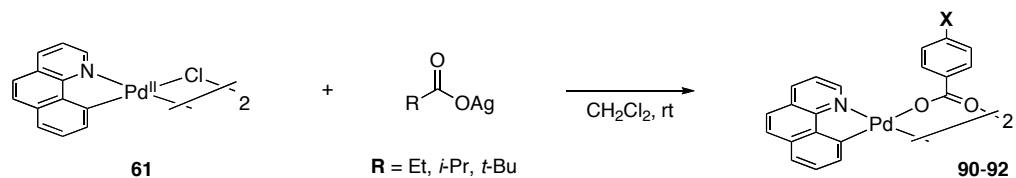
Scheme 5.57 Proposed Mechanism for the Formation of the Two Isomers Formed in **Scheme 5.56**.



Thus, our efforts focused on a methodical study of effect of the both the sterics and electronics of the carboxylate and quinone ligands on the regioselectivity of the reaction.

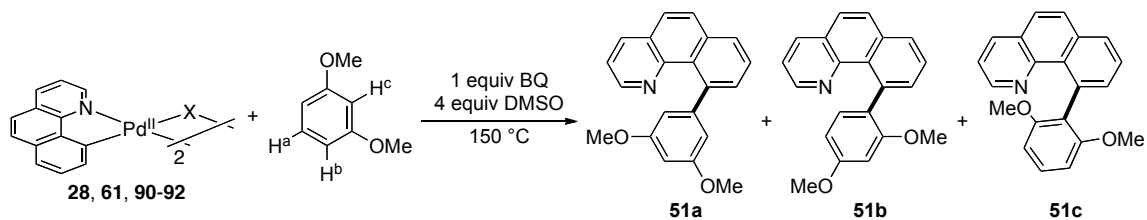
Carboxylate Ligand. Our initial experiments probed the effect of the carboxylate on the regioselectivity of the oxidative cross-coupling reaction. The reactions were run with stoichiometric Pd, so that the oxidant Ag_2CO_3 would not be required, as it would supply a second anionic ligand to the reaction (along with the carboxylate) and complicate the data analysis. The requisite palladium complexes **90-92** were synthesized as described in Scheme 5.58.

Scheme 5.58 Synthesis of BzqPd Carboxylate Complexes **90-92**



We first explored the effect of carboxylate sterics on the regioselectivity of the oxidative coupling reaction. A series of reactions were run with [BzqPd(O₂R)]₂ (**28**) (0.01 mmol, 1 equiv (based on Pd)), benzoquinone (BQ) (2.2 mg, 0.02 mmol, 1 equiv), DMSO (5.7 μL, 0.08 mmol, 4 equiv), nonadecane (internal standard, 2.7 mg, 0.01 mmol, 0.5 equiv) and 1,3-dimethoxybenzene (0.8 mL) at 150 °C for 12 hours. The reaction yield and isomer ratios were determined by GC analysis.

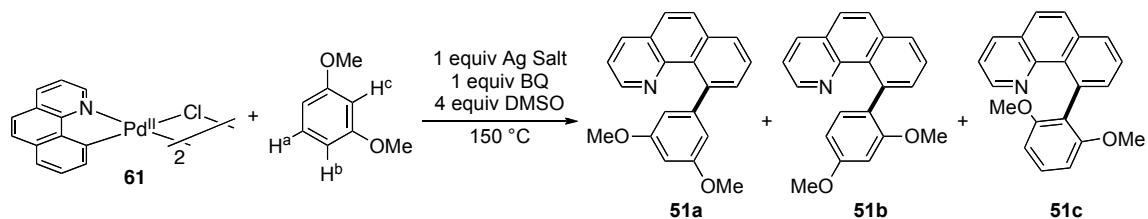
As shown in Table 5.6, the stoichiometric reaction between [BzqPd(OAc)]₂ (**28**) and 1,3-dimethoxybenzene afforded the oxidative coupled product with greater selectivity for isomer A than the catalytic reaction, 7.7 : 1 compared to 2.7 : 1, respectively (Table 5.6, entries 1 and 2). Importantly, in the catalytic reaction, both acetate and carbonate anions are present. Thus, this result suggested that the carbonate might be responsible for eroding the selectivity. Indeed, when the reaction is run with carbonate as the counter anion (via the *in situ* reaction between [BzqPdCl]₂ (**61**) and Ag₂CO₃), the regioselectivity was completely reversed and **51b** is now the major product (Table 5.6, entry 3). Interestingly, when CO₃²⁻ was the anion, small amounts of **51c** are also observed, indicating that the steric hindrance of the two methoxy groups no longer prevented functionalization at H^c. This exciting result suggested that conditions might be developed for the Pd-catalyzed oxidative cross-coupling reaction that would selectively form **51a** or **51b** by simply switching the anionic ligand employed in the reaction from AcO⁻ to CO₃²⁻.

Table 5.6 Effects of Changing the Sterics of the Carboxylate.

Entry	X	% yield	51a : 51b : 51c
1	AcO ⁻ and CO ₃ ²⁻ *	75%	2.7 : 1 : 0
2	AcO ⁻	76%	7.7 : 1 : 0
3	Cl ⁻ and Ag ₂ CO ₃	48%	1 : 8.8 : 1.1
4	EtCO ₂ ⁻	86%	8.7 : 1 : 0
5	<i>i</i> -PrCO ₂ ⁻	88%	12.1 : 1 : 0
6	<i>t</i> -BuCO ₂ ⁻	71%	11.3 : 1 : 0

* yield and ratio are from the catalytic reaction, shown in Scheme 5.56

There are at least three possible factors that may influence this reversal in selectivity. First, the AgCO₃⁻ or CO₃²⁻ anions may have less influence over steric environment at the Pd center, therefore they may allow for easier C–H activation at the more hindered C–H bond. Second, softer AgCO₃⁻ may be less coordinating anion than AcO⁻, and therefore may render the Pd more electrophilic enhancing its reactivity with the more electron rich C–H bond. To test this hypothesis, a variety of other less coordinating anions, including as SbF₆⁻, BF₄⁻ and SO₄²⁻, were screened yet there was no clear trend with coordinating ability and the ratio of isomers formed (Table 5.7, entries 3-5). Finally, the reverse reaction of C–H activation, protonation of the Pd–C bond, may be slower when carbonate is the anion, as HCO₃⁻ (pK_a = 10.3) is less acidic than AcOH (pK_a = 4.8).⁵⁷ However, when a variety of anions were studied with varying basicities, there was no clear trend with selectivity (Table 5.7, entries 1-7). PO₄³⁻ is more basic than CO₃²⁻, however it gives **51a** selectively over **51b**. However, the less basic anions, such as SF₆⁻, BF₄⁻ and SO₄²⁻ were unreactive under the reaction conditions (Table 5.7, entries 3-5). Tom Lyons is currently conducting studies to determine the source of the reversal in regioselectivity when silver carbonate is employed.

Table 5.7 Effects of Changing the Sterics of the Carboxylate.

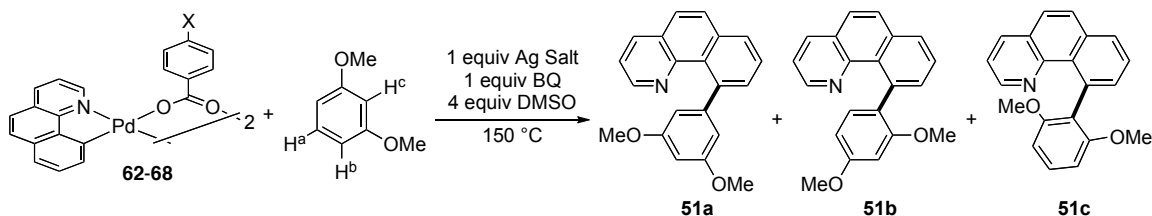
Entry	X	pK _a	% yield	51a : 51b : 51c
1	AgOAc	4.76	58%	9 : 1 : 0
2	Ag ₂ CO ₃	10.3, 3.6	48%	1 : 8.8 : 1.1
3	AgBF ₄	-0.4	0%	- : - : -
4	AgSbF ₆	-25	0%	- : - : -
5	Ag ₂ SO ₄	1.99, -3.0	0%	- : - : -
6	AgTFA	-0.25	8%	7.6 : 1 : 0
7	Ag ₃ PO ₄	12.32, 7.21, 2.12	29%	3.1 : 1 : 0

We also examine carboxylates that are more sterically encumbering than AcO⁻ (Table 5.6, entries 2, 4-6). When switching from MeCO₂⁻ (OAc) to EtCO₂⁻, the selectivity for **51a** was only moderately increased; this is not surprising as the *a*-values for Me and Et are both 1.8. Increasing the substitution further, to *i*-PrCO₂ and *t*-BuCO₂ increased the selectivity for **51a**, suggesting that the steric hindrance of the carboxylate can have a significant effect on the regioselectivity of the oxidative coupling reaction. Importantly, the pK_a values for AcOH, EtCO₂H, *i*-PrCO₂H, and *t*-BuCO₂H are 4.79, 4.88, 4.84, and 5.01, respectively, suggesting that there is little electronic difference between the four carboxylates. Therefore, the observed effects are likely primarily due to their steric differences. The increase in sterics may be slowing the C–H activation adjacent to H^b, thus making k_2^b smaller relative to k_2^a and favoring the formation of **51a** (Scheme 5.57, page 163).

Next, we aimed to study the effect of the electronics of the carboxylate on the regioselectivity of the reaction. By exchanging the AcO⁻ ligand for *para*-substituted benzoates, the electronics of the ligand can be varied without altering the steric environment at the metal center. Interestingly, the substituted benzoate derivatives all afforded the desired cross-coupled products with relatively similar selectivities, where

51a was favored. There was no trend between the selectivity of the reaction and the electron donating/withdrawing nature of the carboxylate, and when the selectivities were plotted against σ , $\rho = 0.56$ and $R^2 = 0.27$, indicating a lack of correlation. This suggests that the change in the electronics of the carboxylate has approximately the same effect on the relative rates of formation of both **51a** and **51b**.

Table 5.8 Changing the Electronics of the Carboxylate.



Entry	X	σ value	% yield	51a : 51b : 51c
1	NO ₂	0.78	39%	14.2 : 1 : 0
2	CF ₃	0.53	45%	11.2 : 1 : 0
3	Cl	0.24	56%	12.1 : 1 : 0
4	F	0.15	67%	13.5 : 1 : 0
5	H	0	62%	12.0 : 1 : 0
6	OMe	-0.27	58%	11.2 : 1 : 0

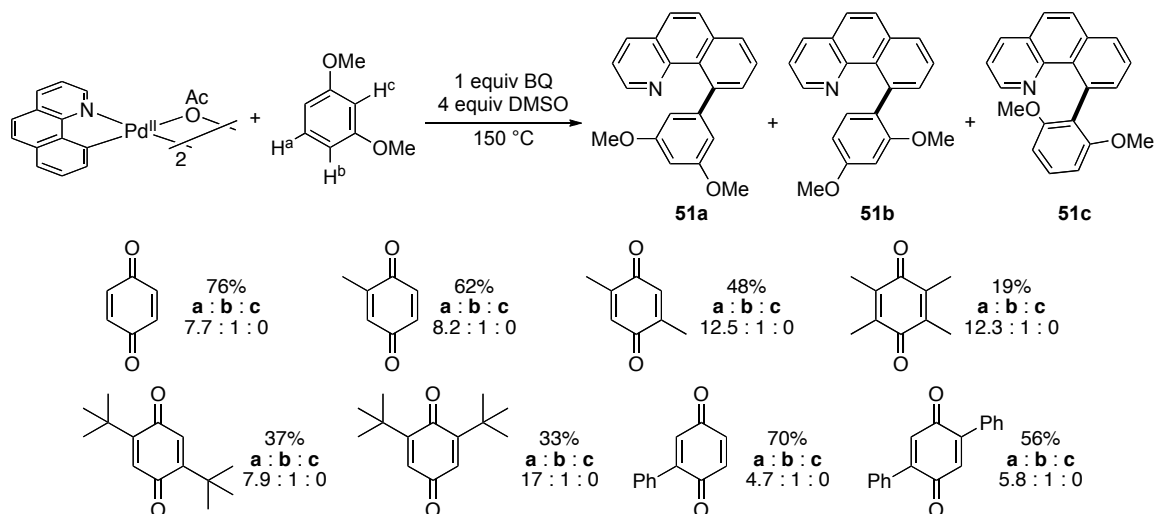
To summarize, the steric environment about the carboxylate anion does have a significant influence on the regioselectivity of the oxidative coupling. Increasing the steric bulk of the carboxylate increases the selectivity for functionalization at the less sterically hindered C–H bond. However, the selectivity is not influenced significantly by electronic modification of the carboxylate. Additionally, the selectivity can be switched to favor the **51b** by using carbonate as the counter ion in place of a carboxylate. Although the origin of this effect needs to be studied in further detail, it is presumably due to the more electrophilic nature and/or irreversibility of the C–H activation.

Quinone Ligand. We next sought to gain a better understanding of the effect of the quinone on the regioselectivity in the Pd-catalyzed oxidative cross-coupling reaction. Previously, we demonstrated that the ratio of regioisomers formed in the oxidative coupling of benzo[*h*]quinoline (**33**) with anisole changed with additional substitution on the benzoquinone (Scheme 5.28, page 144). In order to study the effects of the quinone

ligand on the oxidative coupling reaction systematically, we choose to investigate the oxidative coupling between 1,3-dimethoxybenzene and either [BzqPdOAc]₂ (**28**) or [BzqPdCl]₂ (**61**) in the presence of a variety of sterically and electronically differentiated benzoquinone derivatives.

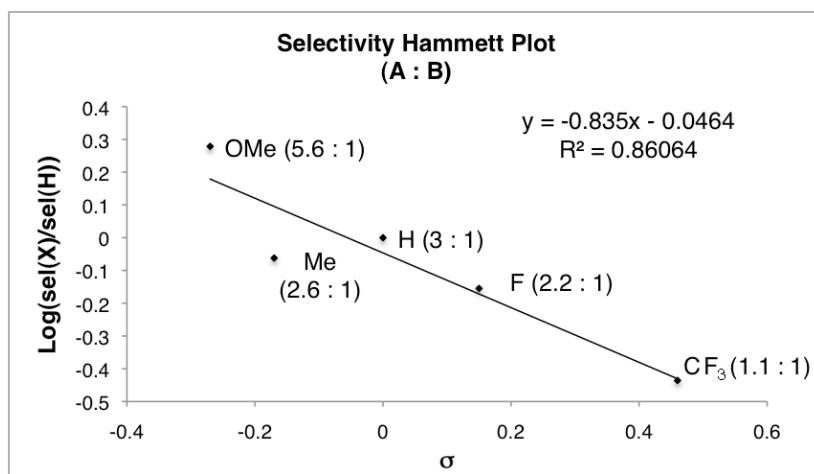
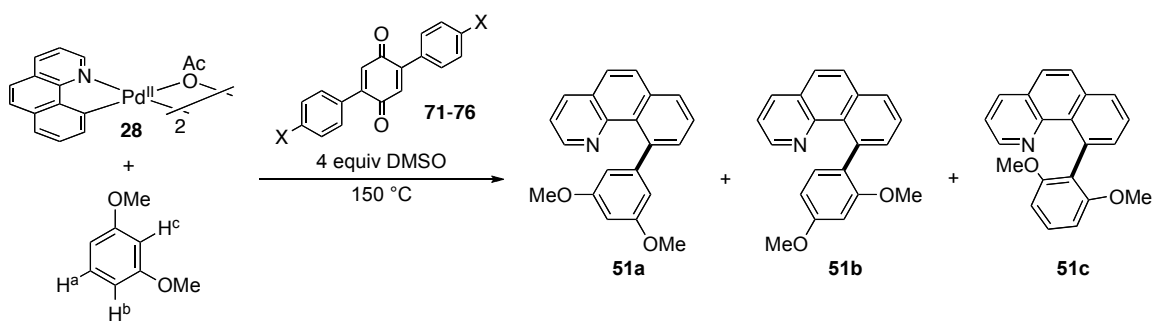
A series of reactions were run with [BzqPdOAc]₂ (**28**) (6.9 mg, 0.01 mmol, 1 equiv (based on Pd)), “BQ” derivative (0.02 mmol, 1 equiv), DMSO (5.7 μL, 0.08 mmol, 4 equiv), nonadecane (internal standard, 2.7 mg, 0.01 mmol, 0.5 equiv) and 1,3-dimethoxybenzene (0.8 mL) at 150 °C for 12 hours. The reaction yield and isomer ratios were determined by GC analysis. The benzoquinone derivatives with increasing substitution, going from benzoquinone, to 2-methyl, 2,5-dimethyl, and tetramethylbenzoquinone did increase the regioselectivity, favoring **51a**. 2,5-Dimethyl- and tetramethylbenzoquinone both afforded the desired product in approximately the same 12 : 1 (**51a** : **51b**) selectivity. Increasing the steric hindrance of the ligand even more (going to 2,6-di-*tert*-butylbenzoquinone) increased the selectivity further; however, this reaction afforded the products **51a** and **51b** in only 33% total yield. Interestingly, 2,5-di-*tert*-butylbenzoquinone afforded the product in approximately the same regioisomeric ratio as BQ. Importantly, increasing the substitution on the BQ also affects the electronic nature of this ligand, as alkyl groups are relatively electron donating. This effect is seen when 2-phenyl- and 2,5-diphenylbenzoquinone were utilized as the π-acid catalyst, and the regioselectivity of the reaction decreased to 4.7 : 1 and 5.5 : 1 (**51a** : **51b**), respectively. Relative to the methyl group, a phenyl ring is both larger and more electron withdrawing; therefore, this loss in regioselectivity may be explained by the electron poor nature of the quinone ligand.

Scheme 5.59 Effect of Changing the Benzoquinone on the Regioselectivity.



In order to deconvolute the steric and electronic effects, the regioselectivity was determined using a variety of *para*-substituted 2,5-diphenylbenzoquinone derivatives. There was little effect on the rate of the oxidative coupling reaction when the electronics of the benzoquinone were systematically changed (Scheme 5.45, page 156). A series of reactions were run with [BzqPdOAc]₂ (**28**) (6.9 mg, 0.01 mmol, 1 equiv (based on Pd)), 2,5-di(*p*-X-Ph)-benzoquinone (0.02 mmol, 1 equiv), DMSO (5.7 μL, 0.08 mmol, 4 equiv), nonadecane (internal standard, 2.7 mg, 0.01 mmol, 0.5 equiv) and 1,3-dimethoxybenzene (0.8 mL) at 150 °C for 12 hours. The reactions were then analyzed by GC and the product ratio of **51a** : **51b** : **51c** was determined. A Hammett plot was constructed, plotting $\log\left(\frac{(\mathbf{51a}/(\mathbf{51a} + \mathbf{51b} + \mathbf{51c}))_X}{(\mathbf{51a}/(\mathbf{51a} + \mathbf{51b} + \mathbf{51c}))_H}\right)$ versus σ (Scheme 5.60). The resulting ρ -value was -0.84 ± 0.19 suggests that the electronic nature of the BQ does have an affect on the regioselectivity in the oxidative coupling between [BzqPdOAc]₂ (**b28**) and 1,3-dimethoxybenzene. This moderate negative value indicates that electron rich BQ ligands increase the selectivity for formation of isomer **51a**, while electron withdrawing groups favor **51b**. For example, when 2,5-di(*p*-CF₃-phenyl)benzoquinone was employed the reaction proceeded to give a 1.1 : 1 mixture of **51a** : **51b**.

Scheme 5.60 Selectivity Hammett Plot for the Quinone Ligand.



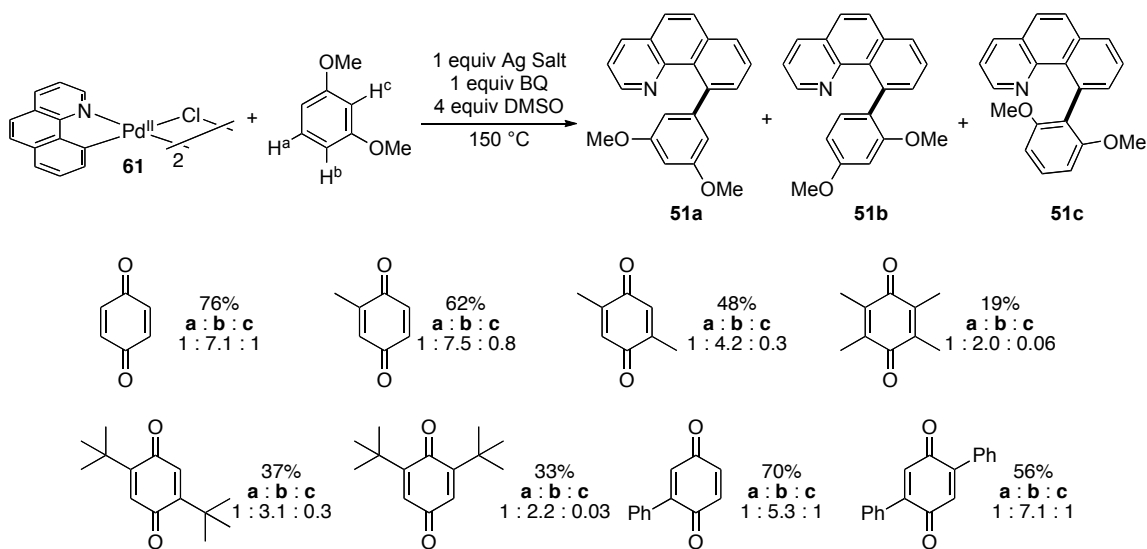
There are two possible explanations for the electronic effects of the BQ on the regioselectivity of the oxidative coupling reaction. First, the benzoquinones substituted with electron withdrawing groups are better π -acids, and therefore may be more reactive. An increase in reactivity often leads to a concomitant decrease in selectivity. However, our mechanistic studies revealed that there was little effect of the electronics of the BQ on the rate of the reaction; therefore this switch in reactivity is unlikely to be result from the increased reactivity of the electron poor benzoquinone. A second possible explanation is that the Pd–C bond of **89b** that leads to **51b** is relatively electron rich, as the carbon is both *ortho* and *para* to methoxy groups, while the Pd-complex **89a** that leads to **51a** has a relatively electron poor Pd–C bond. The electron poor benzoquinone may be relatively faster at reacting with the electron rich Pd-complex than an electron rich BQ.

Our studies on the carboxylate ligand found that **51b** is favored when carbonate is the anionic ligand rather than acetate and trace amounts of **51c** are formed (Table 5.6, page 165). We were interested in determining the effect of the quinone ligand on

reactions that favor the formation of **51b**. More specifically, we hoped to be able to tune the reaction to form **51b** with high selectivity over both isomers **51a** and **51c**.

To study the affect of the sterics of the BQ on the coupling reaction between [BzqPdCl]₂ (**61**) with Ag₂CO₃ a series of reactions were run with [BzqPdCl]₂ (**61**) (6.4 mg, 0.01 mmol, 1 equiv (based on Pd)), Ag₂CO₃ (5.5 mg, 0.02 mmol, 1 equiv), “BQ” derivative (0.02 mmol, 1 equiv), DMSO (5.7 μL, 0.08 mmol, 4 equiv), nonadecane (internal standard, 2.7 mg, 0.01 mmol, 0.5 equiv) and 1,3-dimethoxybenzene (0.8 mL) at 150 °C for 12 hours. The reactions were then analyzed by GC and the product ratio of **51a** : **51b** : **51c** was determined. As seen in Scheme 5.61, increasing the number of methyl groups on the BQ favored the formation of **51a**, though the selectivity never reversed to make **51a** the major isomer. Also, when 2-phenyl and 2,5-diphenylbenzoquinone are used, the selectivity was again similar to that of BQ suggesting that electron withdrawing groups favor the formation of **51b**.

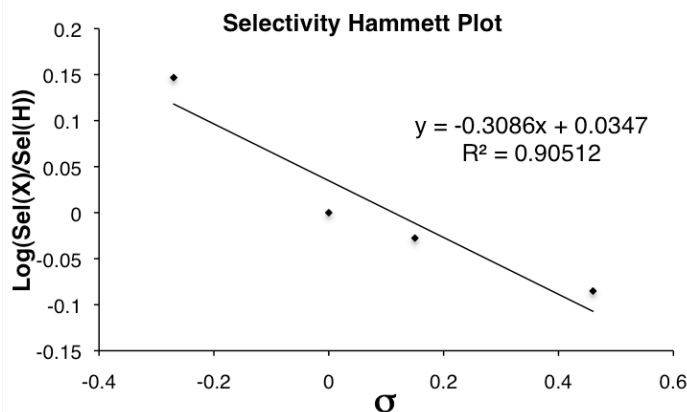
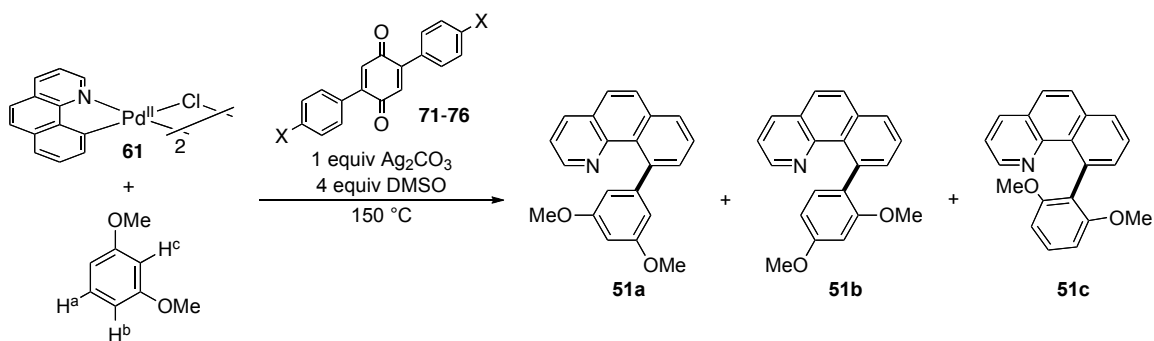
Scheme 5.61 Effect of the Benzoquinone Ligand with Carbonate Anions.



To study the affect of the electronics of the BQ on the coupling reaction between [BzqPdCl]₂ (**61**) with Ag₂CO₃ a series of reactions were run with [BzqPdCl]₂ (**61**) (6.4 mg, 0.01 mmol, 1 equiv (based on Pd)), Ag₂CO₃ (5.5 mg, 0.02 mmol, 1 equiv), 2,5-di(p-X-Ph)-benzoquinone (0.02 mmol, 1 equiv), DMSO (5.7 μL, 0.08 mmol, 4 equiv),

nonadecane (internal standard, 2.7 mg, 0.01 mmol, 0.5 equiv) and 1,3-dimethoxybenzene (0.8 mL) at 150 °C for 12 hours. The reactions were then analyzed by GC and the product ratio of **51a** : **51b** : **51c** was determined. A Hammett plot was constructed, plotting $\log((\mathbf{51a}/(\mathbf{51a} + \mathbf{51b} + \mathbf{51c}))_X/(\mathbf{51a}/(\mathbf{51a} + \mathbf{51b} + \mathbf{51c}))_H)$ versus σ (Scheme 5.61). The Hammett plot shows that electron donating groups favor the formation of **51a** while electron withdrawing groups favor **51b**, similar to the studies with the AcO^- anion. This again suggest that electron poor benzoquinones may bind better to electron rich palladium centers, therefore they favor the formation of **51b**.

Scheme 5.62 Selectivity Hammett Plot for the Electronics of the Quinone Ligand with Carbonate Anions



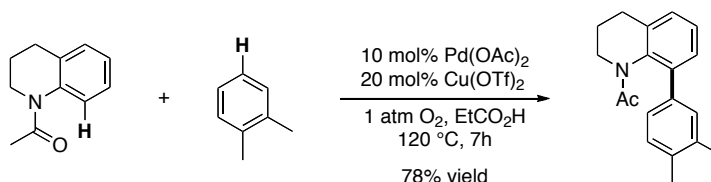
To summarize, both of the ancillary ligands – the carboxylate and the benzoquinone – influence the regioselectivity of the Pd-mediated oxidative cross-coupling reaction. Sterically bulky carboxylates and sterically bulky, electron rich benzoquinones favor the formation of **51a**. When the anionic ligand on the Pd-complex is a carbonate and relatively electron poor benzoquinones are employed, **51b** is favored.

Although **51c** is a minor product when carbonate ligands are employed, conditions to form this as the major regioisomer have not yet been identified.

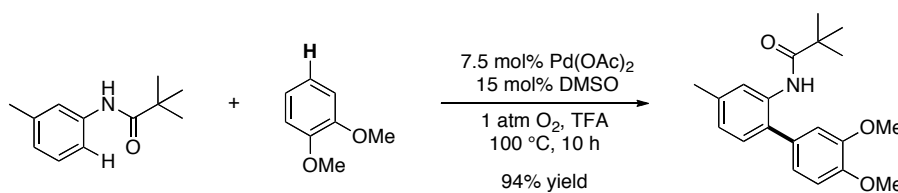
5.5 Subsequent Examples

Several groups have reported simultaneous efforts towards related regioselective Pd-catalyzed oxidative cross-coupling reactions. For example, shortly after our initial publication, Shi demonstrated that *N*-acetanilides can be oxidatively coupled with arenes in the presence of a co-catalytic amount of copper using O₂ as the terminal oxidant (Scheme 5.63).⁵⁸ Buchwald demonstrated that the Cu co-catalyst was not required if the reaction was run in TFA with 15 mol % of DMSO (Scheme 5.64).⁵⁹ Both groups saw similar selectivity, where the functionalization on the substrate lacking a directing group occurred at the less sterically hindered C–H bond. However, they were both limited to fairly electron rich arenes, fluorobenzene and benzene were the most electronically poor arenes used, respectively. Additionally, the reactions lacked any ancillary ligands, which might be changed to tune the regioselectivity in the reactions - these reactions did not require benzoquinone to promote the reductive elimination and as the reactions are run in carboxylic acid solvents, the tuning of the carboxylate is limited.

Scheme 5.63 Shi's Example of Amide Directed Oxidative Cross-Coupling of C–H Bonds⁵⁸

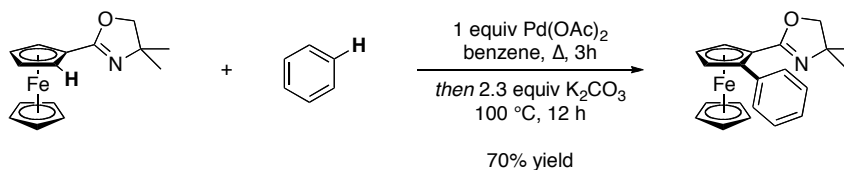


Scheme 5.64 Buchwald's Cu-Free Conditions⁵⁹



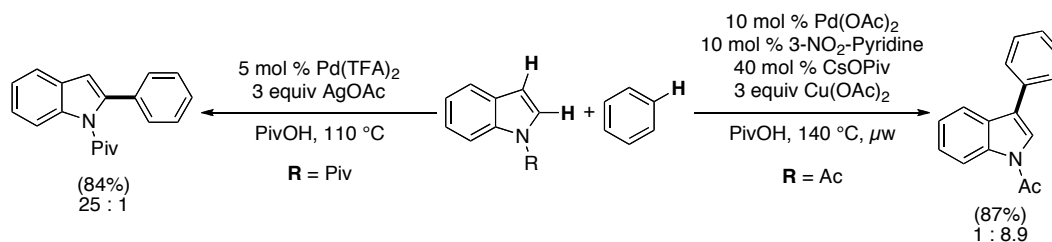
The stoichiometric oxidative coupling of ferrocenyl oxazoline derivatives was also demonstrated. You reported that the reaction went through an initial cyclopalladation of the ferrocene followed by a C–H activation of benzene.⁶⁰ Although initial attempts to make the reaction catalytic are reported, the conditions developed were not general to arenes other than benzene.

Scheme 5.65 Pd-Mediated Oxidative Cross-Coupling of Ferrocenyl Oxazolines and Benzene⁶⁰



The substrate scope for the oxidative coupling of activated heterocycles and arenes has also been expanded. Fagnou demonstrated that pyrroles were also effective substrates, acting as the nucleophilic heterocycles, and were selectively functionalized at the 2-position.²¹ Additionally, both Fagnou and DeBoef found that using AgOAc as the oxidant in place of Cu(OAc)₂, leads to a reversal of the regioselectivity of the indole activation to the 2-position (Scheme 5.66).^{21, 23} Finally, as with observed in our oxidative coupling reactions, when 1,2-disubstitued arenes were employed, the less hindered C–H bond is selectively functionalized.

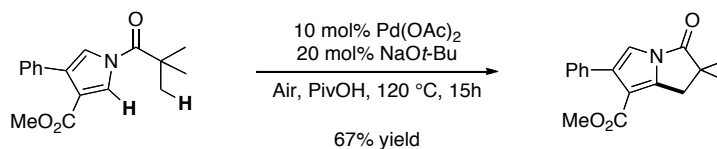
Scheme 5.66 Tunable Selectivity Dependant on the Oxidant Employed.^{20, 21}



Finally, the intramolecular oxidative coupling between an activated heterocycle and an unactivated sp³ C–H bond has been demonstrated (Scheme 5.67).⁶¹ The authors propose a mechanism involving initial electrophilic palladation followed by C–H

activation of the sp^3 C–H bond, and finally reductive elimination to form the new C–C bond. They observed that primary C–H bonds were selectively functionalized over secondary and that sp^2 C–H bonds were selectively functionalized over sp^3 .

Scheme 5.67 Intramolecular Oxidative Cross-Coupling to Form an sp^3 – sp^2 C–C Bond.



5.6 Conclusions

We have demonstrated that palladium can catalyze the oxidative cross-coupling of C–H bonds in the presence of a catalytic amount of BQ. Our approach couples a substrate containing a cyclometallating ligand with a simple arene, through two sequential C–H activation steps: first a cyclopalladation at Pd^{II} on the substrate containing the ligand directing group, followed by a second, undirected C–H activation. The undirected C–H activation generally occurs at the least sterically hindered C–H bond, despite the electronic environment on the aromatic ring. However, when the substituents are relatively small, such as methoxy groups, and the C–H bonds are electronically inequivalent, mixtures of regioisomers form. We were interested in studying the mechanism of the oxidative coupling reaction and the affect of both the benzoquinone and carboxylate ligands on the regioselectivity of the reaction.

We focused our efforts on understanding the mechanism of the second C–H activation/reductive elimination steps, in order to determine the role of the benzoquinone ligand. Through intense mechanistic investigations, we determined that under the reaction conditions the second C–H activation is rapid and reversible, the transient Pd-bisaryl intermediate reacts with a molecule of BQ, which catalyzes the reductive elimination to form the new C–C bond and Pd^0 .

When the oxidative coupling reactions are unselective, due to relatively small functionalities and electronically inequivalent C–H bonds, the regioselectivity of the reaction can be tuned by changing either the carboxylate anion on the Pd or the

benzoquinone ligand employed. Sterically bulky carboxylate ligands and sterically bulky, electron rich benzoquinones favor the functionalization at the less hindered C–H bond and un-coordinating, basic carbonate ligands and electron poor benzoquinones favor the oxidative functionalization at the electronically rich C–H bond.

This methodology is still in the early stages of development. Now that there is better understanding of the mechanism that is occurring and factors that influence the regioselectivity, conditions that use only catalytic Pd^{II} salts can be developed to oxidatively couple the C–H bonds with higher and tunable levels of regioselectivity by simply changing the ancillary ligands employed in the reaction.

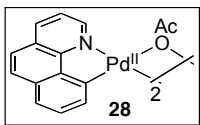
5.7 Experimental Procedure

General Procedures: NMR spectra were obtained on a Varian Inova 500 (499.90 MHz for ¹H; 125.70 MHz for ¹³C), a Varian Inova 400 (399.96 MHz for ¹H; 100.57 MHz for ¹³C; 376.34 MHz for ¹⁹F), or a Varian Mercury 300 (300.07 MHz for ¹H; 75.45 MHz for ¹³C NMR; 282.35 MHz for ¹⁹F) spectrometer. ¹H and ¹³C NMR chemical shifts are reported in parts per million (ppm) relative to TMS, with the residual solvent peak used as an internal reference. ¹⁹F NMR are referenced based on the unified scale, where the frequency of the residual solvent peak in the ¹H NMR spectrum acts as the single primary reference.⁶² ¹⁹F NMR are proton coupled. Multiplicities are reported as follows: singlet (s), doublet (d), doublet of doublets (dd), doublet of doublet of doublets (ddd), doublet of triplets (dt), doublet of quartets (dq), triplet (t), triplet of doublets (td), quartet (q), quartet of doublets (qd), and multiplet (m). Unless otherwise indicated, the ¹H and ¹³C NMR spectra were recorded at room temperature.

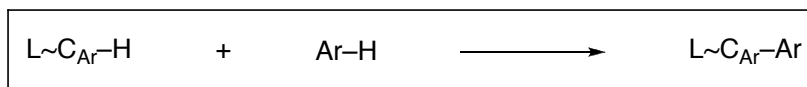
Materials and Methods: Benzo[*h*]quinoline (**33**) was obtained from Pfaltz and Bauer, 8-methylquinoline was purchased from Acros, Ag₂CO₃ was obtained from Acros, and Pd(OAc)₂ was obtained from Pressure Chemical. All were used as received. Benzoquinone was obtained from Acros and was further purified by vacuum sublimation. The arene coupling partners were obtained from commercial sources and used without further purification. *N*-(*m*-Tolyl)-pyrazole was prepared using a Cu-catalyzed *N*-arylation reaction,⁶³ and 2-(*m*-tolyl)-pyrimidine and 2-(*m*-methoxyphenyl)-pyridine were synthesized via Suzuki coupling.⁶⁴ Flash chromatography was performed on EM Science silica gel 60 (0.040-0.063 mm particle size, 230-400 mesh), and thin

layer chromatography was performed on Merck TLC plates pre-coated with silica gel 60 F₂₅₄. Gas chromatography was carried out using a Shimadzu 17A using a Restek Rtx®-5 (Crossbond 5% diphenyl – 95% dimethyl polysiloxane; 15 m, 0.25 mmID, 0.25 mmID, 0.25 μm df) column. HPLC was performed on a Varian ProStar 210 HPLC using Waters μPorasil® 10 μm silica (19 x 300 mm) columns. Control reactions (in the absence of Pd catalyst) were run for each substrate, and showed none of the desired coupled product under our standard reaction conditions. All GC and isolated yields are the average of two reactions.

Experimental Procedures

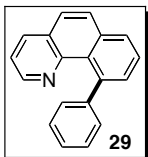


1: Palladacycle **28** was prepared as reported in the literature.²⁹



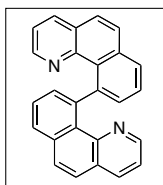
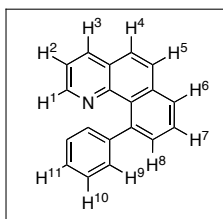
General Procedure: Pd(OAc)₂ (9.6 mg, 0.048 mmol, 10 mol %), benzoquinone (23.7 mg, 0.22 mmol, 0.5 equiv), Ag₂CO₃ (237.2 mg, 0.86 mmol, 2 equiv), and the directed C–H activation substrate (L~C_{Ar}–H) (if solid) (0.43 mmol, 1 equiv) were weighed into a 20 mL scintillation vial equipped with a 15 x 5 mm egg-shaped Teflon stirbar. The arene (Ar–H) (3.75 mL) was added, followed by L~C_{Ar}–H (if oil) (0.43 mmol, 1 equiv), and finally, 125 μL of DMSO (1.45 mmol, 3.4 equiv). The resulting mixture was sealed with a Teflon-lined cap and heated in an aluminum reaction block with vigorous stirring (IKA RCT Basic Hot Plate Stirrer with stirring set at 11). Note: consistent stirring was critical for the reproducibility of these reactions. Reactions run in the absence of stirring showed a significant decrease in yield.* The reaction mixtures generally turned grey/brown upon heating. The reaction was cooled to room temperature, filtered through a plug of silica, and the silica was washed with copious EtOAc (150 mL). The filtrate was concentrated and then evaporated to dryness under high vacuum, and the resulting oils/solids were purified by column chromatography.

* If the reactions were heated in an oil bath, the best results were obtained when they were prestirred prior to heating and the stirring rate was monitored throughout.



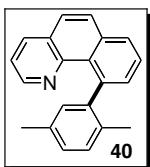
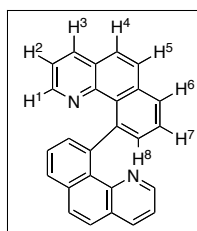
Product 29. L-C_{Ar}-H = benzo[*h*]quinoline (**33**); Ar-H = benzene; temperature = 130 °C. The product was isolated as a white crystalline solid (98 mg, 89% yield, mp = 90.6–92.5 °C, rf = 0.11 in 98% hexanes/2% EtOAc). ¹H NMR (400 MHz, acetone-*d*₆): δ 8.36 (H¹, dd, *J* = 4.0, 2.0 Hz, 1H), 8.21 (H³, dd, *J* = 8.0, 1.6 Hz, 1H), 7.99 (H⁸, dd, *J* = 7.8, 1.4 Hz, 1H), 7.93 (H⁴, d, *J* = 8.8 Hz, 1H), 7.79 (H⁵, d, *J* = 8.8 Hz, 1H), 7.69 (H⁷, dd, *J* = 8.0, 7.2 Hz, 1H), 7.48 (H⁶, dd, *J* = 7.4, 1.4 Hz, 1H), 7.40–7.25 (H², H⁹-H¹¹, multiple peaks, 6H); ¹³C NMR (100 MHz, acetone-*d*₆): δ 147.61, 147.47, 147.43, 142.65, 136.22, 135.98, 132.22, 129.71, 129.50, 129.11, 128.95, 128.18, 128.05, 127.95, 126.98, 126.36, 122.19. HRMS ESI with Formic Acid (*m/z*): [M+H]⁺ calcd for C₁₉H₁₄N, 256.1126; found, 256.1115.

Note: The absence of Ph-Ph (**35**) in the crude reaction mixture was determined by GC analysis versus an authentic sample of biphenyl. The absence of the Bzq oxidative coupling product (Bzq-Bzq) (**34**) was determined by ¹H NMR spectroscopy of the crude reaction mixture, where the diagnostic peak at 6.41 ppm (see below) was not observed.

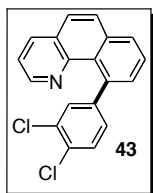
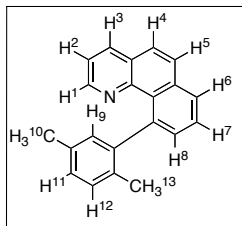


An authentic sample of the Bzq oxidative dimerization product (**34**) was obtained

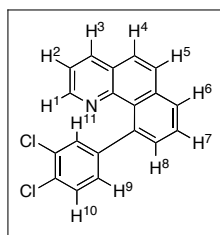
according to the procedure in ref.⁶⁵ The characterization data for this compound are as follows: ¹H NMR (400 MHz, benzene-*d*₆): δ 7.86 (H⁸, dd, *J* = 7.6, 1.6 Hz, 2H), 7.83 (H¹, dd, *J* = 4.2, 1.8 Hz, 2H), 7.76 (H⁴, d, *J* = 8.8 Hz, 2H), 7.60–7.51 (H³, H⁷, multiple peaks, 4H), 7.37 (H⁶, dd, *J* = 8.0, 1.2 Hz, 2H), 7.33 (H⁵, d, *J* = 8.8 Hz, 2H), 6.41 (H², dd, *J* = 8.0, 4.4 Hz, 2H); ¹³C {¹H} NMR (CDCl₃): δ 147.41, 146.67, 145.99, 134.67, 134.33, 130.39, 128.75, 128.63, 127.20, 126.63, 125.21, 120.27 (2 carbon peaks coincidentally overlap); MS-electrospray (*m/z*): [M+H]⁺ calcd for C₂₆H₁₇N₂, 357.1392; Found, 357.1396.



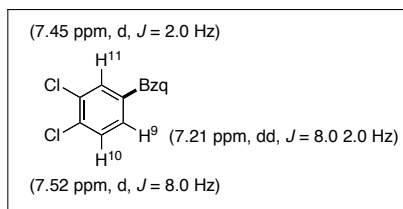
Product 40. Reaction was run at five times the scale of the general procedure above. L~C_{Ar}-H = benzo[*h*]quinoline (**33**); Ar-H = *p*-xylene; temperature = 150 °C. The product was isolated as a clear oil (22 mg, 5% yield, rf = 0.24 in 98% hexanes/2% EtOAc). Trace amounts (<5%) of the Bzq-Bzq dimer were observed in the ¹H NMR spectrum of the crude reaction mixture. ¹H NMR (400 MHz, CDCl₃): δ 8.46 (H¹, dd, *J* = 4.2, 1.8 Hz, 1H), 8.08 (H³, dd, *J* = 8.2, 1.8 Hz, 1H), 7.94 (H⁸, dd, *J* = 8.0, 1.2 Hz, 1H), 7.88 (H⁴, d, *J* = 8.8 Hz, 1H), 7.74–7.67 (H⁵, H⁷, multiple peaks, 2H), 7.48 (H⁶, dd, *J* = 7.2, 1.2 Hz, 1H), 7.32 (H², dd, *J* = 8.0, 4.0 Hz, 1H), 7.16–7.09 (H¹¹, H¹² multiple peaks, 2H), 7.04 (H⁹, bs, 1H), 2.39 (H¹³, s, 3H), 1.80 (H¹⁰, s, 3H). ¹³C {¹H} NMR (100 MHz, CDCl₃): δ 147.45, 147.01, 146.19, 141.15, 134.99, 134.57, 134.30, 132.76, 130.81, 129.43, 128.61, 128.51, 128.42, 127.76, 127.18, 126.88, 126.49, 125.74, 120.91, 21.15, 19.67; MS-electrospray (*m/z*): [M+H]⁺ calcd for C₂₁H₁₈N, 284.1439; Found, 284.1437.

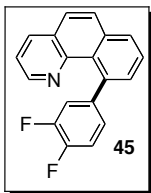


Product 43. L~C_{Ar}-H = benzo[*h*]quinoline (**33**); Ar-H = *o*-dichlorobenzene; temperature = 130 °C. The product was isolated as a pale yellow solid (130 mg, 93% yield, mp = 117.8–121.7 °C, rf = 0.22 in 98% hexanes/2% EtOAc). ¹H NMR (500 MHz, acetone-*d*₆): δ 8.44 (H¹, dd, *J* = 4.0, 2.0 Hz, 1H), 8.28 (H³, dd, *J* = 8.0, 2.0 Hz, 1H), 8.06 (H⁸, dd, *J* = 7.8, 1.3 Hz, 1H), 7.97 (H⁴, d, *J* = 8.5 Hz, 1H), 7.85 (H⁵, d, *J* = 8.5 Hz, 1H), 7.73 (H⁷, dd, *J* = 8.0, 7.5 Hz, 1H), 7.52 (H¹⁰, d, *J* = 8.0 Hz, 1H), 7.49 (H⁶, dd, *J* = 7.3, 1.3 Hz, 1H), 7.45 (H¹¹, d, *J* = 2.0 Hz, 1H), 7.45 (H², dd, *J* = 8.0, 4.5 Hz, 1H), 7.21 (H⁹, dd, *J* = 8.0, 2.0 Hz, 1H); ¹³C NMR (125 MHz, acetone-*d*₆): δ 148.05, 147.89, 147.04, 139.70, 136.61, 136.04, 132.01, 131.42, 131.41, 130.13, 129.96, 129.85, 129.73, 129.43, 129.13, 128.40, 128.14, 127.31, 122.58. HRMS ESI with Formic Acid (*m/z*): [M+H]⁺ calcd for C₁₉H₁₂NCl₂, 324.0347; found, 324.0337.

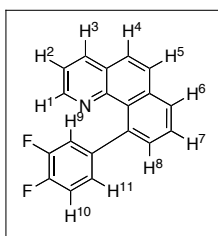


Confirmation of regioselectivity (assignments based on COSY analysis)

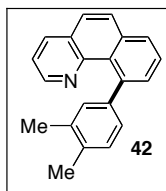
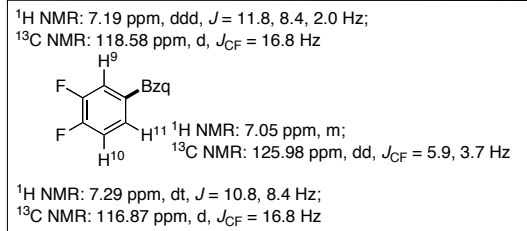




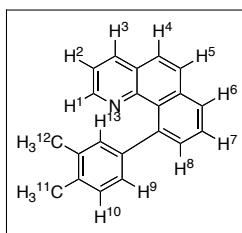
Product 45. $L\sim C_{Ar}\text{-H}$ = benzo[*h*]quinoline (**33**); $Ar\text{-H}$ = *o*-difluorobenzene; temperature = 150 °C. The crude product was a 10:1 mixture of regioisomers (as determined by crude ^{19}F NMR spectroscopy of the reaction mixture). A pure sample of the major regioisomer was isolated as a pale orange viscous oil (61 mg, 49% yield, mp = 123.2–125.2 °C, rf = 0.17 in 98% hexanes/2% EtOAc). Trace amounts (<5%) of the Bzq-Bzq dimer were observed in the ^1H NMR spectrum of the crude reaction mixture. The structure of the major regioisomer was confirmed by GCOSY and HSQC. ^1H NMR (400 MHz, acetone- d_6): δ 8.46 (H^1 , dd, J = 4.4, 2.0 Hz, 1H), 8.28 (H^3 , dd, J = 8.0, 2.0 Hz, 1H), 8.06 (H^8 , dd, J = 8.0, 1.2 Hz, 1H), 7.97 (H^4 , d, J = 8.8, 1H), 7.85 (H^5 , d, J = 8.8 Hz, 1H), 7.73 (H^7 , t, J = 8.0 Hz, 1H), 7.50 (H^6 , dd, J = 7.2, 1.6 Hz, 1H), 7.46 (H^2 , dd, J = 8.0, 4.0 Hz, 1H), 7.29 (H^9 , dt, J = 10.8, 8.4 Hz, 1H), 7.19 (H^{11} , ddd, J = 11.8, 8.4, 2.0 Hz, 1H), 7.05 (H^{10} , m, 1H); ^{13}C NMR (100 MHz, acetone- d_6): δ 150.36 (dd, J = 242.1, 12.8 Hz), 149.65 (dd, J = 241.7, 12.5 Hz), 147.91, 147.18, 144.82 (dd, J = 6.4, 3.6 Hz), 140.25 (d, J = 1.4 Hz), 136.54, 136.05, 132.03, 129.68, 129.63, 129.14, 128.41, 128.06, 127.27, 125.98 (dd, J = 5.9, 3.7 Hz), 122.49, 118.58 (d, J = 16.8 Hz), 116.87 (d, J = 16.8 Hz); ^{19}F NMR (acetone- d_6): δ -142.50 (m, 1F), -145.13 (m, 1F). HRMS ESI with Formic Acid (m/z): $[\text{M}+\text{H}]^+$ calcd for $\text{C}_{19}\text{H}_{12}\text{NF}_2$, 292.0938; found, 292.0930.



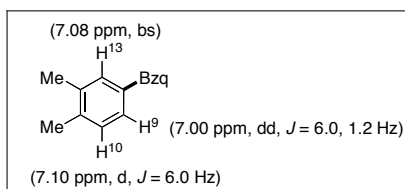
Confirmation of regioselectivity (assignments based on GCOSY, HSQC, and coupling constant analysis)

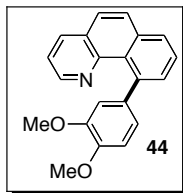


Product 42. L~C_{Ar}-H = benzo[*h*]quinoline (**33**); Ar-H = *o*-xylene; temperature = 130 °C. The product was isolated as an off-white solid (81 mg, 67% yield, mp = 111.5–114.6 °C, rf = 0.11 in 98% hexanes/2% EtOAc). ¹H NMR (500 MHz, acetone-*d*₆): δ 8.39 (H¹, dd, *J* = 3.4, 1.4 Hz, 1H), 8.24 (H³, dd, *J* = 6.4, 1.6 Hz, 1H), 7.99 (H⁸, dd, *J* = 6.2, 1.0 Hz, 1H), 7.94 (H⁴, d, *J* = 7.2 Hz, 1H), 7.81 (H⁵, d, *J* = 7.2 Hz, 1H), 7.70 (H⁷, t, *J* = 6.0 Hz, 1H), 7.48 (H⁶, dd, *J* = 5.6, 1.2 Hz, 1H), 7.41 (H², dd, *J* = 6.4, 3.2 Hz, 1H), 7.10 (H¹⁰, d, *J* = 6.0 Hz, 1H), 7.08 (H¹³, bs, 1H), 7.00 (H⁹, dd, *J* = 6.0, 1.2 Hz, 1H), 2.32 (H¹¹ or H¹², s, 3H), 2.26 (H¹¹ or H¹², s, 3H); ¹³C NMR (125 MHz, acetone-*d*₆): δ 147.72, 147.61, 145.04, 142.94, 136.26, 136.13, 135.70, 134.09, 132.49, 130.80, 129.87, 129.35, 129.23, 128.77, 128.25, 127.98, 127.23, 126.97, 122.24, 19.99, 19.66. HRMS ESI with Formic Acid (*m/z*): [M+H]⁺ calcd for C₂₁H₁₇N, 284.1439; found, 284.1426.

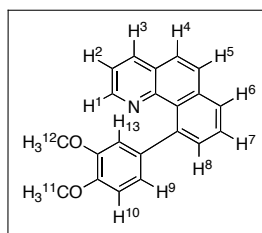


Confirmation of regioselectivity (assignments based on COSY analysis)

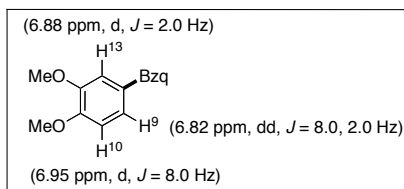


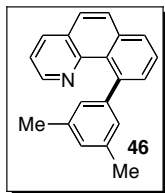


Product 7. $L\sim C_{Ar}-H$ = benzo[*h*]quinoline (**33**); $Ar-H$ = *o*-dimethoxybenzene; temperature = 130 °C. The product was isolated as a off-white crystalline solid (88 mg, 66% yield, mp = 133.6–134.4 °C, rf = 0.11 in 90% hexanes/10% EtOAc). Trace amounts (<5%) of the Bzq-Bzq dimer were observed in the 1H NMR spectrum of the crude reaction mixture. 1H NMR (400 MHz, acetone- d_6): δ 8.46 (H^1 , dd, $J = 4.2, 1.8$ Hz, 1H), 8.27 (H^3 , dd, $J = 8.0, 2.0$ Hz, 1H), 8.01 (H^8 , dd, $J = 7.8, 1.4$ Hz, 1H), 7.96 (H^4 , d, $J = 8.8$ Hz, 1H), 7.83 (H^5 , d, $J = 8.8$ Hz, 1H), 7.71 (H^7 , t, $J = 7.6$ Hz, 1H), 7.53 (H^6 , dd, $J = 7.2, 1.2$ Hz, 1H), 7.44 (H^2 , dd, $J = 8.0, 4.4$ Hz, 1H), 6.95 (H^{10} , d, $J = 8.0$ Hz, 1H), 6.88 (H^{13} , d, $J = 2.0$ Hz, 1H), 6.82 (H^9 , dd, $J = 8.0, 2.0$ Hz, 1H), 3.87 (H^{11} or H^{12} , s, 3H), 3.70 (H^{11} or H^{12} , s, 3H); ^{13}C NMR (100 MHz, acetone- d_6): δ 149.52, 148.94, 147.72, 147.71, 142.66, 140.31, 136.32, 136.18, 132.51, 129.94, 129.24, 128.84, 128.31, 128.00, 127.03, 122.29, 121.59, 114.89, 112.20, 56.25, 56.20. HRMS ESI with Formic Acid (m/z): $[M+H]^+$ calcd for $C_{21}H_{17}O_2N$, 316.1338; found, 316.1324.

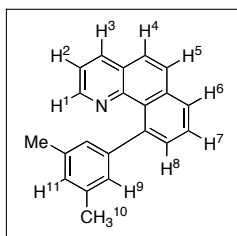


Confirmation of regioselectivity (assignments based on COSY analysis)

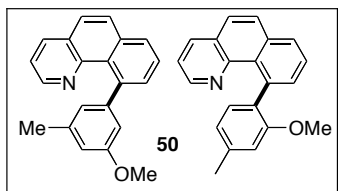
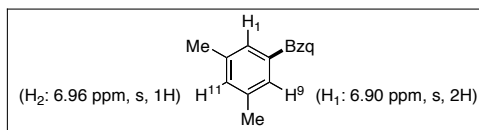




Product 46. $L\sim C_{Ar}\text{-H}$ = benzo[*h*]quinoline (**33**); Ar-H = *m*-xylene; temperature = 150 °C. The product was isolated as a pale orange viscous oil (84 mg, 69% yield, rf = 0.11 in 98% hexanes/2% EtOAc). Trace amounts (<5%) of the Bzq-Bzq dimer were observed in the ^1H NMR spectrum of the crude reaction mixture. ^1H NMR (400 MHz, acetone- d_6): δ 8.41 (H^1 , dd, J = 4.4, 2.0 Hz, 1H), 8.25 (H^3 , dd, J = 8.0, 2.0 Hz, 1H), 8.00 (H^8 , dd, J = 8.0, 1.2 Hz, 1H), 7.96 (H^4 , d, J = 8.8 Hz, 1H), 7.82 (H^5 , d, J = 8.8 Hz, 1H), 7.70 (H^7 , t, J = 7.6 Hz, 1H), 7.48 (H^6 , dd, J = 7.6, 1.2 Hz, 1H), 7.42 (H^2 , dd, J = 8.0, 4.0 Hz, 1H), 6.96 (H^{11} , s, 1H), 6.90 (H^9 , s, 2H), 2.30 (H^{10} , s, 6H); ^{13}C NMR (100 MHz, CDCl_3): δ 146.82, 146.08, 141.88, 136.58, 135.10, 134.98, 131.52, 129.57, 128.98, 128.29, 127.72, 127.31, 127.15, 126.98, 126.55, 125.79, 121.00, 21.45. HRMS ESI with Formic Acid (m/z): $[\text{M}+\text{H}]^+$ calcd for $\text{C}_{21}\text{H}_{18}\text{N}$, 284.1439; found, 284.1429.



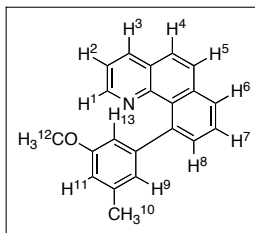
Confirmation of regioselectivity



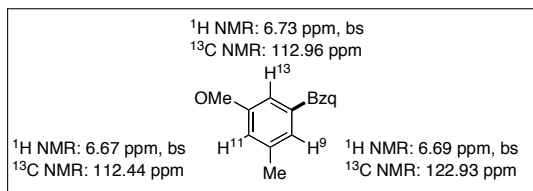
Product 50. $L\sim C_{Ar}\text{-H}$ = benzo[*h*]quinoline (**33**); Ar-H = 3-methylanisole; temperature = 150 °C. The products were isolated as a mixture of isomers, a pale yellow oil (rf = 0.26 in 95% hexanes/5% EtOAc, 90.0 mg, 70% yield, 2.5 : 1 ratio of the 1,3,5 : 1,3,4 isomers).

Trace amounts (<5%) of the Bzq-Bzq dimer were observed in the ^1H NMR spectrum of the crude reaction mixture. Isomers were separated by HPLC to afford each isomer as pale yellow oils.

1,3,5 isomer. ^1H NMR (400 MHz, acetone- d_6): δ 8.44 (H^1 , dd, $J = 4.4, 2.0$ Hz, 1H), 8.26 (H^3 , dd, $J = 8.0, 2.0$ Hz, 1H), 8.02 (H^8 , dd, $J = 7.8, 1.4$ Hz, 1H), 7.96 (H^4 , d, $J = 8.8$ Hz, 1H), 7.83 (H^5 , d, $J = 8.8$ Hz, 1H), 7.71 (H^7 , t, $J = 7.6$ Hz, 1H), 7.51 (H^6 , dd, $J = 7.2, 1.2$ Hz, 1H), 7.43 (H^2 , dd, $J = 8.0, 4.4$ Hz, 1H), 6.73 (H^9 or H^{11} or H^{13} , bs, 1H), 6.69 (H^9 or H^{11} or H^{13} , bs, 1H), 6.67 (H^9 or H^{11} or H^{13} , bs, 1H), 3.74 (H^{12} , s, 3H), 2.32 (H^{10} , s, 3H); ^{13}C NMR (100 MHz, acetone- d_6): δ 160.14, 148.60, 147.77, 147.56, 142.76, 138.55, 136.27, 136.06, 132.09, 129.82, 129.19, 128.96, 128.29, 127.97, 127.04, 122.93, 122.30, 112.96, 112.44, 55.41, 21.78. HRMS ESI with Formic Acid (m/z): $[\text{M}+\text{H}]^+$ calcd for $\text{C}_{21}\text{H}_{18}\text{NO}$, 300.1388; found, 300.1382.

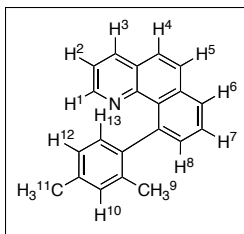


Confirmation of Regioselectivity (assignments based on COSY and HSQC)

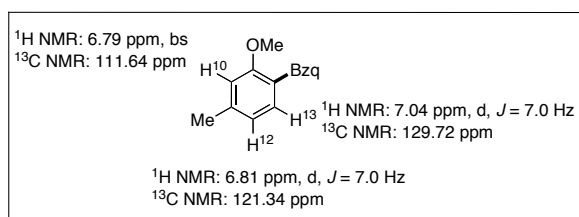


1,2,4 isomer. Regiochemistry confirmed by GCOSY and HSQC. ^1H NMR (400 MHz, acetone- d_6): δ 8.42 (H^1 , dd, $J = 4.2, 1.8$ Hz, 1H), 8.24 (H^3 , dd, $J = 8.0, 2.0$ Hz, 1H), 7.99 (H^8 , dd, $J = 7.8, 1.0$ Hz, 1H), 7.94 (H^4 , d, $J = 8.8$ Hz, 1H), 7.80 (H^5 , d, $J = 8.8$ Hz, 1H), 7.71 (H^7 , t, $J = 7.4$ Hz, 1H), 7.45 (H^6 , dd, $J = 7.4, 1.0$ Hz, 1H), 7.41 (H^2 , dd, $J = 8.0, 4.0$ Hz, 1H), 7.04 (H^{12} , d, $J = 7.2$ Hz, 1H), 6.84–6.78 (H^{10} and H^{13} , multiple peaks, 2H), 3.36 (H^9 , s, 3H), 2.43 (H^{11} , s, 3H); ^{13}C NMR (100 MHz, acetone- d_6): δ 158.43, 148.20, 147.81, 139.44, 137.68, 136.07, 135.64, 134.21, 132.36, 130.89, 129.72, 129.31, 128.82,

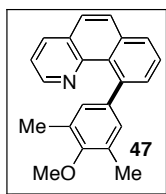
128.08, 127.81, 126.74, 122.04, 121.34, 111.64, 55.31, 21.81. HRMS ESI with Formic Acid (m/z): $[M+H]^+$ calcd for $C_{21}H_{18}NO$, 300.1388; found, 300.1393.



Confirmation of regioselectivity (assignments based on GCOSY and HSQC)

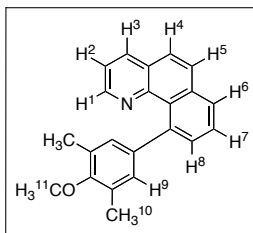


The assignment of the benzoquinoline coupled *ortho* to the OMe rather than the Me is based on the ^{13}C NMR chemical shifts of the C–H₂ and C–H₃. As seen 1,3,5-isomer (above), a C_{Ar}–H *ortho* to a C_{Ar}–OMe is expected to appear at between 110–115 ppm in the ^{13}C NMR. Only one C_{Ar}–H appears in this region of the ^{13}C NMR spectrum of this compound, and this is identified as C–H₁.

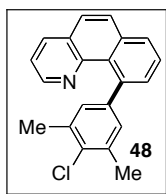
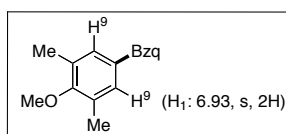


Product 47. L~C_{Ar}–H = benzo[*h*]quinoline (**47**); Ar–H = 2,6-dimethylanisole; temperature = 150 °C. The product was isolated as a pale orange viscous oil (89 mg, 66% yield, $r_f = 0.14$ in 95% hexanes/5% EtOAc). Trace amounts (<5%) of the Bzq-Bzq dimer were observed in the 1H NMR spectrum of the crude reaction mixture. 1H NMR (400 MHz, acetone- d_6): δ 8.42 (H¹, dd, $J = 4.0, 2.0$ Hz, 1H), 8.24 (H³, dd, $J = 8.0, 2.0$ Hz, 1H), 7.98 (H⁸, dd, $J = 8.0, 1.6$ Hz, 1H), 7.94 (H⁴, d, $J = 8.8$ Hz, 1H), 7.81 (H⁵, d, $J = 8.8$ Hz, 1H), 7.69 (H⁷, dd, $J = 8.0, 7.2$ Hz, 1H), 7.49 (H⁶, dd, $J = 7.2, 1.6$ Hz, 1H), 7.41 (H², dd, $J = 8.0, 4.0$ Hz, 1H), 6.93 (H⁹, bs, 2H), 3.78 (H¹¹, s, 3H), 2.27 (H¹⁰, s, 6H); ^{13}C NMR (100 MHz, acetone- d_6): δ 149.52, 148.94, 142.65, 140.31, 136.31, 136.19, 132.51, 129.94,

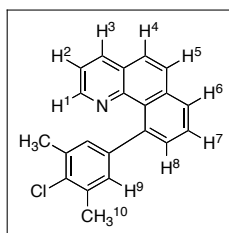
129.24, 128.84, 128.30, 128.00, 127.03, 122.29, 121.59, 114.89, 112.20, 55.42, 21.78.
 HRMS ESI with Formic Acid (m/z): $[M+H]^+$ calcd for $C_{22}H_{20}NO$, 314.1545; found, 314.1544.



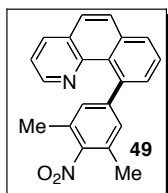
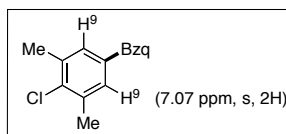
Confirmation of Regioselectivity



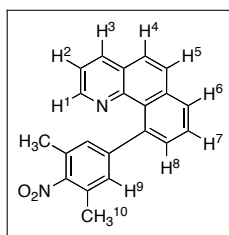
Product 11. L~C_{Ar}-H = 7,8-benzo[*h*]quinoline; Ar-H = 2-chloro-*m*-xylene; temperature = 150 °C. The product was isolated as off-white solid (101 mg, 74% yield, mp = 118.0–121.7 °C, rf = 0.19 in 98% hexanes/2% EtOAc). ¹H NMR (400 MHz, acetone-*d*₆): δ 8.42 (H¹, dd, *J* = 4.4, 2.0 Hz, 1H), 8.26 (H³, dd, *J* = 8.0, 2.0 Hz, 1H), 8.02 (H⁸, dd, *J* = 8.0, 1.2 Hz, 1H), 7.96 (H⁴, d, *J* = 8.8 Hz, 1H), 7.83 (H⁵, d, *J* = 8.8 Hz, 1H), 7.71 (H⁷, t, *J* = 7.6 Hz, 1H), 7.47 (H⁶, dd, *J* = 7.2, 1.2 Hz, 1H), 7.43 (H², dd, *J* = 8.0, 3.6 Hz, 1H), 7.07 (H⁹, s, 2H), 2.37 (H¹⁰, s, 6H); ¹³C NMR (100 MHz, CDCl₃): δ 146.86, 146.66, 144.08, 140.67, 135.20, 134.97, 134.81, 132.06, 131.44, 128.84, 128.81, 128.25, 128.02, 127.18, 126.98, 125.91, 121.11, 20.78. HRMS ESI with Formic Acid (m/z): $[M+H]^+$ calcd for $C_{21}H_{17}NCl$, 318.1050; found, 318.1042.



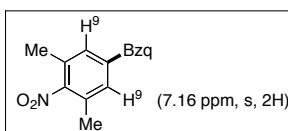
Confirmation of Regioselectivity

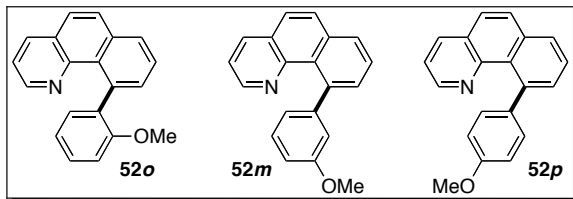


Product 12. $L\sim C_{Ar}-H = 7,8\text{-benzo}[h]\text{quinoline}$; $Ar-H = 2\text{-nitro-}m\text{-xylene}$; temperature = 150 °C. GC analysis of the crude reaction mixture showed an ~20:1 ratio of regioisomers. The major isomer was isolated as white solid and was purified from the 1,2,3,4 isomer by HPLC (79 mg, 56% yield, $r_f = 0.17$ in 95% hexanes/5% EtOAc). Trace amounts (<5%) of the Bzq-Bzq dimer were observed in the ¹H NMR spectrum of the crude reaction mixture. By GC the a peak which may correspond to the 1,2,3,4 isomer is present, in a >18 : 1 ratio. ¹H NMR (400 MHz, acetone-*d*₆): δ 8.46 (H¹, dd, $J = 4.2, 1.8$ Hz, 1H), 8.32 (H³, dd, $J = 8.0, 2.0$ Hz, 1H), 8.10 (H⁸, dd, $J = 8.0, 1.2$ Hz, 1H), 8.01 (H⁴, d, $J = 8.8$ Hz, 1H), 7.89 (H⁵, d, $J = 8.8$ Hz, 1H), 7.77 (H⁷, t, $J = 7.6$ Hz, 1H), 7.52 (H⁶, dd, $J = 7.4, 1.0$ Hz, 1H), 7.49 (H², dd, $J = 7.8, 4.2$ Hz, 1H), 7.16 (H⁹, s, 2H), 2.33 (H¹⁰, s, 6H); ¹³C NMR (100 MHz, acetone-*d*₆): δ 149.74, 147.89, 147.13, 140.67, 136.58, 136.08, 132.00, 130.14, 129.71, 129.51, 129.18, 129.17, 128.43, 128.14, 127.29, 122.62, 17.65 (two carbons are coincidentally overlapping). HRMS ESI with Formic Acid (m/z): $[M+H]^+$ calcd for C₂₁H₁₆N₂O₂ 329.1279; found, 329.1290.



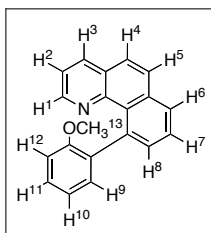
Confirmation of Regioselectivity



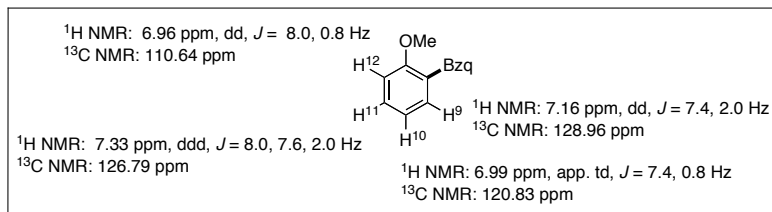


Product 13: L~C_{Ar}-H = benzo[*h*]quinoline (**33**); Ar-H = anisole; temperature = 130 °C. The products were isolated as a mixture of isomers as a pale orange viscous oil (rf = 0.13 in 95% hexanes/5% EtOAc, 99 mg, 80% yield, the *o:m:p* ratio of 1 : 2.6 : 3.3 was determined by GC analysis of crude reaction mixture). Trace amounts (<5%) of the Bzq-Bzq dimer were observed in the ¹H NMR spectrum of the crude reaction mixture. The three regioisomers were separated by HPLC.

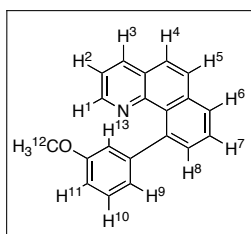
ortho isomer: ¹H NMR (400 MHz, acetone-*d*₆): δ 8.40 (H¹, dd, *J* = 4.4, 2.0 Hz, 1H), 8.26 (H³, dd, *J* = 8.0, 2.0 Hz, 1H), 8.02 (H⁸, dd, *J* = 8.2, 1.4 Hz, 1H), 7.96 (H⁴, d, *J* = 8.8 Hz, 1H), 7.82 (H⁵, d, *J* = 8.8 Hz, 1H), 7.73 (H⁷, t, *J* = 7.6 Hz, 1H), 7.47 (H⁶, dd, *J* = 7.2, 1.2 Hz, 1H), 7.42 (H², dd, *J* = 8.0, 4.0 Hz, 1H), 7.33 (H¹¹, ddd, *J* = 8.0, 7.6, 2.0 Hz, 1H), 7.16 (H⁹, dd, *J* = 7.4, 2.0 Hz, 1H), 6.99 (H¹⁰, app. td, *J* = 7.4, 0.8 Hz, 1H), 6.96 (H¹², dd, *J* = 8.0, 0.8 Hz, 1H), 3.39 (H¹³, s, 3H); ¹³C NMR (100 MHz, acetone-*d*₆): δ 158.56, 148.07, 147.88, 139.34, 137.04, 136.11, 135.62, 132.15, 130.76, 129.89, 129.30, 128.96, 128.24, 128.12, 127.83, 126.79, 122.11, 120.83, 110.64, 55.37. HRMS ESI with Formic Acid (*m/z*): [M+H]⁺ calcd for C₂₀H₁₆NO, 286.1232; found, 286.1219.



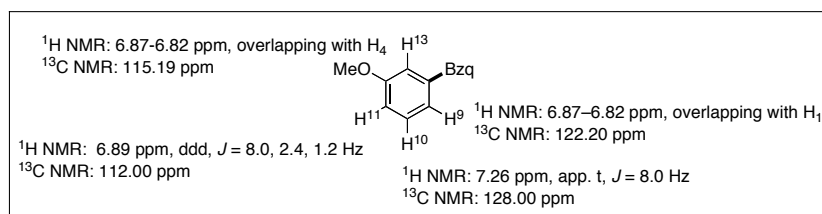
Confirmation of Regioselectivity (assignments based on COSY and HSQC)



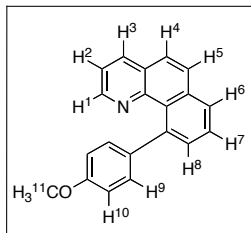
meta isomer: ^1H NMR (400 MHz, acetone- d_6): δ 8.42 (H^1 , dd, $J = 4.4, 2.0$ Hz, 1H), 8.27 (H^3 , dd, $J = 8.0, 1.6$ Hz, 1H), 8.03 (H^8 , dd, $J = 8.0, 1.2$ Hz, 1H), 7.97 (H^4 , d, $J = 8.8$ Hz, 1H), 7.84 (H^5 , d, $J = 8.8$ Hz, 1H), 7.73 (H^7 , dd, $J = 8.0, 7.2$ Hz, 1H), 7.51 (H^6 , dd, $J = 7.2, 1.2$ Hz, 1H), 7.43 (H^2 , dd, $J = 8.0, 4.4$ Hz, 1H), 7.26 (H^{10} , app. t, $J = 8.0$ Hz, 1H), 6.89 (H^{11} , ddd, $J = 8.0, 2.4, 1.2$ Hz, 1H), 6.87–6.82 (H^9 and H^{13} , multiple peaks, 2H), 3.77 (H^{12} , s, 3H); ^{13}C NMR (100 MHz, acetone- d_6): δ 160.12, 148.86, 147.76, 147.48, 142.54, 136.30, 136.04, 132.09, 129.78, 129.16, 129.05, 129.01, 128.28, 128.00, 127.07, 122.30, 122.20, 115.19, 112.00, 55.43. HRMS ESI with Formic Acid (m/z): $[\text{M}+\text{H}]^+$ calcd for $\text{C}_{20}\text{H}_{16}\text{NO}$, 286.1232; found, 286.1220.



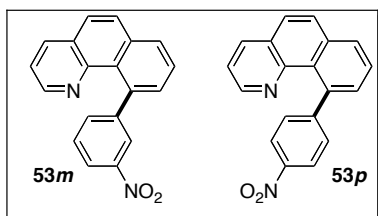
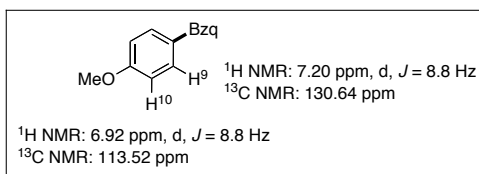
Confirmation of Regioselectivity (assignments based on COSY and HSQC)



para isomer: ^1H NMR (400 MHz, acetone- d_6): δ 8.43 (H^1 , dd, $J = 4.2, 1.8$ Hz, 1H), 8.26 (H^3 , dd, $J = 8.0, 2.0$ Hz, 1H), 7.99 (H^8 , dd, $J = 7.9, 1.4$ Hz, 1H), 7.95 (H^4 , d, $J = 8.8$ Hz, 1H), 8.82, (H^5 , d, $J = 8.8$ Hz, 1H), 7.71 (H^7 , t, $J = 7.6$ Hz, 1H), 7.49 (H^6 , dd, $J = 7.2, 1.6$ Hz, 1H), 7.43 (H^2 , dd, $J = 8.0, 4.4$ Hz, 1H), 7.20 (H^9 , d, $J = 8.8$ Hz, 2H), 6.92 (H^{10} , d, $J = 8.8$ Hz, 2H), 3.86 (H^{11} , s, 3H); ^{13}C NMR (100 MHz, acetone- d_6): δ 159.02, 147.74, 147.68, 142.54, 139.78, 136.34, 136.19, 132.56, 130.63, 129.92, 129.25, 128.80, 128.27, 128.03, 127.01, 122.27, 113.51, 55.49. HRMS ESI with Formic Acid (m/z): $[\text{M}+\text{H}]^+$ calcd for $\text{C}_{20}\text{H}_{16}\text{NO}$, 286.1232; found, 286.1224.

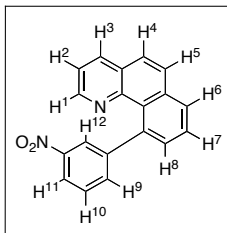


Confirmation of Regioselectivity (assignments based on COSY and HSQC)



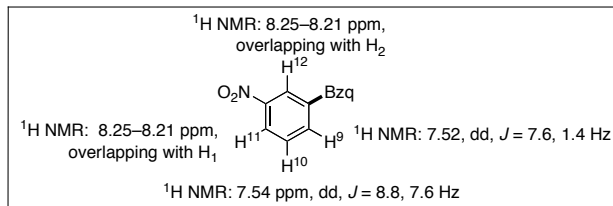
Product 14: $L\sim C_{Ar}\text{-H} = 7,8\text{-benzo}[h]\text{quinoline}$; $Ar\text{-H} = \text{nitrobenzene}$; temperature = 130 °C. The products were isolated as a mixture of isomers as a pale orange viscous oil (rf = 0.13 in 95% hexanes/5% EtOAc, 100 mg, 77% yield, the *o:m:p* ratio of 0 : 3.5 : 1 was determined by GC analysis of crude reaction mixture). Trace amounts (<5%) of the Bzq-Bzq dimer were observed in the $^1\text{H NMR}$ spectrum of the crude reaction mixture. The two regioisomers were separated by HPLC.

meta isomer: $^1\text{H NMR}$ (400 MHz, CDCl_3): 8.36 (H^1 , dd, $J = 4.2, 1.8$ Hz, 1H), 8.25–8.21 (H^{11} and H^{12} , multiple peaks, 2H), 8.12 (H^3 , dd, $J = 8.0, 2.0$ Hz, 1H), 8.00 (H^8 , dd, $J = 8.0, 1.2$ Hz, 1H). 7.89 (H^4 , d, $J = 8.8$ Hz, 1H), 7.74 (H^5 , d, $J = 8.8$ Hz, 1H), 7.72 (H^7 , t, $J = 7.6$ Hz, 1H), 7.69 (H^9 , dt, $J = 8.0, 1.3$ Hz, 1H), 7.54 (H^{10} , dd, $J = 8.8, 7.6$ Hz, 1H), 7.52 (H^6 , dd, $J = 7.6, 1.4$ Hz, 1H), 7.35 (H^2 , dd, $J = 8.0, 4.4$ Hz, 1H); $^{13}\text{C NMR}$ (100 MHz, CDCl_3): δ 147.89, 147.70, 146.88, 146.14, 138.91, 135.52, 135.07, 134.98, 131.18, 128.96, 128.65, 128.22, 127.98, 127.35, 127.13, 126.27, 123.93, 121.41, 120.80. HRMS ESI with Formic Acid (m/z): $[\text{M}+\text{H}]^+$ calcd for $\text{C}_{20}\text{H}_{16}\text{NO}$, 286.1232; found, 286.1220.

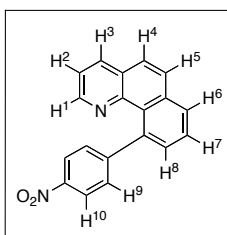


Confirmation of Regioselectivity

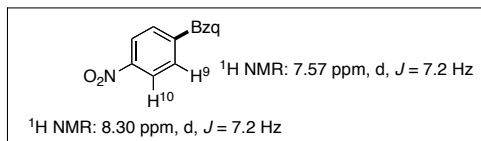
(assignments based on COSY and chemical shift analysis)

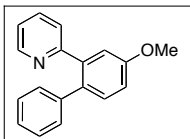


para isomer: $^1\text{H NMR}$ (400 MHz, acetone- d_6): δ 8.42 (H^1 , dd, $J = 3.4, 1.4$ Hz, 1H), 8.36 (H^3 , dd, $J = 6.4, 1.6$ Hz, 1H), 8.30 (H^{10} , d, $J = 7.2$ Hz, 2H), 8.17 (H^8 , dd, $J = 6.4, 1.2$ Hz, 1H), 8.06 (H^4 , d, $J = 7.2$ Hz, 1H), 7.94 (H^5 , d, $J = 7.2$ Hz, 1H), 7.84 (H^7 , dd, $J = 6.2, 5.8$ Hz, 1H), 7.57 (H^9 and H^6 , multiple peaks, 3H), 7.51 (H^2 , dd, $J = 6.4, 3.2$ Hz, 1H). $^{13}\text{C NMR}$ (100 MHz, CDCl_3): δ 153.71, 146.84, 146.13, 145.93, 139.21, 135.56, 134.92, 130.69, 129.53, 128.98, 128.21, 127.38, 127.15, 126.28, 122.82, 121.47 (a seventeenth signal was not resolved due to too little sample or overlapping signals).

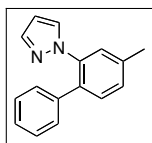
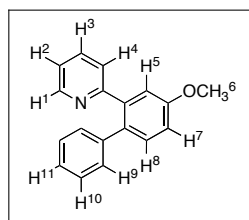


Confirmation of Regioselectivity

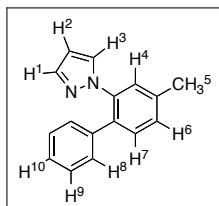


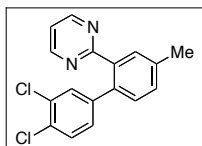


Product 36: $L\sim C_{Ar}\text{-H}$ = 2-(*m*-methoxyphenyl)pyridine; Ar-H = benzene; temperature = 150 °C. The product was isolated as a pale orange viscous oil (52 mg, 46% yield, rf = 0.05 in 90% hexanes/10% EtOAc). ^1H NMR (400 MHz, acetone- d_6): δ 8.58 (H¹, ddd, J = 3.6, 1.2, 0.8 Hz, 1H), 7.46 (H³, td, J = 6.0, 1.5 Hz, 1H), 7.35 (H⁷, d, J = 6.8 Hz, 1H), 7.25–7.17 (H⁸, H⁹, H¹⁰, multiple peak, 5H), 7.11–7.05 (H², H⁴, H⁶, multiple peaks, 3H), 6.92 (H⁵, dt, J = 5.2, 0.8 Hz, 1H), 3.88 (H⁶, s, 3H); ^{13}C NMR (100 MHz, CDCl₃): δ 160.04, 160.00, 150.30, 142.29, 141.86, 136.10, 134.10, 132.54, 130.52, 128.93, 127.22, 126.03, 122.51, 116.55, 115.14, 57.80. HRMS ESI with Formic Acid (m/z): [M+H]⁺ calcd for C₁₈H₁₆NO 262,1232; found, 262.1227.

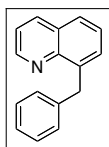
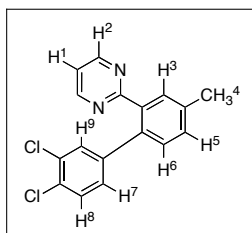


Product 39: $L\sim C_{Ar}\text{-H}$ = 1-(*m*-tolyl)pyrazole); Ar-H = benzene; temperature = 130 °C. The product was isolated as yellow oil (rf = 0.11 in 95% hexanes/5% EtOAc, 26 mg, 26% yield). ^1H NMR (500 MHz, CD₂Cl₂): δ 7.59 (H³, d, J = 2.0 Hz, 1H), 7.40 (H⁴, bs, 1H), 7.37 (H⁷, d, J = 8.0 Hz, 1H), 7.30 (H⁶, bd, J = 8.0 Hz, 1H), 7.29–7.25 (H⁹, H¹⁰, multiple peaks, 3H), 7.13 (H¹, d, J = 2.5 Hz, 1H), 7.10–7.07 (H⁸, m, 2H), 6.20 (H², t, J = 2.3 Hz, 1H), 2.45 (H⁵, s, 3H); 20.94 (two carbon peaks coincidentally overlap). HRMS ESI with Formic Acid (m/z): [M+H]⁺ calcd for C₁₆H₁₄N₂ 235.1235; found, 235.1232.





Product 37: $L\sim C_{Ar}\text{-H}$ = 2-*m*-tolylpyrimidine; Ar-H = benzene; temperature = 150 °C. The product was isolated as white solid (93 mg, 69% yield, mp = 132.7–135.8 °C, rf = 0.09 in 90% hexanes/10% EtOAc). ^1H NMR (500 MHz, acetone- d_6): 8.69 (H², d, J = 4.0 Hz, 2H), 7.70 (H³, bs, 1H), 7.41-7.35 (H⁵, H⁶, H⁹, multiple peaks, 3H), 7.30 (H¹, t, J = 4.0 Hz, 2H), 7.28 (H⁹, d, J = 1.2 Hz, 1H), 6.98 (H⁷, dd, J = 8.3, 2.3 Hz, 1H), 2.46 (H⁴, s, 3H); ^{13}C NMR (125 MHz, acetone- d_6): 167.93, 157.88, 143.77, 139.29, 138.82, 137.23, 132.49, 132.07, 131.77, 131.33, 131.01, 130.73, 130.63, 130.13, 120.03, 21.14. HRMS ESI with Formic Acid (m/z): $[\text{M}+\text{H}]^+$ calcd for $\text{C}_{11}\text{H}_{11}\text{N}_2$, 315.0456; found, 315.0447.



Product 38: $L\sim C_{Ar}\text{-H}$ = 8-methylquinoline; Ar-H = benzene; temperature = 150 °C. The product was isolated as white solid (rf = 0.08 in 98% hexanes/2% EtOAc, 45 mg, 48% yield). Spectroscopic data were identical to the literature data.^{30, 30}

Scheme 5.19: Palladacycle **1** [148 mg, 0.215 mmol, 0.5 equiv (1 equiv based on Pd)] and benzoquinone (47 mg, 0.43 mmol, 1 equiv) were vigorously stirred in 3.75 mL benzene at 130 °C for 12 h. The reaction mixture was filtered through silica gel and washed with 150 mL ethyl acetate. Product **2** was isolated by column chromatography as a crystalline white solid (80 mg, 73% yield).

Scheme 5.27: (a) Used the general procedure for the reaction set up; L~C_{Ar}-H = 7,8-benzo[*h*]quinoline; Ar-H = 2,6-dimethylanisole (2.44 mL, 17.2 mmol, 40 equiv) and *m*-xylene (2.10 mL, 17.2 mmol, 40 equiv); temperature = 150 °C. Upon cooling, methyl naphthalene was added as an internal standard, and the corrected yields were determined by GC analysis.

(b) Used the general procedure for the reaction set up; L~C_{Ar}-H = 7,8-benzo[*h*]quinoline; Ar-H = 2-nitro-*m*-xylene (2.34 mL, 17.2 mmol, 40 equiv) and *m*-xylene (2.10 mL, 17.2 mmol, 40 equiv); temperature = 150 °C. Upon cooling, methyl naphthalene was added as an internal standard, and the corrected yields were determined by GC analysis.

(c) Used the general procedure for the reaction set up; L~C_{Ar}-H = 7,8-benzo[*h*]quinoline; Ar-H = 2-nitro-*m*-xylene (2.34 mL, 17.2 mmol, 40 equiv) and 2,6-dimethylanisole (2.44 mL, 17.2 mmol, 40 equiv); temperature = 150 °C. Upon cooling, methyl naphthalene was added as an internal standard, and the corrected yields were determined by GC analysis.

Scheme 5.28: Used the general procedure for the reaction setup on 1/5 the scale; L~C_{Ar}-H = 7,8-benzo[*h*]quinoline; Ar-H = anisole; temperature = 130 °C. Upon cooling, methyl naphthalene was added as an internal standard, and the corrected yields were determined by GC analysis.

General Procedure for Kinetic Experiments. The initial rates of each set of conditions were determined by monitoring the product formation in six identical reactions, set up

simultaneously. As seen in Scheme 5.33, the standard reaction conditions were [BzqPdOAc]₂ (**28**) (6.9 mg, 0.01 mmol, 0.5 equiv (1 equiv per Pd)) weighed directly into a vial, then 0.806 mL of a standard solution containing (per aliquot) benzoquinone (BQ) (2.2 mg, 0.02 mmol, 1 equiv), DMSO (5.7 μL, 0.08 mmol, 4 equiv), nonadecane (internal standard) (2.7 mg, 0.01 mmol, 0.5 equiv), 1,2-dimethoxybenzene (0.14 mL, 1.1 mmol, 55 equiv), and *p*-xylene (0.66) was added via a 1 mL Hamilton airtight syringe. The reactions were then allowed to stir at room temperature for > 30 s and then at 130 °C for X min in an aluminum reaction block while stirring at the highest rpm (IKA stirplate setting of 11). After the allotted period of time (time ≈ n*(time to reach 10% yield)/6, (n = 1-6)), each reaction was taken out sequentially, cooled to 0 °C in an ice bath, then diluted with CH₂Cl₂. The reaction was then analyzed by GC twice and the yield of **44** determined by comparison to a calibration against the nonadecane internal standard. Importantly, the reactions did not progress after the work-up, a reaction analyzed immediately and 12 hours later gave the same GC yield. Additionally, under the reaction conditions none of **40**, where the *p*-xylenes is oxidatively coupled, was observed. The reported initial rate values are the average of three unique kinetic experiments.

Table 5.5: [BzqPdOAc]₂ (**28**) (6.9 mg, 0.02 mmol, 1 equiv), AcOD (12-115 μL, 10-100 equiv), 1,2-dimethoxybenzene (0.8 mL) were heated at 130 °C for 12 hours. Then 20.5 μL nitrobenzene-*d*₅ was added as an internal standard. Deuterium incorporation was determined by ²H NMR, by integration against the internal standard.

Scheme 5.54: [BzqPdOAc]₂ (**28**) (6.9 mg, 0.01 mmol, 1 equiv (based on Pd)) tributylphenyltin (**85**) (6.5 μL, 0.02 mmol, 1 equiv), benzoquinone (0 or 2.2 mg, 0 or 1 equiv) and DMSO (5.7 μL, 0.08 mmol, 4 equiv) were heated to 130 °C in *p*-xylene for 12 h. The products were analyzed by GC and yields determined by comparison to the internal standard nonadecane.

Table 5.6: [BzqPdO₂R]₂ (0.01 mmol, 1 equiv (based on Pd)), benzoquinone (BQ) (2.2 mg, 0.02 mmol, 1 equiv), DMSO (5.7 μL, 0.08 mmol, 4 equiv), nonadecane (internal

standard, 2.7 mg, 0.01 mmol, 0.5 equiv) and 1,3-dimethoxybenzene (0.8 mL) at 150 °C for 12 hours. The reaction yield and isomer ratios were determined by GC analysis.

Table 5.7: [BzqPdCl]₂ (**61**) (6.4 mg, 0.01 mmol, 1 equiv (based on Pd)), Ag salt (0.02 mmol, 1 equiv), benzoquinone (BQ) (2.2 mg, 0.02 mmol, 1 equiv), DMSO (5.7 μL, 0.08 mmol, 4 equiv), nonadecane (internal standard, 2.7 mg, 0.01 mmol, 0.5 equiv) and 1,3-dimethoxybenzene (0.8 mL) at 150 °C for 12 hours. The reaction yield and isomer ratios were determined by GC analysis.

Table 5.8: [BzqPdO₂R]₂ (0.01 mmol, 1 equiv (based on Pd)), benzoquinone (BQ) (2.2 mg, 0.02 mmol, 1 equiv), DMSO (5.7 μL, 0.08 mmol, 4 equiv), nonadecane (internal standard, 2.7 mg, 0.01 mmol, 0.5 equiv) and 1,3-dimethoxybenzene (0.8 mL) at 150 °C for 12 hours. The reaction yield and isomer ratios were determined by GC analysis.

Scheme 5.59: [BzqPdOAc]₂ (**28**) (6.9 mg, 0.01 mmol, 1 equiv (based on Pd)), “BQ” derivative (0.02 mmol, 1 equiv), DMSO (5.7 μL, 0.08 mmol, 4 equiv), nonadecane (internal standard, 2.7 mg, 0.01 mmol, 0.5 equiv) and 1,3-dimethoxybenzene (0.8 mL) at 150 °C for 12 hours. The reaction yield and isomer ratios were determined by GC analysis.

Scheme 5.60: [BzqPdOAc]₂ (**28**) (6.9 mg, 0.01 mmol, 1 equiv (based on Pd)), 2,5-di(*p*-X-Ph)-benzoquinone (0.02 mmol, 1 equiv), DMSO (5.7 μL, 0.08 mmol, 4 equiv), nonadecane (internal standard, 2.7 mg, 0.01 mmol, 0.5 equiv) and 1,3-dimethoxybenzene (0.8 mL) at 150 °C for 12 hours. The reactions were then analyzed by GC and the product ratio of **51a** : **51b** : **51c** was determined.

Scheme 5.61: [BzqPdCl]₂ (**61**) (6.4 mg, 0.01 mmol, 1 equiv (based on Pd)), Ag₂CO₃ (5.5 mg, 0.02 mmol, 1 equiv), “BQ” derivative (0.02 mmol, 1 equiv), DMSO (5.7 μL, 0.08 mmol, 4 equiv), nonadecane (internal standard, 2.7 mg, 0.01 mmol, 0.5 equiv) and 1,3-dimethoxybenzene (0.8 mL) at 150 °C for 12 hours. The reactions were then analyzed by GC and the product ratio of **51a** : **51b** : **51c** was determined.

Scheme 5.62: [BzqPdCl]₂ (**61**) with Ag₂CO₃ a series of reactions were run with [BzqPdCl]₂ (**61**) (6.4 mg, 0.01 mmol, 1 equiv (based on Pd)), Ag₂CO₃ (5.5 mg, 0.02 mmol, 1 equiv), 2,5-di(*p*-X-Ph)-benzoquinone (0.02 mmol, 1 equiv), DMSO (5.7 μL, 0.08 mmol, 4 equiv), nonadecane (internal standard, 2.7 mg, 0.01 mmol, 0.5 equiv) and 1,3-dimethoxybenzene (0.8 mL) at 150 °C for 12 hours. The reactions were then analyzed by GC and the product ratio of **51a** : **51b** : **51c** was determined.

5.8 References

- (1) Hassan, J.; Sevignon, M.; Gozzi, C.; Schulz, E.; Lemaire, M. *Chem. Rev.* **2002**, *102*, 1359-1469.
- (2) Unger, M. O.; Fouty, R. A. *J. Org. Chem.* **1969**, *34*, 18-21.
- (3) Kozhevnikov, I. V. *React. Kinet. Cat. Lett.* **1976**, *5*, 415-419.
- (4) Kozhevnikov, I. V. *React. Kinet. Cat. Lett.* **1976**, *4*, 451-458.
- (5) Mennenga, G. U.; Rudenkov, A. I.; Matveev, K. I.; Kozhevnikov, I. V. *React. Kinet. Cat. Lett.* **1976**, *5*, 401-406.
- (6) Kozhevnikov, I. V. *React. Kinet. Cat. Lett.* **1977**, *6*, 401-407.
- (7) Yatsimirskii, A. K.; Deiko, S. A.; Ryabov, A. D. *Tetrahedron* **1983**, *39*, 2381-2392.
- (8) Shiotani, A.; Itatani, H.; Inagaki, T. *J. Mol. Catal.* **1986**, *34*, 57-66.
- (9) Fuchita, Y.; Taga, M.; Kawakami, M.; Kawachi, F. *Bull. Chem. Soc. Jpn.* **1993**, *66*, 1294-1296.
- (10) Lee, S. H.; Lee, K. H.; Lee, J. S.; Jung, J. D.; Shim, J. S. *J. Mol. Catal. A* **1997**, *115*, 241-246.
- (11) Iretskii, A. V.; Sherman, S. C.; White, M. G.; Kenvin, J. C.; Schiraldi, D. A. *J. Catal.* **2000**, *193*, 49-57.
- (12) Mukhopadhyay, S.; Rothenberg, G.; Lando, G.; Agbaria, K.; Kazanci, M.; Sasson, Y. *Adv. Syn. Catal.* **2001**, *343*, 455-459.
- (13) Okamoto, M.; Yamaji, T. *Chem. Lett.* **2001**, 212-213.
- (14) Okamoto, M.; Watanabe, M.; Yamaji, T. *J. Organomet. Chem.* **2002**, *664*, 59-65.

- (15) Ackerman, L. J.; Sadighi, J. P.; Kurtz, D. M.; Labinger, J. A.; Bercaw, J. E. *Organometallics* **2003**, *22*, 3884-3890.
- (16) Masui, K.; Ikegami, H.; Mori, A. *J. Am. Chem. Soc.* **2004**, *126*, 5074-5075.
- (17) Negishi, E. I., Ed.; In *Handbook of Organopalladium Chemistry for Organic Synthesis*; Wiley-Interscience: New York, 2002.
- (18) Tamao, K.; Miyaura, N. *Top. Curr. Chem.* **2002**, *219*, 1-9.
- (19) Li, B.; Yang, S.; Shi, Z. *Synlett* **2008**, 949-957.
- (20) Stuart, D. R.; Fagnou, K. *Science* **2007**, *316*, 1172-1175.
- (21) Stuart, D. R.; Villemure, E.; Fagnou, K. *J. Am. Chem. Soc.* **2007**, *129*, 12072-12073.
- (22) Dwight, T. A.; Rue, N. R.; Charyk, D.; Josselyn, R.; DeBoef, B. *Org. Lett.* **2007**, *9*, 3137-3139.
- (23) Potavathri, S.; Dumas, A. S.; Dwight, T. A.; Naumiec, G. R.; Hammann, J. M.; DeBoef, B. *Tetrahedron Lett.* **2008**, *49*, 4050-4053.
- (24) Li, R.; Li, J.; Lu, W. *Organometallics* **2006**, *25*, 5973-5975.
- (25) Itahara, T. *Synthesis* **1979**, 151-152.
- (26) Itahara, T.; Kawasaki, K.; Ousetto, F. *Bull. Chem. Soc. Jpn.* **1984**, *57*, 3488-3493.
- (27) Itahara, T. *J. Org. Chem.* **1985**, *50*, 5272-5275.
- (28) Desai, L. V.; Hull, K. L.; Sanford, M. S. *J. Am. Chem. Soc.* **2004**, *126*, 9542-9543.
- (29) Dick, A. R.; Hull, K. L.; Sanford, M. S. *J. Am. Chem. Soc.* **2004**, *126*, 2300-2301.
- (30) Kalyani, D.; Deprez, N. R.; Desai, L. V.; Sanford, M. S. *J. Am. Chem. Soc.* **2005**, *127*, 7330-7331.
- (31) Hull, K. L.; Anani, W. Q.; Sanford, M. S. *J. Am. Chem. Soc.* **2006**, *128*, 7134-7135.
- (32) Kalyani, D.; Dick, A. R.; Anani, W. Q.; Sanford, M. S. *Tetrahedron* **2006**, *62*, 11483-11498.
- (33) Hull, K. L.; Lanni, E. L.; Sanford, M. S. *J. Am. Chem. Soc.* **2006**, *128*, 14047-14049.
- (34) Hull, K. L.; Sanford, M. S. *J. Am. Chem. Soc.* **2007**, *129*, 11904-11905.
- (35) Constable, A. G.; McDonald, W. S.; Sawkins, L. C.; Shaw, B. L. *J. Chem. Soc., Dalton Trans* **1980**, 1992-2000.

- (36) Dupont, J.; Consorti, C. S.; Spencer, J. *Chem. Rev.* **2005**, *105*, 2527-2571.
- (37) Ryabov, A. D. *Inorg. Chem.* **1987**, *26*, 1252-1260.
- (38) Ryabov, A. D.; Yatsimirskii, A. K.; Abicht, H. P. *Polyhedron* **1987**, *6*, 1619-1620.
- (39) Chen, X.; Li, J.; Hao, X.; Goodhue, C. E.; Yu, J. *J. Am. Chem. Soc.* **2006**, *128*, 78-79.
- (40) Grennberg, H.; Gogoll, A.; Baeckvall, J. E. *Organometallics* **1993**, *12*, 1790-1793.
- (41) Tanaka, D.; Romeril, S. P.; Myers, A. G. *J. Am. Chem. Soc.* **2005**, *127*, 10323-10333.
- (42) Chen, M. S.; White, M. C. *J. Am. Chem. Soc.* **2004**, *126*, 1346-1347.
- (43) Chen, M. S.; Prabakaran, N.; Labenz, N. A.; White, M. C. *J. Am. Chem. Soc.* **2005**, *127*, 6970-6971.
- (44) Shiotani, A.; Shiotani, J. *Mol. Cat.* **1983**, *18*, 23.
- (45) Cho, J.; Iverson, C. N.; Smith, M. R., III *J. Am. Chem. Soc.* **2000**, *122*, 12868-12869.
- (46) Ishiyama, T.; Takagi, J.; Ishida, K.; Miyaura, N.; Anastasi, N. R.; Hartwig, J. F. *J. Am. Chem. Soc.* **2002**, *124*, 390-391.
- (47) Maleczka, R. E., Jr.; Shi, F.; Holmes, D.; Smith, M. R. *J. Am. Chem. Soc.* **2003**, *125*, 7792-7793.
- (48) Lawrence, J. D.; Takahashi, M.; Bae, C.; Hartwig, J. F. *J. Am. Chem. Soc.* **2004**, *126*, 15334-15335.
- (49) Fairlamb, I. J. S. *Org. Biomol. Chem.* **2008**, *6*, 3645-3656.
- (50) Palmgren, A.; Thorarensen, A.; Backvall, J. *J. Org. Chem.* **1998**, *63*, 3764-3768.
- (51) Davies, D. L.; Donald, S. M. A.; Macgregor, S. A. *J. Am. Chem. Soc.* **2005**, *127*, 13754-13755.
- (52) Ryabov, A. D.; Sakodinskaya, I. K.; Yatsimirsku, A. K. *J. Chem. Soc. Dalton Trans.* **1985**, 2629-2638.
- (53) Rubina, M.; Gevorgyan, V. *J. Am. Chem. Soc.* **2001**, *123*, 11107-11108.
- (54) Shilov, A. E.; Shul'pin, G. B. *Chem. Rev.* **1997**, *97*, 2879-2932.
- (55) Lafrance, M.; Fagnou, K. *J. Am. Chem. Soc.* **2006**, *128*, 16496-16497.
- (56) Yoneyama, T.; Crabtree, R. H. *J. Mol. Catal. A* **1996**, *108*, 35-40.

- (57) Anslyn, E. V.; Dougherty, D. A. *Modern Physical Organic Chemistry*; University Science Books: Sausalito, CA, 2006.
- (58) Cai, G.; Fu, Y.; Li, Y.; Wan, X.; Shi, Z. *J. Am. Chem. Soc.* **2007**, *129*, 7666-7673.
- (59) Brasche, G.; Garcia-Fortanet, J.; Buchwald, S. L. *Org. Lett.* **2008**, *10*, 2207-2210.
- (60) Xia, J.; You, S. *Organometallics* **2007**, *26*, 4869-4871.
- (61) Lafrance, M.; Gorelsky, S. I.; Fagnou, K. *J. Am. Chem. Soc.* **2007**, *129*, 14570-14571.
- (62) Harris, R. K.; Becker, E. D.; Cabral De Menezes, S. M.; Goodfellow, R.; Granger, P. *Pure Appl. Chem.* **2001**, *73*, 1795-1818.
- (63) Cristau, H.; Cellier, P. P.; Spindler, J.; Taillefer, M. *Eur. J. Org. Chem.* **2004**, 695-709.
- (64) Littke, A. F.; Dai, C.; Fu, G. C. *J. Am. Chem. Soc.* **2000**, *122*, 4020-4028.
- (65) Dick, A. R. *Ph.D Thesis*, University of Michigan: Ann Arbor, MI, **2007**.